Towards the assembly of higher-order DNA nanostructures: DNA nanotube dynamics and railroad tracks for DNA 'super-origami'

By

Janane Farid Rahbani

A thesis submitted to McGill University in partial fulfillment of the requirements for the degree of Doctor of Philosophy

Department of Chemistry, McGill University

Montréal, Quebec, Canada

August, 2017

© Janane Farid Rahbani, 2017



Abstract

DNA is the molecule that encodes our genetic information. DNA nanotechnology is the field that uses the information given by DNA to build materials in the nanoscale. Through Watson-Crick base pairing, a wide range of DNA-based geometrical motifs self-assemble into programmable and well-defined one-, two- and three-dimensional nanostructures. The remarkable accuracy provided by DNA had an impressive impact on the field of nanotechnology and has been utilized by biologists, chemists, physicists and engineers. However, the generation of higher-order DNA nanostructures remains challenging and often requires hundreds of DNA strands. This thesis tackles this limitation using three approaches. (i) In the first strategy, we develop dynamic DNA nanotubes based on 11 unmodified strands. Simply, triangular rung units are connected via three linking strands to grow tubes up to 2 µm. The symmetry incorporated within the repeating units of the tubes allow them to amplify motion in response to external stimuli. (ii) The second method introduces hydrophobic interactions to enlarge the structural and functional range of our nanotubes. Several parameters were studied to understand the chemistry between the alkyl chains and the nanostructures. Mainly, nanotubes able to encapsulate and selectively release cargo are assembled when the DNA alkyl chains interact intramolecularly within the cavities of the tubes. When the interaction between the DNA amphiphiles becomes intermolecular, an extended network of DNA bundles is formed. Thus, introducing orthogonal hydrophobic interactions into DNA nanotubes can significantly affect their self-assembly, ability for guest encapsulation, cell uptake and intracellular behavior. (iii) In the third strategy, we create DNA super-origami without dramatically increasing the number of synthesized strands. This approach is based on custom-made repetitive DNA backbones that can arrange up to five rectangular origami tiles in high yields. The production of these single-stranded scaffolds, up to ~1000 bases, is cost-effective, user-defined and offers a unique tool to control the final shape of DNA nanostructures. Together, the three approaches developed in this thesis can be employed to expand DNA nanostructure functionalities and geometries without increasing synthetic effort and cost.

Résumé (Translated by Laure Kayser)

L'ADN est la molécule qui code notre information génétique. La nanotechnologie ADN est le domaine dans lequel l'information donnée par l'ADN est utilisée pour construire des matériaux à l'échelle nanométrique. À travers l'appariement de paires de bases Watson-Crick, une large gamme de motifs géométriques basés sur l'ADN s'auto-assemblent en nanostructures mono-, di- et tridimensionnelles programmables et bien définies. La remarquable précision fournie par l'ADN a eu un impact impressionnant dans le domaine de la nanotechnologie et a été utilisée par les biologistes, chimistes, physiciens et ingénieurs. Cependant, la génération de structures d'ADN d'ordre supérieur reste un défi et requiert souvent des centaines de brins d'ADN. Cette thèse s'attaque à ce problème via trois approches. (i) Dans la première stratégie, nous avons développé des nanotubes dynamiques d'ADN basés sur 11 brins non modifiés. Des échelons fait d'unités triangulaires sont simplement connectés par trois brins unifiants pour former des tubes allant jusqu'à 2 µm de longueur. La symétrie incorporée dans les unités de base des tubes leur permet d'amplifier le mouvement de réponse vis-à-vis d'un stimuli extérieur. (ii) La deuxième méthode introduit des interactions hydrophobiques pour augmenter la gamme structurelle et fonctionnelle de nos nanotubes. Plusieurs paramètres ont été étudiés pour comprendre la chimie entre les chaînes alkyles et les nanostructures. En particulier, des nanotubes capables d'encapsuler et de relâcher leur cargaison de manière sélective sont assemblés lorsque les chaînes alkyles de l'ADN interagissent intramoléculairement dans les cavités des tubes. Lorsque l'interaction entre les ADN amphiphiles devient intermoléculaire, un réseau étendu d'ensemble d'ADN est formé. L'introduction d'interactions hydrophobiques orthogonales dans les nanotubes d'ADN peut donc fortement influencer leur auto-assemblage, leur capacité à encapsuler une molécule, leur absorption cellulaire et leur comportement intracellulaire. (iii) Dans la troisième stratégie, nous créons des superorigamis d'ADN sans augmenter dramatiquement le nombre de brins synthétisés. Cette approche est basée sur des squelettes d'ADN répétitifs fait sur mesure qui peuvent arranger jusqu'à cinq tuiles rectangulaires d'origami avec un haut rendement. La production de ces brins uniques, jusqu'à environ 1000 bases, est rentable, définie par l'utilisateur et offre un unique outil de contrôle sur la structure finale des nanostructures d'ADN. Ensemble, les trois approches développées dans cette thèse peuvent être employées pour étendre les fonctionnalités et géométries des nanostructures d'ADN sans augmenter les efforts de synthèse ni les coûts.

Acknowledgements

First and foremost, I present my sincerest gratefulness to my advisor Prof. Hanadi Sleiman for her excellence guidance, thoughtful criticism, and providing me with congenial atmosphere for carrying out my research. I accredit the level of my degree to her support and without her this thesis would not have been fulfilled or written.

I would also like to record my gratitude to Prof. Gonzalo Cosa for his constructive collaboration and for his assistance, advice and helpful discussions in the experimental work.

I convey special acknowledgement to Prof. Jean-Marie Lehn for giving me the opportunity to work in his laboratory in ISIS, Strasbourg University. This experience has helped me expand my knowledge in supramolecular chemistry.

I am most grateful to Karina Carneiro for always being available and for her dynamism and great efforts in affording me with necessary resources during my first PhD years. It is a pleasure to express my gratitude wholeheartedly to Graham Hamblin for his support and assistance throughout my first year.

In my daily work, I have been blessed with a friendly and cheerful group of fellow students. I thank Pongphak, John, Dani, Johans, Albert, Amani, Janet, Tolu, Kitty, Fiora, Andrea, Danny, Xin, Justin, Tom, Mohammed, Farhad and Alex P. for the stimulating discussions, for the sleepless nights we were working together before deadlines, and for all the fun we have had in the last five years.

I owe Pongphak Chidchob for several hundred hours of brainstorming and origami synthesis supervision. Whenever things get tough, Pongphak is always there to calm me down.

Johans Fakhoury and John Hsu introduced me to the world of molecular cloning. Besides being judgmental on every decision I make, Johans has been the big brother that looked after me in

Montreal. In turn, I have been the annoying old brother to John, I made sure to always pick up on him.

Dani Saliba put in a great effort in synthesizing gold nanoparticles. He is the chosen one to transfer the nanotubes legacy to the coming generation of Sleimanites.

I am thankful to Empar Vengut-Climent for carrying out tens of confocal microscopy experiments in live cells. However, the main question remains: where is the DNA labelled strand going?

I am thankful to Amani Hariri for her work on TIRFM. Her presence positively affected the quality of my research.

I am grateful to Petr Fiurasek, Beatrice Lego, and Mohini Ramkaran for help with various instruments, and Chantal Marotte for answering countless of stupid questions graduate students ask. I would also like to thank all the staff members in the Chemistry Department for providing a friendly working environment.

Above all, I would like to thank my brother Rami who has given his unequivocal support throughout, as always, for which my mere expression of thanks likewise does not suffice.

Finally, I thank my friends whose love, dedication, and persistent confidence in me has taken the load off my shoulder. My friends Mary, Madhu, Monika, Rafi, Nassir, Jack, Luca, Diogo, Laure, Jory, Huizhi, Shadi, Mahmoud and Ghislaine who provided me a new home in Montreal deserve a special mention.

Table of Contents

Chapter 1: Introduction	1
1.1 DNA Nanotechnology	1
1.1.1 Overview and Early Examples	1
1.1.2 DNA Origami	8
1.1.3 DNA Nanotubes and Other Dynamic Nanostructures	15
1.1.4 Higher-Order DNA Nanostructures	22
1.2 Scope of Thesis Research	29
1.3 References	31
Chapter 2: Dynamic DNA Nanotubes: Reversible Switching between Single and Double-Stranded Forms, and Effect of Base Deletions	40
2.1 Introduction	40
2.2 Results and Discussions	42
2.2.1 Designing and Assembling DNA Nanotubes	42
2.2.2 Reversible Switching Between Double- and Single-Stranded Nanotubes	48
2.2.3 Site Specific Base Deletions	56
2.2.4. Optimization of Biotin-Streptavidin Interaction	63
2.3 Conclusions	66
2.4 Experimental	67
2.4.1 Materials	67
2.4.2 Instrumentation	68
2.4.3 Sequence Design and Synthesis	69
2.4.4 Total Internal Reflection Fluorescence Microscopy	72
2.5 References	74

-	Tube-like versus bundle-like DNA Nanostructures: Towards orms for cellular Delivery and Guest Encapsulation	79
3.1 Introduct	ion	79
3.2 Results a	nd Discussions	82
3.2.1	Self-Assembly of DNA Nanotubes with Hydrophobic Microenvironment	82
3.2.2	Self-Assembly of DNA Bundles with Hydrophobic Patches	88
3.2.3	Effect of Alkyl Chain Lengths on the Assembly of Nanotubes and Bundles	89
3.2.4	Self-Assembly of DNA Nanotubes and Bundles at Higher Concentrations	91
3.2.5	Step by Step Assembly of Nanotubes and Bundles	94
3.2.6	Conversion from Nanotubes to Bundles	96
3.2.7	Effect of Magnesium Concentration on the Assembly of Bundles	97
3.2.8	Cellular Uptake of Unmodified versus Amphiphilic Nanostructures	100
3.3 Conclusio	ons	104
3.4 Experime	ental	105
3.4.1	Materials	105
3.4.2	System Design	105
3.4.3	DNA Synthesis and Purification	108
3.4.4	Nile Red Encapsulation Protocol	110
3.4.5	Cellular Uptake Study	112
3.5 Reference	es	120
_	: Single-Stranded DNA Templates as 'Railroad Tracks' Origami Formation	127
4.1 Introduct	ion	127
4.2 Results a	nd Discussions	130
4.2.1	Synthesis of Single-stranded DNA Backbones ss-AB[10] (or ss[10])	130
4.2.2	Synthesis of Single-Stranded DNA Backbones ss[20]	134

4.2.3 Organization of Three Origami Tiles	136
4.2.4 Self-Assembly of a Nano-Railroad Track	142
4.3 Conclusions	144
4.4 Experimental	145
4.4.1 Materials	145
4.4.2 Instrumentation	146
4.4.3 Sequential Growth of ds[10]	147
4.4.4 Transformation of pUC19-AB[10]	149
4.4.5 Magnetic Beads Separation of ss[10]	150
4.4.6 Synthesis of ds[20] and ss[20]	151
4.4.7 Preparation of the 3-Tile System	158
4.4.8 Preparation of the 5-Tile System	161
4.4.9 Additional AFM images on 3- and 5-Tiles Systems	165
4.4.10 DNA Sequences	167
4.5 References	176
Chapter 5: Conclusions and Future Work	180
5.1 Conclusions	180
5.2 Suggestions for Future Work	
5.3 List of Publications	184
Appendix 1: Rearrangement of DNA Nanotubes into Long Fibers Mediated by Gold Nanoparticles	186
A1.1 Introduction	186
A1.2 Results and Discussions	187
A1.2.1 System Design	187
A1.2.2 Self-Assembly of Long Fibers and Needle-Like Structures	188

A1.3 Conclusion	ons	195
A1.4 Experimental		196
A1.4.1	Materials	196
A1.4.2	Instrumentation	197
A1.4.3	Synthesis of Gold Nanoparticles	197
A1.4.4	DNA Sequences	199
A1.5 References		200

List of Figures

Figure 1.1.	DNA structure.	2
Figure 1.2.	Examples of supramolecular assemblies	3
Figure 1.3.	DNA geometrical motifs	5
Figure 1.4.	Double- and triple crossover motifs	6
Figure 1.5.	Three-dimensional DNA nanostructures	7
Figure 1.6.	DNA origami	9
Figure 1.7.	DNA origami with complex geometries	11
Figure 1.8.	Higher-order nanostructures of DNA origami	13
Figure 1.9.	DNA origami interactions with biomolecules	14
Figure 1.10	Strategies for assembling DNA nanotubes	16
Figure 1.11.	Strand displacement approach	18
Figure 1.12.	DNA nanomachines	20
Figure 1.13.	Modular DNA nanotubes	21
Figure 1.14.	Patterning DNA nanostructures on surfaces	24
Figure 1.15.	Organization of AuNPs into a hexagonal pattern	25
Figure 1.16.	Combining coordination chemistry and DNA	26
Figure 1.17.	Formation of higher-order DNA nanostructures via orthogonal interactions	27
Figure 2.1.	Previous designs of tubes synthesized in the Sleiman group	41
Figure 2.2.	New DNA nanotube design	43
Figure 2.3.	Characterization of nanotubes by AGE, AFM and TIRFM	45
Figure 2.4.	Detailed TIRFM study on the nanotubes	47
Figure 2.5.	Characterization of open tubes	48
Figure 2.6.	Strand displacement experiment	51
Figure 2.7.	Reversible switching between single- and double-stranded forms	52
Figure 2.8.	AGE characterization of the dynamic behavior of the tubes	53
Figure 2.9.	Single-molecule characterization of the reversible switching between the tubes	55
Figure 2.10.	Site specific mismatches study	57
Figure 2.11.	AFM characterization of site specific mismatches on the nanotubes	60
Figure 2.12.	PAGE showing the assembly of dimers	62
Figure 2.13.	Introducing distortion to the tubes via strand displacement approach	64

Figure 2.14.	TIRFM studying the effect of biotin concentration on the deposition of the tubes	65
Figure 2.15.	Photobleaching intensity traces examples from a series of samples	66
Figure 2.16.	DNA nanotubes design as modelled by Gideon	70
Figure 3.1.	Introducing orthogonal modes of assembly to DNA	80
Figure 3.2.	Illustrations of the assembly of amphiphilic rungs	83
Figure 3.3.	Assembly of nanotubes with hydrophobic pockets	85
Figure 3.4.	TIRFM characterization of the encapsulation/release of Nile Red	87
Figure 3.5.	Assembly of bundles	89
Figure 3.6.	AFM characterization of tubes having various alkyl chain lengths	90
Figure 3.7.	Effect of alkyl chain lengths on the assembly of bundles	91
Figure 3.8.	PAGE characterization of amphiphilic rungs at higher concentrations	92
Figure 3.9.	AFM characterization of amphiphilic nanotubes at higher concentrations	93
Figure 3.10.	AFM characterization of bundles at higher concentrations	95
Figure 3.11.	AFM micrographs displaying the formation of nanotubes and bundles	96
Figure 3.12.	AFM characterization of the conversion of individual tubes to bundles	98
Figure 3.13.	AFM characterization of the bundles at low concentrations of Mg^{2+}	99
Figure 3.14.	PAGE displaying the integrity of the nanostructures at low Mg ²⁺ concentrations	100
Figure 3.15.	Spectral imaging of nanostructures incubated in HeLa cells at 6 and 24 h	103
Figure 3.16.	DMT-dodecane-Diol phosphoramidite purchased from ChemGenes	109
Figure 3.17.	Reverse-phase HPLC traces of sequence-defined DNA amphiphiles	110
Figure 3.18.	Emission spectra of Nile Red	112
Figure 3.19.	3D reconstructed images of bundles/nanotubes incubated in HeLa cells for 24 h	113
Figure 3.20.	Spectral imaging of the bundles/nanotubes incubated in HeLa cells for 7 and 24 h $$	115
Figure 3.21.	Spectral imaging of various structures incubated in HeLa cells for 24 h	118
Figure 3.22.	Serum stability assays of structures prepared at higher concentrations	119
Figure 3.23.	Serum stability assays of structures prepared at 75 nM then concentrated	120
Figure 4.1.	Different techniques to assemble larger origami structures	129
Figure 4.2.	Synthesis of a DNA backbone in a temporal controlled manner	132
Figure 4.3.	Production of pUC19-AB[20] from pUC19-AB[10]	135
Figure 4.4.	AGE characterization of the successful insertion of ds-AB[20] into the pUC19	136
Figure 4.5.	3-tiles system assembly	138

Figure 4.6.	Effect of the number of sticky ends on the assembly of 3-tiles system	140
Figure 4.7.	Assembly of 3-tiles system at different ss[10] concentrations	141
Figure 4.8.	Railroad track assembly	144
Figure 4.9.	Generation of two DNA fragments M and N via two PCR reactions	152
Figure 4.10.	AGE showing colonies containing the insert	155
Figure 4.11.	Single strand conversion of ds[20]	157
Figure 4.12.	AFM of individual origami tiles	159
Figure 4.13.	3-tile system assembly through stepwise addition of individual tiles	160
Figure 4.14.	AFM characterization of the stepwise assembly of 3-tile system	161
Figure 4.15.	AGE characterization of the railroad track	162
Figure 4.16.	Assembly of railroad track at different temperatures	164
Figure 4.17.	Assembly of railroad track at room temperature	164
Figure 4.18.	Effect of the number of sticky ends on the assembly of railroad track	165
Figure 4.19.	AFM images of 3-tiles system	166
Figure 4.20.	AFM images of railroad track	167
Figure A1.1	. AFM micrographs of short and big nanotubes	188
Figure A1.2	. AGE characterization of the three versions of the tubes	189
Figure A1.3	. Effect of AuNPs quantity on the assembly of long fibers	190
Figure A1.4	. Effect of AuNPs size and polyT length on the formation of long fibers	192
Figure A1.5	. Effect of AuNPs size and polyT length on the formation of short fibers	193
Figure A1.6	. Effect of nanotubes concentration on the formation of long fibers	194
Figure A1.7	. Effect of the buffer on the formation of long fibers	195

List of Tables

Table 2.1.	Sequences of all the strands used in chapter 2.	71
Table 3.1.	Sequences of all the strands used in chapter 3.	107
Table 4.1.	Duplex Seed Sequences for AB[10].	148
Table 4.2.	Optimized PCR conditions to exctract ds[10] from pUC19-AB[10].	151
Table 4.3.	PCR conditions to generate M and N fragments.	153
Table 4.4.	Digestion conditions of pUC19 and M and N fragments with BsmBI.	154
Table 4.5.	Ligation conditions of pUC19 and M and N fragments with T7 ligase.	154
Table 4.6.	Digestion conditions of pUC19-[AB]20 with BsmBI.	155
Table 4.7.	Lambda Exonuclease digestion of ds[20].	157
Table 4.8.	Modification of staple strands in 3-tile system.	167
Table 4.9.	Modification of staple strands in 5-tile system (version 1).	168
Table 4.10.	Modification of staple strands in 5-tile system (version 2).	169
Table A1.1.	Effect of AuNPs size and polyT length on the formation of fibers.	190
Table A1.2.	Sequences of the strands used to build the nanotubes.	199

List of abbreviations

1D One-dimensional

2D Two-dimensional

3D Three-dimensional

A Adenine

AFM Atomic force microscopy

AGE Agarose gel electrophoresis

ATP Adenosine triphosphate

AuNPs Gold nanoparticles

C Cytosine

DNA Deoxyribonucleic acid

ds Double-stranded

DMEM Dulbecco's Modified Eagle Medium

dNTP Deoxynucleotide triphosphates

DX Double-crossover

EDTA Ethylenediaminetetraacetic acid

FBS Fetal bovine serum

G Guanine

HEG Hexaethylene glycol

HeLa Cervical cancer cell line

PAGE Polyacrylamide gel electrophoresis

PBS Phosphate buffered saline

PCR Polymerase chain reaction

PEG Poly(ethylene glycol)

RCA Rolling circle amplification

ss Single-stranded

SST Single-stranded tile

T Thymine

TEM Transmission electron microscopy

TIRFM Total internal reflection fluorescence microscope

Author Contributions

Prof. Hanadi F. Sleiman granted funding, provided research objectives, and intellectual supervision for all of the projects reported in this thesis.

Prof. Gonzalo Cosa provided supervision over all TIRFM experiments.

Chapter 2

Hariri A.A. performed all the TIRFM experiments throughout this chapter.

Chapter 3

Chidchob P. carried out the TIRFM experiments in section 3.2.1. **Gidi Y.** performed the analysis on the TIRFM images in section 3.2.1. **Vengut-Climent E.** performed all the confocal microscopy measurements and serum stability assays in sections 3.2.8 and 3.4.5. **Trinh T.** synthesized few strands named 5'-HE(n)-8T-LS1*, 5'-HE(n)-LS1*, 5'-HE(n)-8T-LS2/3* and 5'-HE(n)-LS2/3*.

Chapter 4

Hsu J. performed the transformation of ds[10] into pUC19. He designed the synthesis of ds[20] and optimized its transformation into pUC19. Sections 4.2.2 and 4.4.6 were carried out in close collaboration with **Hsu J. Chidchob P.** helped in the preparation of many samples in sections 4.2.3 (~70%), 4.4.7 (50%) and 4.4.8 (20%). He also performed many gel electrophoresis experiments throughout this chapter.

Appendix A1

Saliba D. helped in preparing few samples (~40%) and synthesizing gold nanoparticles. He also performed the gel electrophoresis experiments in this appendix.

Chapter 1:

Introduction

1.2 DNA Nanotechnology

During the past 30 years, the field of DNA nanotechnology has witnessed significant development and has been applied in various other fields such as biology, physics, chemistry and engineering.¹⁻³ The number of laboratories working on this topic has expanded immensely, leading to the generation of a variety of two and three-dimensional nanostructures. These novel constructs were incorporated in the creation of nanomechanical devices and contributed in the advancement of medical applications.^{4,5}

1.1.1 Overview and Early Examples

DNA (Deoxyribonucleic acid) is the molecule that encodes our genetic information. Since Watson and Crick revealed the recognition motifs of DNA, biologists have been further exploiting the chemical basis underlying our genes. In particular, the hydrogen bonding between adenine (A)/thymine (T) and guanine (G)/cytosine (C) is called Watson-Crick base-pairing (Figure 1.1). However, biology is no longer the sole area of science in which DNA is playing a crucial role. According to Professor Nadrian Seeman, founder of DNA nanotechnology: "It is now possible to exploit DNA complementarity to control the structure of matter."

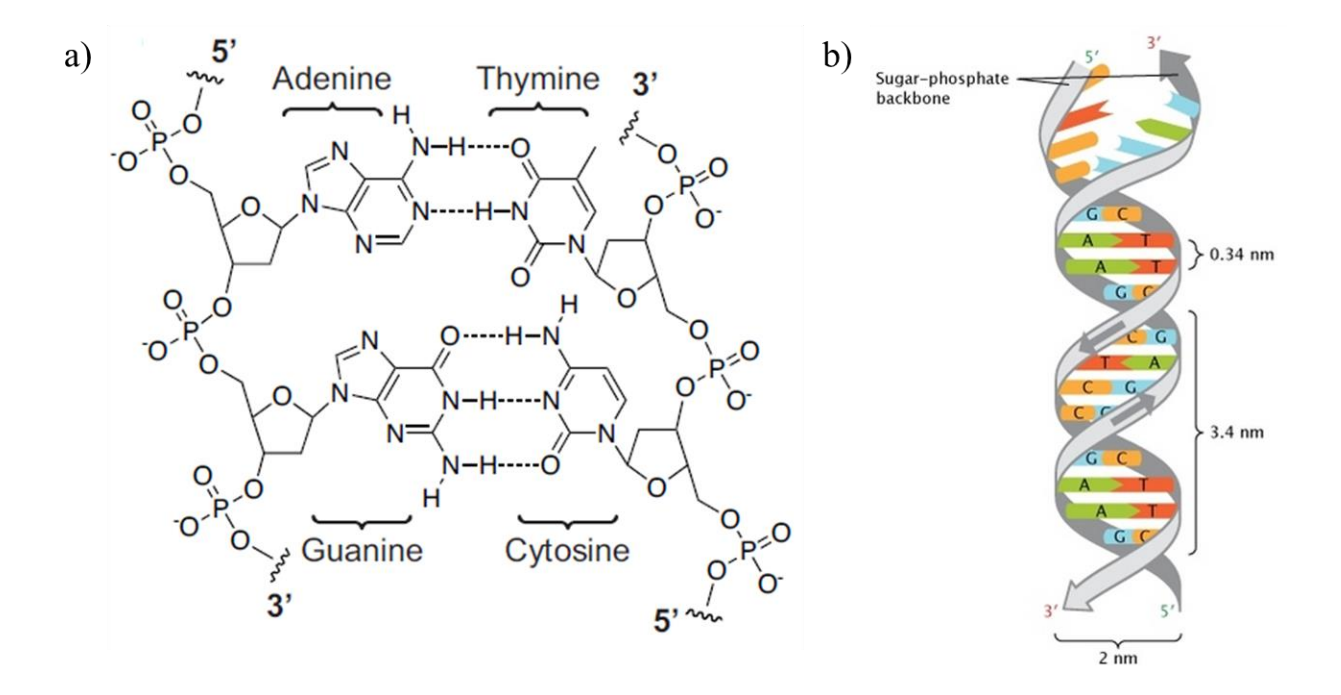


Figure 1.1: Watson-Crick base pairing. a) Three hydrogen bonds linking nucleobases G and C versus two hydrogen bonds linking nucleobases A and T. b) B-DNA: right handed helical sense, a 3.4 Å helical rise per base pair, a width of 2 nm and a 10.5 base pairs per helical turn. Adapted with permission from reference 6 (Nature Publishing Group, 2008).⁶

In the last few decades, researchers have focused on building materials and technologies on the nanometer size regime (1-100 nm).⁷ Working at this length scale offers a variety of appealing opportunities since the properties of nanoparticles can be highly dependent on their sizes.⁸ Indeed, the shape and length of nanoparticles can dramatically manipulate their electronic, optical, chemical and magnetic properties. Since nanomaterials are generally smaller than 100 nm, their structural properties are influenced by their surrounding molecules and the interaction between the particles often generate unique optical and electronic properties.

Despite the existence of two common approaches, top-down and bottom-up, in building nanomaterials, it is still challenging to construct materials at this scale. The top-down strategy refers to breaking down large structures into smaller dimensions required for processing.⁹ This

method is widely used in fabricating nanodevices, yet it requires external and expansive tools to achieve smaller sizes in the molecular scale. Alternatively, bottom-up techniques are able to produce devices through the autonomous self-assembly of small building blocks. ¹⁰ Indeed, the idea of supramolecular self-assembly involves the creation of novel materials with unique chemical compositions and properties (Figure 1.2). ¹¹ This concept is mainly based on non-covalent interactions such as hydrogen-bonding, π - π stacking, the hydrophobic effect and so on. The self-assembly of DNA is the result of these interactions through Watson-Crick base pairing.

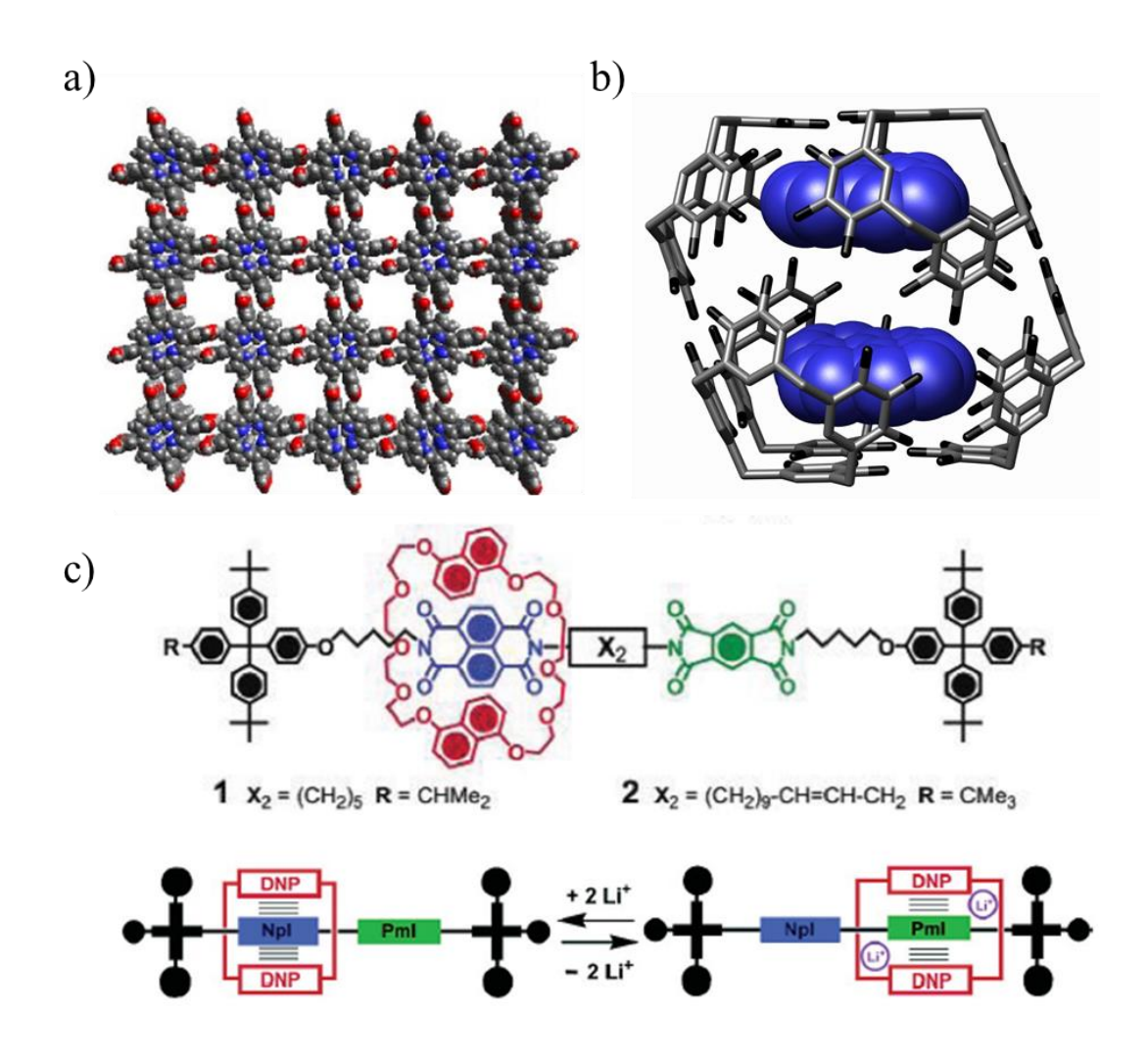


Figure 1.2. (a) Crystal structure of an octahydroxy porphyrin network: 5,10,15,20-tetrakis(3',5'-dihydroxy-phenyl) porphyrin. Based on the position of hydroxyl groups and the nature of metals, the size of the pores varies. Adapted with permission from reference 12 (Taylor and Francis, 1998). (b) Crystal structure of resolved pyrene fragments inside a hexameric assembly. Adapted with permission from reference 13 (Science, 2005). (c) Schematic representation of a switchable bistable rotaxane. The blue and green colored docking sites are π -electron poor, whereas the red ring is π -electron rich. The addition/removal of lithium cations induce the switching between the two docking sites. Adapted with permission from reference 14 (ACS Publishing, 2004).

Inspired by the helical structure of DNA and aiming at designing periodic lattices from short oligonucleotides, Nadrian Seeman established the field of DNA nanotechnology in 1982. 15 Because DNA is inherently linear, he introduced specific geometrical motifs that can dictate the final size and shape of the nanostructures. Figure 1.3 shows early examples of branched junctions reported in literature. In order to better understand how these nanostructures assemble, it is important to define concepts such as non-natural hybridization and stable stick-ends and explain appropriate strategies to design sequences. For instance, the Holliday junction presents a simple example of unusual arrangement of two helices to produce a four-way junction. 16 When the 5'-and/or 3'-ends of the junctions are extended by a defined number of unhybridized bases (sticky ends or overhangs), a 2D/3D lattice can be produced depending on the complementarity of the sticky-ends. Figure 1.3 depicts the formation of a quadrilateral from a sticky-ended branched junction.

Following the invention of the Holliday junction, Seeman found that the construction of larger patterns requires more rigid geometrical motifs. Thus, he developed double crossover motifs (DX) to build defined 2D networks.¹⁷ The DX motif was shown to be approximately twice as rigid as

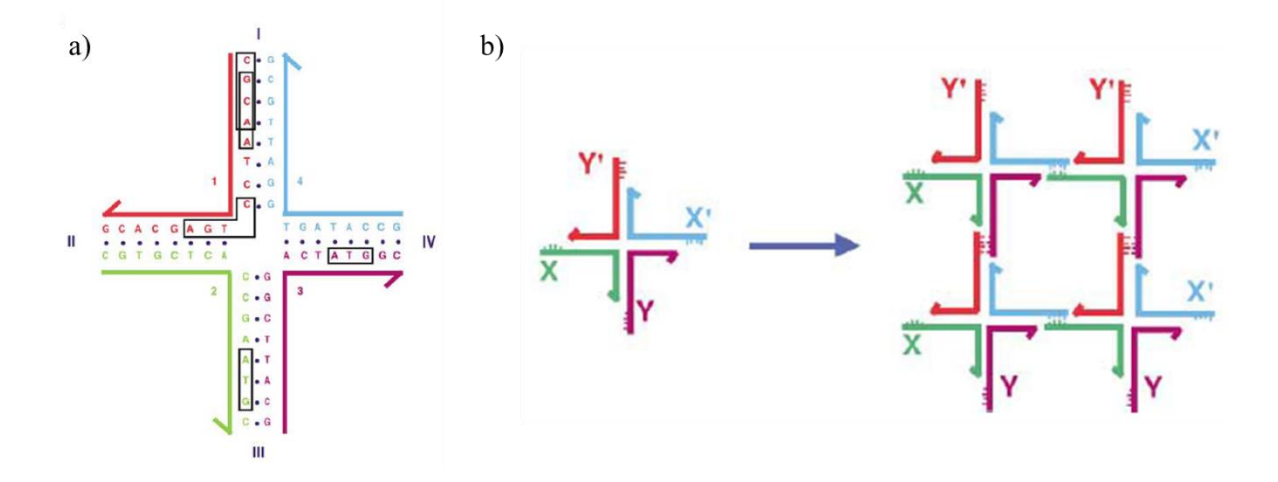


Figure 1.3. (a) A stable branched junction composed of four DNA strands. (b) A four-way sticky-ended branched junction induces the assembly of a quadrilateral. Adapted with permission from reference 18 (Elsevier Publishing, 2003).¹⁸

equivalent linear double-stranded DNA due to the two crossover points, the points at which individual strands cross between two domains, that provide a defined orientation of DNA and confine their mobility. Triple crossover (TX) motifs¹⁹ were developed to further increase the rigidity of branched junctions, yet they were not as widely used as DX motifs. Figure 1.4c displays the assembly of a 2D array due to the interaction between two DX motifs programmed to come together via Watson-Crick base pairing.²⁰ Note that changing the number of bases between crossovers or modifying the size and/or sequences of sticky-ends leads to the formation of nanotubes instead of planar sheets (section 1.1.3). Therefore, it is critical to consider the helicity of DNA when designing any structure.

Because of its ease of synthesis and programmability, DNA has been used to produce a wide range of structures. Several geometrical motifs and branching junctions have been created to assemble cubes,²¹ nanotubes,^{22,23} tetrahedra^{24,25} and so on. Other factors including stochiometric ratios between DNA strands, annealing temperatures, stepwise versus one-pot assemblies play an

important role in determining the final geometry and shape of the structures. For example, Sleiman and coworkers reported the assembly of DNA cubes made up of four strands mixed and annealed

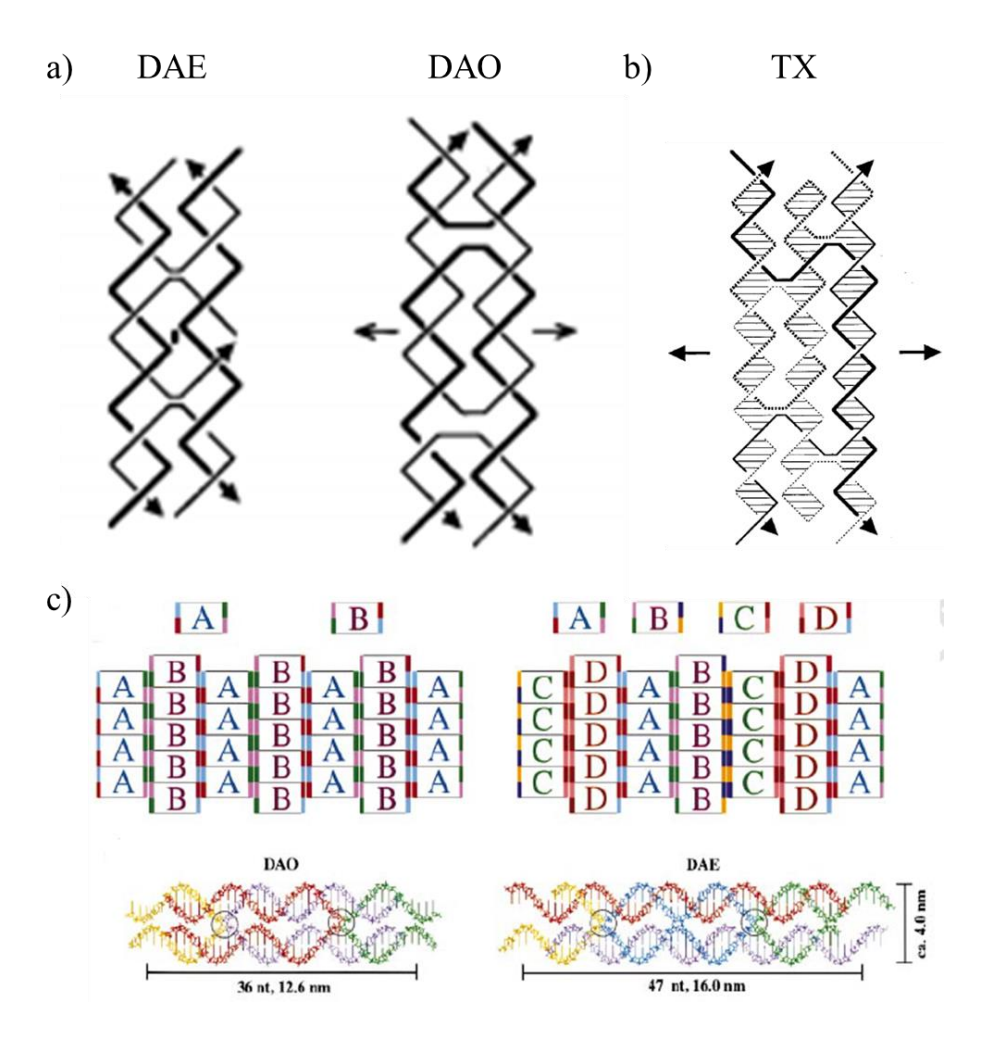


Figure 1.4. (a) Schematic representation of two types of double-crossover structures (D). A: antiparallel refers to the orientation of the two helical domains. E: even and O: odd refer to the number of helical turns between the two crossover points. Adapted with permission from reference 17 (ACS Publishing, 1993). (b) Scheme of a triple-crossover complex consisting of three helices having coplanar axes. The complex is made up of four strands. Adapted with permission from reference 26 (ACS Publishing, 2000). (c) Generation of 2D networks from DX tiles bearing different overhang addressabilities. Adapted with permission from reference 20 (Nature Publishing Group, 1998).

together at 95°C then cooled down to 4°C for 6 hours (Figure 1.5).²⁷ Changing the conditions of assembly by adding one component in excess or mixing the strands at room temperature leads to the formation of other byproducts and dramatically affects the yield of the desired discrete shape. DNA tetrahedron is another geometry reported by Turberfield's research group constituting of four strands (Figure 1.5).²⁸ The latter example illustrates how the shape of the nanostructure is determined by the designed sequences of the original motif.

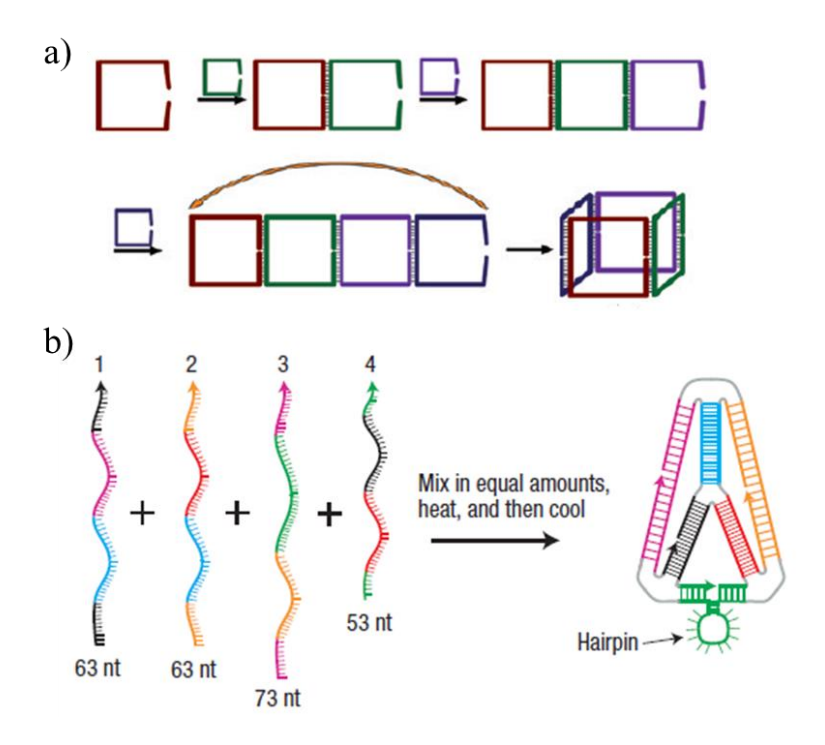


Figure 1.5. (a) Scheme showing the clip-by-clip approach for the synthesis of DNA cubes from four strands. Adapted with permission from reference 27 (ACS Publishing, 2016). (b) Scheme representing the synthesis of a DNA tetrahedron from four strands. The hairpin region acts as a toehold for further strand displacement experiments. Adapted with permission from reference 28 (Nature Publishing Group, 2008).

Following the successful generation of large 2D arrays and a wide range of 3D systems based on DNA molecules, researchers have employed DNA nanostructures to arrange proteins, ^{29,30} small

molecules³¹ and nanoparticles^{32,33} with nanoscale precision, optimize biological probes,³⁴ create novel drug delivery vehicles^{35,36} and combine the traditional synthesis of DNA with lithographic techniques.^{37,38} Knowing that real-world applications require a large-scale production of DNA, ongoing efforts have been focusing on developing inexpensive routes such as on-chip DNA synthesis to produce oligonucleotides in high yields.³⁹ Finally, because DNA is limited by the four-letter genetic code, it becomes extremely difficult to assemble a large number of strands without avoiding undesired secondary interactions. In order to solve this problem, various orthogonal interactions such as the hydrophobic effect were introduced to increase the complexity and functional range of DNA structures. In the following sections, we will further elaborate on different strategies employed to create higher-order nanostructures and will discuss their impact on the field.

1.1.2 DNA Origami

Two decades after the generation of the initial geometrical motifs, Paul Rothemund revolutionized the field of DNA nanotechnology through a use of a long strand of DNA to build nanostructures. He used a strand of genomic viral DNA M13mp18 and folded it around more than 200 short strands (called staples strands) obtained synthetically, to form various DNA geometries and shapes with the aid of a computer software (Figure 1.6). Unlike Seeman's 2D arrays, the assembly of DNA origami does not rely on sticky-end cohesion of DX motifs. Instead, crossover points were generated through the assembly of these short and unique strands at predesigned positions with the long scaffold. Compared to other assembly modes of DNA nanostructures, DNA origami offers many advantages: (i) Based on the locations/sequences of

staples strands, a wide range of morphologies can be created, (ii) Origami structures are more rigid than DX tiles since crossovers are continuously connected by a single backbone and (iii) because of their structural robustness, it is easy to characterize origami tiles and study their assemblies via AFM, TEM, single molecule fluorescence and so on. In this section, we will be describing some of the origami designs and their emerging applications ranging from nanodevices to drug delivery.

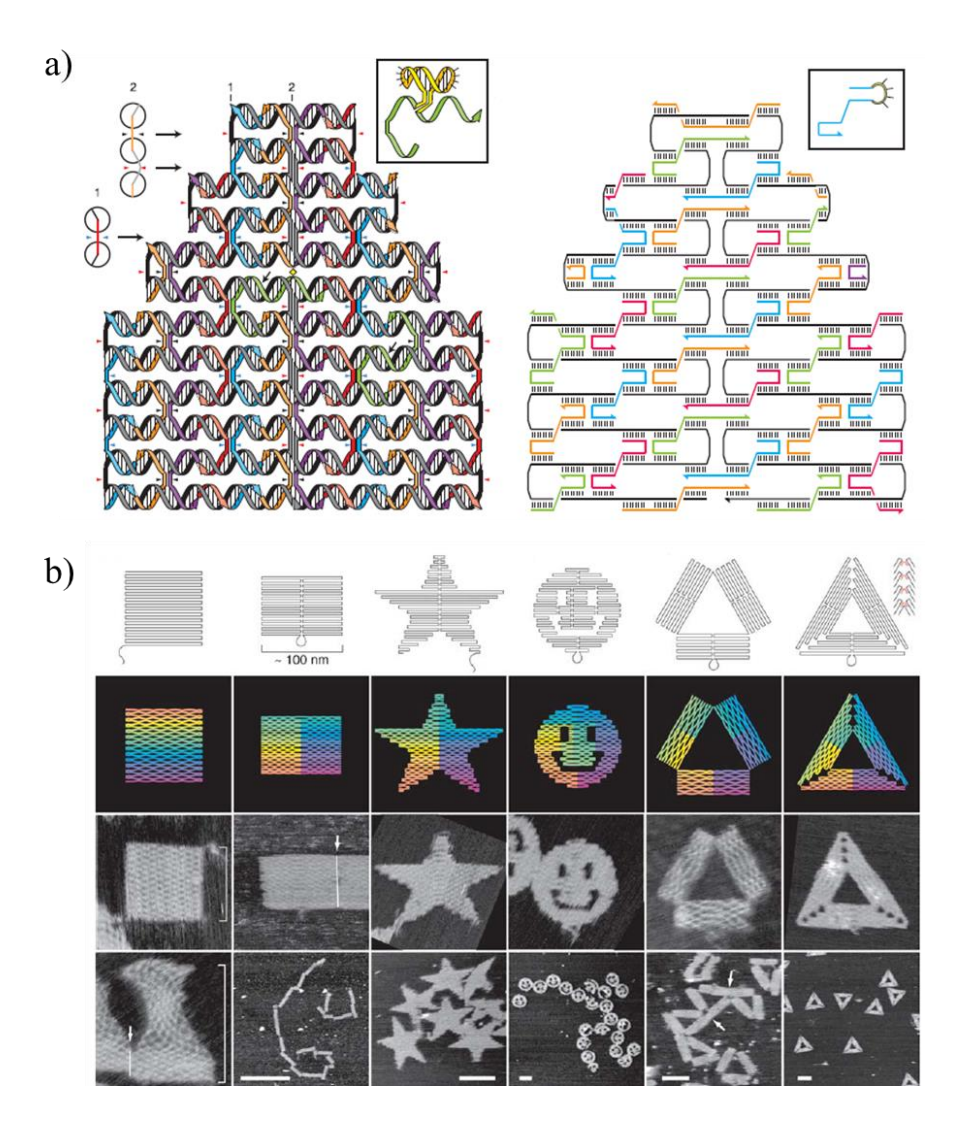


Figure 1.6. (a) A long strand (7249-nt) is folded into various shapes through hybridization to staples strands of unique sequences. While running through every helix, crossover points are generated to increase the rigidity of the final structure. (b) Images of some 2D structures

produced using this technique. Adapted with permission from reference 40 (Nature Publishing Group, 2006).

Based on the origami approach developed by Rothemund, Shih and coworkers aimed at designing 3D origami structures. They put together an innovative software named "cadnano" to improve the production of random 3D nanostructures through a user-friendly interface.⁴¹ The Shih group reported the assembly of square lattices using this program (Figure 1.7a).⁴² Besides designing stable and rigid nanostructures, curvature of origami tiles was introduced by Yan et al. They found that adding/erasing bases between crossover points drastically alters the planarity of the structure (Figure 1.7b).⁴³ However, while the surface area of a single origami can provide around ~200 templating sites, it remains a challenge to assemble higher-order nanostructures that are capable of accomplishing complicated functions. For most of practical applications, assembling larger origami is required to allow wiring of multi-component electronic devices, 44,45 to amplify optical effects as observed in optical metasurfaces⁴⁶ or simply to template proteins and nanoparticles over bigger areas. The main limitation arises from the scarce sources for long singlestranded DNA (ssDNA) scaffolds of different lengths and random sequences at a large scale. To overcome this problem, ongoing efforts have been focusing on exploring the folding of DNA origami into 2D arrays by means of multiple tiles. 47-49 Other promising strategies include the selfassembly of individual origami tiles into super-origami through surface diffusion on a solid substrate, ⁵⁰ or by gold nanoparticle bridges. ⁵¹ While it is important to balance construct simplicity with complex function, higher-order nanostructures should maintain their addressability and geometric versatility. In chapter 4, we examine the organization of the origami tiles via an external scaffold made up of custom-made repetitive sequences to address this need.

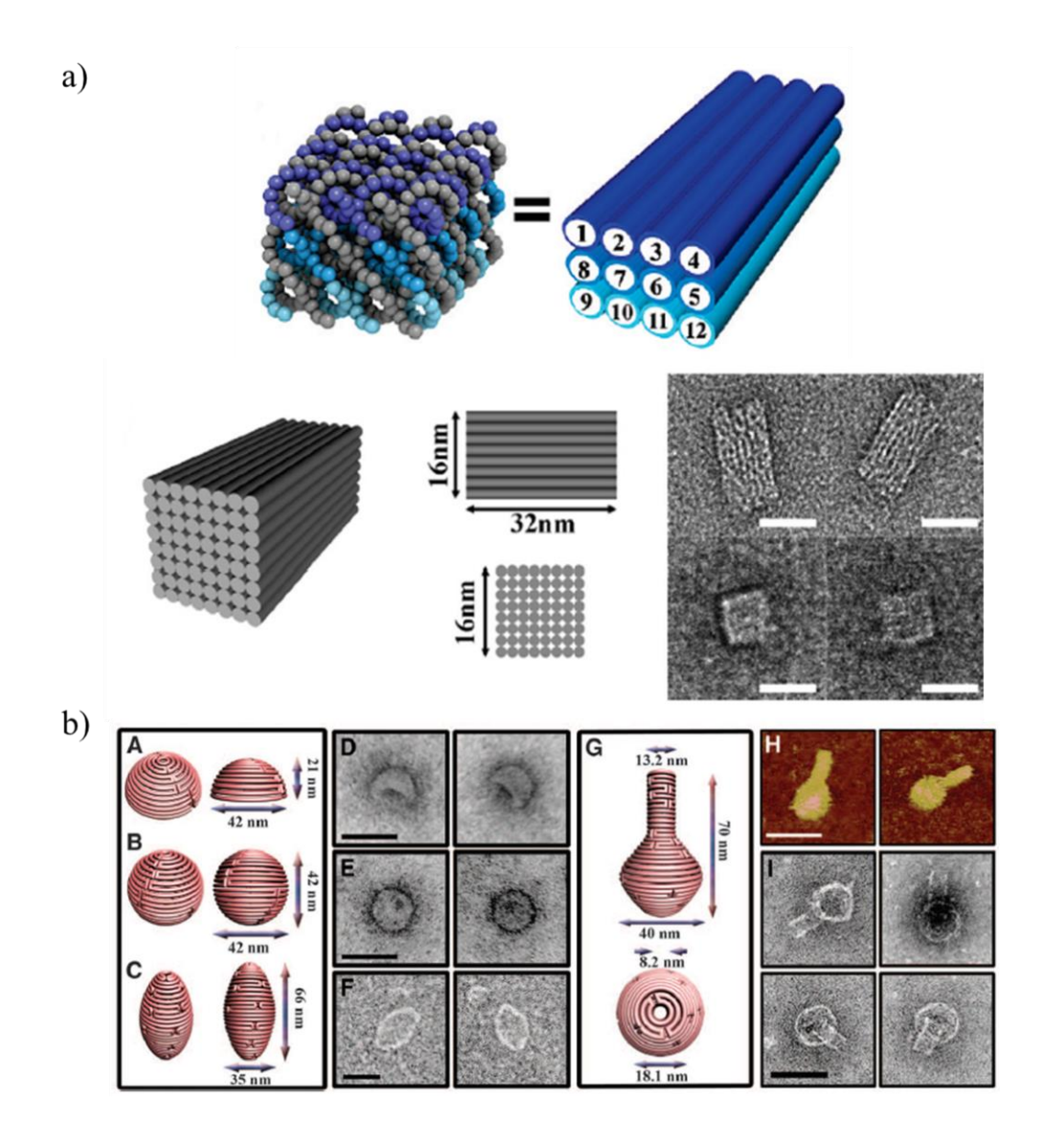


Figure 1.7. (a) Schematic representation of 3D DNA origami square-lattice structure. The gray color refers to the scaffold strand and the blue colors refer to the staple strands. To simplify the scheme, each cylindrical rod on the right represents one double helix. The eight-layer structure is visualized by TEM (scale bar is 20 nm). Adapted with permission from reference 42 (ACS Publishing, 2009). (b) Complex curvatures were introduced in the design of origami structures. A: hemisphere, B: sphere, C: ellipsoid, D: TEM micrographs of the hemisphere, E: TEM micrographs of the sphere, F: TEM micrographs of the ellipsoid (scale bar is 50 nm), G: nanoflask, H: AFM micrographs of the nanoflask (scale bar is 75 nm) and I: TEM micrographs of the nanoflask (scale bar is 50 nm). Adapted with permission from reference 43 (Science 2011).

To increase the utility of DNA origami, many researchers have been labeling DNA with nanoparticles,⁵² enzymes,⁵³ polymers⁵⁴ or small molecules⁵⁵ and so on. These units either direct the assembly of higher-order origami structures or the origami platforms are used to control their positions in 2D and 3D. The main goal in both cases is building efficient systems capable of displaying new properties at the macroscopic level. For example, gold nanoparticles (AuNPs) and nanorods have been commonly used in the fabrication of novel materials due to their unique optical properties. In this regard, DNA nanostructures are employed to manipulate light by controlling the distance between nanoparticles. Since AuNPs are easily conjugated to thiolated DNA strands, Gang and colleagues reported the assembly of a network of AuNPs captured inside a cross-shaped DNA origami (Figure 1.8a). 56 Turberfield et al. organized AuNPs via DNA nanoflowers to control photonic properties (Figure 1.8b).⁵⁷ Molecular patterning onto AuNPs was demonstrated by Wei and coworkers after attaching the nanoparticles to origami at defined positions then removing the template under specific conditions.⁵⁸ It is noteworthy that this strategy was reported first by Sleiman's group on nanocubes.⁵⁹ Furthermore, DNA origami presents an ideal tool to build plasmonic materials since the distance between particles can be addressed within a nanoscale precision. This concept was demonstrated by Schmidt's research group who was able to template AuNPs on nanotubes by tuning various parameters affecting the interaction of DNA with the gold surface (Figure 1.8c).⁶⁰

Alternatively, researchers envisioned the use of DNA origami as a tool to better understand complex biological systems. As such, a variety of macromolecules were templated on the origami surface in order to (i) develop enzymatic nanoreactors,⁶¹ (ii) build more efficient drug delivery vehicles⁶² and (iii) improve current biosensing devices.⁶³ Yan and coworkers employed origami

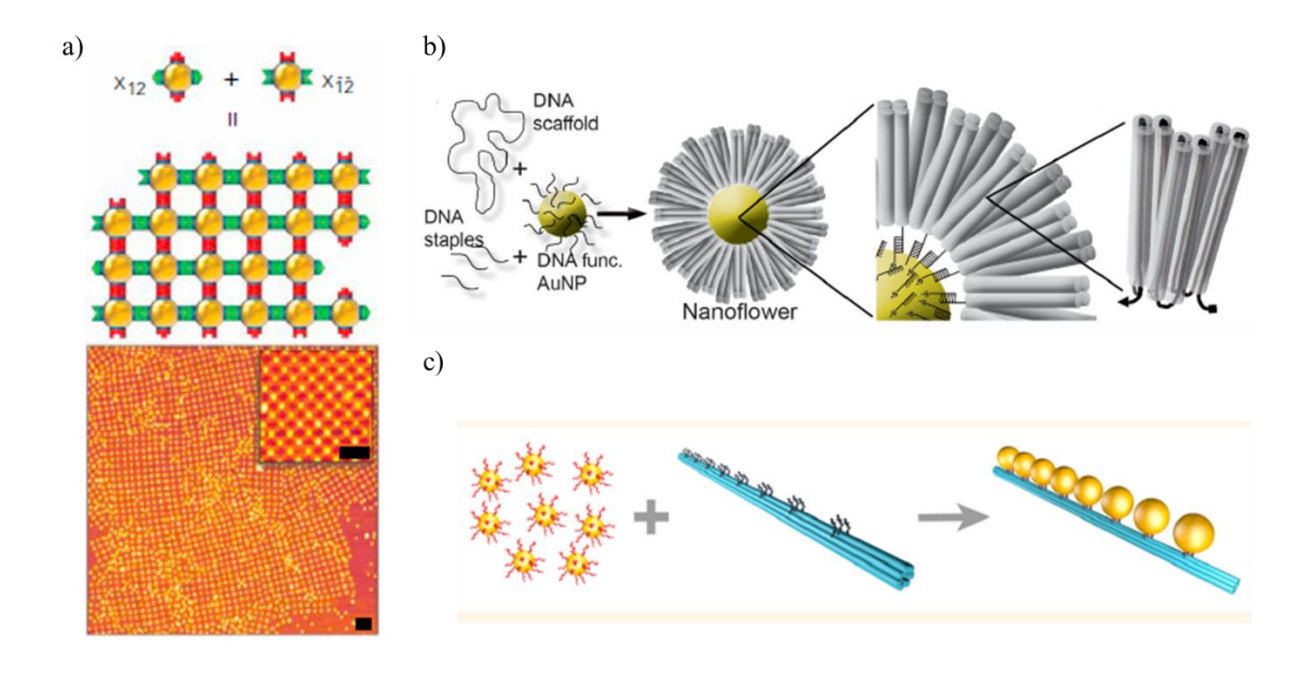


Figure 1.8. (a) Formation of a 2D network of DNA origami mediated by AuNP. Adapted with permission from reference 56 (Nature Publishing Group, 2016). (b) Assembly of nanoflowers mediated by DNA origami. In a one pot reaction: staples strands, scaffold and 15 nm AuNP were mixed. Adapted with permission from reference 57 (ACS Publishing, 2016). (c) Scheme showing the assembly of AuNP on DNA nanotubes (six helical bundles) through Watson-Crick base pairing. Adapted with permission from reference 60 (ACS Publishing, 2016).

tiles in an attempt to examine the activity of two enzymes as a function of the distance between them (Figure 1.9a).⁶⁴ Shih's group used the ordering provided by origami nanotubes to aid in the NMR characterization of membrane proteins (Figure 1.9b).⁶⁵ Moreover, various publications described the interaction of functionalized DNA nanostructures with lipid membranes. A study conducted by Walter *et al.* has shown that the number/position of cholesterol barges on origami tiles play a significant role in controlling their dynamics on the bilayer surface. Therefore, these systems can be labelled with fluorescent dyes and used as probes to characterize biological membranes.⁶⁶ In addition to their usage as templating platforms, DNA origami are considered exceptional substrates to perform super-resolution single-molecule experiments based on DNA

PAINT (a variation of super-resolution fluorescence microscopy).⁶⁷ Jungman and coworkers reported the successful imaging of biomolecules within 5 nm resolution using this technique. Briefly, DNA-PAINT is based on the transient interaction between one or more short DNA strands labelled with dyes, typically 9 bases, with specific staple strands on origami (Figure 1.9c).

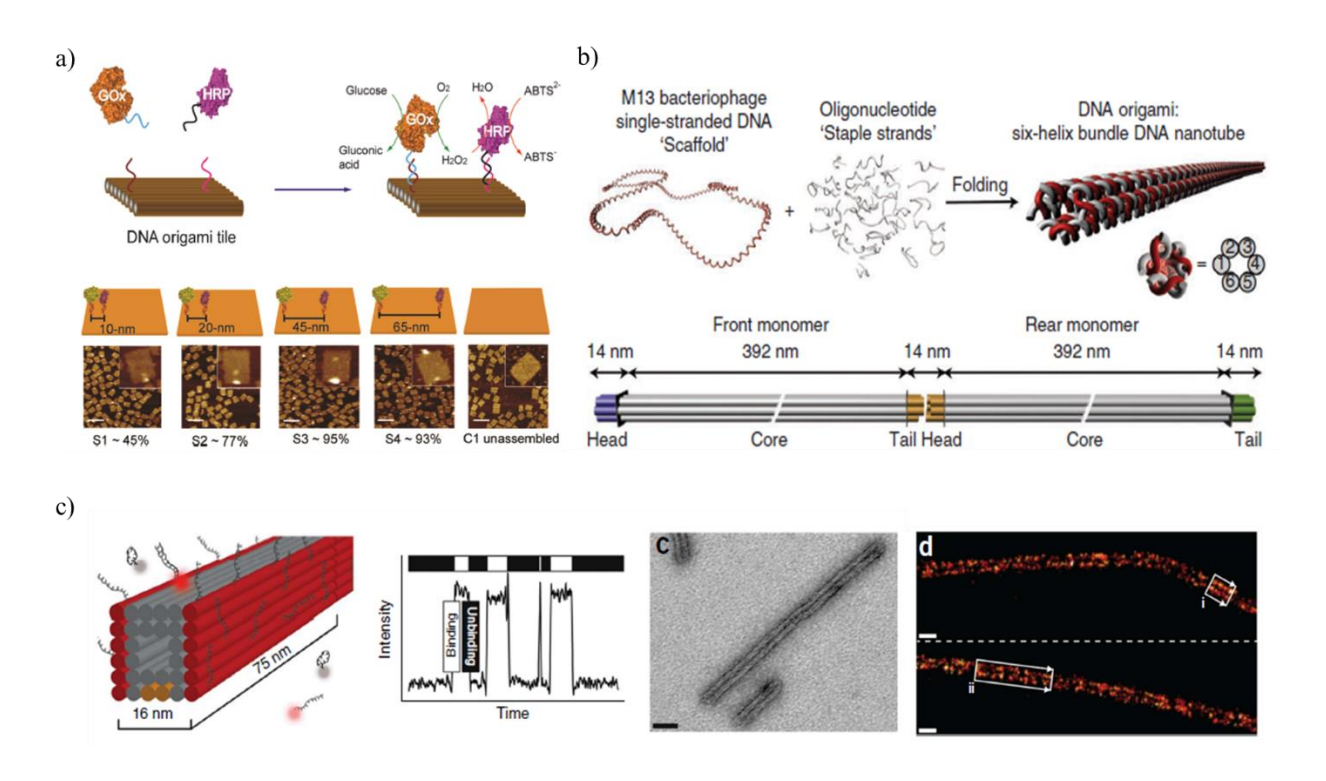


Figure 1.9. (a) DNA origami mediated assembly of glucose oxidase (GOx) and horseradish peroxidase (HRP) enzymes with a defined inter-enzyme distances. The spacing between the two enzymes was observed by AFM (scale bar: 200 nm). Adapted with permission from reference 64 (ACS Publishing, 2012). (b) Scheme showing the formation of a six-helix bundle DNA nanotube using DNA origami approach. The cartoon represents an 800 nm-long six-helix tube. The proteins were later properly aligned on these structures for NMR studies. Adapted with permission from reference 65 (Nature Publishing Group, 2013). (c) From left to right: Schematic representation of a DNA origami looking similar to a microtubule. The distance separating the single-stranded overhangs (9 bases) is 16 nm. The transient binding reaction between these strands and their complementary fluorescent strands generates fluorescence blinking leading to a stochastic super-resolution imaging. The TEM micrograph displays the morphology of the origami polymers. The origami tubes were also observed via PAINT technique where two well-resolved lines are visible. Adapted with permission from reference 67 (Nature Publishing Group, 2014).

For the fabrication of nanomaterials using DNA origami, the size limitations of the origami substrates present once again the main challenge in developing large-scale assemblies. It seems unlikely that practical devices can be produced from the examples reported in literature. Hence, it is essential to focus on overcoming this limitation while optimizing the structures of DNA origami and their assembly conditions. Furthermore, it is noteworthy to mention that the majority of origami structures are inherently static. An ideal optimization to promote the generation of nanomaterials based on DNA at the macroscopic level is to program their dynamics at the nanoscale level.⁶⁸

1.1.3 DNA Nanotubes and Other Dynamic Nanostructures

The necessity to simplify assembly while preserving programmability and dynamic character is illustrated by the construction of DNA nanotubes. Several strategies based on DX motifs, DNA origami and single-stranded DNA were adopted to build tubes with different shapes and geometries. One of the first methods involved the formation of 2D sheets that fold into nanotubes. The size of these tubes depends highly on the number of bases between two crossover points within the DX motif and the length/position of the sticky ends. ^{22,69} For example, Seeman *et al.* demonstrated the assembly of six- and eight-helix bundles of different inner cavities (Figure 1.10a). ²³ They showed that the connection between two helices at particular positions dramatically affects the angles between DX portions, hence leading to the growth/disassembly of micron-sized tubes. Yin's research group reported the assembly of nanotubes and other complex shapes from single-stranded tiles (SST) made up of 42 bases (Figure 1.10b). ⁷⁰ Each strand consisted of four domains and was able to bind four other strands during assembly. Another strategy to build nanotubes from a single-stranded oligonucleotide was demonstrated by Mao and coworkers. ⁷¹

Inspired by the natural folding of microtubules, the authors aimed at reducing the number of DNA strands by increasing sequence symmetry. They synthesized a strand made up of 52 bases and

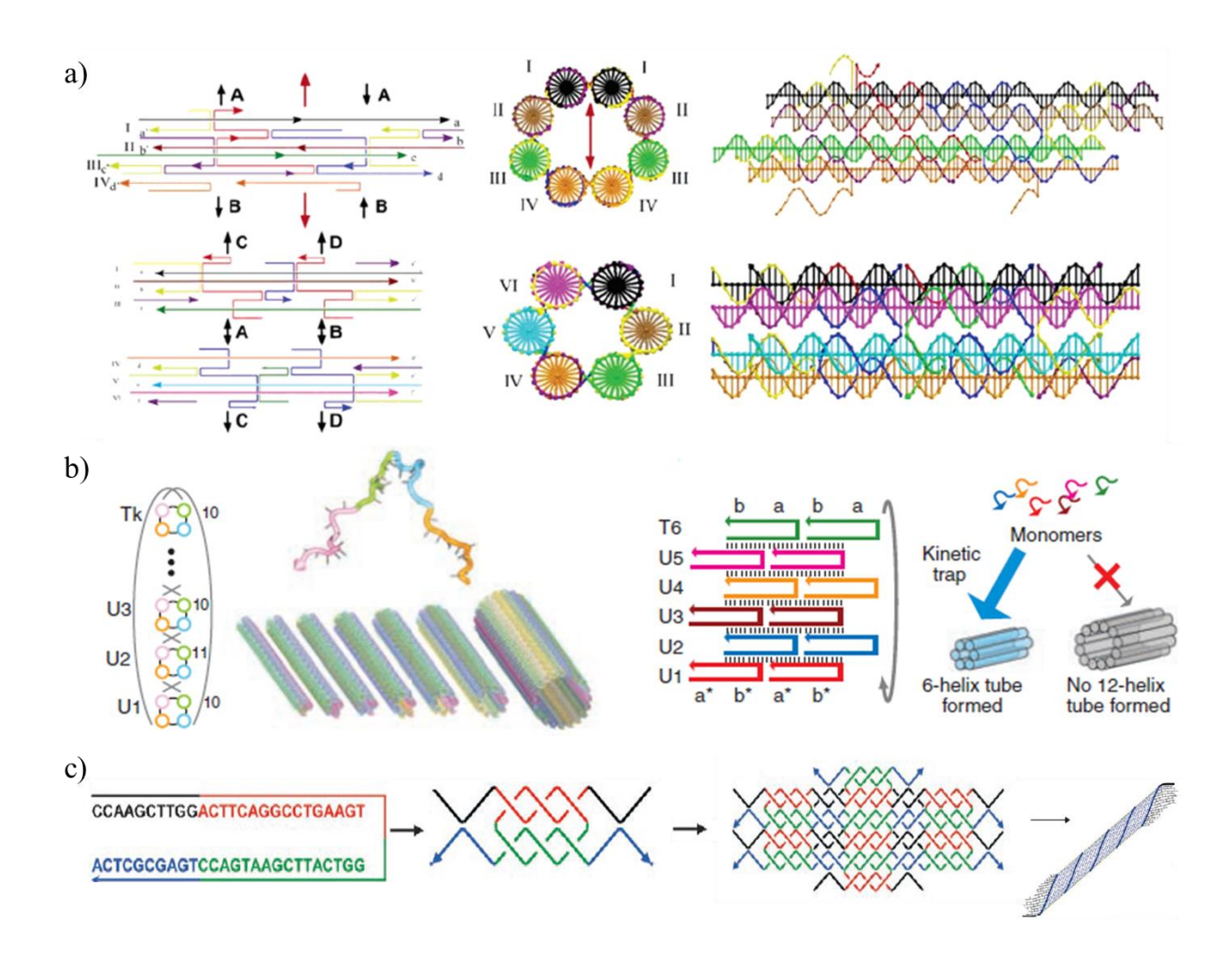


Figure 1.10. (a) Schematic representations of 8- helix (top) and 6-helix (bottom) bundles. The connection between crossovers is illustrated in the left through the letters and arrows. The cross-sections of the tubes are displayed in the center and the helices appear to the right of the panels. Adapted with permission from reference 23 (ACS Publishing, 2007). (b) Scheme showing the formation of DNA nanotubes based on single-stranded tile strategy. Left: 3D illustration of tubes with programmed circumferences. Right: A possible kinetic product (12-helix bundle) during the assembly of 6-helix bundles. Adapted with permission from reference 70 (Science 2008). (c) Schematic drawing of a single-stranded DNA nanotube composed of hour palindromic domains. A two-stranded complex is formed first followed by the assembly of 2D sheets which will fold into tubes. Adapted with permission from reference 71 (RSC Publishing 2006).

divided into four palindromic domains (same sequences when read from 5'- to 3'-end or 3'- to 5'-end). Because of this self-complementarity, 2D lattices were assembled upon the hybridization of the sticky ends followed by the formation of tubes due to the flexibility of the lattices (Figure 1.10c).

Using the DNA origami approach, another generation of DNA nanotubes with defined diameters and lengths was produced. A six-helix bundle tube was achieved when the M13mp18 scaffold was folded around 168 staple strands.³⁰ Each short oligonucleotide consisted of 42 bases and interacted with the scaffold in three regions of 14 bases each. Shih and colleagues showed that such interactions led to the assembly of tubes instead of 2D sheets. Schulman's group made DNA nanotubes via an origami approach tiles and used them as seeds to control the growth of tubes based on DX motifs.⁷² According to the authors, the origami seeds act as nucleation templates, hence accelerating the growth of the tubes with controlled dimensions.

The production of DNA nanotubes is a central area in nanobiotechnology. Besides controlling the dimensions of the tubes, it is crucial to regulate their movements in order to build multicomponent devices. Thus, it is worthwhile to shed more light on a variety of dynamic DNA nanostructures reported in literature before discussing some of the attempts to build dynamic DNA nanotubes.

The idea of isothermal DNA strand displacement was introduced by Neumann and coworkers to construct one of the first molecular machines made up of DNA (Figure 1.11a).⁷³ The nanomechanical switch in this case was based on the interaction between an extended single-stranded overhang (toehold) with its complement component. As a result, the complement strand was able to remove the targeted strand from the machine and allowed the DNA tweezer to open. Since the discovery of strand displacement approach, a variety of DNA walkers have been

demonstrated.⁷⁴⁻⁷⁶ Another type of DNA-based robots was generated by Yan and coworkers by allowing three deoxyribozymes "legs" to interact with prescriptive landscapes (Figure 1.11b).⁷⁷ The directional progress of the robots on the track was followed via single-molecule fluorescence. The authors believed that the potential interaction between these robots might lead to collective behavior as a means of performing more complex tasks.

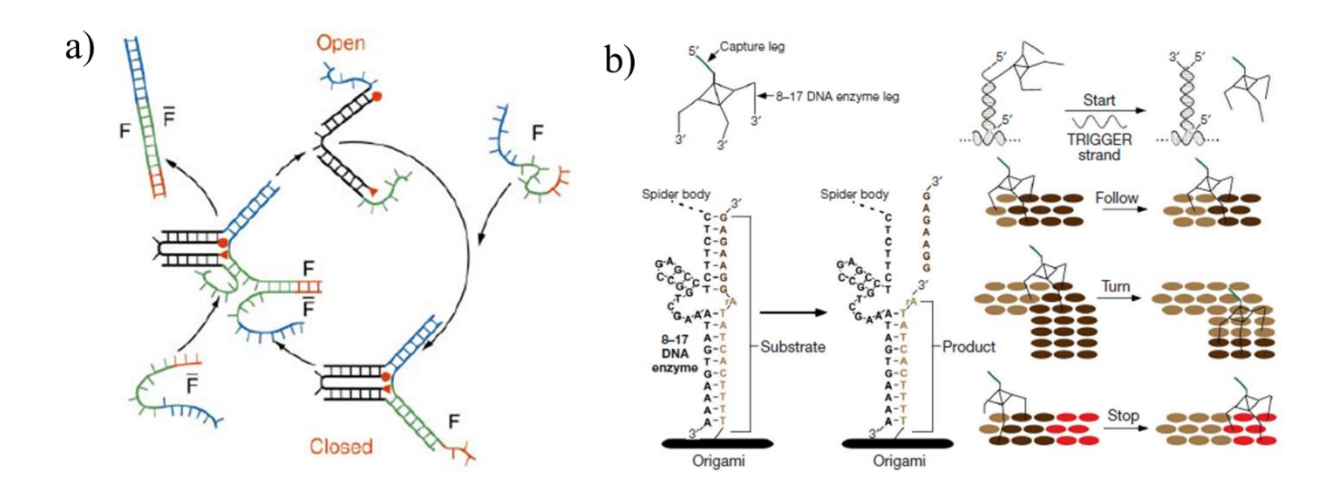


Figure 1.11. (a) Schematic representation of a DNA tweezer. The machine closes upon binding of strand F to the sticky ends of strands B and C. Then, the complement of strand F induces the re-opening of the tweezer. Adapted with permission from reference 73 (Nature Publishing Group, 2000). (b) Scheme showing the movement of a DNA walker in the presence of deoxyribozyme enzyme. The enzyme breaks the substrate specifically at an RNA base, generating two short strands. Following the dissociation of these strands, a new substrate can bind the machine. Adapted with permission from reference 77 (Nature Publishing Group, 2010).

The generation of dynamic DNA nanostructures is becoming more essential to build practical devices. Since the introduction of the new cellular membrane model in the 1970s, researchers have been developing novel techniques to examine membrane's heterogeneity. Various agents have been implemented to the lipid bilayers in order to optimize imaging quality via confocal microscopy and flow cytometry. In this regard, DNA nanostructures offer a remarkable

platform to functionalize the membranes and/or generate artificial nanopores. Howorka and coworkers built a molecular valve able to control the transportation of cargos across the membrane. The valve was demonstrated to be selective towards small charged organic molecules and to experience nanomechanical changes upon binding to the cargo (Figure 1.12a).⁴ Another study published by Seelig et al. employed strand displacement approach to detect collisions between compartments on the cellular membrane (Figure 1.12b).81 This analysis is supposed to help understanding the dynamic behavior of some of the molecules present in the lipid bilayers. Alternatively, DNA nanostructures have been created to deliver cargos to the cells. Ricci and colleagues reported the assembly of DNA nanosystems that are able to encapsulate/release cargo upon binding to antibodies.⁸² One of the antigens used in this study included HIV-related antigen and is suggested to improve future diagnosis of HIV in vivo. A simple DNA-based nanomachine was reported by Liu's research group. The authors employed a C rich sequence called "i-motif" to build a nanomotor.⁸³ Briefly, an oligonucleotide containing CCC stretches forms a quadruplex structure at a pH lower than 5 due to the intramolecular hydrogen bonding between protonated and unprotonated Cytosines. The process is reversible since the duplex form can be easily achieved under neutral or basic pH. However, the incorporation of C rich stretches within nanostructures remains challenging since some systems are not stable at acidic pH. Light driven DNA nanomachines were demonstrated by Asanuma's research group.⁸⁴ They incorporated two azobenzene-modified sequences to open/close a hairpin structure in response to UV light. Once the hairpin opened, the enzymes found the correct topology to cleave protected RNA segments (Figure 1.12c).

The importance of forming dynamic DNA nanotubes, similar to the aforementioned examples, lies in their ability to amplify motion, hence acting as biophysical probes or efficient drug delivery vehicles. However, methods based on DX or TX motifs, single-stranded tiles and origami generate

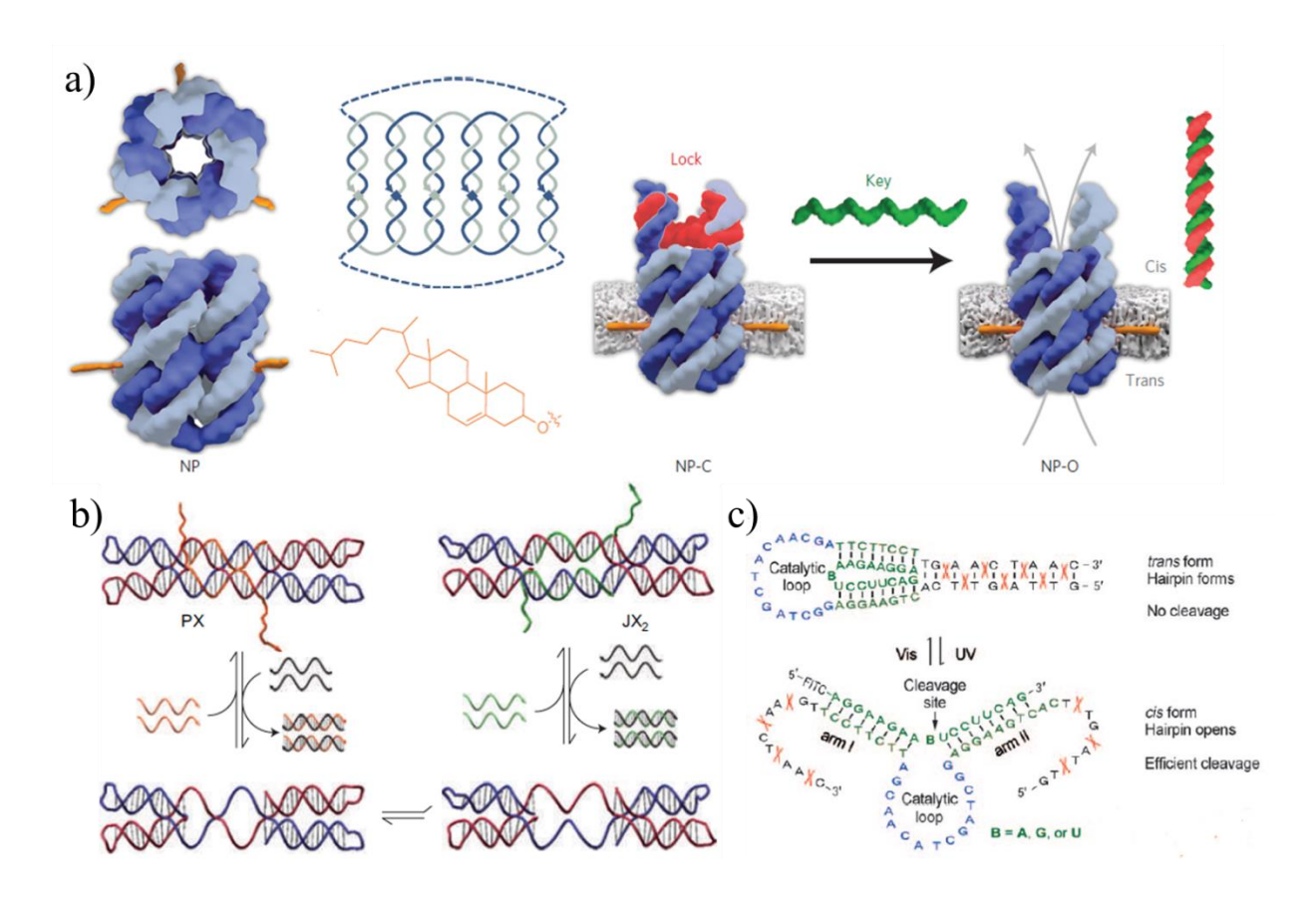


Figure 1.12. (a) Schematic representation of a DNA nanopore that opens upon the hybridization of the key strand (green) to the lock strand (red). Adapted with permission from reference 4 (Nature Publishing Group, 2016). (b) Another DNA switch based on exchanging strands between PX and JX₂ tile motifs. Adapted with permission from reference 81 (Nature Publishing Group, 2011). (c) Scheme displaying a light-responsive DNA based machine. Azobenzene molecules were incorporated in the DNA sequences. The hairpin opens under UV light allowing DNAzymes to cleave the RNA target. Adapted with permission from reference 84 (Wiley-VCH, 2010).

rigid systems that are fully double-stranded and are not inherently dynamic. Therefore, our group has assembled a variety of DNA nanotubes of tunable geometry and rigidity based on sticky end cohesion of DNA polygons on top of one another via linking strands (Figure 1.13a).⁸⁵ Since the linking strands are able to switch between single- and double stranded forms through strand displacement strategy, the resulting tubes were ideal for loading/releasing cargos (Figure 1.13b).⁸⁶

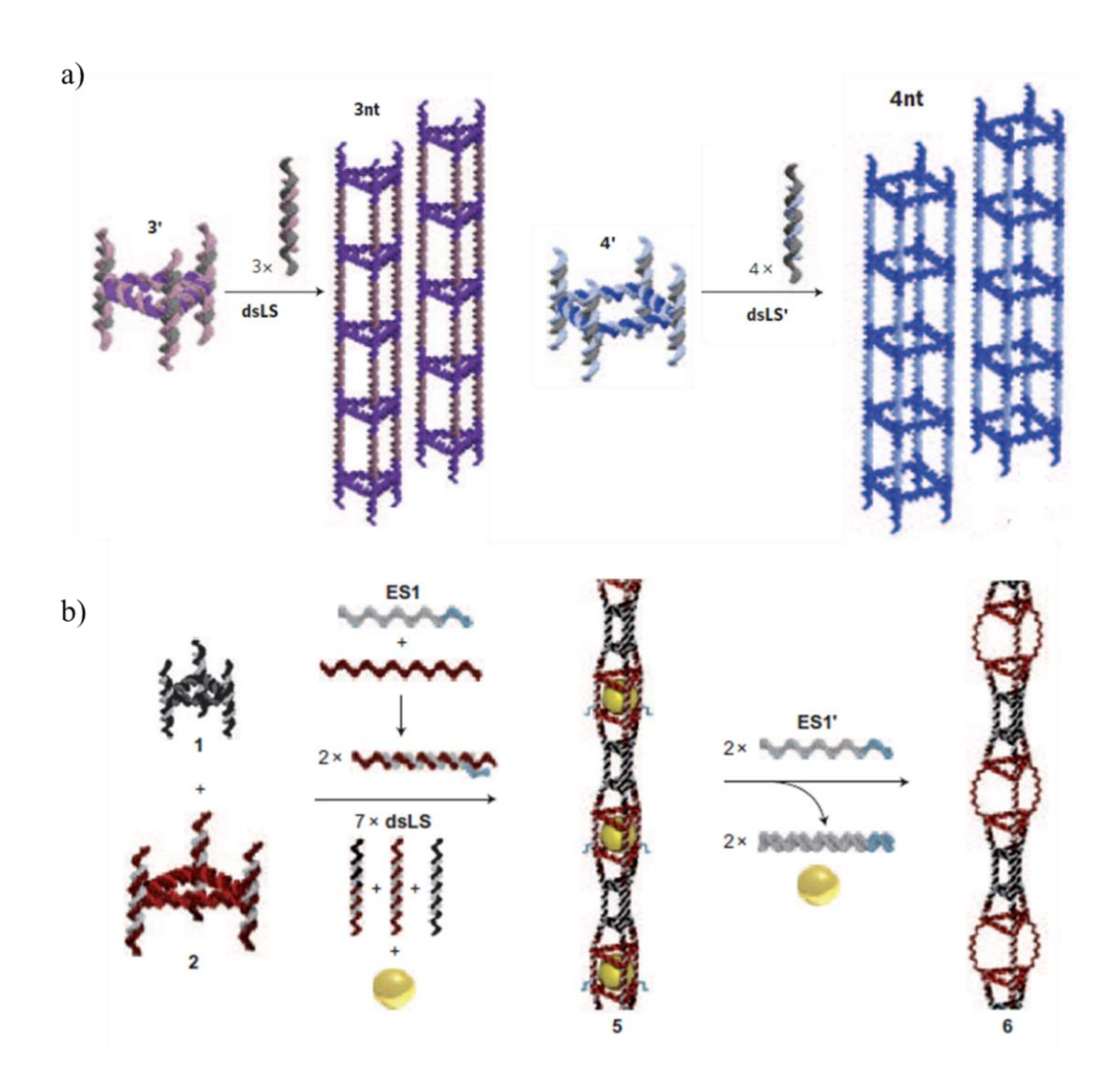


Figure 1.13. (a) Self-assembly of triangular and square nanotubes through sticky-end cohesion between triangular/square units and 3/4 linking strands respectively. Adapted with permission from reference 85 (Nature Publishing Group, 2009). (b) Scheme showing the construction of triangular tubes that are able to encapsulate 15 nm AuNPs, followed by the selective release of

these particles through strand displacement strategy. Adapted with permission from reference 86 (Nature Publishing Group, 2010).

The next chapter will further describe our designs to build nanotubes with intrinsic dynamic behavior and will explain the advantages of our approach compared to the previous strategies reported in literature.

1.1.4 Higher-Order DNA Nanostructures

Natural systems combine many different supramolecular interactions in a hierarchical manner to build functional structures. In contrast, DNA nanotechnology relies almost exclusively on DNA base-pairing for structure generation. Introducing other supramolecular interactions can significantly expand the structural and functional range of DNA assemblies, but this requires an understanding of the interplay between these different interactions within DNA nanostructures. On the other hand, the production of DNA based nanodevices with a resolution on the nanoscale requires the combination of standard nanofabrication methods with bottom-up assembly techniques. Ongoing efforts have been investigating a variety of strategies to assemble higher-order DNA systems and to scale them up. In this section, two main strategies will be discussed: (i) DNA patterning on surfaces and (ii) assembly of supramolecular DNA structures.

Organizing DNA into long-range assemblies in 2D/3D holds great potential for encapsulating/releasing small molecules for drug delivery, arranging nanoparticles to promote the creation of electronic devices and engineering novel biosensors. Ideally, in order to employ oligonucleotides in any device, the DNA motifs must be geometrically well-aligned before the

beginning of the processing step.87 One of the strategies reported to organize DNA involves lithography. 88 Briefly, a substrate is patterned via lithography (soft lithography involving patterned PDMS poly(dimethyl siloxane), for example, can be used to organize biomaterials under mild conditions) followed by the addition of a solution containing DNA strands which are generally integrated into defined areas on the etched surface. The oligonucleotides can be later functionalized with other materials, including gold nanoparticles⁸⁸ (Figure 1.14a) or used to grow other materials.⁸⁹ Alternatively, Rothemund and coworkers reported the organization of origami tiles on a mica surface by controlling the diffusion of cations on the surface. 50 The authors demonstrated that gradually replacing magnesium by sodium cations induced the self-assembly of origami tiles into periodic lattices. According to previous studies, the interaction of negatively charged oligonucleotides with the negatively charged mica surface is highly dependent on the concentration and type of cations. In this paper, the diffusion of cations was suggested to play a key role in controlling the dynamic behavior of origami rectangular tiles and to build a higherorder assembly (Figure 1.14b). Using the AFM cantilever, Liu's research's group generated a pattern of DNA following a specific path. 90 Typically, the material on the surface can be replaced by DNA at particular areas while the AFM tip is travelling across the surface. Note that complex patterns can be created via other techniques such as dip-pen nanolithography, 91 yet these strategies remain expensive for the high-scale production of nanodevices. Moreover, the generation of errorfree assembly procedures via similar approaches still require to be optimized in a more efficient manner. Therefore, other routes including the usage of non-natural bases and various orthogonal interactions were examined to produce higher-order DNA nanostructures.

Non-covalent interactions primarily mediate the supramolecular assembly of basic building blocks within biological systems. This approach is mimicked synthetically to provide a powerful

platform for the organization of various nanostructures, including nanoparticles, ⁹² proteins, ⁹³ and small molecules. ⁹⁴ In DNA nanotechnology, Watson-Crick base-pairing has mainly been used as a model for the assembly of DNA nanostructures, though their complexities are inherently limited by the genetic code. Ongoing efforts have been focusing on introducing orthogonal interactions to increase the complexity of the systems without compromising structural integrity. For instance, synthetic modifications incorporated in DNA double helices such as geometric vertices have a great impact on the rigidity and stability of duplexes. ⁹⁵ They are able to alter the linearity of DNA,

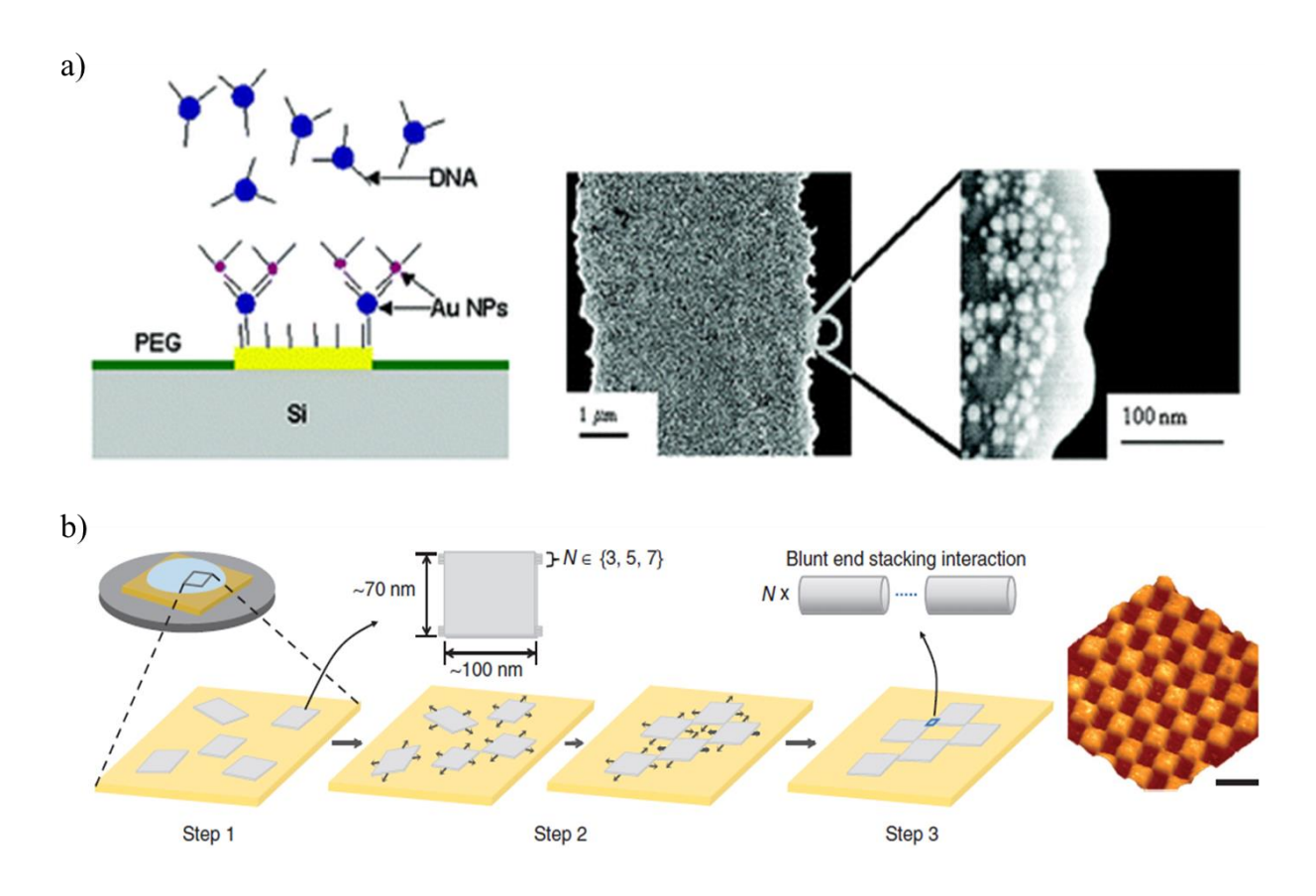


Figure 1.14. (a) Schematic representation of the assembly of two layers of AuNPs on a gold film patterned by photolithography. Adapted with permission from reference 88 (ACS Publishing, 2004). (b) Organization of 2D origami lattices through controlling the diffusion of cations on mica surface. The tiles are immobilized on the surface in the presence of magnesium buffer (step 1). During the second step, sodium buffer was added to allow the diffusion of origami tiles. Finally, the tiles are immobilized again upon the addition of nickel and magnesium buffers. To the right is an AFM micrograph of the resulting structure. Scale bar, 200 nm.

hence producing new geometries without modifying DNA sequences. Sleiman and coworkers synthesized an m-terphenyl-based vertex and attached it to DNA overhangs at both ends (Figure 1.15). The resulting final structure was rigidified by the inserted vertex and was used to organize six gold nanoparticles. Using the same concept, Richert's research group examined the formation of tetrahedral lattices by inserting four-way junctions within duplexes. Similarly, large networks of DNA were created after incorporating six-way insertions.

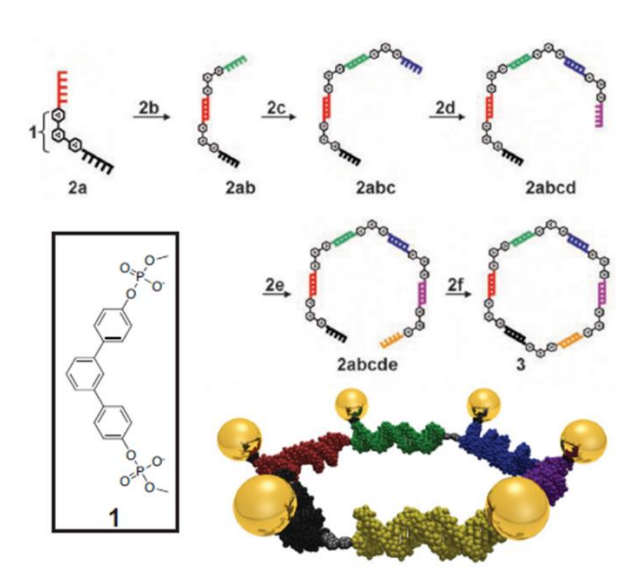


Figure 1.15. Organization of AuNPs into a hexagonal pattern. Adapted with permission from reference 96 (Wiley-VCH, 2006).

The desire to further expand the DNA "alphabet" while preserving the ability to predict the geometry of DNA-based structures encouraged scientists to combine coordination chemistry and DNA. Similar to the field of metallosupramolecular chemistry, the inserted ligands can precisely arrange metal complexes and provide DNA nanostructures with new functionalities for applications in nanoelectronics, optics, charge transport and catalysis. In turn, nucleic acids are

one of the few materials that are suited for controlling the position of transition metals and the assembly of 3D metal frameworks. A variety of approaches were reported to incorporate metals into DNA such as metal binding to artificial or natural nucleic acids, ^{99,100} addition of metal complexes to DNA, ¹⁰¹ and integration of ligands to DNA for subsequent coordination to transition metals. ¹⁰² Through metal binding to natural nucleobases, a molecular logic gate (Figure 1.16a), for example, was generated. ¹⁰³ DNA polymerases were only activated in the presence of specific mismatches and Hg²⁺/Ag⁺ cations. Hannon and coworkers produced bi-metallic helicate structures, pre-assembled metallosupramolecular structures, that can bind DNA similar to other natural DNA binders (Figure 1.16b). ¹⁰⁴ Sleiman's research group reported the addition of diphenylphenanthroline ligands (dpp) into a prism. Subsequent to the addition of metals, the metal-DNA cages were found to be more stable, hence more suitable for future applications (Figure 1.16c). ¹⁰²

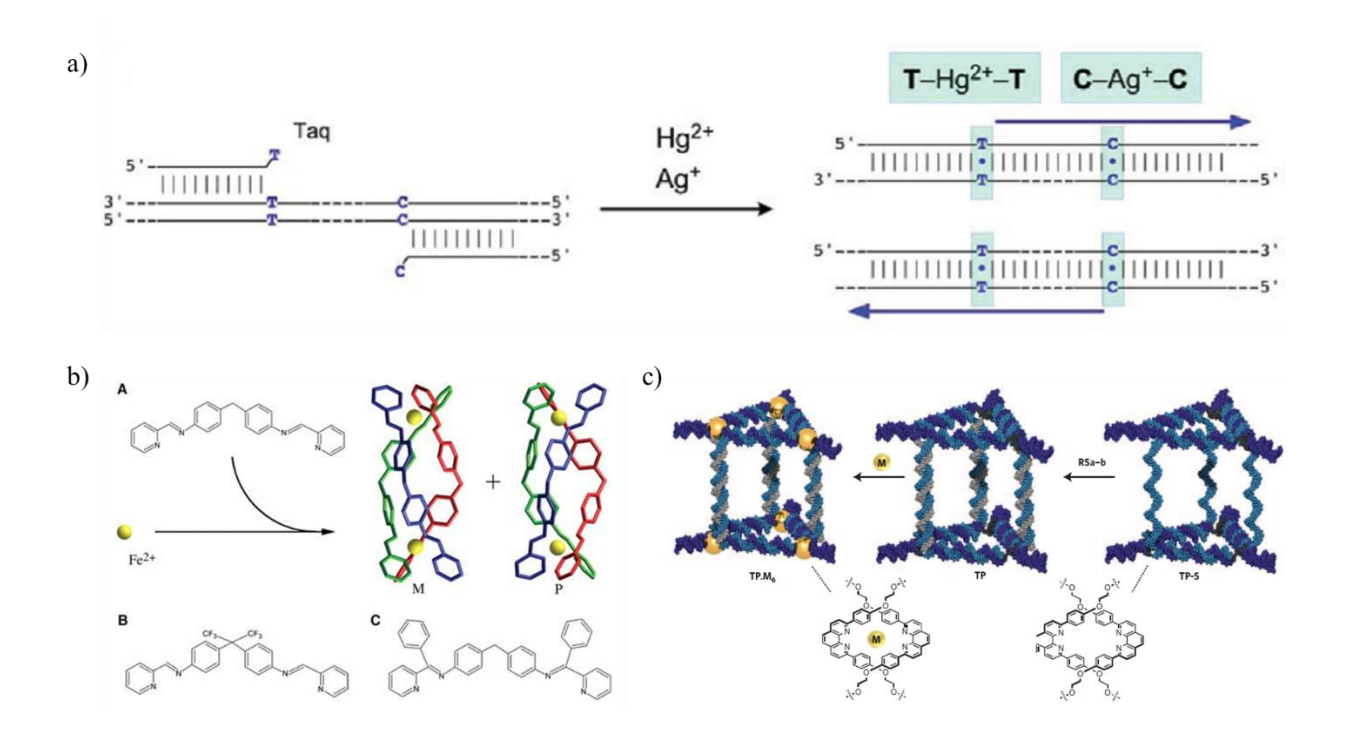


Figure 1.16. (a) Generation of an AND logic gate through T-Hg²⁺-T and C-Ag⁺-C base pairs. Adapted with permission from reference 103 (ACS Publishing, 2012). (b) 3D representation of the metallosupramolecular structures obtained by X-ray crystallography. M: $[Fe_2L_3]^{4+}$ and P- $[Fe_2L_3]^{4+}$; L=C₂₅H₂₀N₄. Adapted with permission from reference 104 (Oxford Press, 2008). (c) Schematic drawing of the production of 3D DNA prism followed by site-specific metalation. Adapted with permission from reference 102 (Nature Publishing Group, 2009).

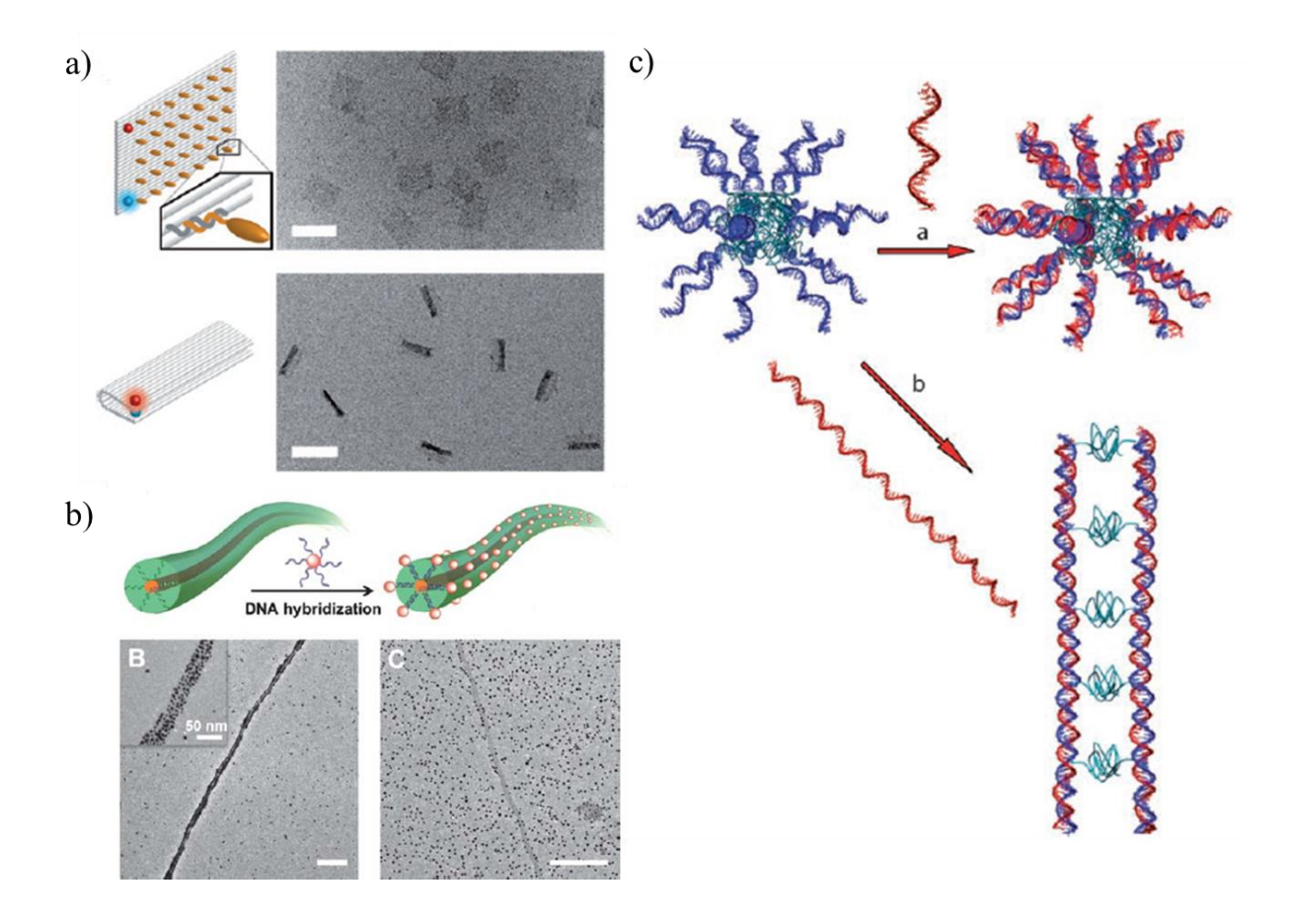


Figure 1.17. (a) Top: TEM micrograph of origami tiles consisting of 24 double helices. The positions of the strands functionalized with cholesterol are displayed in orange. Bottom: TEM image showing the intramolecular hydrophobic interaction between cholesterol moieties attached on origami. Scale bar, 100 nm. Adapted with permission from reference 106 (Wiley-VCH, 2014). (b) Schematic representation of the interaction between DNA nanofibers (made up of single-stranded DNA amphiphile) and functionalized AuNPs. TEM B: oligonucleotide on AuNPs is complementary to nanofibers. TEM C: complementarity is absent. Scale bar, 200 nm. Adapted with permission from reference 112 (RSC Publishing 2011). (c) Schematic drawing of hybridization of short versus long ss DNA to micelles made up of DNA amphiphiles. Adapted with permission from reference 113 (Wiley-VCH, 2007).

One of the main advantages of the method used in our lab is its ability to introduce a wide range of orthogonal interactions into DNA in a sequence-controlled manner. In particular, hydrophobic modifications have been employed to trigger DNA assembly into higher-order structures. 105 For instance, Simmel and coworkers have shown the formation of DNA sandwiched structures through the hydrophobic aggregation of cholesterol-modified DNA origami (Figure 1.17a). 106 Lipid-DNA conjugates have been employed to improve the stability of nanostructures in cells, to facilitate vesicle fusion and to create synthetic membrane nanopores. 107-109 In addition, hydrophobic chains were attached to individual nucleobases to form "nucleolipids" capable of selfassembling into spherical micelles in an aqueous buffer. 110 Yanagawa and collegues reported the creation of helical fibers from nucleolipids at certain conditions. 111 Long-range assembly of amphiphilic DNA polymers were demonstrated by Herrmann et al. through microphase separations. The authors described the formation of a large 1D morphology via microphase separation of a long DNA strand attached to a hydrophobic polymer made up of polypropylene oxide (Figure 1.17b).¹¹² Moreover, attaching dentritic polybenzylether to DNA induced the generation of long fibers as reported by Liu's research group (Figure 1.17c). 113

Recently, our group devised a method for positioning sequence-controlled hydrophobic polymers on small DNA cages to direct their assembly.^{31,114} The length and placement of the hydrophobic chains on the small cages were important determinants of their hydrophobically-driven assembly, defining whether it is intra- or intermolecular, and how large the aggregation number is.¹¹⁵ The strategy developed in our lab and its application on DNA nanotubes will be further discussed in chapter 3.

1.3 Scope of Thesis Research

Since the establishment of the field, researchers have been extensively exploring the usage of DNA-based nanostructures to develop progressively functional systems for a wide range of applications. However, many structural and synthetic aspects need to be improved before achieving superior levels of complexity and control. Many of these limitations were described in the previous sections, thus we will be focusing in this part on our contribution to overcome some of these problems within the context of this thesis.

After more than a decade of work in the field of DNA nanotechnology, the Sleiman's group have pioneered a variety of systems that can be potentially employed to build DNA-based nanodevices or drug delivery vehicles. 31,86 Our laboratory has focused on designing nanostructures using the minimum number of strands required to achieve a define 3D architecture. 116 We have extensively examined a large number of synthetic modifications allowing our constructs to form through various orthogonal interactions. 102,117 Hence, our work had a great impact on the progression of supramolecular DNA assemblies. This thesis summarizes our efforts during the last past five years to build one of the simplest dynamic DNA nanotubes that are responsive towards external stimuli. We later modified 6 components of the tubes with alkyl chains in a sequence controlled manner to study the assembly of higher-order nanostructures. Aiming at producing a "super-origami", we have developed a new approach to link rectangular origami tiles without amplifying design challenges.

Chapter 2 describes the synthesis of DNA nanotubes from 11 unmodified DNA strands and the examination of their dynamic behavior by AFM and TIRFM. Our strategy allows the programmable site-specific insertion of structural changes within the cages of the nanotubes. We produced and analyzed fully double-stranded nanotubes, and switched them to tubes with partially

or fully single-stranded sides, via strand displacement approach. We later inserted DNA strands that reduce two sides of the nanotubes at site specific regions, while retaining the size of the third side. This method generates dynamic tubes that can potentially magnify biologically related DNA distortions through a minimum number of DNA strands.

In chapter 3, we demonstrate that the orientation of hydrophobic chains on a triangular rung unit can lead to two distinct modes of orthogonal association. In the absence of a spacer between the binding region and the hydrophobic chains, the rungs and linking strands associated intermolecularly into extended networks via hydrophobic interactions and Watson-Crick base-pairing. On the other hand, these DNA amphiphiles gathered together intramolecularly to generate micellar microenvironments along the repeating units of the nanotubes in the presence of 8T spacers on the amphiphilic strands. These nanotubes can encapsulate and conditionally release small molecules when a specific DNA strand was added, as monitored by both ensemble and insitu single-molecule fluorescence microscopy, and the process can be repeated on the same nanotubes. Nonetheless, under physiological conditions, the resulting hydrophobically assembled bundles disassembled into smaller nanostructures of optimal size to enter the cells and were found to be less susceptible towards nuclease degradation for more than 24 hours. We believe that the integrity of lipophilic DNA based systems is better preserved, compared to bare DNA nanostructures, which can lead to a decrease in non-specific cellular uptake.

Chapter 4 focuses on the synthesis of long DNA backbones containing repeating sequences in a temporally controlled way. Following the scaffolds production, we hybridized the edges of preassembled DNA origami to our backbones (one consisting of 500 nt and the second containing 100 nt) to geometrically align three and five origami tiles respectively. By the aid of two sets of backbones (one backbone hybridized to the top of the tiles and another to the bottom), a nano-

"railroad track" was created. This approach provides a unique platform for the organization, addition or removal of any tile, an option that has not been offered by previous approaches. Future studies of design area and fine-tuning of binding interactions between the tiles are expected to scale up the production of complex nanostructures for practical applications.

1.4 References

- (1) Zhang, F.; Nangreave, J.; Liu, Y.; Yan, H. J. Am. Chem. Soc. **2014**, 136, 11198.
- (2) Chen, Y.-J.; Groves, B.; Muscat, R. A.; Seelig, G. Nature Nanotechnol. 2015, 10, 748.
- (3) Pan, J.; Li, F.; Cha, T.-G.; Chen, H.; Choi, J. H. Curr. Opin. Biotechnol. 2015, 34, 56.
- (4) Burns, J. R.; Seifert, A.; Fertig, N.; Howorka, S. Nature Nanotechnol. 2016, 11, 152.
- (5) Angell, C.; Xie, S.; Zhang, L.; Chen, Y. *Small* **2016**, *12*, 1117.
- (6) Pray, L. Nat. Education **2008**, 1, 100.
- (7) Hashimoto, M.; Tong, R.; Kohane, D. S. *Mol. Pharm.* **2013**, *10*, 2127.
- (8) Hobson, D. W. Wiley Interdisciplinary Reviews: Nanomedicine and Nanobiotechnology **2009**, *1*, 189.
- (9) Seeman, N. C. *Nature* **2003**, *421*, 427.
- (10) Seeman, N. C.; Belcher, A. M. *Proc. Natl. Acad. Sci.* **2002**, *99*, 6451.
- (11) Lehn, J.-M. Science **1993**, 260, 1762.
- (12) Bhyrappa, P.; Wilson, S. R.; Suslick, K. S. Supramol. Chem. **1998**, 9, 169.
- (13) Dalgarno, S. J.; Tucker, S. A.; Bassil, D. B.; Atwood, J. L. Science **2005**, 309, 2037.
- (14) Vignon, S. A.; Jarrosson, T.; Iijima, T.; Tseng, H.-R.; Sanders, J. K.; Stoddart, J. F. *J. Am. Chem. Soc.* **2004**, *126*, 9884.
- (15) Seeman, N. C. J. Theor. Biol. **1982**, 99, 237.

- (16) Mao, C.; Sun, W.; Seeman, N. C. J. Am. Chem. Soc. **1999**, 121, 5437.
- (17) Fu, T. J.; Seeman, N. C. *Biochemistry* **1993**, *32*, 3211.
- (18) Seeman, N. C. Chem. Biol. 2003, 10, 1151.
- (19) Mao, C.; LaBean, T. H.; Reif, J. H.; Seeman, N. C. Nature 2000, 407, 493.
- (20) Winfree, E.; Liu, F.; Wenzler, L. A.; Seeman, N. C. *Nature* **1998**, *394*, 539.
- (21) Aldaye, F. A.; Palmer, A. L.; Sleiman, H. F. Science 2008, 321, 1795.
- (22) Rothemund, P. W.; Ekani-Nkodo, A.; Papadakis, N.; Kumar, A.; Fygenson, D. K.; Winfree, E. J. Am. Chem. Soc. 2004, 126, 16344.
- (23) Kuzuya, A.; Wang, R.; Sha, R.; Seeman, N. C. *Nano Lett.* **2007**, *7*, 1757.
- (24) Walsh, A. S.; Yin, H.; Erben, C. M.; Wood, M. J.; Turberfield, A. J. *ACS Nano* **2011**, *5*, 5427.
- (25) Goodman, R. P.; Berry, R. M.; Turberfield, A. J. Chem. Commun. 2004, 1372.
- (26) LaBean, T. H.; Yan, H.; Kopatsch, J.; Liu, F.; Winfree, E.; Reif, J. H.; Seeman, N. C. *J. Am. Chem. Soc.* **2000**, *122*, 1848.
- (27) McLaughlin, C. K.; Hamblin, G. D.; Hänni, K. D.; Conway, J. W.; Nayak, M. K.; Carneiro,
 K. M.; Bazzi, H. S.; Sleiman, H. F. *J. Am. Chem. Soc.* 2012, *134*, 4280.
- (28) Goodman, R. P.; Heilemann, M.; Doose, S.; Erben, C. M.; Kapanidis, A. N.; Turberfield, A. J. *Nat. Nanotechnol.* **2008**, *3*, 93.
- (29) Yan, H.; Park, S. H.; Finkelstein, G.; Reif, J. H.; LaBean, T. H. Science **2003**, 301, 1882.
- (30) Douglas, S. M.; Chou, J. J.; Shih, W. M. Proc. Natl. Acad. Sci. 2007, 104, 6644.
- (31) Edwardson, T. G.; Carneiro, K. M.; McLaughlin, C. K.; Serpell, C. J.; Sleiman, H. F. *Nat. Chem.* **2013**, *5*, 868.
- (32) Zhao, Z.; Jacovetty, E. L.; Liu, Y.; Yan, H. Angew. Chem. Intl. Ed. **2011**, 50, 2041.

- (33) Sharma, J.; Chhabra, R.; Liu, Y.; Ke, Y.; Yan, H. Angew. Chem. Intl. Ed. 2006, 45, 730.
- (34) Pei, H.; Lu, N.; Wen, Y.; Song, S.; Liu, Y.; Yan, H.; Fan, C. Adv. Mat. **2010**, 22, 4754.
- (35) Lu, C.-H.; Willner, B.; Willner, I. ACS Nano **2013**, 7, 8320.
- (36) Labhasetwar, V. Curr. Opin. Biotechnol. 2005, 16, 674.
- (37) Deng, Z.; Mao, C. Angew. Chem. Intl. Ed. 2004, 43, 4068.
- (38) Diagne, C. T.; Brun, C.; Gasparutto, D.; Baillin, X.; Tiron, R. ACS Nano 2016, 10, 6458.
- (39) Marchi, A. N.; Saaem, I.; Vogen, B. N.; Brown, S.; LaBean, T. H. *Nano Lett.* **2014**, *14*, 5740.
- (40) Rothemund, P. W. Nature **2006**, 440, 297.
- (41) Douglas, S. M.; Marblestone, A. H.; Teerapittayanon, S.; Vazquez, A.; Church, G. M.; Shih, W. M. *Nucleic acids Res.* **2009**, *37*, 5001.
- (42) Ke, Y.; Douglas, S. M.; Liu, M.; Sharma, J.; Cheng, A.; Leung, A.; Liu, Y.; Shih, W. M.; Yan, H. *J. Am. Chem. Soc.* **2009**, *131*, 15903.
- (43) Han, D.; Pal, S.; Nangreave, J.; Deng, Z.; Liu, Y.; Yan, H. *Science* **2011**, *332*, 342.
- (44) Maune, H. T.; Han, S.-P.; Barish, R. D.; Bockrath, M.; Goddard III, W. A.; Rothemund, P. W.; Winfree, E. *Nat. Nanotechnol.* **2010**, *5*, 61.
- (45) Bui, H.; Onodera, C.; Kidwell, C.; Tan, Y.; Graugnard, E.; Kuang, W.; Lee, J.; Knowlton,
 W. B.; Yurke, B.; Hughes, W. L. *Nano Lett.* 2010, 10, 3367.
- (46) Holloway, C. L.; Kuester, E. F.; Gordon, J. A.; O'Hara, J.; Booth, J.; Smith, D. R. *IEEE Antennas Propag. Mag.* **2012**, *54*, 10.
- (47) Wu, N.; Willner, I. *Nano Lett.* **2016**, *16*, 2867.
- (48) Chen, H.; Zhang, H.; Pan, J.; Cha, T.-G.; Li, S.; Andréasson, J.; Choi, J. H. ACS Nano **2016**, 10, 4989.

- (49) Liu, W.; Zhong, H.; Wang, R.; Seeman, N. C. Angew. Chem. 2011, 123, 278.
- (50) Woo, S.; Rothemund, P. W. Nat. Commun. 2014, 5, 4889.
- (51) Yao, G.; Li, J.; Chao, J.; Pei, H.; Liu, H.; Zhao, Y.; Shi, J.; Huang, Q.; Wang, L.; Huang,W. Angew. Chem. Intl. Ed. 2015, 54, 2966.
- (52) Shen, X.; Song, C.; Wang, J.; Shi, D.; Wang, Z.; Liu, N.; Ding, B. J. Am. Chem. Soc. **2011**, 134, 146.
- (53) Numajiri, K.; Yamazaki, T.; Kimura, M.; Kuzuya, A.; Komiyama, M. J. Am. Chem. Soc.2010, 132, 9937.
- (54) Krissanaprasit, A.; Madsen, M.; Knudsen, J. B.; Gudnason, D.; Surareungchai, W.; Birkedal, V.; Gothelf, K. V. *ACS Nano* **2016**, *10*, 2243.
- (55) Song, S.; Fan, C. In *Rolling Circle Amplification (RCA)*; Springer: 2016, p 151.
- (56) Liu, W.; Halverson, J.; Tian, Y.; Tkachenko, A. V.; Gang, O. *Nat. chem.* **2016**, *8*, 867.
- (57) Schreiber, R.; Santiago, I.; Ardavan, A.; Turberfield, A. J. ACS Nano 2016, 10, 7303.
- (58) Zhang, Y.; Chao, J.; Liu, H.; Wang, F.; Su, S.; Liu, B.; Zhang, L.; Shi, J.; Wang, L.; Huang,W. Angew. Chem. 2016, 128, 8168.
- (59) Edwardson, T. G.; Lau, K. L.; Bousmail, D.; Serpell, C. J.; Sleiman, H. F. *Nat. Chem.* **2016**, 8, 162.
- (60) Gür, F. N.; Schwarz, F. W.; Ye, J.; Diez, S.; Schmidt, T. L. ACS Nano **2016**, 10, 5374.
- (61) Linko, V.; Eerikäinen, M.; Kostiainen, M. A. Chem. Commun. **2015**, *51*, 5351.
- (62) Zhang, Q.; Jiang, Q.; Li, N.; Dai, L.; Liu, Q.; Song, L.; Wang, J.; Li, Y.; Tian, J.; Ding, B. *ACS Nano* **2014**, *8*, 6633.
- (63) Tintoré, M.; Gállego, I.; Manning, B.; Eritja, R.; Fàbrega, C. Angew. Chem. Intl. Ed. 2013, 52, 7747.

- (64) Fu, J.; Liu, M.; Liu, Y.; Woodbury, N. W.; Yan, H. J. Am. Chem. Soc. 2012, 134, 5516.
- (65) Bellot, G.; McClintock, M. A.; Chou, J. J.; Shih, W. M. Nat. Protoc. 2013, 8.
- (66) Johnson-Buck, A.; Jiang, S.; Yan, H.; Walter, N. G. ACS Nano **2014**, 8, 5641.
- (67) Jungmann, R.; Avendaño, M. S.; Woehrstein, J. B.; Dai, M.; Shih, W. M.; Yin, P. *Nat. Methods* **2014**, *11*, 313.
- (68) Wang, P.; Meyer, T. A.; Pan, V.; Dutta, P. K.; Ke, Y. Chem 2017, 2, 359.
- (69) Mathieu, F.; Liao, S.; Kopatsch, J.; Wang, T.; Mao, C.; Seeman, N. C. *Nano Lett.* **2005**, *5*, 661.
- (70) Yin, P.; Hariadi, R. F.; Sahu, S.; Choi, H. M.; Park, S. H.; LaBean, T. H.; Reif, J. H. *Science* **2008**, *321*, 824.
- (71) Liu, H.; Chen, Y.; He, Y.; Ribbe, A. E.; Mao, C. Angew. Chem. Intl. Ed. **2006**, 45, 1942.
- (72) Mohammed, A. M.; Schulman, R. *Nano lett.* **2013**, *13*, 4006.
- (73) Yurke, B.; Turberfield, A. J.; Mills, A. P.; Simmel, F. C.; Neumann, J. L. *Nature* **2000**, 406, 605.
- (74) Yan, H.; Zhang, X.; Shen, Z.; Seeman, N. C. *Nature* **2002**, *415*, 62.
- (75) Dirks, R. M.; Pierce, N. A. *Proc. Natl. Acad. Sci. U.S.A.* **2004**, *101*, 15275.
- (76) Sherman, W. B.; Seeman, N. C. *Nano Lett.* **2004**, *4*, 1203.
- (77) Lund, K.; Manzo, A. J.; Dabby, N.; Michelotti, N.; Johnson-Buck, A.; Nangreave, J.; Taylor, S.; Pei, R.; Stojanovic, M. N.; Walter, N. G. *Nature* **2010**, *465*, 206.
- (78) Singer, S. J.; Nicolson, G. L. *Science* **1972**, *175*, 720.
- (79) Korlach, J.; Schwille, P.; Webb, W. W.; Feigenson, G. W. *Proc. Natl. Acad. Sc.* **1999**, *96*, 8461.
- (80) Dive, C.; Watson, J. V.; Workman, P. Cytometry Part A 1990, 11, 244.

- (81) Zhang, D. Y.; Seelig, G. *Nat. Chem.* **2011**, *3*, 103.
- (82) Ranallo, S.; Prévost-Tremblay, C.; Idili, A.; Vallée-Bélisle, A.; Ricci, F. *Nat. Commun.* **2017**, 8.
- (83) Liu, D.; Balasubramanian, S. Angew. Chem. Intl. Ed. 2003, 42, 5734.
- (84) Zhou, M.; Liang, X.; Mochizuki, T.; Asanuma, H. Angew. Chem. 2010, 122, 2213.
- (85) Aldaye, F. A.; Lo, P. K.; Karam, P.; McLaughlin, C. K.; Cosa, G.; Sleiman, H. F. *Nat. Nanotechnol.* **2009**, *4*, 349.
- (86) Lo, P. K.; Karam, P.; Aldaye, F. A.; McLaughlin, C. K.; Hamblin, G. D.; Cosa, G.; Sleiman, H. F. *Nat. Chem.* **2010**, *2*, 319.
- (87) Hung, A. M.; Noh, H.; Cha, J. N. *Nanoscale* **2010**, 2, 2530.
- (88) Kannan, B.; Kulkarni, R. P.; Majumdar, A. *Nano Lett.* **2004**, *4*, 1521.
- (89) Becerril, H. A.; Woolley, A. T. Chem. Soc. Rev. **2009**, *38*, 329.
- (90) Liu, M.; Amro, N. A.; Chow, C. S.; Liu, G.-y. *Nano Lett.* **2002**, 2, 863.
- (91) Piner, R. D.; Zhu, J.; Xu, F.; Hong, S.; Mirkin, C. A. Science **1999**, 283, 661.
- (92) Daniel, M.-C.; Astruc, D. Chem. Rev. 2004, 104, 293.
- (93) Liu, G.-Y.; Amro, N. A. Proc. Natl. Acad. Sci. 2002, 99, 5165.
- (94) Liu, Z.; Sun, X.; Nakayama-Ratchford, N.; Dai, H. ACS Nano **2007**, 1, 50.
- (95) Shi, J.; Bergstrom, D. E. Angew. Chem. Intl. Ed. **1997**, 36, 111.
- (96) Aldaye, F. A.; Sleiman, H. F. *Angew. Chem. Intl. Ed.* **2006**, *45*, 2204.
- (97) Meng, M.; Ahlborn, C.; Bauer, M.; Plietzsch, O.; Soomro, S. A.; Singh, A.; Muller, T.; Wenzel, W.; Bräse, S.; Richert, C. *ChemBioChem* **2009**, *10*, 1335.
- (98) Singh, A.; Tolev, M.; Meng, M.; Klenin, K.; Plietzsch, O.; Schilling, C. I.; Muller, T.; Nieger, M.; Bräse, S.; Wenzel, W. *Angew. Chem. Intl. Ed.* **2011**, *50*, 3227.

- (99) Kuklenyik, Z.; Marzilli, L. G. Inorg. Chem. 1996, 35, 5654.
- (100) Miyake, Y.; Togashi, H.; Tashiro, M.; Yamaguchi, H.; Oda, S.; Kudo, M.; Tanaka, Y.; Kondo, Y.; Sawa, R.; Fujimoto, T. *J. Am. Chem. Soc.* **2006**, *128*, 2172.
- (101) Bond, P.; Langridge, R.; Jennette, K.; Lippard, S. Proc. Natl. Acad. Sci. 1975, 72, 4825.
- (102) Yang, H.; McLaughlin, C. K.; Aldaye, F. A.; Hamblin, G. D.; Rys, A. Z.; Rouiller, I.; Sleiman, H. F. *Nature Chem.* **2009**, *1*, 390.
- (103) Takezawa, Y.; Shionoya, M. Acc. Chem. Res. 2012, 45, 2066.
- (104) Malina, J.; Hannon, M. J.; Brabec, V. *Nucleic Acids Res.* **2008**, *36*, 3630.
- (105) Börjesson, K.; Lundberg, E. P.; Woller, J. G.; Nordén, B.; Albinsson, B. Angew. Chem.
 Intl. Ed. 2011, 50, 8312.
- (106) List, J.; Weber, M.; Simmel, F. C. Angew. Chem. Intl. Ed. 2014, 53, 4236.
- (107) Langecker, M.; Arnaut, V.; Martin, T. G.; List, J.; Renner, S.; Mayer, M.; Dietz, H.; Simmel, F. C. *Science* **2012**, *338*, 932.
- (108) Burns, J. R.; Stulz, E.; Howorka, S. *Nano Lett.* **2013**, *13*, 2351.
- (109) Wilks, T. R.; Bath, J.; de Vries, J. W.; Raymond, J. E.; Herrmann, A.; Turberfield, A. J.; O'Reilly, R. K. ACS Nano 2013, 7, 8561.
- (110) Kwak, M.; Herrmann, A. Chem. Soc. Rev. 2011, 40, 5745.
- (111) Yanagawa, H.; Ogawa, Y.; Furuta, H.; Tsuno, K. J. Am. Chem. Soc. 1989, 111, 4567.
- (112) Ding, K.; Alemdaroglu, F. E.; Börsch, M.; Berger, R.; Herrmann, A. Angew. Chem. Intl. Ed. 2007, 46, 1172.
- (113) Wang, L.; Feng, Y.; Sun, Y.; Li, Z.; Yang, Z.; He, Y.-M.; Fan, Q.-H.; Liu, D. *Soft Matter* **2011**, *7*, 7187.
- (114) Chidchob, P.; Edwardson, T. G.; Serpell, C. J.; Sleiman, H. F. J. Am. Chem. Soc. 2015.

- (115) Serpell, C. J.; Edwardson, T. G.; Chidchob, P.; Carneiro, K. M.; Sleiman, H. F. J. Am. Chem. Soc. **2014**, 136, 15767.
- (116) Hamblin, G. D.; Carneiro, K. M.; Fakhoury, J. F.; Bujold, K. E.; Sleiman, H. F. *J. Am. Chem. Soc.* **2012**, *134*, 2888.
- (117) Carneiro, K. M.; Hamblin, G. D.; Hänni, K. D.; Fakhoury, J.; Nayak, M. K.; Rizis, G.; McLaughlin, C. K.; Bazzi, H. S.; Sleiman, H. F. *Chem. Sci.* **2012**, *3*, 1980.

Chapter 2:

Dynamic DNA Nanotubes: Reversible Switching between Single and

Double-Stranded Forms, and Effect of Base Deletions

Reproduced in part with permission from: "Dynamic DNA Nanotubes: Reversible Switching between Single and Double-Stranded Forms, and Effect of Base Deletions", Rahbani J. F., Hariri A. A., Cosa G., and Sleiman H. F. *ACS Nano.*, **2015**, *9*, 11898–11908. American Chemical Society (2015).

Author Contributions: Hariri A. A. carried out all the TIRFM experiments.

2.1 Introduction

Extended DNA nanostructures with high aspect ratio have the potential to amplify biologically relevant DNA distortions. In particular DNA nanotubes having repeating units over micron sizes provide an efficient platform to organize many objects using a limited amount of starting materials. As mentioned in the introduction, our group has previously reported the synthesis of DNA nanotubes of tunable rigidity and geometry, by organizing triangular or square DNA polygons on top of one another using linking strands. The resulting tubes can be built in single- or double stranded forms, and the nanotubes can encapsulate cargo and release it by strand displacement. This approach required the synthesis of DNA polygons with rigid organic molecules at their corners by cyclization and chemical ligation. The rolling circle amplification (RCA) process was then used to coarsely tune nanotube length and enhance stability, but this method involves cyclization, ligation and enzymatic replication, and it yields double-stranded nanotubes (Figure 2.1a). Recently, we reported two methods to control the length, circumference and patterns on

every position of DNA nanotubes, using a temporal growth strategy to sequentially add building blocks (Figure 2.1).^{4,5} Thus, when nanotubes need to be fully controlled in length and at every one of their positions, the use of DNA origami or sequential construction methods is necessary.

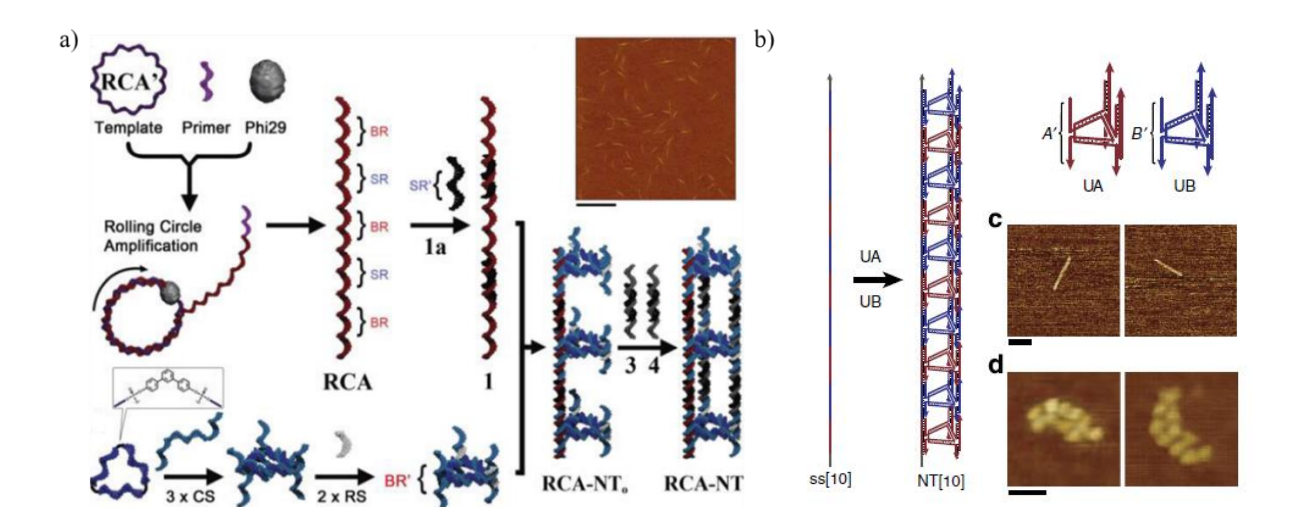


Figure 2.1. (a) Scheme showing the construction of RCA nanotube from a cyclic template and predesigned triangular units. The RCA is synthesized by mixing a cyclic template with polymerase Phi29. The template is designed to bind the tiangular units which interact with two other linking strands to close the tubes. Right: AFM micrograph confirming the assembly of the tubes, Scale bar 2.5 µm. Adapted with permission from reference 3 (ACS Publishing, 2012). (b) Monodispersed DNA nanotubes were assembled by combining rung units with single-stranded scaffold ss[10]. AFM micrographs confirm the production of the nanotubes.

In addition to encapsulation and release, the capability of nanotubes to be dynamic allows their potential use as probes of DNA deformation. DNA can undergo bending, looping and twisting when it interacts with proteins, small molecules, or ions.^{6,7} Because of its fundamental significance, DNA distortion has been the subject of extensive investigation.^{8,9} DNA nanotubes are stiff, extended polymers with repeating segments. As a result, they are potentially capable of binding macromolecules such as proteins and amplifying the distortion into a macroscopic change in morphology.¹⁰ However, to our knowledge, this morphological switching has not been

previously studied. A DNA nanoactuator was incorporated into a 2D-tile lattice by the group of Yan,33 and DNA structural dynamics have been probed using high speed atomic force microscopy on origami substrates by Sugiyama *et al.*¹¹

Here, we describe a simplified, modular synthesis of DNA nanotubes, and investigate their structural switching by strand displacement strategies, using atomic force microscopy and in situ single molecule fluorescence microscopy. These nanotubes have controlled geometry and circumference, and can be site-specifically and reversibly switched between single and doublestranded forms. The method relies on only 11 unmodified DNA strands and involves no ligation or RCA steps, thus it can be readily applied by any laboratory. The unique architecture of our nanotube is capable of amplifying DNA distortion into a measurable morphological change. First, we "peel off" and "refill" strands in different numbers and locations on an immobilized nanotube, examine the stability of the single-stranded version of the design, and study the morphological switching between the single and double-stranded forms. Second, we increasingly shorten two nanotube sides while keeping the third constant, resulting in length mismatch in each repeat unit. We show the bending of the nanotubes, until the distortion is significant enough to shorten the nanotube, as measured by AFM and by single molecule photobleaching studies. The latter method quantifies the number of repeat units within the nanotube. 12,13 We explore the mechanism that underlies the formation and elongation of the nanotube, and the appearance of shorter tubes with increasing length mismatch.

2.2 Results and Discussion

2.2.1. Designing and Assembling of DNA Nanotubes

Our nanotube synthesis starts with a triangular "core" unit (**U**), composed of 6 unmodified DNA strands (Figure 2.2). The mixture is annealed at 95°C then slowly cooled down to 4°C over 4 h to give (**U**) in quantitative yield (Figure 2.2, left, polyacrylamide gel electrophoresis (PAGE)). The core structure (**U**) possesses extensions from the top and bottom of the triangular plane, in order to hybridize via sticky-end cohesion to three linking strands (LS1-3), which result in nanotube formation. To maximize the yield of fully formed nanotubes and prevent cross-linking, our method uses linking strands that are different from one another (Figure 2.2). The first, LS1 is

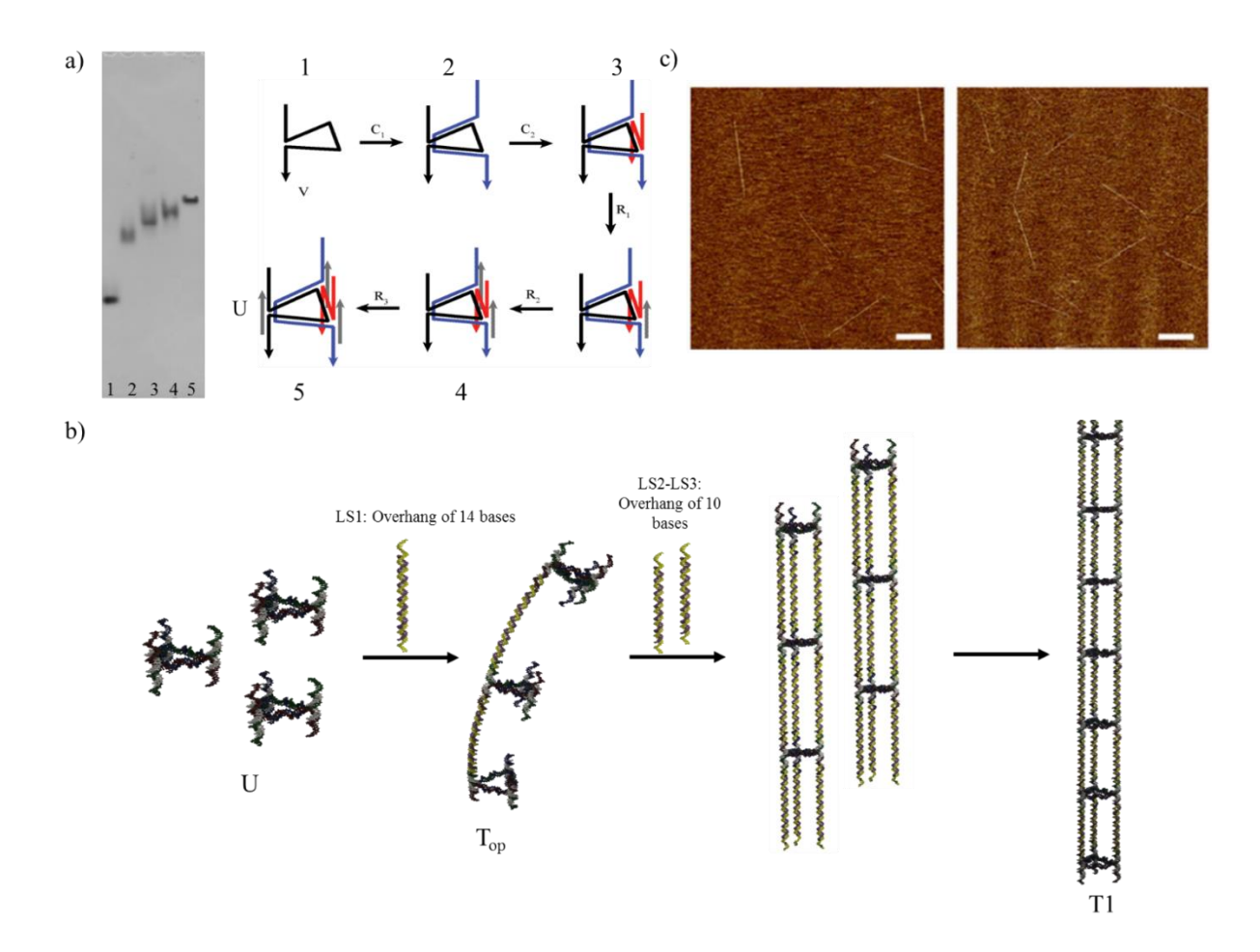


Figure 2.2. DNA nanotube design. (a) Assembly of the triangular core unit U from 6 unmodified DNA strands. Right: Design of U: Strand V (black) binds with

complementary strand C1 (blue), which spans its internal section and creates a core triangular frame. Complementary strand C2 (red) binds the third edge. Rigidifying strands R1, R2 and R3 (gray) bind the overhangs of C1 and C2, holding them out of plane from the triangular core, to create the vertical sticky-ends of the rung. Left: 8% nondenaturing Polyacrylamide gel electrophoresis (PAGE) characterization of the stepwise assembly of the triangular core unit **U**. (b) Stepwise nanotube formation through sticky-end cohesion of the rung units to LS1 first, to form **T**_{op} (open tube), then of LS2/LS3, followed by tube elongation. (c) AFM images displaying the morphology of the tubes, Scale bar 500 nm.

designed with longer sticky-ends (14 nucleotides, nt), and the other two (LS2, LS3) with shorter sticky-ends (10 nt). The nanotubes **T1** are formed through a stepwise, hierarchical mechanism. Linking strand LS1 is first added (heating to 56°C then cooling to 22°C), resulting in the formation of an open structure **T**_{0p} with the triangular rungs positioned on top of one another (Figure 2.2). Then linking strands LS2 and LS3 are added (44 to 22°C) to close the structure **T**_{0p} with preorganized triangles, into the full nanotube. Finally, the elongation of the tubes occurs when the strands are geometrically well aligned, as demonstrated below. The self-assembly of tubes **T1** was initially examined by nondenaturing agarose gel electrophoresis (AGE) and atomic force microscopy (AFM). AGE shows the formation of a nonpenetrating band consistent with a large structure, while AFM shows long and stiff tubes ranging between 1 and 3 μm in length (Figure 2.3, mean length: 1403 nm; standard deviation (SD): 796.1 nm).

Single-molecule total internal reflection fluorescence microscopy (TIRFM) was used to obtain quantitative information on the nanotube formation. For this, we created a nanotube **T1** where the core triangular unit is singly labeled with a Cy3 dye (Figure 2.3 and 2.4; LS2 and LS3 have the same sequence in the middle, double stranded portions, but different sequences at their sticky-end regions). In order to immobilize the nanotubes on a coverslip surface, 5% of one of the strands

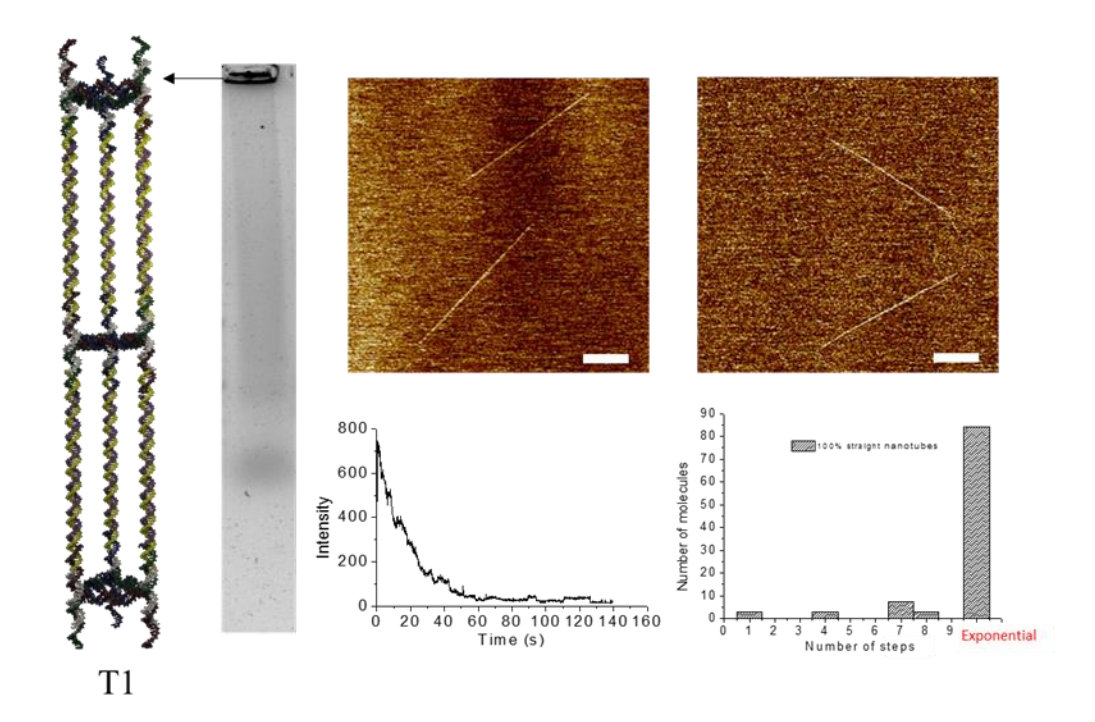


Figure 2.3. Characterization of the nanotube formation by AGE, AFM and TIRFM. 1% nondenaturing agarose gel of tubes **T1** shows a nonpenetrating band. The two AFM micrographs display straight nanotubes with a length ranging from ~1 to 3 μm, Scale bar 500 nm. Typical intensity-time trajectory acquired for a single nanotube with a histogram showing the distribution of the number of steps (Cy3 dyes) obtained from photobleaching curves (See Figure 2.4).

within the triangular core were also labeled with biotin (Figure 2.4). The 5% average biotin labeling represents a compromise between specifically immobilizing the nanotubes on the coverslip surface and maintaining their dynamic character. Polycarbonate film imaging chambers were assembled onto glass coverslips, coated with a mixture of polyethylene glycol (PEG) and biotin-tagged PEG to prevent nonspecific adsorption. Individual dye-labeled nanotubes were next specifically immobilized on the coverslips via biotin streptavidin interactions. ¹⁴ We expect most nanotubes to bind partially in a side-on manner to the PEG-streptavidin surface (Figure 2.4). Regions were excited using a TIRF setup with an evanescent field employing the 532 nm output

of a diode laser. Images corresponding to a field of view of ca. 70 μm × 35 μm were acquired on an EMCCD camera. Typically, 150 single DNA nanotubes were simultaneously imaged within this field of view (Figure 2.4). We used single molecule photobleaching to count the number of Cy3 dyes, and thus the number of repeat units, in each single nanotube imaged. Here, images were acquired for extended periods of time enabling visualization of the intensity time profile of individual nanotubes. 15,16 Conditions were optimized to work under the full dynamic range of the imaging camera, avoiding saturation by the larger structures. Considering that the structures are ~2 µm long on average by AFM, we expect an average of 70 Cy3 dyes per nanotube. Given the noise in single molecule trajectories, we have observed that up to 10 dyes in a structure may yield discrete photobleaching steps in the intensity-time trajectory, essentially a "staircase" photobleaching pattern. The number of intensity steps may be counted and the number of Cy3 repeats and thus the nanotube length can thus be quantified. Nanotubes with more than ca. 11 dyes exhibit however steps that are too small, and not sufficiently separated over time, to be unambiguously assigned. In this case the intensity time trajectory shows rather an exponentially decreasing intensity over time. In the case of tube **T1**, we observed photobleaching patterns with an exponentially decreasing intensity for the majority (90%) of the single nanotubes imaged. A histogram reflecting the Cy3 count distribution is displayed in Figure 2.4.

We next performed single molecule photobleaching studies to determine whether the elongation of our nanotubes into micron-sized structures occurs in the first step of their formation (upon LS1 binding) or in the second step (upon LS2/3 binding). We assembled the 5%-biotin and Cy3-labeled nanotubes by solution annealing the components with LS1 only, but without LS2 and LS3. This is expected to give a Cy3-labeled open, intermediate structure T_{op} (Figure 2.5). Gel

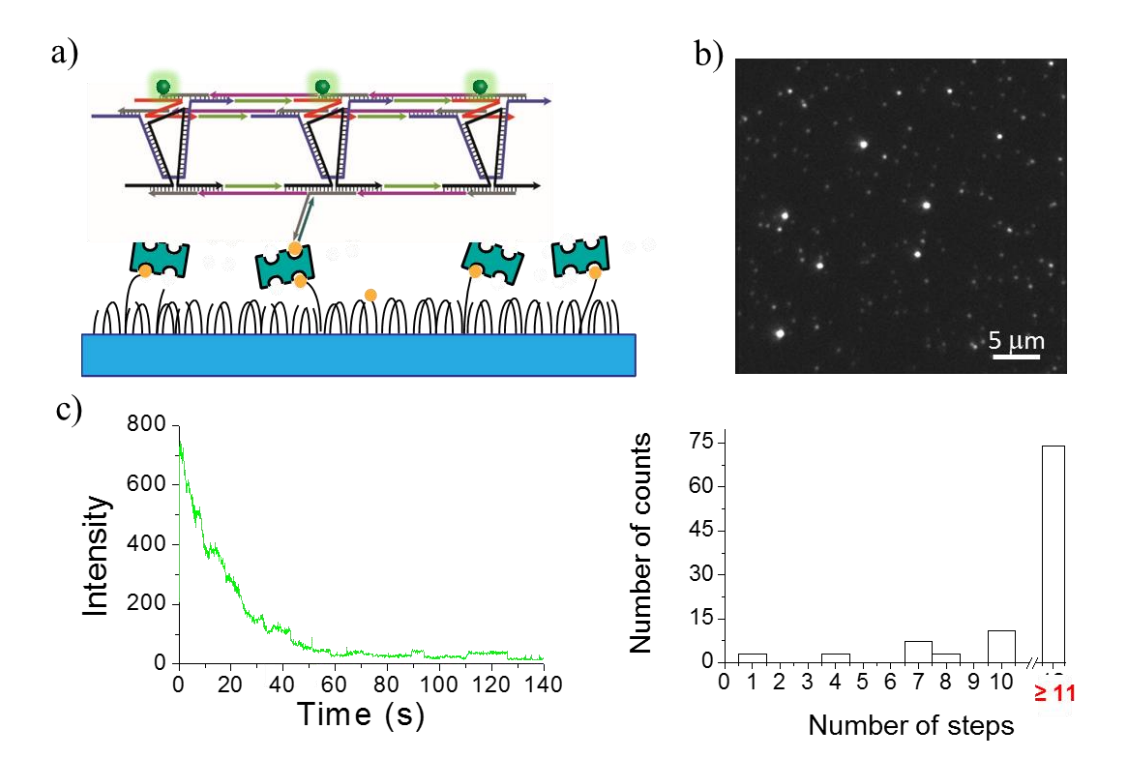


Figure 2.4. (a) Schematic illustration showing the immobilized nanotubes on the PEG-streptavidin coated coverslip surface. (b) Typical TIRFM image of surface-bound Cy3 labeled nanotubes, scale bar 5 µm. (c) Typical intensity-time trajectory acquired for a single nanotube with a histogram showing the distribution of the number of steps (Cy3 dyes) obtained from photobleaching curves.

electrophoresis shows bands of higher mobility compared to the full nanotube band (Figure 2.5), consistent with shorter features. Attachment of these open forms onto the coverslip surface and examination of their length by single-molecule TIRFM with photobleaching revealed a maximum of 10 rungs in the histograms, and the complete absence of structures with exponential intensity decrease traces (Figure 2.5). These observations are consistent with the formation of relatively short structures in the first step (Figure 2.2). We believe that LS2 and LS3 bind these open structures to form short closed tubes that are geometrically well-aligned now to grow and elongate through base pairing of the sticky ends. (Figure 2.2).

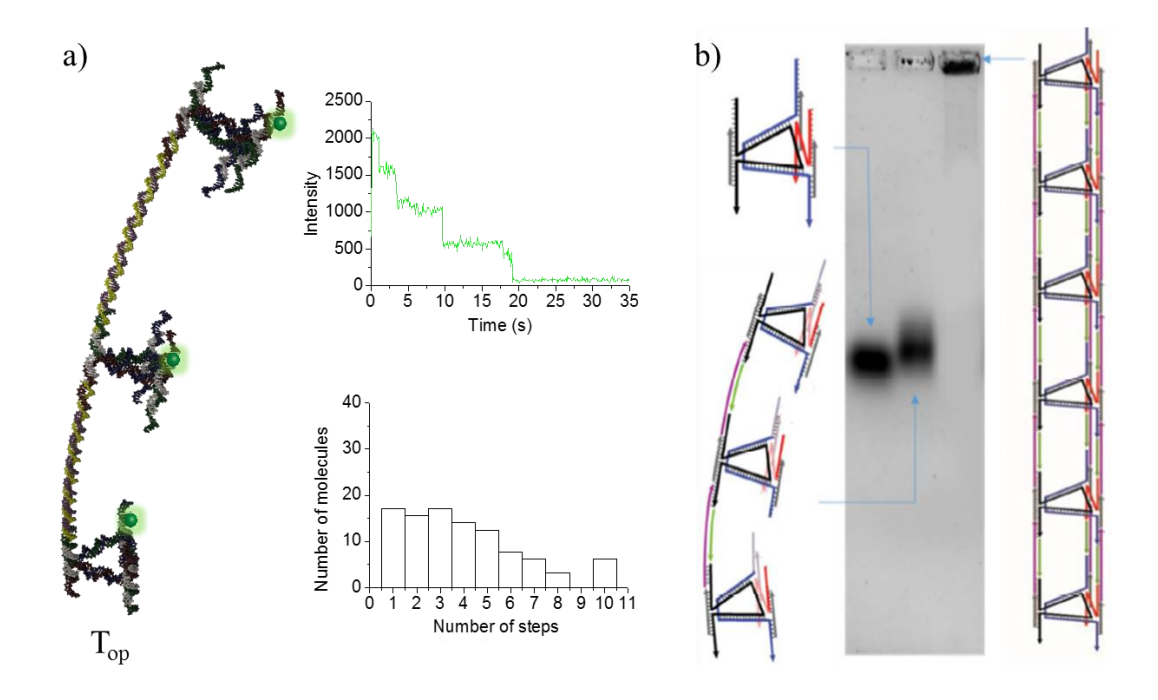


Figure 2.5. (a) Single molecule characterization of the open tube. Left: Schematic illustration of the Cy3-labeled open tube immobilized on coverslips via biotin-streptavidin interactions, and studied by TIRF. Top right: Typical intensity time trajectory acquired for a single open nanotube, displaying 5 steps (dyes). Bottom right: Histogram showing the distribution of the number of steps (Cy3 dyes) obtained from photobleaching curves of the open nanotube samples. (b) 1% non-denaturing AGE showing the growth of the nanotubes from individual rung units.

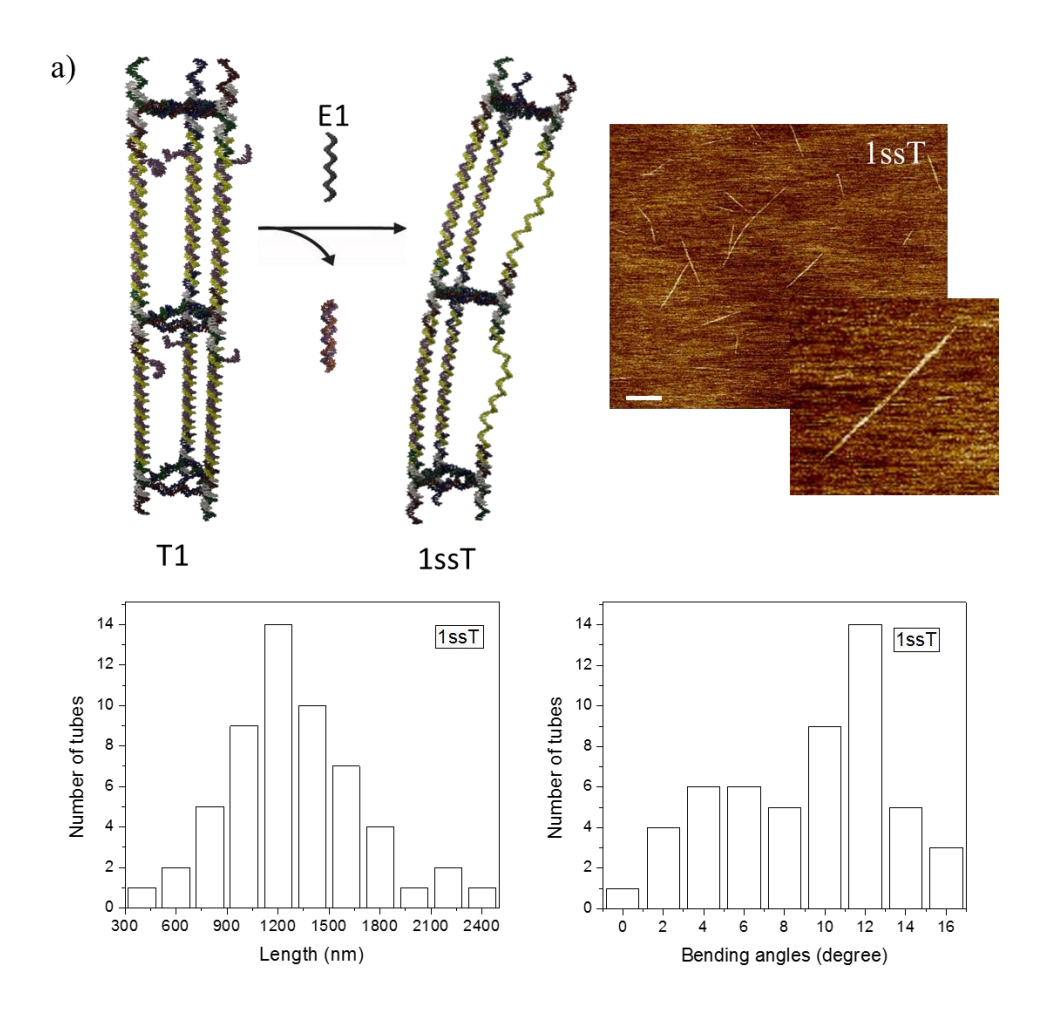
2.2.2. Reversible Switching between Double- and Single-Stranded Nanotubes

We next explored the potential to address DNA nanotubes in response to site-specific DNA hybridization events. To date, DNA nanotubes have not been employed as potential nanomechanical devices. A key challenge is to develop an understanding of their collective structural changes in response to modifications in their repeat unit. In the present nanotubes, the linking strands LS1, LS2, and LS3 can be independently addressed (note that LS2 and LS3 have the same sequence in their middle, double-stranded portions, but different sequences at their sticky-end regions). Two strategies were used: (i) switching between single and double-stranded forms of the nanotube upon displacing one, two and three complementary strands of the linking

strands (LS1-3), and (ii) switching to nanotubes where two sides are shorter than the third one, by a specified number of bases. We investigated the morphological changes by AFM and single-molecule fluorescence microscopy, including in situ experiments. For the latter experiments, in addition to Cy3 labeling of the core triangular units, we labeled the two linking strands bearing short sticky ends (LS2 and LS3) with the red emitting dye Atto647N. Using two different diode lasers, regions were excited with an evanescent field first at 641 nm and then at 532 nm. This sequential recording of the frames minimized artifacts that arise from the bleeding of Atto647N emission into the green channel and of Cy3 emission into the red channel. Single frames (200 ms) were acquired to prevent the photobleaching of the dyes. For the doubly labeled surface-anchored nanotube, we observed the spatial colocalization of the two dyes (Cy3 and Atto647), consistent with retention of nanotube integrity upon immobilization.

We first applied a strand displacement strategy to erase and refill the complementary strands of LS1, LS2 and LS3 in solution. To accomplish this experiment, we built the tubes using extended linking strands LS1-3*, bearing the same sequence as the original LS1-3, but additionally carrying a 10-base overhang. We then added fully complementary strands (eraser strands E1-3) that are expected to bind to each of LS1-3* thus displacing them one by one from the nanotube. This leaves the nanotube single-stranded on one, two and three sides respectively (1ssT, 2ssT and 3ssT). We examined each state of these tubes in situ by TIRFM and observed their conformation by AFM. The partially single-stranded tubes 1ssT and 2ssT were deposited on a freshly cleaved mica surface. Interestingly, AFM (in air) shows that making one- or two sides single-stranded does not significantly change the average tube length (Figure 2.6). The average length of partially single stranded tubes 1ssT (mean length value ($\bar{x} = \frac{\Sigma x}{N}$ where x represents each value of the sample and

N is the sample size): 1342 nm; standard deviation (SD = $\sqrt{\frac{\Sigma(x-\overline{x})^2}{N-1}}$): 421.6 nm) and 2ssT (mean length value: 1386 nm; SD: 686.5 nm). However, one can immediately notice the shift from straight tubes on the mica surface to curved, especially in 2ssT (where the mean bending angle value is 20° and the standard deviation (SD) is 6.9°, see Figure 2.6), when two sides were single-stranded.



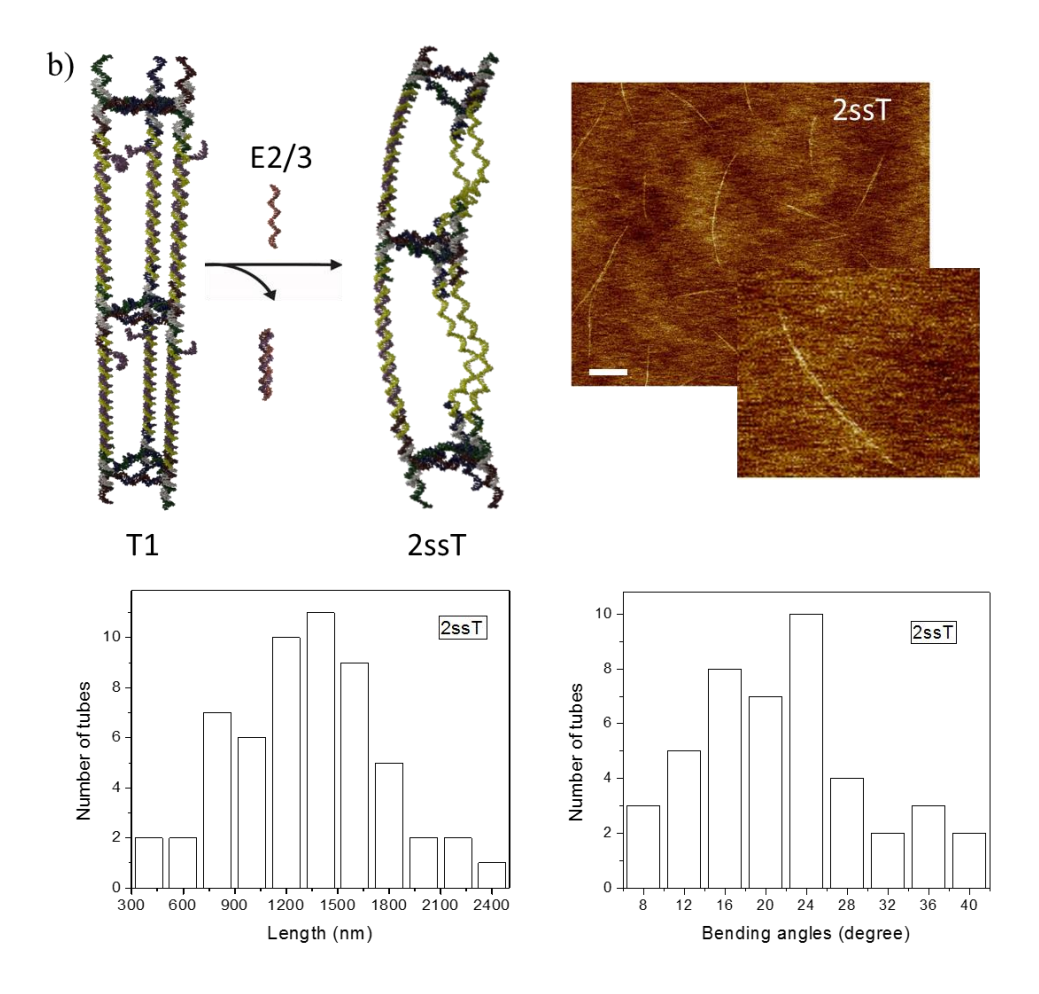
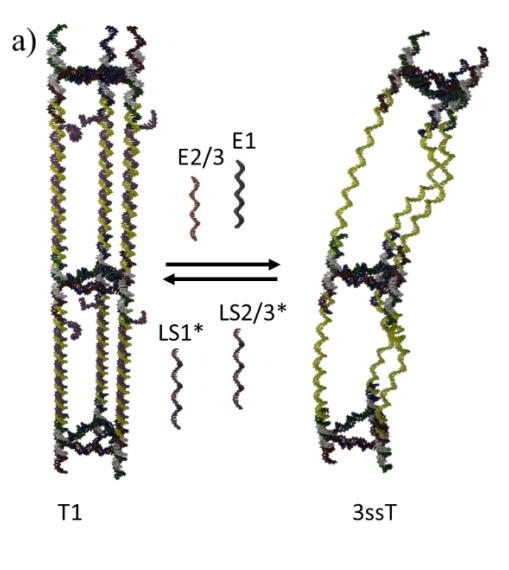


Figure 2.6. Strand displacement experiment. (a) Schematic showing the addition of the erasing strand E1 to generate tubes with one single-stranded side **1ssT**. Dry AFM micrographs (Scale bar 500 nm) depicting the morphological changes of the tubes upon E1 addition (insets are magnified images for single features. In these images, care was taken to avoid washing the mica surface with water after deposition, in order to preserve the native nanotube structure. Bottom: Statistical analysis on the tubes **1ssT** displaying the changes in size distribution and bending angle distribution upon erasing one linking strand at every repeat unit of the nanotubes. (b) The bending angles increase upon erasing 2 linking strands to produce tubes **2ssT**.

The fully single-stranded tubes **3ssT** (Figure 2.7) revealed curvature (97% curved tubes, mean angle value: 25°; SD: 9.1°, mean length value: 1538 nm; SD: 728.2 nm), with a decrease in the population of individual tubes on the surface. At the same concentration, **3ssT** tubes tended to form bundles under the dry AFM conditions (possibly due to their increased flexibility). We



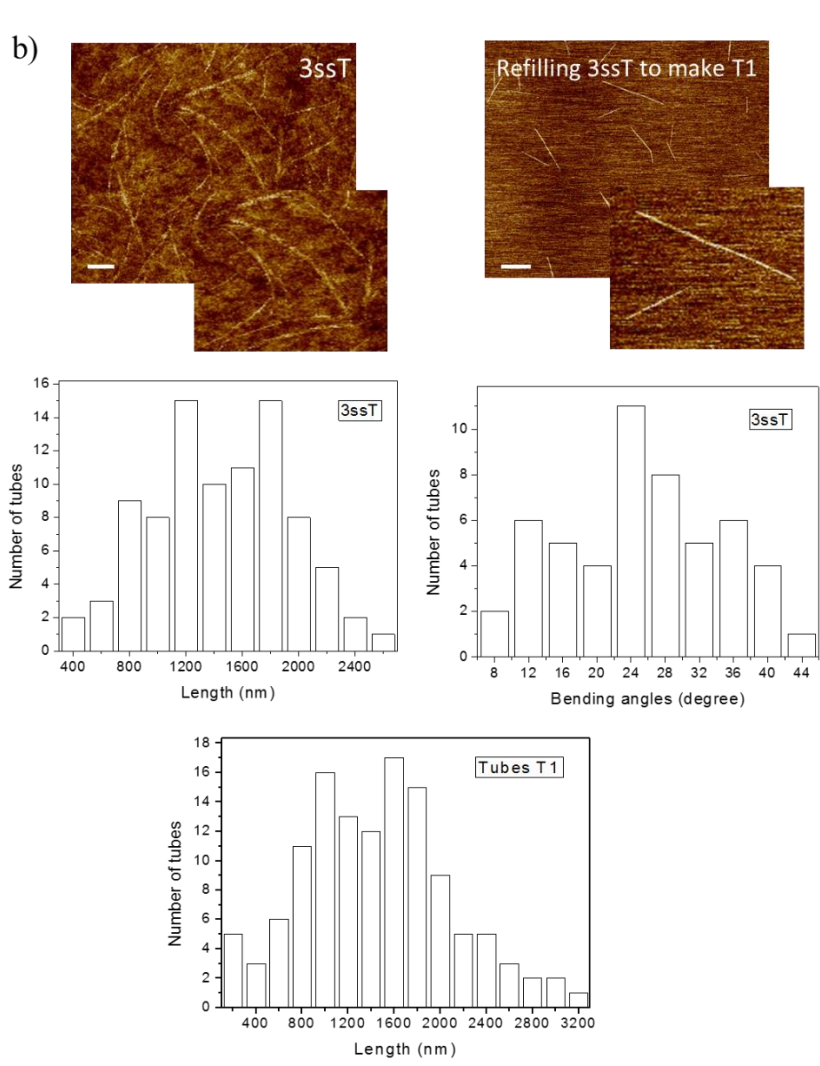


Figure 2.7. Reversible switching between single- and double-stranded forms. (a) Schematic displaying the addition of the erasing strands E1 and E2/3 to produce tubes **3ssT**. The original tube **T1** is reconstituted upon addition of LS1* and LS2/3* to **3ssT**. (b) Dry AFM micrographs (Scale bar 500 nm) depicting the morphological changes of the tubes upon E1 and E2/3 addition. The curvature of the constructs increases as they become more single-stranded. The initial linear morphology is recovered after refilling these single-stranded portions. Bottom: Statistical analysis on the tubes **3ssT** and **T1**.

then added LS1-3* again to the fully single-stranded tubes **3ssT** in solution, to examine whether we could reconstitute their double-stranded form. By AFM, the tubes adopted again their original linear conformation. Interestingly, reconstituted tubes have similar length distribution as the original versions (mean length value: 1400 nm; SD: 800 nm), as depicted in Figure 2.7.

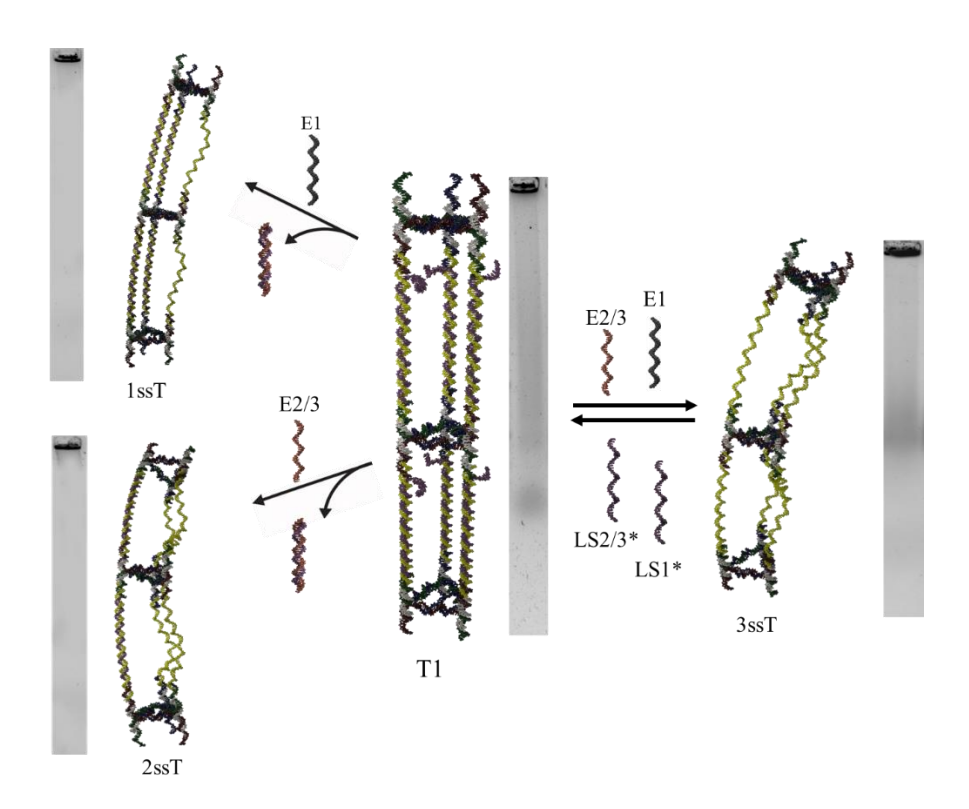
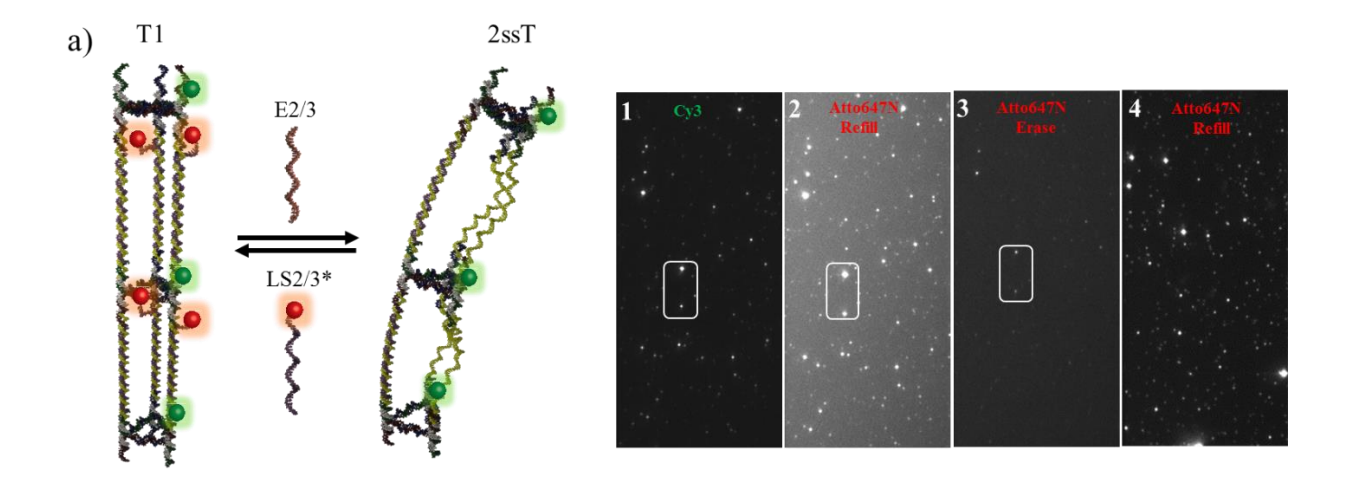


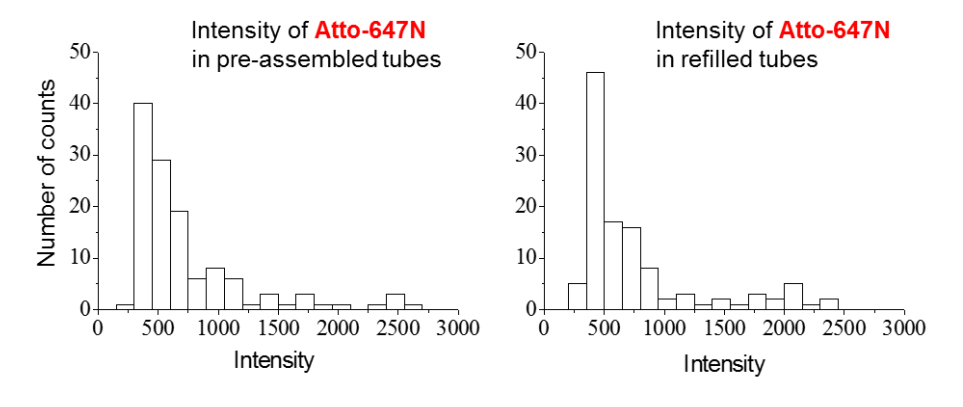
Figure 2.8. 1% non-denaturing AGE characterization of the tubes upon adding E1 and/or E2/3.

Whether left partially/fully single stranded or refilled with the matching strands, the impact of strand displacement process on the stability and robustness of our tubes was investigated by agarose gel electrophoresis (AGE). Figure 2.8 demonstrates that the three nanotube forms (double, partially single, and single-stranded) all showed nonpenetrating bands, indicating the assembly of large structures consistent with the AFM results.

To further examine the system dynamics, we carried out in situ single molecule TIRF studies. We immobilized the nanotubes T1 labeled with Cy3 and 5% biotin as before, but we used in this case ATTO647N-labeled LS2/3*, containing 10-bases overhangs. We once again observed the spatial colocalization of the two dyes in most of the imaged structures (Figure 2.9). We then added the erasing strand E2/3 at a concentration of 500 nM (in excess), to form the immobilized, partially single-stranded nanotube 2ssT. This was followed by a washing step with 1×TAMg buffer (50 μL). Consistent with two sides of the nanotube losing the labeled LS2/3* and becoming single stranded, no emission was detected on the red channel (Atto647N) following the above 2 steps. We next added and incubated fresh ATTO647N-LS2/3* solution at a concentration of 500 nM (in excess) followed by a washing step with 1×TAMg buffer (50 µL). Co-localization of the two dyes indicated the success of the refilling experiment. Interestingly, refilling the partially singlestranded tube 2ssT with strands was qualitatively slow, taking tens of minutes in contrast with the near immediate removal of the strands from double-stranded tube T1. When we compare the intensity ratios of the two dyes before and after erasing/refilling, we notice a high refilling percentage after 1 h incubation. These observations provide evidence of the stability of the tubes in both single- and double-stranded forms and their ability to restore the initial design without degradation (Figure 2.9). We note the difference in the background between panel 2 and panel 3, and between panel 2 and panel 4 in Figure 2.9. This difference is due to the incubation of the



b) Intensity-based analysis histograms



c) Step photobleaching-based analysis histograms

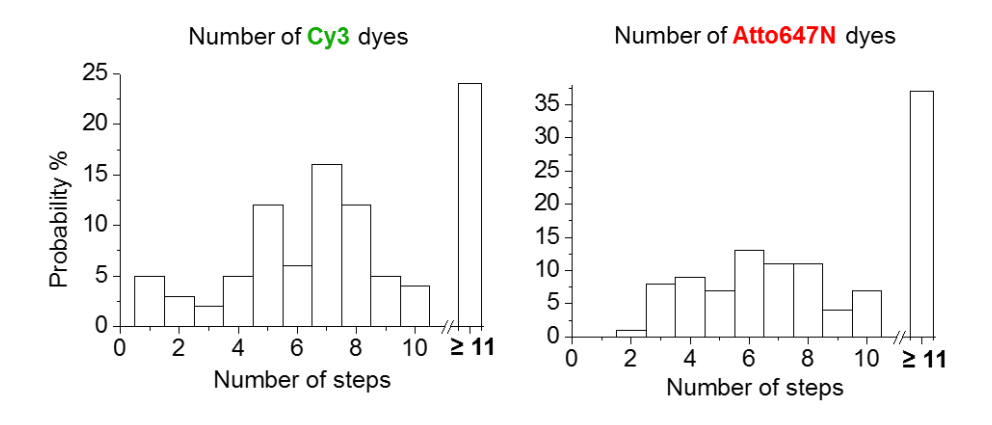


Figure 2.9. Single-molecule characterization of the reversible switching between tubes T1 and 2ssT, immobilized on coverslips using biotin-streptavidin interactions. (a) Schematic showing

the removal of the strands labeled with Atto647N and their re-addition. Right: Series of TIRFM images (70 μm × 35 μm) displaying the colocalization of the two dyes prior to the removal of the labeled LS2/3* (panels 1 and 2), the disappearance of the Atto647N emission upon adding E2/3 (panel 3) and its reappearance after LS2/3* hybridization (panel 4). (b) Histograms depicting the intensity distribution of Atto647N in preassembled versus refilled tubes **T1**, consistent with efficient refilling with LS2/3*. (c) Histograms showing the distribution of the number of steps (Cy3 dyes and Atto-647N) obtained from photobleaching curves in refilled tubes **T1**.

Atto647N labeled DNA in the chamber (panel 2) giving higher background, which is rinsed thoroughly (panel 3) after erasing. Panel 4 is also a refill with Atto647N labeled DNA but in this case after rinsing thoroughly, not during incubation as in panel 2.

These experiments are consistent with the ability to reversibly cycle the nanotube system between double stranded, partially single-stranded and fully single stranded forms. The nanotubes are increasingly curved as they become more single-stranded in character (AFM). Our preliminary evidence shows that the surface attached single-stranded nanotubes are slower to rehybridize into their double-stranded form (TIRF), possibly consistent with increased DNA deformation and/or compaction and decreased accessibility. The switching processes are reversible, and the nanotube retains its length and robustness as it changes between these forms.

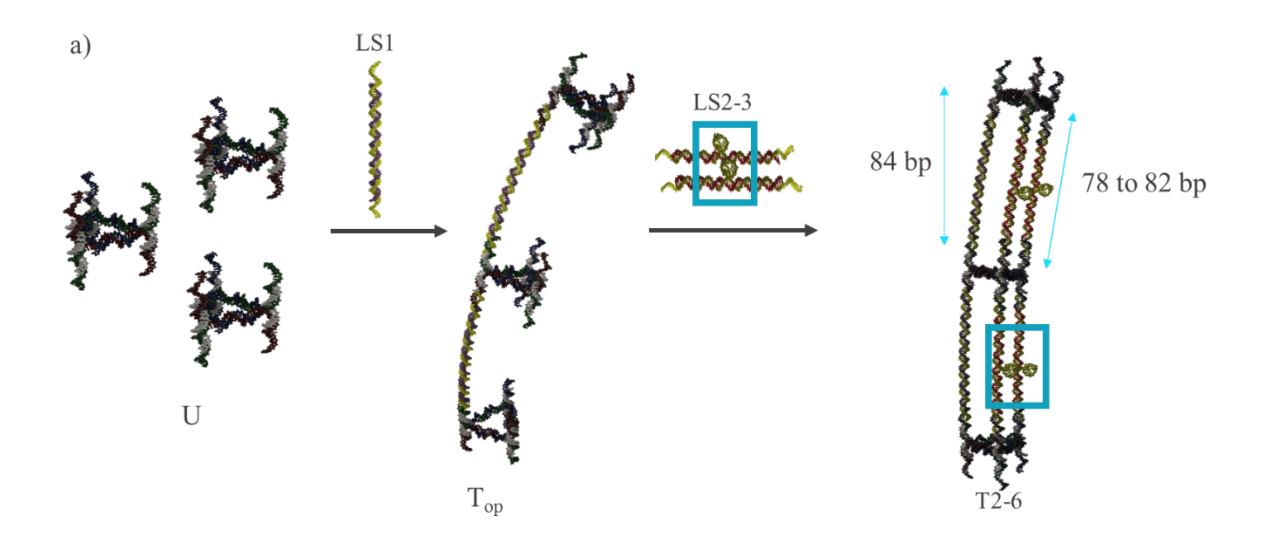
2.2.3. Site Specific Base Deletions

In the next set of experiments, we modified the length of the strand complementary to the two linking strands (LS2/3* as shown in Figure 6A) by removing 2 to 6 bases. By hybridizing to LS2/3*, these shorter strands likely cause the formation of internal loops of 2 to 6 bases. As a result, on one side of the nanotube, two consecutive triangular cores are separated by 84 bases

(~28.6 nm) and on the other two sides they are separated by shorter DNA stretches: 82 for **T2** (~27.9nm), 81 for **T3** (~27.5nm), 80 for **T4** (~27.2nm), 79 for **T5** (~26.9 nm) and 78 bases for **T6** (~26.5 nm) respectively. This size mismatch repeats over the whole length of the nanotube at each constitutive polygon (a 1 μ m nanotube has ~35 repeat LS units).

Strategies for bending DNA nanostructures have been developed by the Shih, Yin and Yan groups, by introducing insertions and deletions, or placing designed crossover and nick points at specific positions. ^{18,19,20} Here, rather than introducing static structural changes, we examine the dynamic switching mismatch between the tube sides serves as a model for a local DNA structural change in the repeat unit (distortion/bending as a result of protein or small molecule binding). We were interested to probe whether this mismatch results in morphological changes in the nanotubes, and at which point this bending/distortion would disrupt nanotube formation.

We used two methods for the generation of these modified nanotubes. First, the nanotubes were preassembled in solution by mixing and annealing all strands. They were studied by nondenaturing AGE, AFM under dry conditions and TIRFM. As described earlier, fully double-



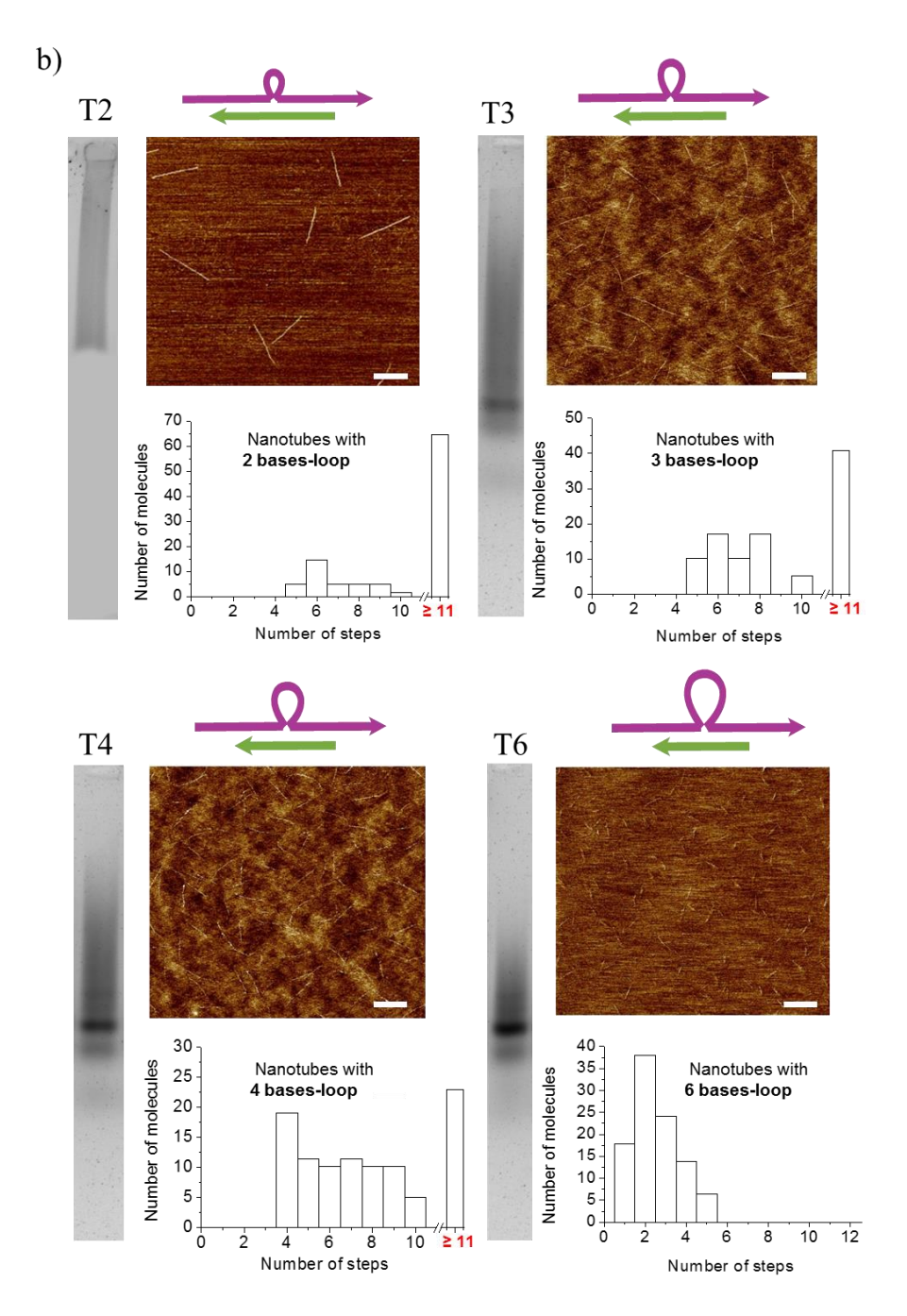
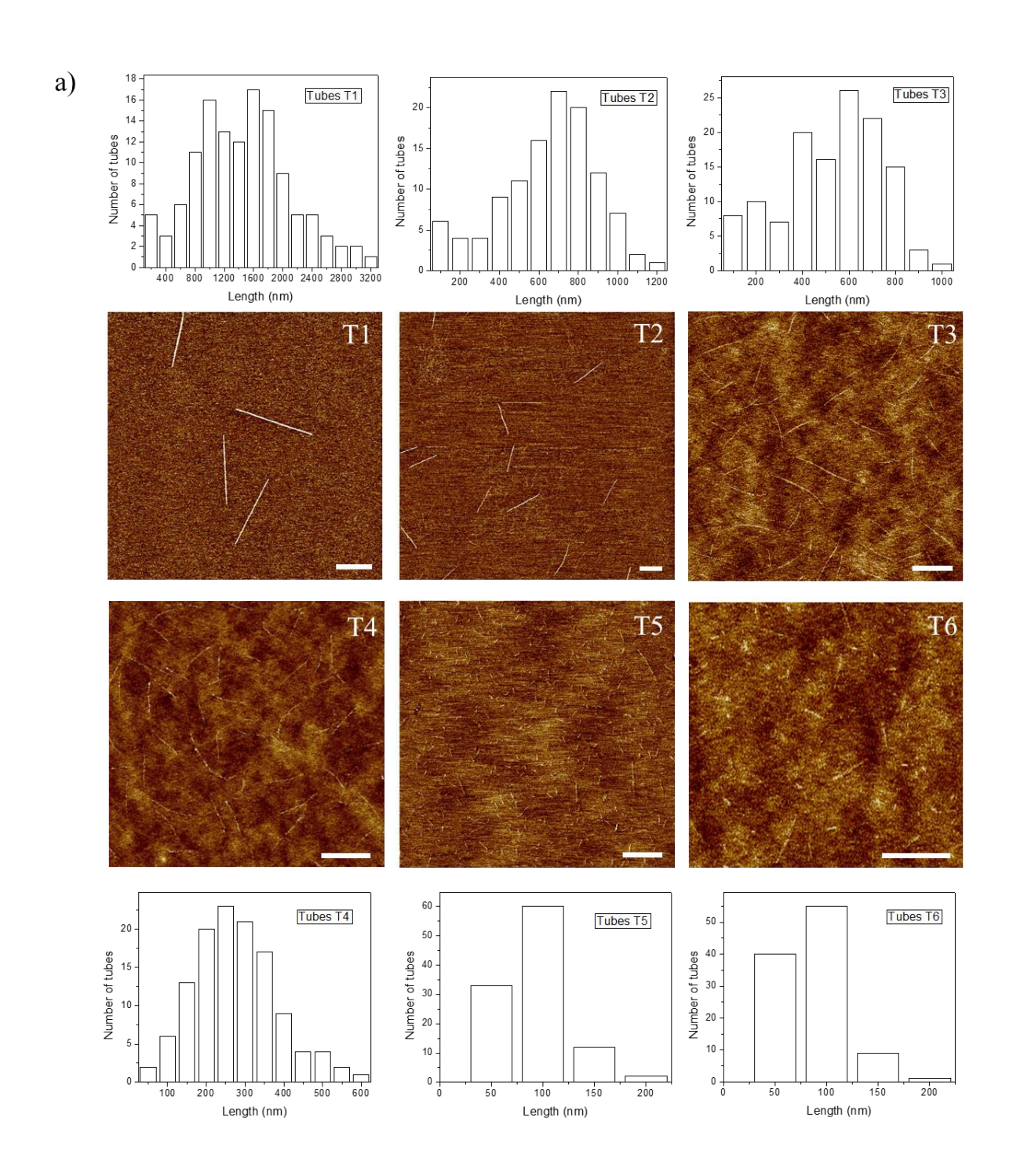


Figure 2.10. Study of the robustness and morphological changes of the tubes by increasing length mismatches between the vertical strands of the repeat units. (a) Schematic representing the introduction of a size mismatch between LS2-3 strands and LS2/3* through a gradual decrease of the length of LS2/3* strand. (b) Characterization of the effect of these mismatches on the shape and size distribution of the tubes by 1% nondenaturing AGE, AFM (Scale bar 500 nm) and TIRFM. The average length of the tubes decreases with increasing the mismatch length; a mismatch of 5 bases is enough to break the tubes into small pieces of 5 rungs at most. For the AGE of **T2**, the band of very low mobility is faint; we speculate that the length mismatch in **T2** slightly weakens its sticky-end interactions, such that the tube fragments as it travels down the AGE gel.

stranded **T1** shows a nonpenetrating band by AGE, straight and long features by AFM (~70 rungs) and exponential traces in intensity trajectories. As the length difference between the tube sides increases (T2-T6), AGE shows smeared bands of progressively higher gel mobility, consistent with shorter nanotubes (Figure 2.10). By AFM, tubes **T2** with a difference of 2 bases were not able to grow more than $\sim 1 \mu m$ ($\sim 35 \text{ rungs}$, Figures 2.10, 2.11). The mean length was calculated to be 720 nm (SD: 375.3 nm) and 80% of these tubes were curved (Figure 2.11). 94% of tubes T3 showed a certain degree of curvature with a mean bending value of 19° (SD: 8.4°) (Figure 2.11), and structures with a mean length value of 590 nm (SD: 186.6 nm) were imaged. Single molecule TIRFM photobleaching experiments for T2 and T3 showed an exponential decay for the majority of the tubes, with a slight increase in the population of shorter tubes made up of 5 to 10 repeat units (Figure 2.10). With a 4 bases difference between LS1 and LS2/3, 96% of the tubes appeared to be curved (mean: 21°; SD: 9.7°) but with a length of ~500 nm (~18 rungs) at most (mean length: 226 nm; SD: 96.2 nm). By TIRFM, **T4** exhibits a large increase in the population of shorter tubes ranging from 4 to 10 rungs, with only ~33% of the tubes showing an exponential decay (Figure 2.10).

A difference between the three sides of the tubes of 5 and 6 bases induced the assembly of small features of ~150 nm and less (~5 rungs, Figure 2.11). Using single molecule photobleaching, we generate histograms of the distribution of the number of steps in the nanotubes, where tubes **T5** and **T6** showed short nanotubes with no more than 5 repeat units (Figure 2.10). Thus, the introduction of length mismatch in the repeat units of DNA nanotubes results in bending for differences of 2-3 bases, with relative maintenance of the tube length. On the other hand, a mismatch greater than 4 bases introduces sufficient distortion to cause nanotube shortening, which becomes significant for differences of 5-6 bases. We have carried out control experiments on a

DNA dimer model of the nanotube, to verify proper hybridization of the length mismatched form (Figure 2.12).



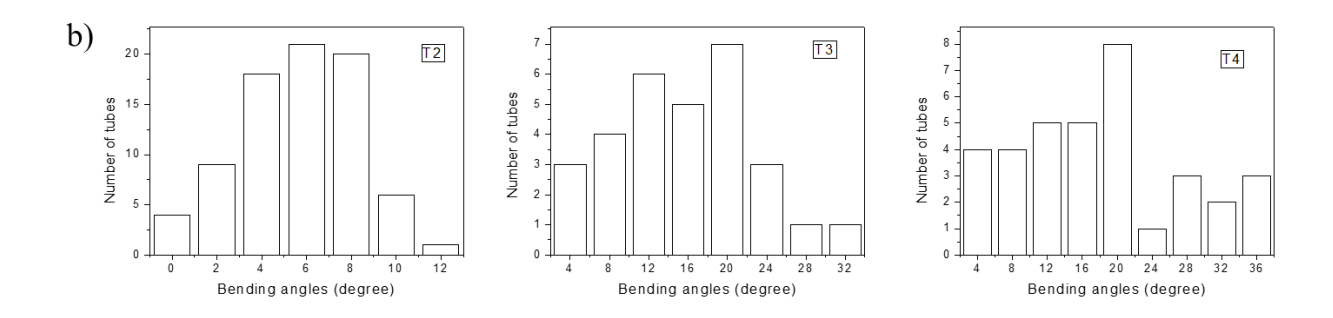


Figure 2.11. AFM images at a scale bar of 500 nm of tubes **T1** to **T6** prepared in solution then immobilized on the mica surface. (a) Statistical analysis reveals clearly the effect of length mismatches on the overall size distribution of the tubes. (b) Analysis showing the length mismatches effect on the bending angles of tubes **T2**, **T3** and **T4**.

During the growth process, nanotubes of various size distribution were developed and studied. Since it was difficult to characterize the structure of our tubes from non-penetrating bands displayed in the agarose gels, we designed various dimers of two rung units linked on one side by LS1 of ~28.56 nm in length (84 bases) and on two sides by LS2 and LS3 of ~27.88 nm (82 bases), ~27.54 nm (81 bases), ~27.2 nm (80 bases), ~26.86 nm (79 bases) and ~26.52 nm (78 bases) in length. We have also performed the strand displacement strategy on the dimer (**D1**) having three sides of equivalent length.

To inhibit the formation of larger tubes and favor dimer formation, we introduced two types of triangular cores. For the top rung, the three overhangs above the plane were removed while the other three sticky-ends remained. On the other hand, the three overhangs below the plane of the bottom rung were removed (Figure 2.12). Subsequently, all dimers were constructed through the addition of LS1 first then LS2 and LS3 as described before. The PAGE gel displayed in Figure 2.12 shows the assembly of clean rungs top (lane 1), rungs bottom (lane 2), open dimers with LS1 only (lane 3), closed dimers with three sides of same length (lane 4). Length mismatched dimers

were pre-assembled in solution by mixing and annealing all strands (+ control) or generated from the dimer version of the partially single stranded form 2ssT. In Figure 2.12, we demonstrate the formation of five kinds of dimers having a length mismatch starting from 2 to 6 bases. The mobility of the discrete band shown in each lane with respect to its corresponding positive control provides additional evidence for the stability of the partially single-stranded dimers. The second band of higher mobility was the result of the interaction of E2/3 with the initial LS2/3* strands.

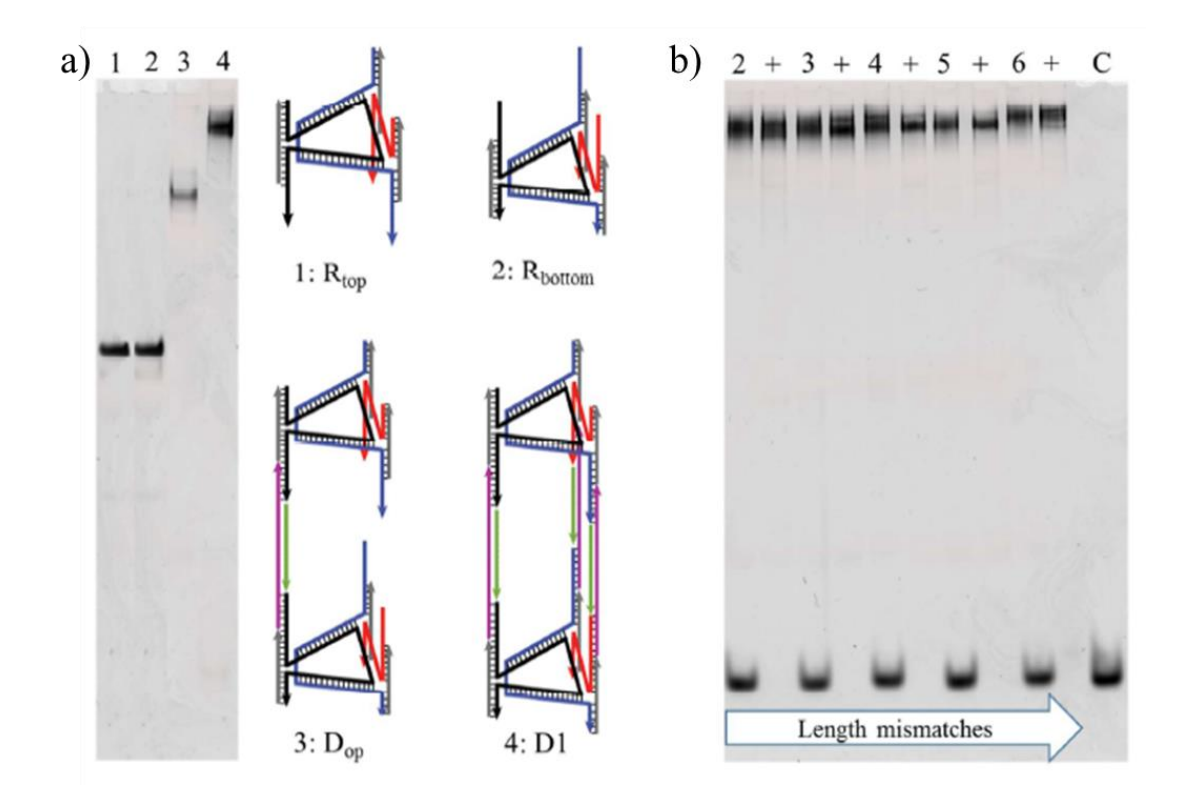


Figure 2.12. (a) 6% non-denaturing PAGE depicting the assembly of dimers **D1** from rungs top and rungs bottom. (b) 6% native PAGE showing the formation of different types of dimers via (i) generation of 2ssT by strand displacement, followed by addition of the length mismatched dimer (for example, lane 2) or (ii) annealing all strands, including length mismatched together (the lanes labelled +). The lane labels 2 to 6 represent the dimers with a length mismatch of 2 to 6 bases (**D2-D6**). The last lane C represents the double stranded DNA resulting from the hybridization of E2/3 to LS2/3*.

Length mismatched nanotubes can also be generated directly from the partially single stranded form **2ssT**. In particular, we were interested to see if an initially long single-stranded nanotube **2ssT** can be fragmented and shortened upon addition of length mismatched strands, even under mild conditions. In solution, we generated **2ssT**, by starting with double-stranded **T1** and strand displacement of LS2/3 (Figure 2.13). We next refilled the tube with the 5-bases shorter complements (LS2/3* 37) labeled with Atto647N, in solution at room temperature (1 h incubation). Figure 2.13 illustrates the effect of LS2/3* binding in disassembling the preformed long structures. Note the absence of the non-penetrating band after LS2/3* 5-base shorter strand binding and the appearance of new bands with higher mobility similar to tubes **T6** reported in Figure 2.10. The AFM micrograph shown in Figure 2.13 confirms the AGE observations as small features of ~150 nm at most were imaged on the surface of mica. Thus, pre-annealing nanotubes **T5** with length mismatch, or generating them from single-stranded forms produce similar populations of shortened nanotubes.

2.2.4. Optimization of Biotin-Streptavidin Interaction

In order to immobilize our nanotubes on the coverslips, we extended one of the rigidifier strands (R3ov) by 20 bases and we synthesized its complementary strand decorated with biotin moiety (Bio-R3ov*). Since the interaction of biotin on our constructs with strepdavidin on the surface determined the dynamics and the stability of the tubes during the TIRFM measurements, we varied the amount of biotin attached to our nanotubes from 100% to 5%. A 100% biotin was referred to a 1:1 ratio of the biotinylated strand with respect to the rung. However, at a percentage

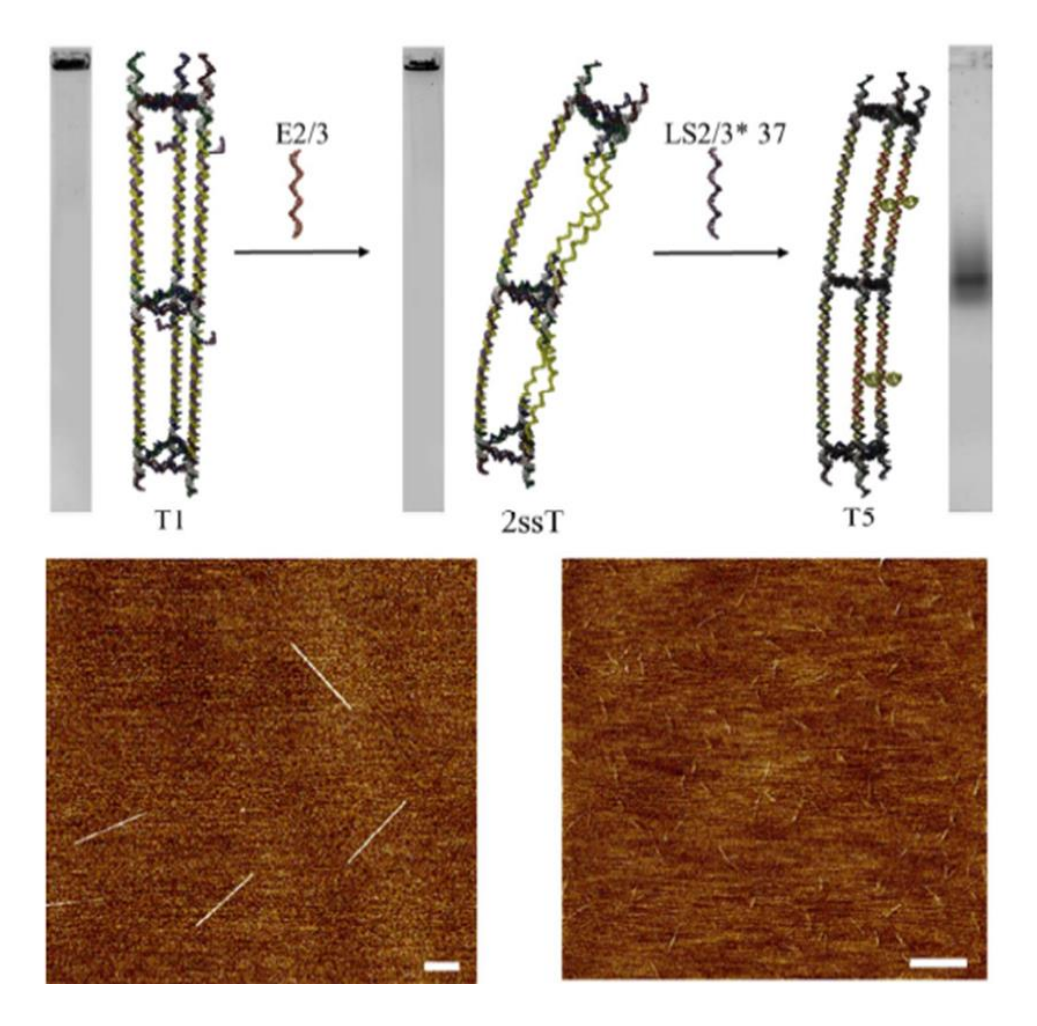


Figure 2.13. Study of the morphological changes by non-denaturing AGE (1%) and AFM after the addition of LS2/3* (5-bases shorter than LS1) to the tubes **2ssT**.

of 5% for example, 5% of the rigidifier (R3) were hybridized to the strand tagged with biotin and to the triangular core while the remaining 95% consisted of R3 lacking the 20 bases sticky-end. Since the rigidifier R1 was labelled with a Cy3 dye, the emission of nanotubes bearing 100%, 80%, 60%, 40%, 20%, 10% and 5% of biotin molecules was detected into the red channel (Figure 2.14). Interestingly, the visualization of the tubes was possible even at the lowest percentage tested indicating that a minimal percentage of biotin label is sufficient to deposit the tubes on the surface. Because the biotin-streptavidin interaction can restrain the movement of the tubes, 5% biotin labels

were employed in all studies in order to allow a certain degree of freedom of the tubes on the surface.

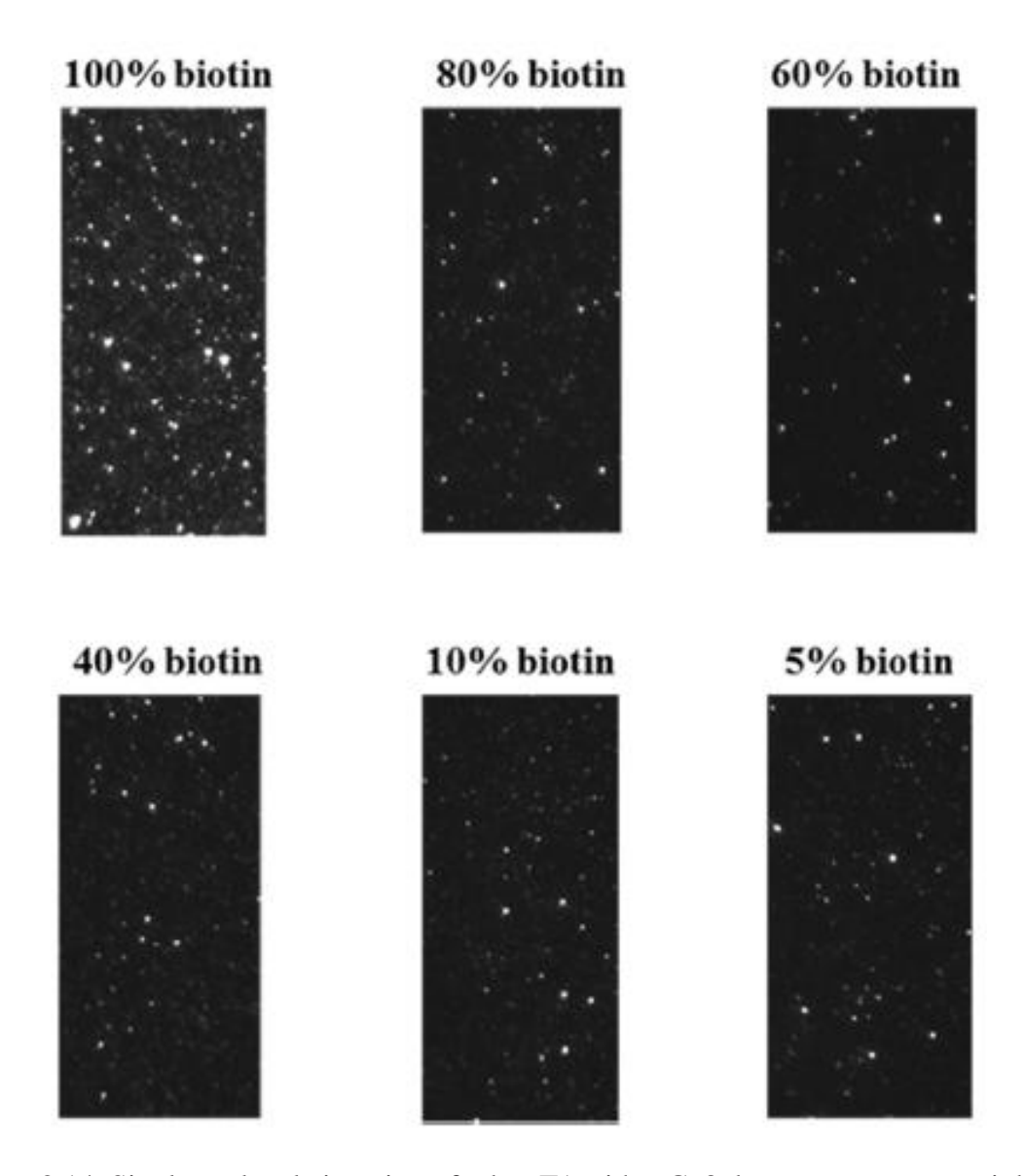


Figure 2.14. Single-molecule imaging of tubes T1 with a Cy3 dye on every rung unit but at different biotin concentrations.

Finally, we show in Figure 2.15 some of the intensity steps corresponding to tubes **T1** to **T6**. As the length mismatch between the tube sides increases, the degree of curvature increases until the distortion is strong enough to disassemble the structure into small fragments.

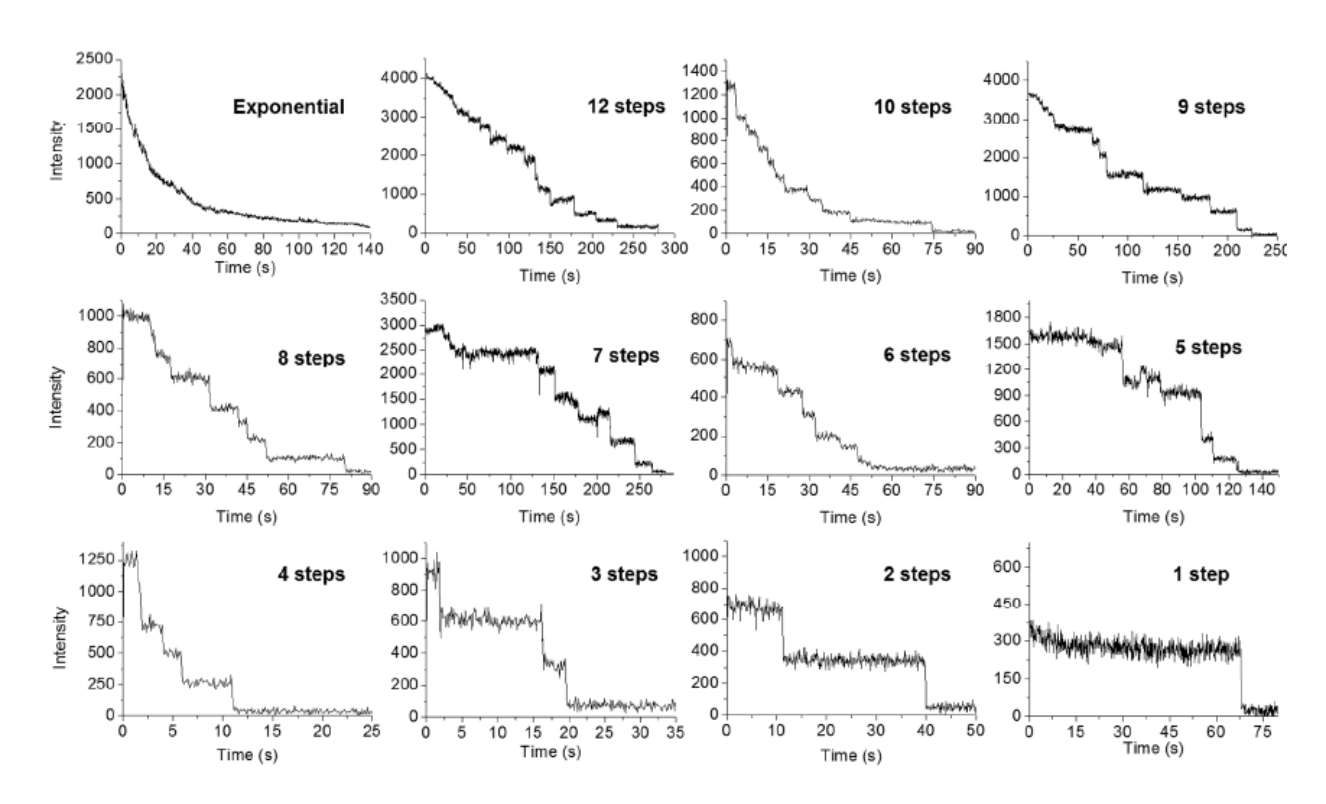


Figure 2.15. Photobleaching intensity traces examples from a series of samples starting from T1 to T6.

2.3 Conclusions

In conclusion, we have shown a simple and efficient synthesis of DNA nanotubes from 11 short unmodified strands. This yields robust structures with controlled geometry and circumference, and site-specific addressability. Unlike tile- or origami-based structures, these nanotubes can be reversibly switched between a fully double-stranded form, and structures with one, two or three

single-stranded repeat units. We show by atomic force microscopy that this results in bent and flexible structures. In situ fluorescence microscopy shows that strand displacement from doublestranded forms occurs quickly, but the "refilling" of single-stranded forms occurs more slowly, consistent with their increased flexibility and possible compactness. Interestingly, refilling the single-stranded structures to go back to the double-stranded tube is very efficient, pointing to the robustness of this nanotube "actuator". We introduce an additional morphological change into the nanotubes: an increasing size mismatch between the vertical strands of each repeat unit. This results in nanotube bending, until the introduced distortion disrupts the formation of long nanotubes. Because they have a large number of repeat units down their length, these nanotubes have the potential to amplify biologically relevant DNA distortions. Thus, this method allows the simple and scalable production of dynamic nanotubes, for potential applications as biophysical probes and tools for drug delivery. In particular, the implementation of specific sequences involved in gene silencing and the functionalization of some strands with targeting agents can significantly enhance the therapeutics effect of our system. Furthermore, a variety of real-world applications of DNA tubes might be envisioned, such as the organization of gold nanoparticles within nanoscale precision and the arrangement of components with electronic properties for the creation of functional nanowires. The ability to exchange strands and modify the position of these functional objects down the tube's length is expected to alter the optical and/or electronic properties of materials in a highly programmable manner.

2.4 Experimental

2.4.1 Materials

Acetic acid. boric acid. EDTA. urea. magnesium chloride. GelRed. tris(hydroxymethyl)aminomethane (Tris), D(+) glucose, 2-betamercaptoethanol, and streptavidin were purchased from Aldrich. Nucleoside (1000 Å)-derivatized LCAACPG solid support with loading densities of 25-40 µmol/g, Sephadex G-25 (super fine DNA grade), and reagents for automated DNA synthesis were used as purchased from BioAutomation. Acrylamide (40%)/bisacrylamide 19:1 solution and agarose were purchased from BioShop. For TIRFM sample preparation, 1% v/v Vectabond/acetone was purchased from Vector Laboratories, while poly-(ethylene glycol) succinimidyl valerate MW 5000 (mPEG-SVA) and biotin-PEG-SVA were purchased from Laysan Bio, Inc. Imaging chamber components were purchased from Grace Bio-Lab. AFM cantilevers were purchased from Asylum Research (model AC160TS) and RubyRed mica were ordered from Electron Microscopy Sciences. TBE buffer is composed of 90 mM Tris and boric acid and 1.1 mM EDTA, with a pH of ~8.3. TAMg buffer is composed of 45 mM Tris and 12.5 mM MgCl2 with a pH of ~7.8 adjusted by glacial acetic acid.

2.4.2 Instrumentation

The strands were synthesized via automated solid-phase synthesis carried on a BioAutomation MerMade MM6 DNA synthesizer at 1 µmol scale. Labelled strands were ordered from Integrated DNA Technologies (IDT). The strands were deprotected and cleaved from the solid support in the presence of concentrated ammonium hydroxide solution (60°C, 16 hours).

Polyacrylamide gel electrophoresis (PAGE: 20 x 20 cm vertical Hoefer 600 electrophoresis unit) was employed to purify crude products (8-20% polyacrylamide/8M urea at constant current of 30 mA for 2 hours, with 1xTBE as a running buffer). Following electrophoresis, the desired bands were excised then crushed and incubated in 11 mL of autoclaved water at 60°C for at least 12

hours. After drying the samples to 1.5 mL, we used size exclusion chromatography (Sephadex G-25) to desalt the solution. The strands were quantified (OD260) by UV/vis spectroscopy with a NanoDrop Lite Spectrophotometer and using IDT's extinction coefficient at 260.

AFM was carried on with a MultiMode 8 SPM connected to a NanoscopeTM controller, from the Digital Instruments Veeco Metrology Group. $5\mu L$ of the nanotubes at a concentration of 100 nM (concentration of each of the component strands) in filtered $1\times TAMg$ were deposited on freshly cleaved mica then incubated for at least 1 hour under vacuum. Note that at this concentration, only single nanotubes were observed on the surface with a typical height between 1 and 2 nm. Further washing with water or buffer resulted in collapsed structures on the surface, therefore we preferred to use AFM to visualize the curvature and dynamics of our constructs without losing their original shape through additional rinsing cycles.

Coverslips were washed, labeled with polyethylene glycol, and functionalized with streptavidin as detailed in the Supporting Information. Nanotubes were deposited via biotin-streptavidin interactions then imaged via a two-color total internal reflection fluorescence microscopy setup. The photobleaching events were recorded and fluorescence intensity time traces of individual molecules were analyzed using a self-written algorithm in IDL and Matlab.

2.4.3 Sequence Design and Synthesis

When designing a nanotube composed solely of DNA strands, one should be careful in determining the length of each product, the size of their sticky-ends and the undesirable secondary interactions between them. More importantly, since our constructs possess a geometrically well-defined architecture, each region was modelled to produce the expected assembly with a minimal yield of byproducts. We used Gideon,²¹ a software specifically developed to facilitate the design of various

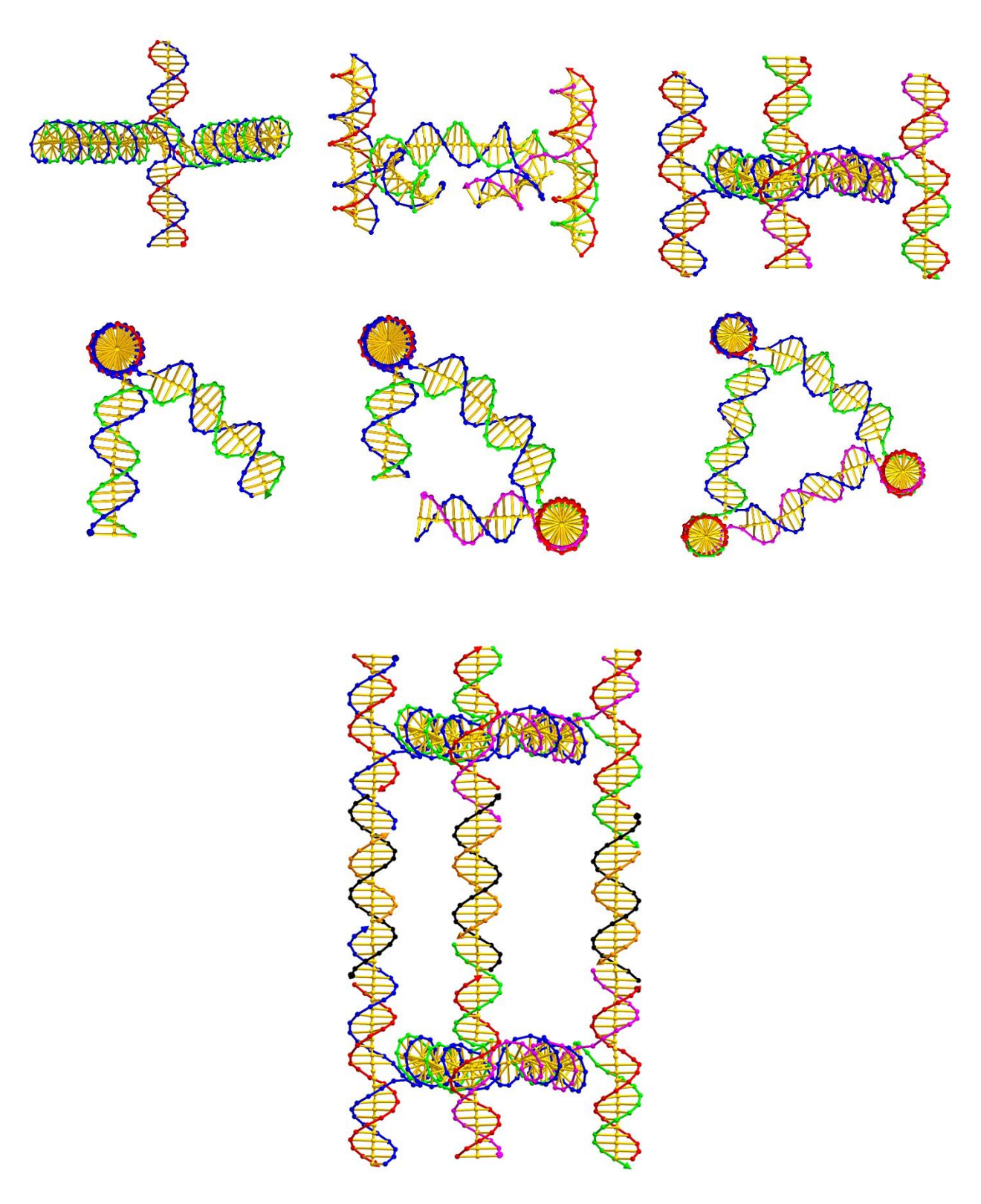


Figure 2.16. DNA nanotubes design as modelled by Gideon.

Table 2.1. Sequences of all the strands used in this chapter

Name	Seuquence 5' to 3'	ε ₂₆₀ (L.mole ⁻¹ .cm ⁻¹)
V	CTCAGCAGCGAAAAACCGCTTTACCACATTCGAGGCACGTTGTACGTC CAC ACT TGGAACCTCATCGCACATCCGCCTGCCACGCTCTTAGCATAGGACGGC GGC GTT AAA TA	1062100
C1	CGGTGCATTTCGACGGTACTTCGTACAACGTGCCTCGAATGTAGAGCGTGGCAGG CGGATGTGAAGCAGTTGCAGCGTACTCGT	803900
C2	TCGGCAGACTAATACACCTGTCGATGAGGTTCCAAGTGTGGATAGCTAGGTAACG GATTGAGC	623300
R1	TGCAACTGCTACCAGGTGTATT	207400
R2	TTACCTAGCTCCAGTACCGTCG	202000
R3	GTCCTATGCTTTGTAAAGCGGT	207400
LS1	TTTTCGCTGCTGAGGTAAGCCTTCGGCGAGCATCTATCTA	563700
LS1*	CGGAGACATAGATAGATGCTCGCCGAAGGCTTA C	337000
LS1*ov	CGACTTCGAGCGGAGACATAGATAGATGCTCGCCGAAGGCTTAC	430500
LS2	AGTCTGCCGACACAGAGATCAGTCGGAAGCATAATATCTTATGTTCGT GAT AAC GAGTACGC	618800
LS3	AAATGCACCGCACAGAGATCAGTCGGAAGCATAATATCTTATGTTCGT GAT AGC TCAATCCG	615100
LS2/3*	TATCACGAACATAAGATATTATGCTTCCGACTGATCTCTGTG	406900
LS2/3*ov	TTTTTTTTTTATCACGAACATAAGATATTATGCTTCCGACTGATCTCTGTG	487900
E1	GTAAGCCTTCGGCGAGCATCTATCTATGTCTCCGCTCGAAGTCG	409100
E2/3*	CACAGAGATCAGTCGGAAGCATAATATCTTATGTTCGTGATAAAAAAAA	546300
R3ov	GTCCTATGCTTTGTAAAGCGGTGCCTGGCCTTGGTCCATTTG	379700
Bio-R3ov*	biotin-CAAATGGACCAAGGCCAGGC	198100
LS2/3*24	TATCACGAACATCTGATCTCTGTG	227600
LS2/3*36	TATCACGAACATAAGATATTCCGACTGATCTCTGTG	352500
LS2/3*37	TATCACGAACATAAGATACTTCCGACTGATCTCTGTG	358700
LS2/3*38	TATCACGAACATAAGATATCTTCCGACTGATCTCTGTG	367800
LS2/3*39	TATCACGAACATAAGATATTCTTCCGACTGATCTCTGTG	375900
LS2/3*40	TATCACGAACATAAGATATTGCTTCCGACTGATCTCTGTG	384800

DNA nanostructures geometries, to build our triangular core unit (rung) with minimal strain between phosphate-backbone linkages (Figure 2.16). The length of each edge and whether it was more favorable to add unpaired nucleotides at the junction points or not were also modelled by the

same program. Subsequently, we determined the length of the linking strands between two rungs to be 84 bases. These dimensions gave us the most relaxed and unstrained structure. The size of the overhangs was 10 (LS2 and LS3) and 14 (LS1) bases (Figure 2.16). After defining the length of each strand, all the sequences were generated via CANADA 2.0 (available online), a program intended to minimize undesirable secondary interactions (Table 2.1). Finally, we used the Integrated DNA Technologies website to double check that the generated sequences did not have any unintended interactions more than 5 bases and that they cannot self-dimerize.

The triangular rung unit was the result of the assembly of 6 unmodified strands (V: 113 bases, C1:84 bases, C2:63 bases and R1, R2 and R3:22 bases) in equimolar mixture with a final concentration of 136 nM in 1×TAMg. The solution was annealed from 95 to 4°C over 3 h 40 min to get the highest yield possible of the clean product. The formation of the rung was confirmed by native polyacrylamide gel electrophoresis (PAGE: 20 × 20 cm vertical Hoefer 600 electrophoresis unit) shown in the Supporting Information. The optimization of the length of the six sticky ends coming out from each rung unit is further discussed in the paper and in the Supporting Information. In order to form the nanotube, 1 equiv. of the first set of linking strands LS1 was added. LS1 hybridized to two sticky ends during an annealing step from 56 to 22°C for 1 h. The preorganized opened assembly was closed to the full nanotube after the addition of 1 equiv. of each of the two linking strands LS2 and LS3 and their complements while annealing the mixture from 44 to 22°C for 45 min. The formation of the tubes was first characterized by a 1% nondenaturing agarose gel (Owl Mini gel electrophoresis unit) stained 20 min in GelRed.

2.4.4 Total Internal Reflection Fluorescence Microscopy (Performed by Hariri A.A.)

Coverslips were soaked in piranha solution (25% H₂O₂ and 75% concentrated H2SO4) and sonicated for 1h, followed by multiple water (molecular biology grade), and acetone (high performance liquid chromatography (HPLC) grade) rinsing cycles. Dry and clean coverslips were then treated with Vectabond/acetone 1% v/v solution for 5 min and then rinsed with H₂O and left in dried state until used. In order to prevent non-specific adsorption of biomolecules onto the glass surface, coverslips were functionalized prior to use with a mixture of poly(ethylene glycol) succinimidyl valerate, MW 5000 (mPEG-SVA) and biotin-PEG-SVA at a ratio of 99/1 (w/w), in a 0.1 M sodium bicarbonate solution for 3h. Excess PEG was rinsed with water, and the coverslips were dried under a N₂ stream. In order to reduce photobleaching events, oxygen scavenger solution was prepared consisting of a triplet quencher agent, β-mercaptoethanol 1% v/v and an oxygen scavenger system (D(+)glucose 3% w/v, glucose oxidase 0.1 mg/mL, and catalase 0.02 mg/mL). Imaging chambers (~8 μL) were constructed by pressing a polycarbonate film with an adhesive gasket onto a PEG-coated coverslip. Two silicone connectors were glued onto the predrilled holes of the film and served as inlet and outlet ports. The surface was incubated with 10 μL of a 0.2 mg/mL streptavidin solution for 10 min. Excess streptavidin was then washed with 100 μL of 1xTAMg buffer. 10 µL of the 600 pM DNA nanotube solution was injected in the chamber. (136 nM solution diluted 200×; ~100 fluorescent spots per 30 μm × 30 μm region). Unbound DNA structures were then flushed out with 50 µL of 1xTAMg buffer.

Fluorescence single molecule experiments were carried out using a total internal reflection fluorescence microscopy setup (TIRFM). The TIRFM setup consisted of an inverted microscope (IX71, Olympus) equipped with a laser-based TIRFM illumination module (IX2-RFAEVA-2, Olympus) coupled to a diode-pumped solid-state green laser (both 532 nm and 638 nm outputs were used, lasers from CrystaLaser). The beam position was adjusted using the illuminator to attain

total internal reflection through an oil-immersion objective (N.A. 1.45, Olympus U PLAN SAPO 60x,). Fluorescence emission was collected through the objective and images were captured with an EMCCD camera (CascadeII: 512B, Photometrics, Roper Scientific). Emission was chromatically separated using dichroic mirrors (640dcxr, Chroma) with the 'green' and 'red' emission filtered through band pass filters (HQ590/70M and HQ685/80M, respectively, from Chroma) before being captured by the EMCCD camera. The camera was controlled using Image-Pro Plus 5.1 (Media Cybernetics), capturing 8-bit 512 x 512 pixel images with an exposure time of 150-200 ms, a conversion gain of 3, and multiplication gain of 3750-4095. To image the Cy3/Atto647N DNA nanotube sample, excitation was carried out with a power output of 6.5 mW (532 nm) and 4.6 mW (638 nm) measured from the objective. Fluorescence intensity time traces of individual molecules were extracted from the movies using a self-written algorithm in IDL and Matlab.

2.5 References

- (1) Aldaye, F. A.; Lo, P. K.; Karam, P.; McLaughlin, C. K.; Cosa, G.; Sleiman, H. F. *Nat. Nanotechnol.* **2009**, *4*, 349.
- (2) Lo, P. K.; Karam, P.; Aldaye, F. A.; McLaughlin, C. K.; Hamblin, G. D.; Cosa, G.; Sleiman, H. F. *Nat. Chem.* **2010**, *2*, 319.
- (3) Hamblin, G. D.; Carneiro, K. M.; Fakhoury, J. F.; Bujold, K. E.; Sleiman, H. F. *J. Am. Chem. Soc.* **2012**, *134*, 2888.
- (4) Hamblin, G. D.; Rahbani, J. F.; Sleiman, H. F. Nat. Commun. 2015, 6.
- (5) Hariri, A. A.; Hamblin, G. D.; Gidi, Y.; Sleiman, H. F.; Cosa, G. *Nat. Chem.* **2015**, *7*, 295.

- (6) Duzdevich, D.; Redding, S.; Greene, E. C. Chem. Rev. **2014**, 114, 3072.
- (7) Travers, A. Philos. *Trans. R. Soc. A* **2004**, *362*, 1423.
- (8) Gaudier, M.; Schuwirth, B. S.; Westcott, S. L.; Wigley, D. B. *Science* **2007**, *317*, 1213.
- (9) Jones, S.; van Heyningen, P.; Berman, H. M.; Thornton, J. M. *J. Mol. Biol.* **1999**, 287,

877.

- (10) Gu, H.; Yang, W.; Seeman, N. C. J. Am. Chem. Soc. **2010**, 132, 4352.
- (11) Endo, M.; Sugiyama, H. Acc. Chem. Res. 2014, 47, 1645.
- (12) Johnson-Buck, A.; Nangreave, J.; Jiang, S.; Yan, H.; Walter, N. G. *Nano Lett.* **2013**, *13*, 2754.
- (13) Pinheiro, A. V.; Nangreave, J.; Jiang, S.; Yan, H.; Liu, Y. ACS Nano **2012**, 6, 5521.
- (14) Ngo, A. T.; Karam, P.; Fuller, E.; Burger, M.; Cosa, G. *J. Am. Chem. Soc.* **2008**, *130*, 457.
- (15) Ulbrich, M. H.; Isacoff, E. Y. *Nat. Methods* **2007**, *4*, 319.
- (16) Casanova, D.; Giaume, D.; Moreau, M.; Martin, J.-L.; Gacoin, T.; Boilot, J.-P.; Alexandrou, A. *J. Am. Chem. Soc.* **2007**, *129*, 12592.
- (17) Yurke, B.; Turberfield, A. J.; Mills, A. P.; Simmel, F. C.; Neumann, J. L. *Nature* **2000**, 406, 605.
- (18) Dietz, H.; Douglas, S. M.; Shih, W. M. Science **2009**, 325, 725.
- (19) Han, D.; Pal, S.; Nangreave, J.; Deng, Z.; Liu, Y.; Yan, H. *Science* **2011**, *332*, 342.
- (20) Wei, B.; Ong, L. L.; Chen, J.; Jaffe, A. S.; Yin, P. Angew. Chem. **2014**, 126, 7605.
- (21) Birac, J. J.; Sherman, W. B.; Kopatsch, J.; Constantinou, P. E.; Seeman, N. C. *J. Mol. Graph. Modell.* **2006**, *25*, 470.

Introduction to Chapter 3

Chapter 2 describes the synthesis of dynamic DNA nanotubes made up of 11 unmodified strands. The construct relies exclusively on DNA base-pairing for structure generation. However, introducing other supramolecular interactions can significantly expand the structural and functional range of DNA assemblies. In chapter 3, we report an economic strategy to build DNA nanotubes functionalized with polymers containing long alkyl chains. When these chains are linked to the nanotube via a flexible spacer, they interact together on the inside of the nanotube to create a hydrophobic environment; the nanotube can then encapsulate small molecules and conditionally release them when a specific DNA strand is added, as monitored by single-molecule fluorescence microscopy. When the alkyl chains in the amphiphiles are directly linked to the nanostructure without spacers, they interact intermolecularly to form a large network of DNA bundles. This morphological switch can be directly observed using a strand displacement strategy. The two hydrophobic association modes result in very different cellular uptake behavior. Amphiphilic nanotubes with intramolecular association show a fibrillar pattern inside cells with mitochondrial co-localization. On the other hand, the intermolecularly connected bundles disassemble into smaller alkyl coated nanostructures that slow down and reduce the extent of nonspecific cellular uptake, and result in a punctate intracellular pattern. In addition to uncovering structural parameters to direct the hierarchical assembly of nanostructures intra- or intermolecularly, this approach produces materials that will be useful for applications as selective drug delivery vehicles.

Chapter 3:

Tube-like versus bundle-like DNA Nanostructures: Towards New

Platforms for cellular Delivery and Guest Encapsulation

Author Contributions: Chidchob P. carried out all the TIRFM experiments. Dr. Vengut-Climent E. performed confocal microscopy and serum stability assays. Trinh T. helped in the synthesis of few strands. Gidi Y. performed the analysis on the TIRFM images.

3.1 Introduction

Well-defined DNA nanostructures that rely on Watson-Crick base-pairing have been adopted in growing technologies such as nanoelectronics, ^{1,2} biophysics^{3,4} and nanomedicine^{5,6}. The invention of DNA origami, for instance, has enabled the assembly of two- and three-dimensional nanometer-sized objects with unprecedented nanoscale precision. 8-10 While DNA nanotechnology offers remarkable structural control, it is inherently limited by the four-letter genetic code. Ongoing efforts have focused on incorporating synthetic materials into DNA nanostructures in order to introduce orthogonal modes of assembly. 11,12 This approach has been employed to generate complex and functional systems such as DNA cage assemblies, 13,14 DNA sandwiched structures, 15 and hydrophobic spherical nucleic acids 16-20 for drug delivery applications (Figure 3.1). In particular, synthetic hydrophobic insertions can trigger the assembly of higher-order assemblies and improve their stability in cells among many other advantages.^{21,22}

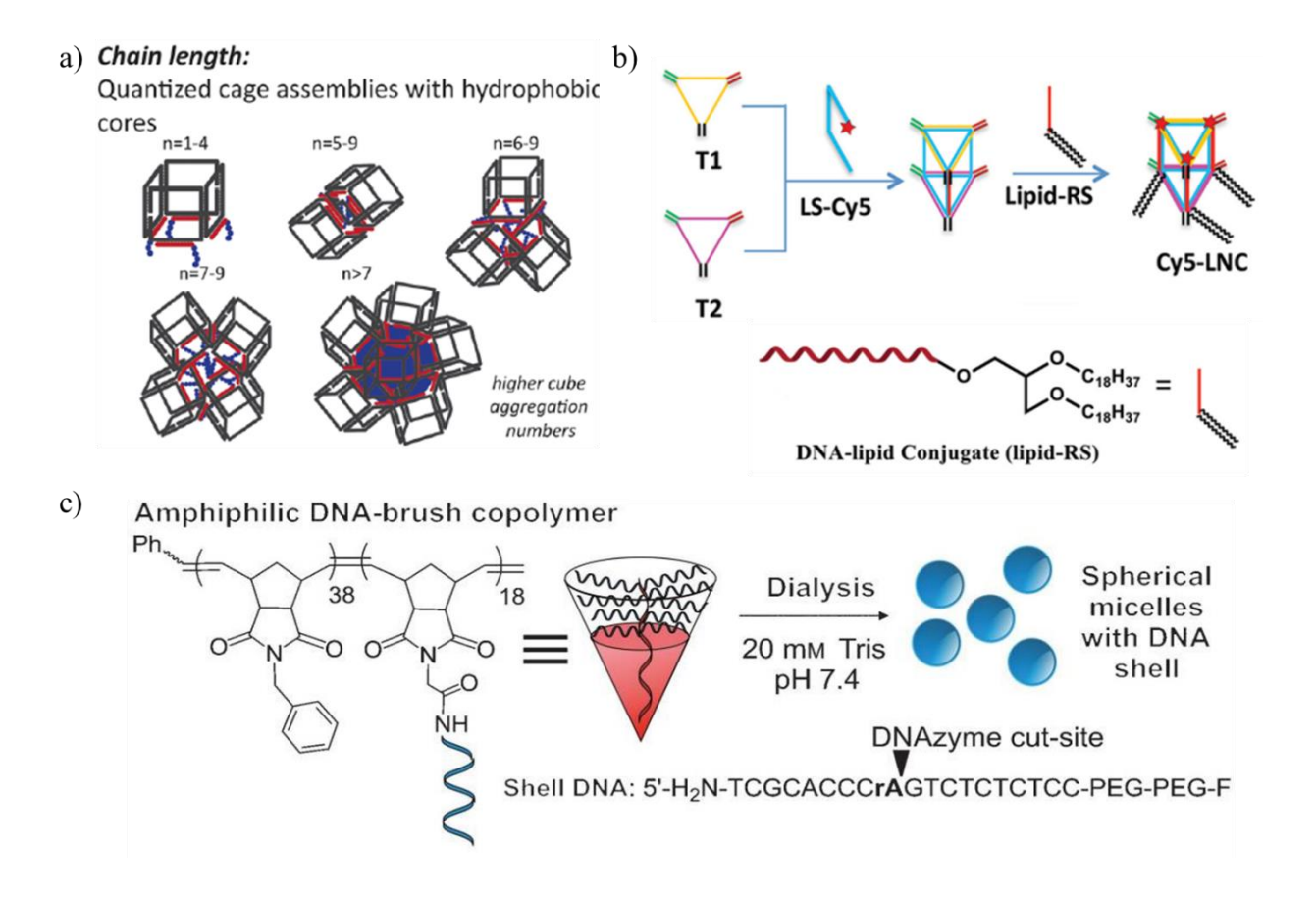


Figure 3.1. (a) Scheme illustrating the effect of alkyl chains lengths on the assembly of DNA nanocages. As the number hydrophobic repeats increases, as the number of cubes aggregating increases. Adapted with permission from reference 14 (ACS Publishing, 2016) (b) Scheme displaying the formation of Cy5-labeled lipid-functionalized DNA nanocage (Cy5-LNCs). Adapted with permission from reference 21 (Wiley-VCH, 2016) (c) Assembly of DNA copolymers into micelles. Adapted with permission from reference 18 (Wiley-VCH, 2010).

Inspired by protein folding such as in coiled-coil motifs and helical bundles, we would like to design DNA modules that hierarchically assemble via base-pairing and hydrophobic interactions in a predictable manner. These higher-order structures can also possibly modulate cellular uptake behavior. Here, we report the assembly of DNA nanotubes with a switchable hydrophobic environment that can encapsulate guest molecules. In this design, a DNA spacer between the alkyl chains and the region hybridized to the nanotube allows the chains to meet on the inside of this

structure, resulting in an internal hydrophobic space. We use single-molecule fluorescence to monitor small molecule guest encapsulation, conditional release of these molecules via strand displacement, and their re-encapsulation upon restoring the hydrophobic pocket.

On the other hand, when the DNA amphiphiles lack a spacer between the alkyl chains and the region hybridized to the tube, the hydrophobic association switches from intramolecular to intermolecular, resulting in a one-dimensional network observed with atomic force microscopy (AFM). To understand this switching mechanism, we start with the nanotube with the intramolecular hydrophobic handshake, and we use strand displacement to progressively replace the spacer-containing amphiphilic strands with their non-spacer counterparts. A simple molecular spacer can thus switch the morphology from DNA nanostructures with an internal 'handshake' of the alkyl chains, to an external interaction that brings nanostructures together into 1D-networks.

DNA architectures are uniquely positioned as drug delivery vehicles. Their size and shape are precisely controlled, they can be monodisperse, nuclease resistant, and they can selectively respond to numerous external stimuli.²³⁻²⁷ Functionalization of DNA nanostructures with hydrophobic domains can modify their cellular delivery profile, and allows them to carry small molecule therapeutics, beyond those that directly bind to DNA (such as Doxorubicin). ²⁸⁻³³ Here, we compare the cellular uptake behavior of the individual tubes containing hydrophobic pockets with that of the intermolecularly associated 1D-networks.

When the alkyl chains are engaged in an intramolecular handshake, dye-mediated co-localization with mitochondria is observed, suggesting dissociation of the dye-labelled strand from the structure. This behavior is similar to that of bare nanotubes without lipidic chains. On the other hand, the 1D-bundles with intermolecular hydrophobic association disassemble into alkyl coated smaller nanostructures in physiological conditions. These structures slow down and reduce the

extent of non-specific strand uptake, and result in punctate intracellular fluorescence. Thus, both the presence of alkyl chains and their ability to result in an intramolecular interaction profoundly influence cellular uptake of their strands.

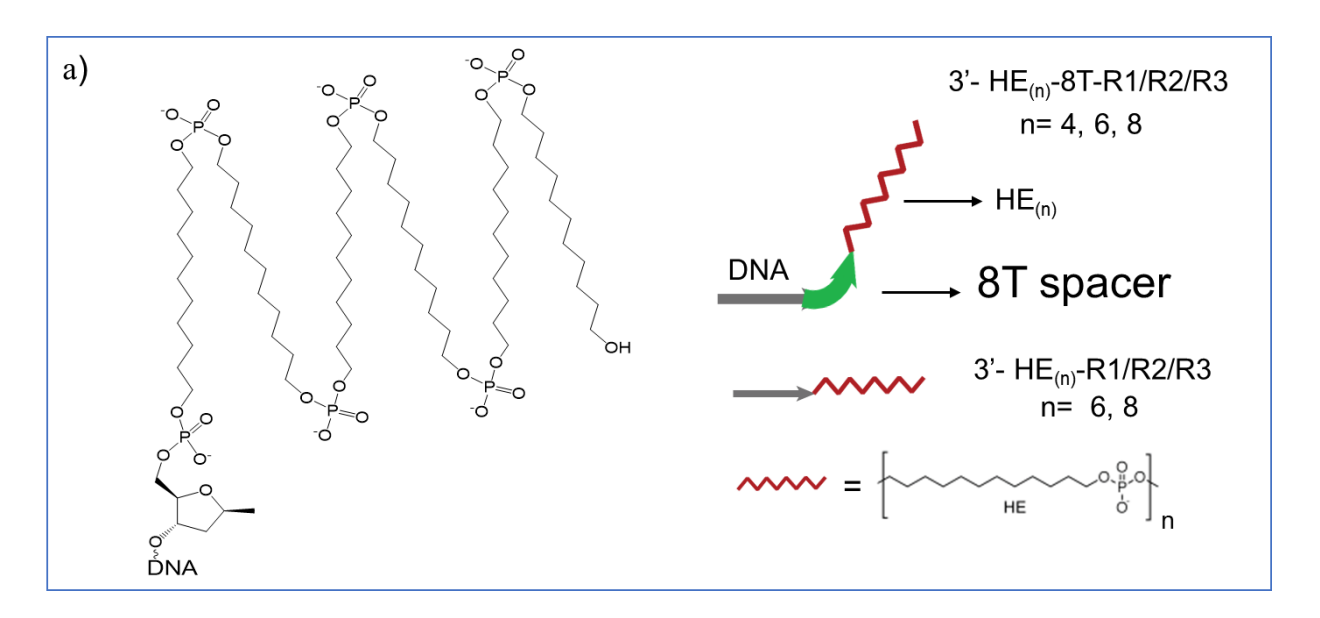
3.2 Results and Discussions

3.2.1 Self-Assembly of DNA Nanotubes with Hydrophobic Microenvironment

A significant consideration in our method is to generate DNA conjugates with a hydrophobic domain, while still allowing the capability of the DNA component to hybridize efficiently. We used amphiphilic DNA-polymer conjugates (R1-R3 and LS1- LS3) that are monodisperse and precisely defined in number of alkyl units. These were prepared in high yield on an automated synthesizer, by sequentially coupling long C12 chains (hexaethylene or HE) to the 3'- or 5'-end of DNA via phosphoramidite chemistry (Figure 3.2, please refer to the experimental section for more details). Commercially available C12 monomer containing DMT on one end and a phosphoramidite on the other was used (Figure 3.2).

The DNA nanotubes are based on a triangular core unit 'rung' (Figure 3.2) and 3 sets of linking strands (Figure 3.3, left). Briefly, the synthesis of the nanotubes starts by assembling the rung from 3 unmodified strands that define the triangular region, and 3 rigidifying strands R1-R3 (Figure 3.2). R1, R2, and R3 are amphiphilic: they possess a DNA region that binds to the triangular unit, and a hydrophobic domain consisting of 6 HE units attached on the 3' end. In rung A, there is an 8T (thymidine) DNA spacer between the binding region and the HE units, while in rung B, the HE units are directly attached to the binding region without a spacer. Modeling this strand shows that the alkyl component should be oriented to the exterior of the rung in the absence of a spacer. (Figure 3.2 and experimental section for more details on the design). At concentrations of 75 nM

or lower, the rungs assembled cleanly upon annealing from 95 to 4°C (Figure 3.2). Higher concentrations resulted in the formation of higher-order products, likely because of intermolecular hydrophobic interactions between the rungs (Figure 3.11).



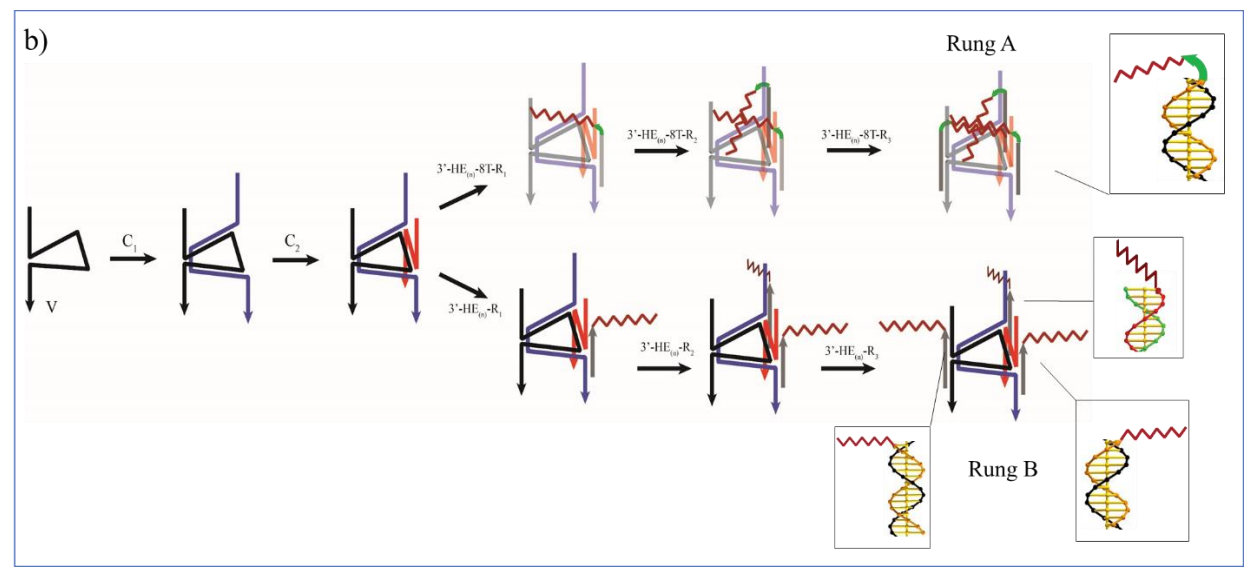


Figure 3.2. (a) Sequential coupling of the alkyl chains to DNA. Chemical structure of the hydrophobic unit (Hexaethylene). HE units were attached to DNA with or without 8T spacers. (b) Scheme illustrating the self-assembly of rungs A and B with the corresponding DNA amphiphiles R1, R2 and R3.

In addition to the hydrophobic domains in the rungs, we designed the linking strands between the rungs so that they also possess hydrophobic units, again with and without 8T spacers (Figure 3.3). To have the nanotube, we sequentially added the first linking strand (LS1) with its complementary amphiphile strand with an annealing step (from 56 to 22°C for 1 hour). This pre-organizes the rungs on top of one another and prevents crosslinking. Finally, the amphiphilic linking strands LS2 and LS3 were added while heating the solution (from 44 to 22°C for 45 min.). The hydrophobic units on the rung R(1-3) and those on the linking strands LS(1-3) are separated from one another by a relatively long stretch of DNA (36 bp between R1 and LS1 and 32 bp for between R2/3 and LS2/3), in order to minimize undesirable hydrophobic interactions during assembly.

We first studied the assembly of the amphiphilic nanotubes in in which 8T spacers separate the hydrophobic unit from the nanotube binding region. Tubes A6, where the amphiphiles possess 6 hexaethylene units, were deposited on a freshly cleaved mica surface. Figure 3.3 shows the assembly of individual tubes with a mean length value of ~870 nm and lengths up to 1.5 μm. AFM micrographs did not reveal any apparent intermolecular hydrophobic interactions between the alkyl moieties on the nanotubes. Instead, the 8T spacers most likely allow the hydrophobic alkyl chains to participate in an intramolecular 'handshake' inside the tube cavities, thus creating internal hydrophobic environments down the tube's length (see below for further evidence).

The micellar environment produced in tubes **A6** is expected to encapsulate hydrophobic small molecules. This phenomenon was studied in situ by using single molecule total internal refection fluorescence microscopy (smTIRFM). The DNA nanotubes were fluorescently labelled with Cy5 at the 5'-end of one of its rigidifying strands (**R1**). Then, the tubes were incubated with a solution

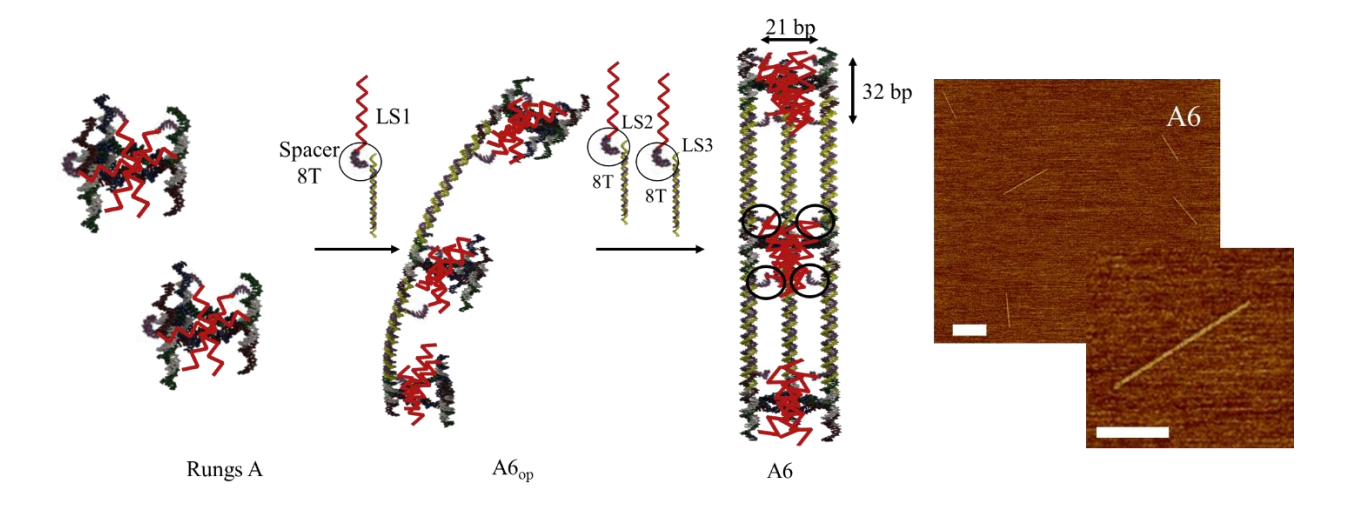


Figure 3.3. Left: schematic illustrating the assembly of nanotubes with hydrophobic pockets. Right: AFM micrographs displaying the formation of individual nanotubes, scale bar 500 nm.

of Nile Red overnight (SI section V) and then surface immobilized using biotin-streptavidin interactions. (Figure 3.4a).

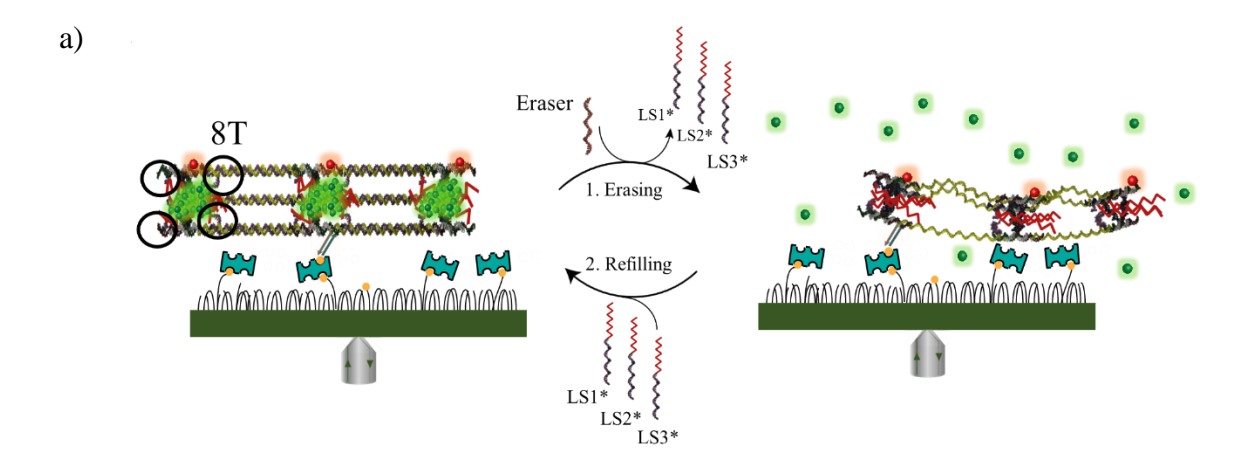
Nile Red is weakly emissive in aqueous solutions, but intensely fluorescent when excited at 532 nm in a hydrophobic environment.^{34,35} Panels 1 and 2 in Figure 3.4 illustrate the high spatial colocalization of the internal marker Cy5 and the Nile Red molecules, consistent with the self-assembly of tubes **A6** with a hydrophobic pocket containing Nile Red molecules in their repeating units.

Using amphiphilic strands with 10-base overhangs, we examined the ability of the nanotubes to release their cargo. The addition of fully complementary erasing strands is expected to remove the amphiphilic linking strands by strand displacement (Figure 3.4, we use a flow cell and each addition step is followed by washing).³⁶ The erasing process leads to the formation of three sides single-stranded tubes containing only 3 hydrophobic regions within the rungs. Single molecule

TIRFM imaging of these nanotubes showed multiple emissive spots in the Cy5 channel, consistent with preservation of the nanotube's integrity.³⁷ However, dim emission was detected in the green channel (Nile Red) after 10 min (panel 4 in Figure 3.4a). This is consistent with release of the hydrophobic guest molecules from the nanotube upon disrupting the micellar environment.

Finally, we re-added the amphiphilic linking strands with spacers (LS1-3s*), thus recreating a hydrophobic environment. When incubated with Nile Red for 30 min, followed by extensive washing, the Nile Red emission from tubes A6 was recovered and significantly co-localized with the emission of the Cy5 dye. That the nanotubes released their Nile Red load upon addition of invading strands to next gain it back once the amphiphilic linking strands with spacers were annealed in the presence of Nile Red, may be also observed from correlation plots in Figure 3.4c. Here the Nile Red emission intensity for every single nanotube (a particle showing both Cy5 and Nile Red emission) was compared before and after adding the eraser strand (Figure 3.4c) and before adding the eraser strand and after adding the eraser strand and refilling. While the former correlation shows that the emission of every particle dropped to close to zero when the eraser strand is added, the latter correlation shows that the emission was restored after refilling. In this second case (Figure 3.4c) the intensity before and after refilling is similar, as may be observed from the slope of the correlation.

The successful sequential erasing-refilling step on single particles illustrated via TIRFM experiments demonstrates that our design can reversibly encapsulate and release small molecules in response to site-specific hybridization events along the repeating units of the nanotube. The experiment underscores the potential application of this and related structures for targeted drug delivery.



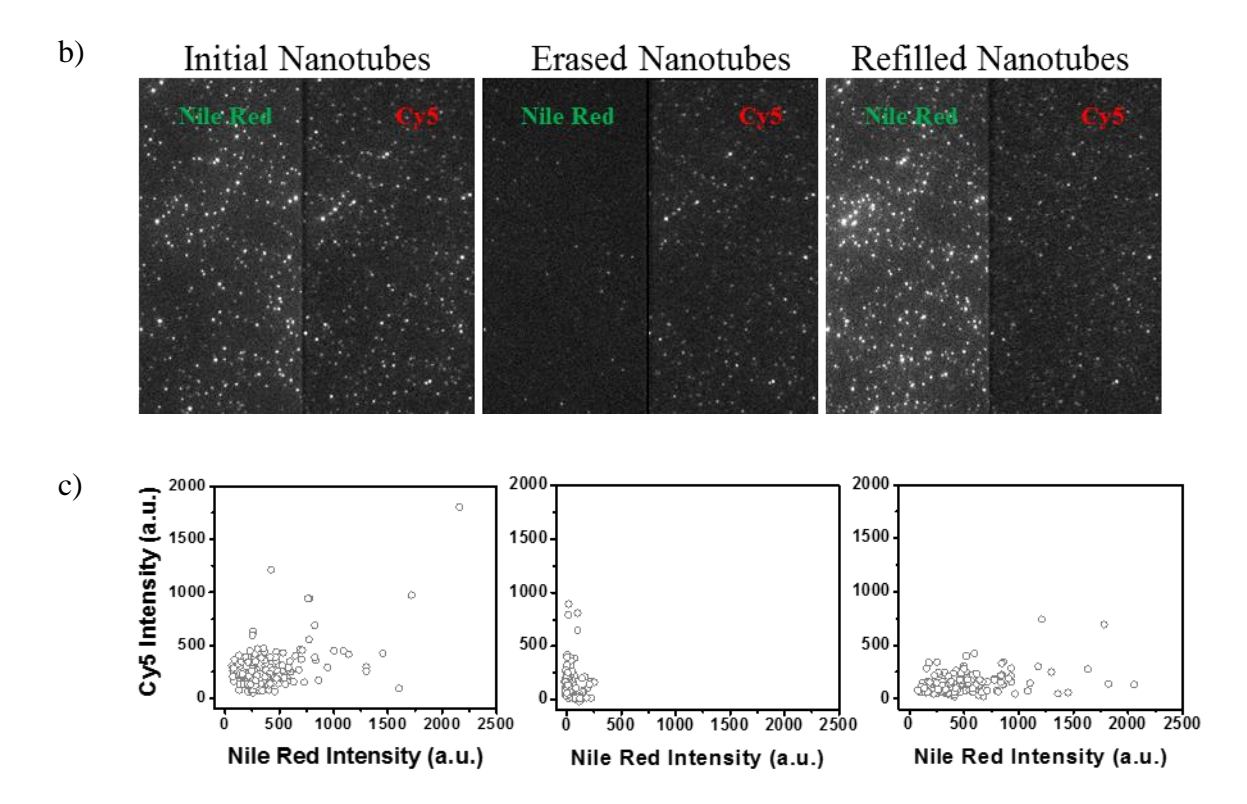


Figure 3.4. Typical TIRFM images of surface-bound Cy5 labeled nanotubes using biotin-streptavidin interactions. (a) Schematic showing the removal of three DNA amphiphiles strands by strand displacement and their readdition. (b) Series of TIRFM images (70 μm × 35 μm²) depicting the co-localization of Cy5 and Nile Red in the original tube A6 (panels 1 and 2). The removal of 5'-(HE)_n-8T-LS1* and 5'-(HE)_n-8T-LS2/3* causes the disappearance of the Nile Red fluorescence signal on the green channel (panel 4), while the Cy5 fluorescence is still detected (panel 3). The emission of Nile Red was detected again upon adding the DNA amphiphiles (panel 6) and is co-localized with Cy5 emission (panel 5). (c) Green and red intensity correlation obtained for each step. TIRFM was performed by Chidcob P. and the analysis by Gidi Y.

3.2.2 Self-Assembly of DNA Bundles with Hydrophobic Patches

In the next set of experiments, we removed the spacers from the 6 DNA amphiphile strands and attached the C12 units directly to the DNA regions hybridized to the rungs and linking strands. The absence of spacers is expected to orient the hydrophobic portions to the outside of the rungs, and decrease the possibility of forming a micellar environment upon the addition of LS1-3. We first characterized the assembly of bundles B6, prepared at 75 nM, via dry/liquid AFM, then we carried out another set of experiments to examine the bundles at higher concentrations (See section 3.4.5). The AFM micrographs in Figure 3.5 did not reveal any monomoric nanotube. Instead, large continuous networked bundles that extend into multiple microns were observed. We next imaged B6 under liquid conditions to verify that the observed structures are not artifacts due to surface drying. The AFM micrographs in Figure 3.5 depict the formation of long bundles that are similar to the images observed under dry conditions. Therefore, we believe that the assembly of these large features is driven by 2 forces: (i) the intermolecular hydrophobic interactions between the amphiphilic rungs and the amphiphilic linking strands and (ii) Watson-Crick base-pairing between the same entities. However, it is most likely that these rungs started to aggregate randomly after the addition of LS1 only (Figure 3.16), thus hindering the formation of individual tubes properly. We were also interested in determining whether these bundles were able to encapsulate small molecules (Figure 3.5c). We thus carried out fluorescence ensemble measurements of the tubes A6 and bundles B6, each incubated with the same amount of Nile Red, using a microplate reader. Interestingly, samples B6 encapsulated Nile red with a higher capacity than the single tubes A6 at the same concentration. This observation can be attributed to the larger volume of hydrophobic environment present in bundles allowing them to retain more small molecules.

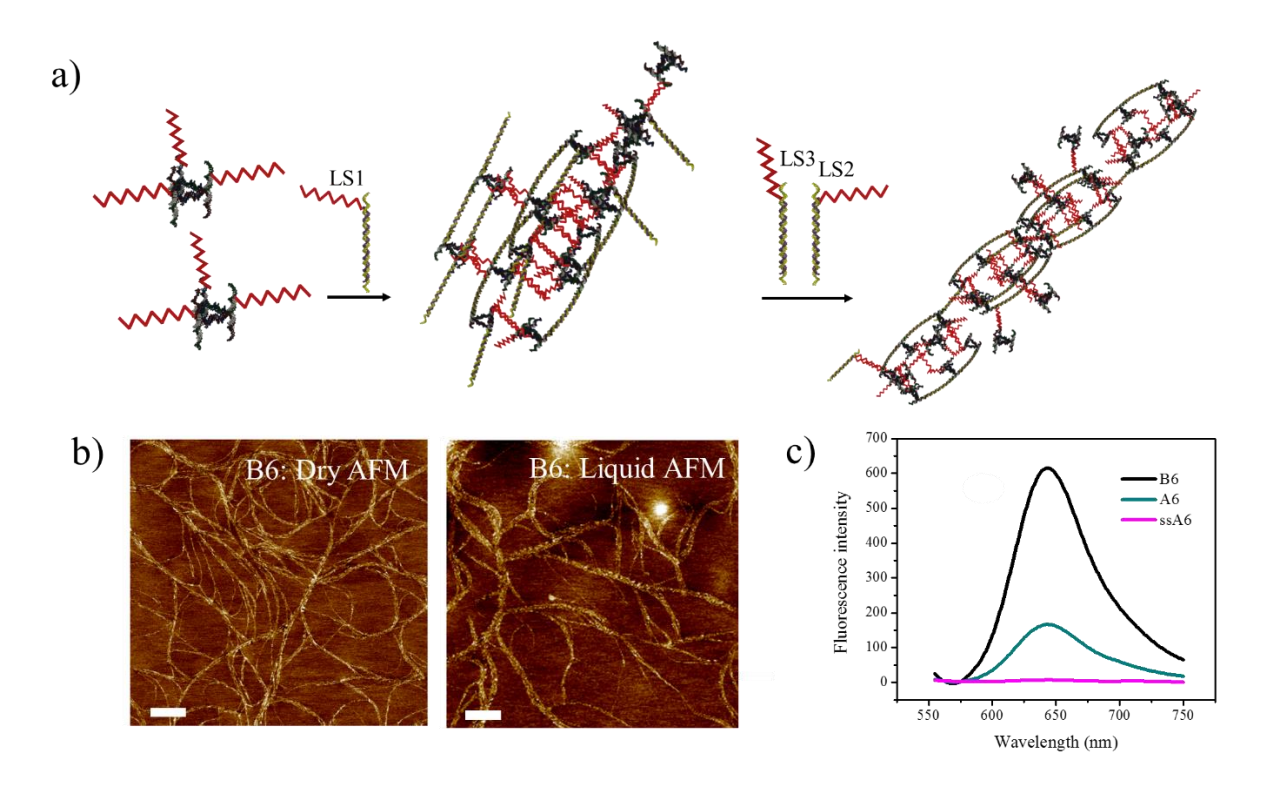


Figure 3.5. (a) schematic illustrating the assembly of a network of DNA nanostructures with hydrophobic regions. (b) dry and liquid AFM micrographs displaying the formation of these large networks, scale bar 500 nm. (c) Emission spectra of Nile Red encapsulated within the hydrophobic pockets of A6, B6, and single-stranded A6.

3.2.3 Effect of Alkyl Chain Lengths on the Assembly of Nanotubes and Bundles

Following the same strategy detailed in section 3.2.1, we sequentially added the first set of linking strands while annealing the mixture from 56 to 22°C for 1 hour. Then we added LS2 and LS3 while annealing the mixture from 44 to 22°C for 45 min. Herein, we conjugated the 5'- end of the complementary strands of LS1 (LS1*), LS2 and LS3 (LS2/3*) with 4, 6 and 8 HE units. 4 µL of the nanotubes at a concentration of 75 nM (concentration of each of the component strands) in filtered 1×TAMg were deposited on freshly cleaved mica then incubated for at least 1 hour under vacuum.

We first studied the assembly of the amphiphilic nanotubes in which 8T spacers separate the hydrophobic unit from the nanotube binding region. Tubes A6-4, A6-6 and A6-8, where the amphiphiles possess 4, 6, and 8 hexaethylene units respectively, were deposited on a freshly cleaved mica surface. Figure 3.6 shows the assembly of individual tubes with lengths up to 1.5 µm. AFM micrographs did not reveal any apparent intermolecular hydrophobic interactions between the alkyl moieties on the nanotubes. Instead, the 8T spacers most likely allow the hydrophobic alkyl chains to participate in an intramolecular 'handshake' inside the tube cavities, thus creating internal hydrophobic environments down the tube's length. Interestingly, increasing the length of the alkyl chains did not affect much the morphology of the tubes.

In the next set of experiments, we removed the spacers from the 6 DNA amphiphile strands and attached the C12 units directly to the DNA regions hybridized to the nanotubes. Figure 3.5 displays the AFM micrographs of bundles B6-6 (with 6 HE units on each amphiphile). Here we are showing two AFM images of bundles B6-8 (with 8 HE units on each amphiphile) under dry and liquid conditions. Figure 3.7 depicts the formation of large DNA bundles that extend into multiple microns similar to the ones shown in Figure 3.5. The size of the hydrophobic chains in this case (B6-6 vs. B6-8) does not seem to create a major difference between the two samples.

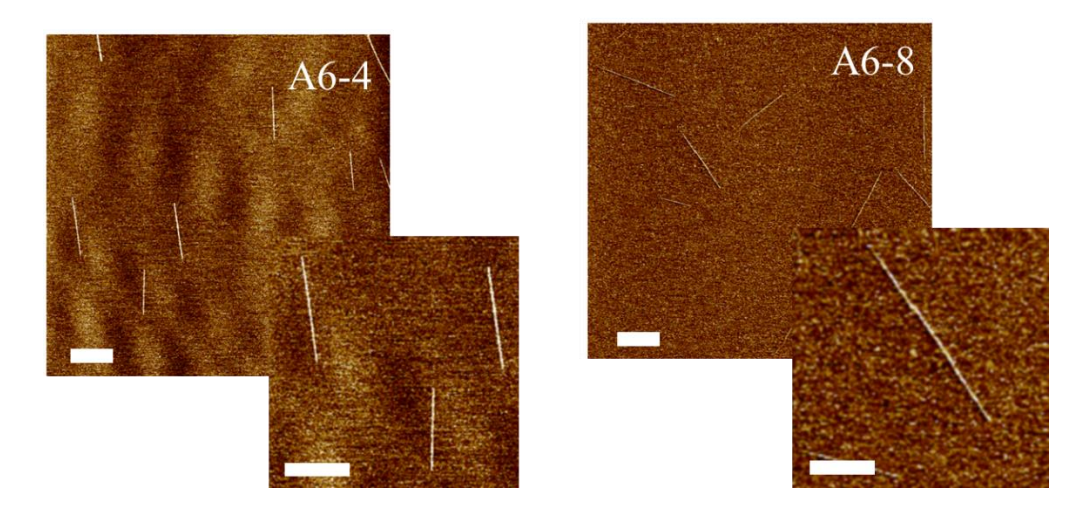


Figure 3.6. AFM micrographs displaying the formation of individual nanotubes, scale bar 500 nm. A6-4 and A6-8 are the fully formed nanotubes with 4 and 8 HE repeats per polymer chain.

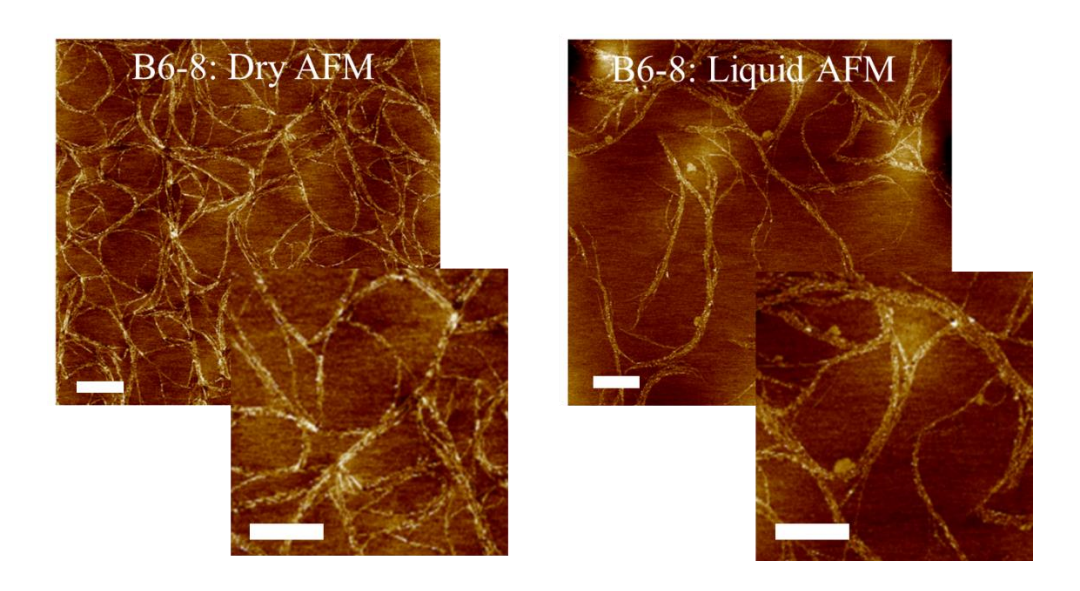


Figure 3.7. Dry and liquid AFM micrographs displaying the formation of large networks of DNA nanostructures, scale bar 500 nm.

3.2.4 Self-Assembly of DNA Nanotubes and Bundles at Higher Concentrations

Our triangular core involves the equimolar assembly of 6 DNA strands (V: 113 bases, C1: 84 bases, C2: 63 bases and R1, R2 and R3: 22 bases) with a final concentration ranging from 75 to 400 nM in 1×TAMg as shown in Figure 3.8. To the 3' end of the rigidifier strands R1, R2 and R3, 4, 6 or 8 HE units were directly attached (rung B) or 8T spacers were added first followed by the attachment of the HE units (rung A). As detailed in the first section, without the spacers, the orientation of the alkyl chains prohibits their intramolecular interaction. However, the introduction of the 8T spacers provides the HE units enough rotational freedom to meet. In the following set of gel electrophoresis experiments, we study the maximum concentration at which both rungs are still

able to self-assemble in high yields without inducing higher order structures. We found that at this low concentration, the assembly of the rungs A and B is not affected by the addition of the hydrophobic chains. Compared to the formation of the control rung unit, which is made up of 6 unmodified DNA strands, only discrete and clean bands appeared for all types of rungs. On the other hand, at 400 nM, the bands resulting from rungs A and B were smeared and other non-penetrating bands started to appear on the wells of the gel (Figure 3.8). We think that above 75 nM, the assembly of the rungs occur above the critical micelle concentration (CMC) of the DNA amphiphiles. Hence, high order structures are likely to grow due to the hydrophobic interaction between the alkyl chains.

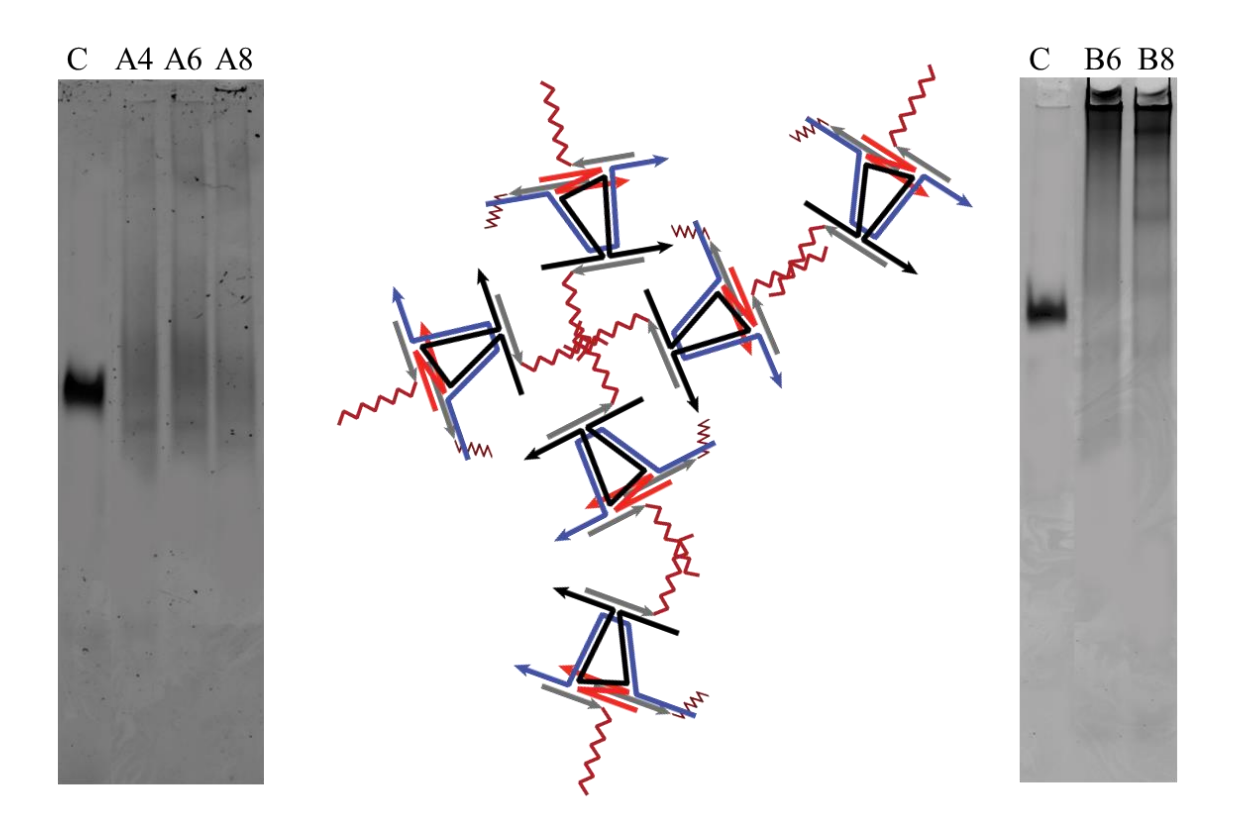


Figure 3.8. 6% PAGE showing the assembly of rungs A and B at 400 nM. C represents the rung with unmodified 6 strands as a control.

At a concentration of 75 nM, only individual structures were imaged on the surface for tubes A6-4, A6-6 and A6-8 with a typical height between 1 and 2 nm. However, we observed a network

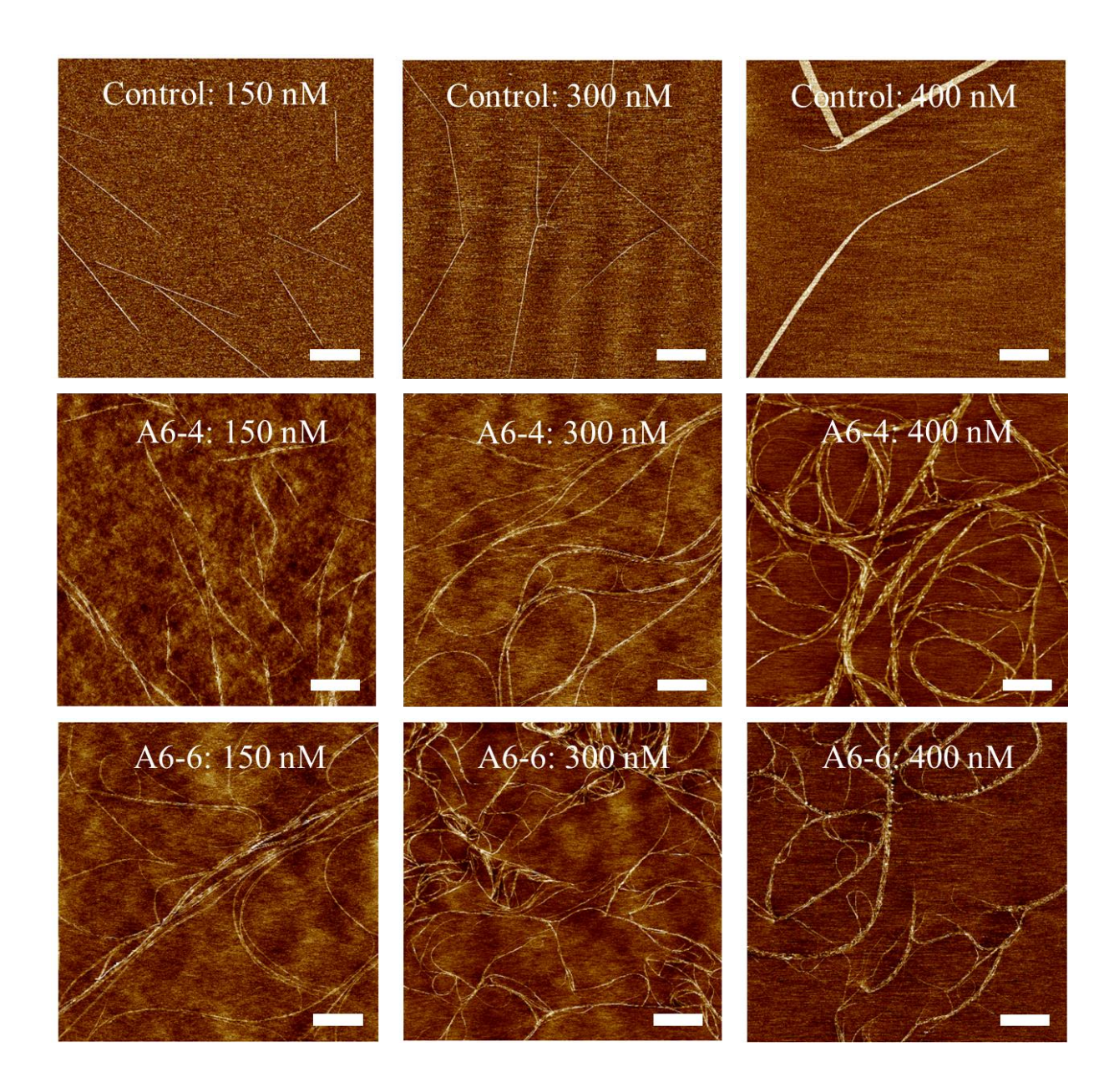


Figure 3.9. Dry AFM micrographs showing the formation of a large network of DNA nanotubes even in the presence of spacers, scale bae 500 nm. Unmodified DNA nanotubes tend to form more rigid and organized bundles at high concentrations.

of DNA fibers when we deposited tubes B6-6 and B6-8 on the mica surface (Figure 3.5 and 3.7). In this section, we visualize the behavior of our constructs under more concentrated conditions (up to 400 nM). Figure 3.9 displays the development of bundles for tubes A6-6 at 150, 300 and 400 nM compared to the original nanotubes where no alkyl chains were incorporated (control). In the absence of hydrophobic units, the nanotubes tend to aggregate at high concentrations into long and straight bundles on the mica surface. The control experiment demonstrates that the network of DNA nanotubes we previously observed is most likely due to the hydrophobic character introduced to the original design. As explained previously, rung A itself starts to form higher-order assemblies at higher concentrations. Therefore, the growth of individual nanotubes becomes more challenging and a network of DNA structures is formed instead. Note that the width of the bundles increases consistently with increasing the concentration of the constructs. Yet, no major differences were observed based on length of the alkyl chains.

The effect of concentration on the assembly of the bundles was also investigated for tubes B6-6 and B6-8. Figure 3.10 depicts the aggregation of DNA nanotructures into large bundles with respect to the concentration of the component strands. Again, the length of the hydrophobic units did not induce severe morphological changes on the mica surface. However, at high concentrations, both tubes B6-6 and B6-8 generate thicker bundles of mostly 90 nm in width.

3.2.5 Step by Step Assembly of Nanotubes and Bundles

In order to better understand the assembly of these amphiphilic nanotubes and bundles, we visualized the intermediate, open form of the tubes A6op and B6op (before the addition of LS2 and LS3) by AFM on mica. Individual small tubes up to 300 nm were observed in the case of tubes

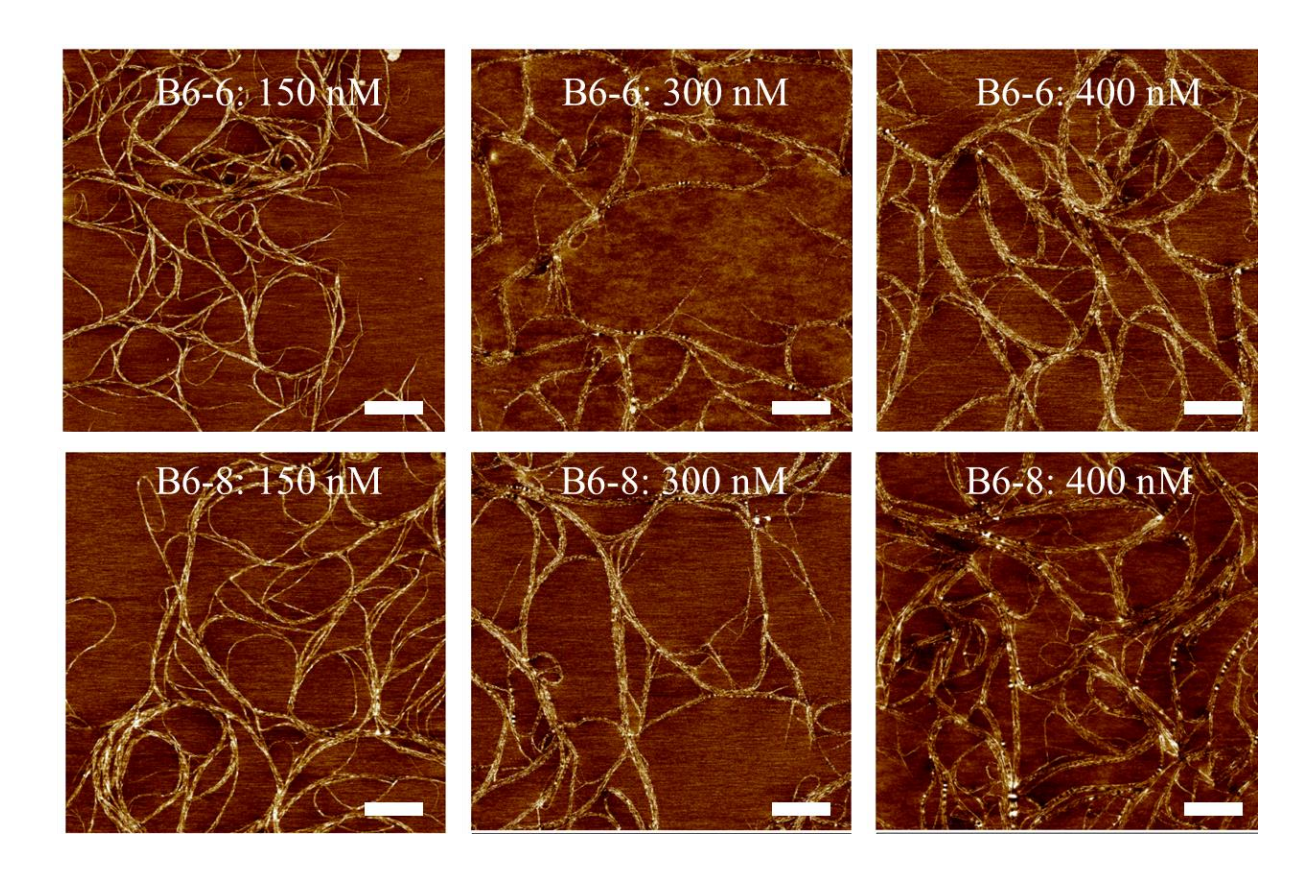


Figure 3.10. Dry AFM micrographs showing the formation of a large network of DNA nanotubes, scale bae 500 nm.

 $A6_{op}$, and aggregates were absent (Figure 3.11). These observations are consistent with the assembly of short structures upon addition of a single set of linking strands, followed by elongation when the nanotube is fully formed. In this open structure, the alkyl chains of R1 and chains of R1 and LS1 are likely interacting intramolecularly. However, unlike $A6_{op}$, the results demonstrate the assembly of intermediate-size bundles instead of small individual open tubes for tubes $B6_{op}$. (Figure 3.11) Thus, the intermediate open tubes undergo intermolecular hydrophobic aggregation prior to their closure with LS2 and LS3 and their elongation.

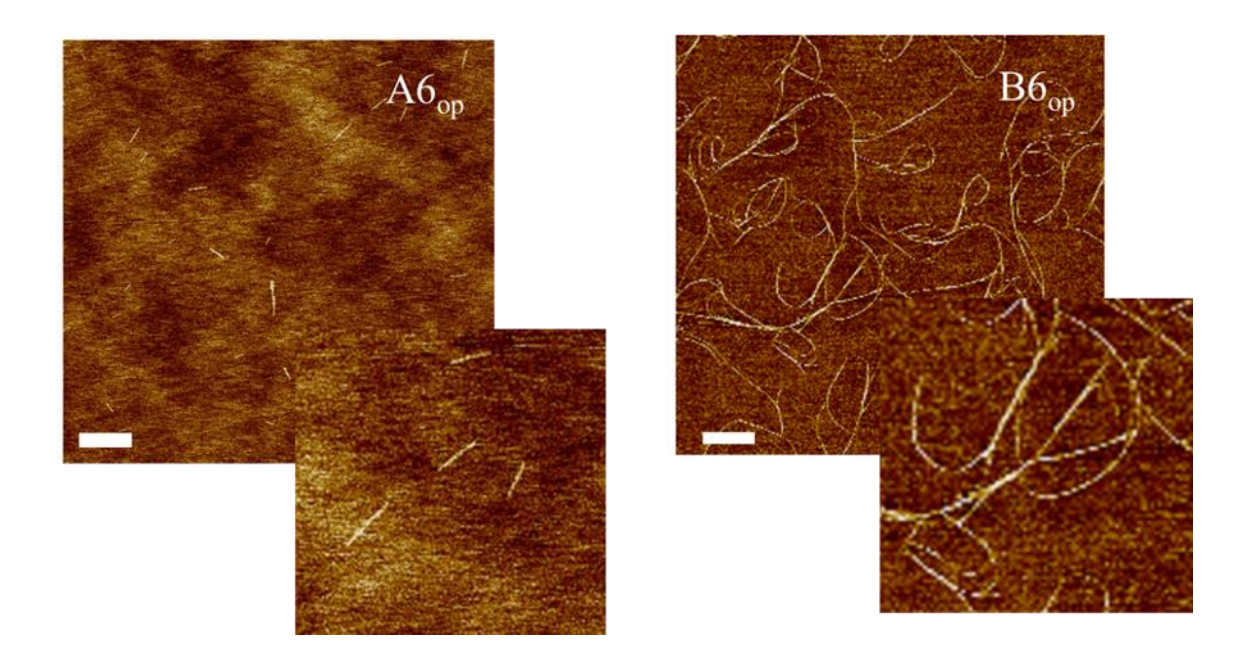


Figure 3.11. AFM micrographs displaying the formation of individual nanotubes and bundles, scale bar 500 nm. A6op and B6op are the intermediate structures before the addition of LS2 and LS3 (6 HE repeats in the polymer).

3.2.6 Conversion from Nanotubes to Bundles

To gain insight on the mechanism of hydrophobic association, we attempted to generate the bundles **B** directly from individual tubes **A** by strand displacement. We were interested in answering the question: what is the minimum number of non-spacer DNA amphiphile strands needed to switch the morphology of the tubes from intra-, to intermolecular?

Starting from A6 with intramolecular handshake, the first amphiphilic strand LS1_s*, containing the 8T spacer was removed by strand displacement, and replaced by strand LS1_{ns}* that lacked the spacer, to form tube (A5)(B1) (Figure 3.12). Individual tubes were still observed with this single replacement. When the same was done for LS2_s* to give tube (A4)(B2), we saw long, straight tubes with some degree of crosslinking. Interestingly, when the third amphiphile LS3_s* was removed and substituted with LS3_{ns}*, we saw a dramatic change in morphology. The rigid tubes

were replaced by long, flexible aggregated bundles, similar to the morphology of **B6** (Figure 3.12). Thus, replacing 3 of the 6 amphiphilic strands with their non-spacer counterparts shifted the hydrophobic interactions from intra- to intermolecular. Interestingly, AFM of the intermediate (A3)(B2), partially single-stranded tube after displacement of the strand **LS3**_s* from (A4)(B2), but before addition of amphiphile strand **LS3**_{ns}*, also showed bundled features.

This dramatic morphological change from monomeric nanotube to flexible bundles is likely due to two factors. First, the hydrophobicity of the nanotube increases when its alkyl chains are no longer pointing to the inside, and thus its tendency to form intermolecular micellar aggregates increases. Second, the alkyl chains on the rung are no longer able to associate with those on the linking strands, thus weakening the cohesion between the nanotube units and aiding disassembly. Both factors contribute to rearrange the tube into hydrophobically associated micellar bundles. Native polyacrylamide gel electrophoresis shows that the intermediate structure (A3)(B3) disassembles into its amphiphilic rung components, confirming that it is composed of loosely held rungs and linking strands.

These strand displacement experiments thus create a kinetically controlled 'tug-of-war' between Watson-Crick base-pairing and hydrophobic intermolecular interactions. Base-pairing interactions on their own would result in an intact nanotube, and hydrophobic interactions favor rearranging the nanotube components into micellar bundles.

3.2.7 Effect of Magnesium Concentration on the Assembly of Bundles

In this section, we studied the disassembly of bundles (A3)(B3) and B6 under low Magnesium cations concentrations \leq 2.5 mM. Since the interaction between the alkyl chains is highly dependent on Mg²⁺, the addition of EDTA (between 10 to 12.5 mM) is expected to induce the disruption of

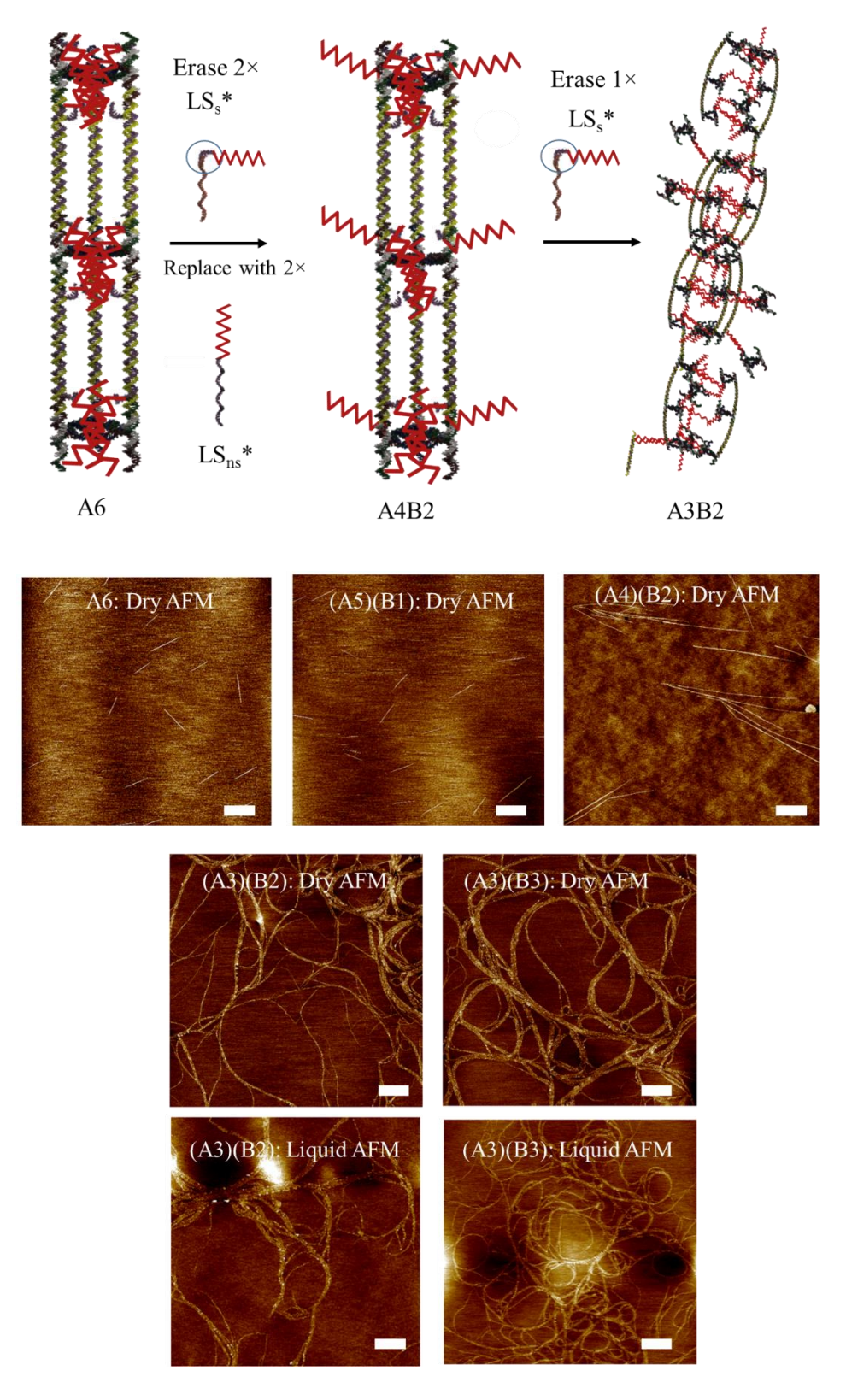


Figure 3.12. AFM characterization of the conversion of individual tubes to bundles, scale bar 500 nm.

the disruption of these bundles into smaller aggregates or nanostructures. The AFM micrographs in Figure 3.13 display this phenomenon where the majority of the features look like small aggregates of individual rungs. The results explain further our observations under confocal microscopy (section 3.2.7) for bundles B6 in which the uptake behavior of amphiphilic rungs B and bundles B6 were found to be similar. Moreover, the dramatic disassembly of bundles (A3)(B3) provides additional evidence that the intermolecular hydrophobic interaction between the C12 chains plays a crucial role in directing the Watson-Crick base-pairing. As such, we think that tubes (A3)(B2) might be partially falling apart and then coming together through these hydrophobic interactions instead of Watson-Crick base-pairing.

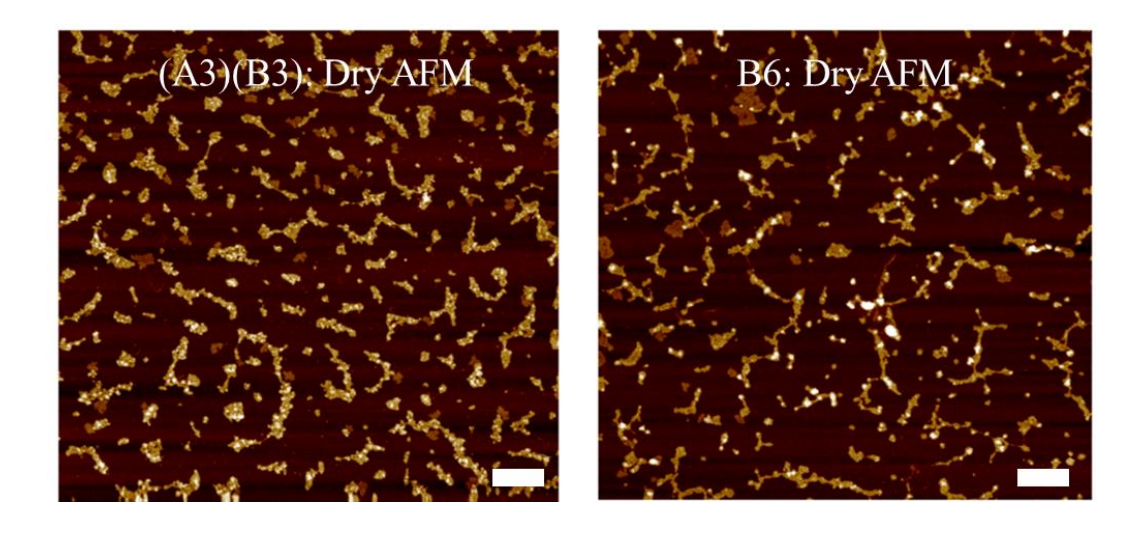


Figure 3.13. AFM characterization of the bundles at low concentrations of Mg²⁺, scale bar 500 nm.

We further followed the conversion from A6 to (A3)(B3) under the same conditions (all samples prepared at 75 nM). As expected, samples that produced tubes under AFM gave mainly non-penetrating bands via PAGE (lanes 1 and 2 in Figure 3.14). Similar to bundles B6 prepared at 75

nM, bundles (A3)(B2) and (A3)(B3) disassembled to smaller nanostructures under these experimental conditions. Hence, this gel demonstrates that bundles have higher chances to fall apart when we decrease the magnesium concentration in the solution. It also proves that the conversion from individual tubes to bundles is dependent on the number of alkyl chains contributing in the intermolecular hydrophobic interaction between the structures.

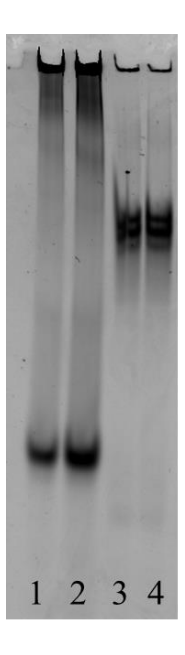


Figure 3.14. 6% PAGE displaying the integrity of the nanostructures at low Mg²⁺ concentrations. Nanotubes A6 prepared at 75 nM (lane 1), (A4)(B2) (lane 2), (A3)(B2) (lane 3) and (A3)(B3) (lane 4).

3.2.8 Cellular Uptake of Unmodified versus Amphiphilic Nanostructures

Knowing that nanostructures bearing amphiphilic molecules are expected to exhibit a distinct cellular uptake behavior, ^{28,38,39} we examined the uptake of the DNA nanotubes and bundles in human cervical cancer (HeLa) cells via confocal microscopy. Single-stranded rigidifier **R1** with a Cy5 dye on its 5'-end (**Cy5-R1**) showed uptake starting at ~2-6 hours (h), and after 24 h a fibrillar

pattern was observed (Figure 3.15 and 3.21). This filamentous pattern of cyanine dye-labelled oligonucleotides has been previously reported, and attributed to mitochondrial localization mediated by the dye.⁴⁰ When **Cy5-R1** was placed on the triangular rung or on nanotubes, we first observed aggregation of these structures, then disassembly of the aggregates accompanied with an increase in intracellular fluorescence at ~ 6-7 h. After 24 hours, the same fibrillar pattern was observed as the major population in cells (Figure 3.15 and 3.21). Thus, the **Cy5-R1** strand may be slowly dissociating from the bare rungs or nanotubes, producing a filamentous intracellular pattern.

Amphiphilic single-stranded **Cy5-R1-HE**₆, 5'-labelled with Cy5 and 3'-labelled with hydrophobic chains showed a similar intracellular fibrillar pattern as **Cy5-R1**. Interestingly however, when three such amphiphilic strands were placed on the rung (rung **A** or **B**), a very different uptake profile was observed: an exclusively punctate fluorescence pattern accompanied with a slower internalization time~12 h and reduced intracellular fluorescence was noted (Figure 3.15 and 3.21), with no fibrillar structure formation. Punctate structures are typically associated with endosomal uptake. Thus, the amphiphilic rung is protecting the cyanine labelled strand, slowing down and reducing its non-specific cellular uptake. This is a desirable property if the structures are used for selective targeting of diseased cells (by attaching targeting ligands). We observed the same punctate pattern whether the amphiphiles had 8T spacers (rung **A**) or not (rung **B**). As described earlier, bundle like structures (**A3**)(**B2**), (**A3**)(**B3**) and **B6** are weakly held together, and dissociate into their component rungs under physiologically relevant conditions. Accordingly, we observed the same intracellular punctate pattern as the amphiphilic rungs when these bundle-like structures were incubated with HeLa cells (Figure 3.15 and 3.21).

Finally, we studied the cellular uptake of **A6**, which is a fully formed nanotube composed of amphiphilic rungs and linking strands with an intramolecular association. Surprisingly, this structure did not behave like its component amphiphilic rungs. Instead, it showed the same internalization time and fibrillar pattern displayed by the unmodified nanotube (Figure 3.15).

To further elucidate the different nature of the uptake, a time-course quantification of mitochondrial co-localization was also carried out (Figure 3.15). Interestingly, the intramolecular 'handshake' **A6** and unmodified rung presented a high Pearson's correlation coefficient (PCC) for mitochondria co-localization. This coefficient increased over incubation time, being 0.75 after 24h incubation. The amphiphilic rung, however, did not present this behavior. Instead, the low PCC value (<0.5) suggests that the structure did not significantly reside within the mitochondria.

These observations point to the different nature of the tube-like, versus bundle-like structures. Bare nanotubes, as well as intramolecular 'handshake' nanotubes do not seem to protect their cyanine-labelled strand, thus mitochondrial co-localization is observed. On the other hand, bundle-like structures dissociate into their amphiphilic rungs. These alkyl coated rungs slow down and reduce the uptake of the cyanine-labelled dye. This may either be due to protection of this strand by steric hindrance of the alkyl chains and decreased access of nucleases, or to binding of the hydrophobic units to serum proteins (such as albumin). (see nuclease stability assays below) Currently, we are further investigating the internalization mechanism of our structures and studying their intracellular fate by changing the position and the nature of the dye.

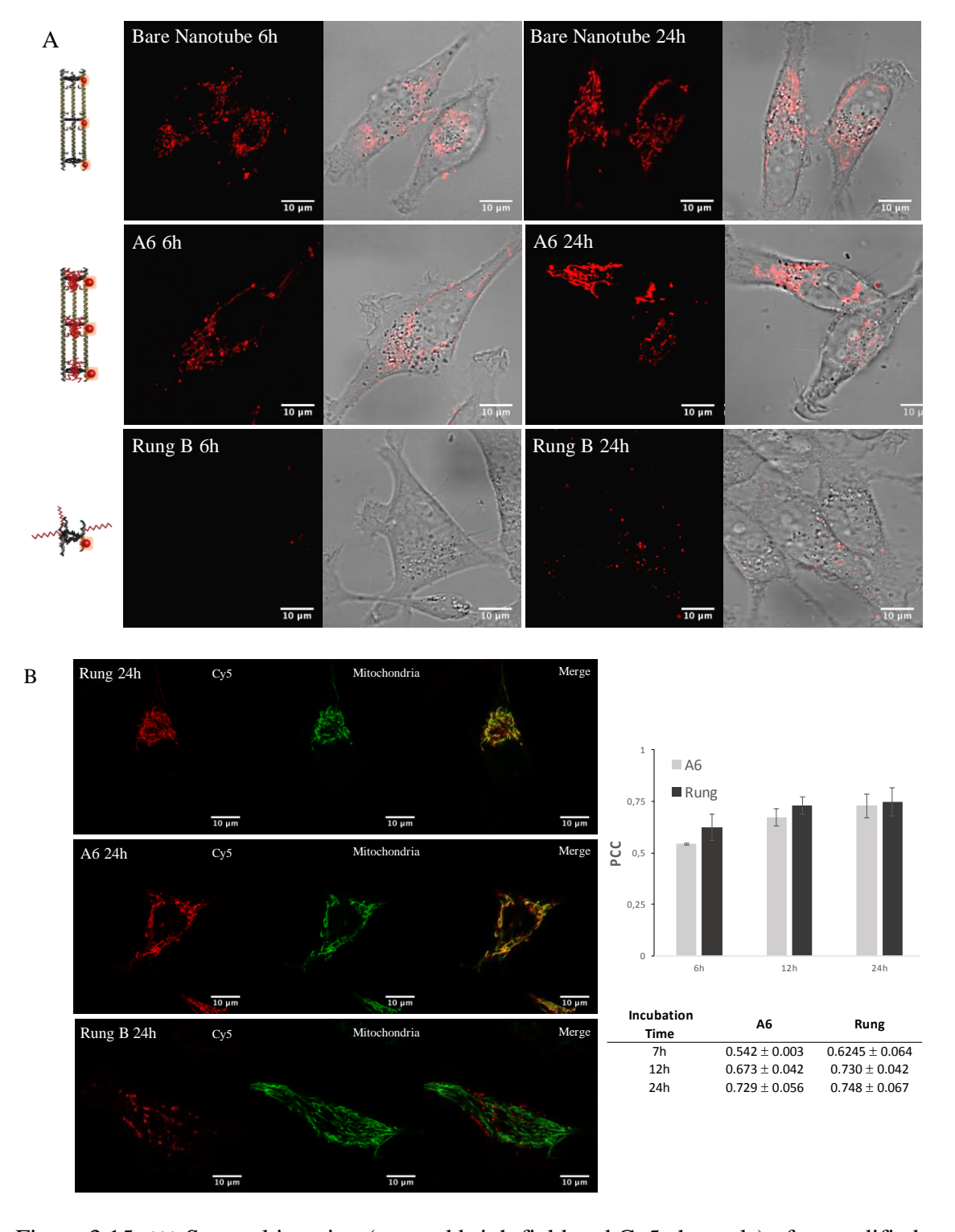


Figure 3.15. (A) Spectral imaging (merged brightfield and Cy5 channels) of unmodified nanotubes, rung **B** and **A6** incubated in HeLa cells at 6 and 24 h. Red sphere represents the Cy5 dye. (B) Left: Spectral imaging of unmodified rungs, rung **B** and **A6** illustrating the mitochondrial co-localization with Cy5 labelled strands. Right: Diagram displaying the PCC values of unmodified rungs and A6. Confocal imaging was Performed by Vengut-Climent E.

3.3 Conclusions

In conclusion, we showed that the orientation of hydrophobic chains on a triangular rung unit can lead to two distinct modes of orthogonal association. In the absence of a spacer, the rungs and linking strands associate intermolecularly into extended networks via hydrophobic interactions and Watson-Crick base-pairing. On the other hand, these DNA amphiphiles gather together intramolecularly to generate micellar microenvironments along the repeating units of the nanotubes in the presence of 8T spacers on the amphiphilic strands. These nanotubes can encapsulate and selectively release small molecules when a specific DNA strand is added, as monitored by both ensemble and in-situ single-molecule fluorescence microscopy, and the process can be repeated on the same nanotubes. With this contribution, we can propose guidelines for combining Watson-Crick base-pairing with hydrophobic interactions in 3D-DNA structures. Whenever the hydrophobic chains can meet and interact on the inside of DNA cages or nanotubes, then an intramolecular 'handshake' is preferred. A simple DNA spacer, such as the 8T used here, allows this to happen. This produces hydrophobic environments within the DNA cages, which make them very useful for selective drug delivery applications. On the other hand, if the hydrophobic chains are incapable of meeting inside the DNA structure, then an intermolecular association of DNA nanostructures into networks occurs. Here, amphiphilic rungs and linking strands come together into filament networks that extend over multiple microns. Under physiological conditions, the resulting bundles disassemble into alkyl coated nanostructures that slow down and reduce non-specific uptake and dye-directed mitochondrial localization, which is an attractive property for the design of targeted therapies. On the other hand, when the alkyl chains are engaged in an intramolecular handshake the biological behavior resembles that of the bare nanotube and we observe mitochondrial co-localization. Thus, introducing orthogonal

hydrophobic interactions into DNA nanotubes can significantly affect their self-assembly, ability for guest encapsulation, cell uptake and intracellular behavior.

While one of the main objectives of our designs is to create universal drug carriers able to transport functional cargos to targeted cells, future studies will further explore the utility of amphiphilic nanostructures in building imaging agents for medical diagnosis of a variety of diseases. Long DNA nanotubes, that are not able to easily access the cells, can play an important role in delivering these agents to the cell surface in order to monitor its progress during the treatment. Moreover, by tuning the chemistry of the DNA-polymer conjugates, we anticipate that various microenvironments can be simultaneously introduced inside the cavities of our construct, allowing the selective encapsulation and release of more than one cargo in response to two or more external stimuli.

3.4 Experimental

3.4.1 Materials

Acetic acid, boric acid, EDTA, magnesium chloride, GelRed, urea, tris(hydroxymethyl)aminomethane (Tris), D(+) glucose, 2-betamercaptoethanol, and streptavidin were purchased from Aldrich. Nucleoside (1000 Å)-derivatized LCAACPG solid support with loading densities of 25-40 µmol/g, Sephadex G-25 (super fine DNA grade), and reagents for automated DNA synthesis were used as purchased from BioAutomation. Acrylamide (40%)/bisacrylamide 19:1 solution and agarose were purchased from BioShop. For TIRFM sample preparation, 1% v/v Vectabond/acetone was purchased from Vector Laboratories, while poly-(ethylene glycol) succinimidyl valerate MW 5000 (mPEG-SVA) and biotin-PEG-SVA were purchased from Laysan Bio, Inc. Imaging chamber components were purchased from Grace BioLab. AFM cantilevers were purchased from Asylum Research (model AC160TS) and RubyRed mica were ordered from Electron Microscopy Sciences. TBE buffer is composed of 90 mM Tris and boric acid and 1.1 mM EDTA, with a pH of ~8.3. TAMg buffer is composed of 45 mM Tris and 12.5 mM MgC12 with a pH of ~7.8 adjusted by glacial acetic acid.

3.4.2 System Design

When creating a nanotube made up of DNA strands only, one should be cautious in designing the length of every strand, the size of their overhangs and the unwanted secondary interactions between them. On the other hand, when DNA strands are coupled to hydrophobic moieties, other orthogonal interactions might be produced and one should be more careful in determining the length, position and orientation of the DNA amphiphiles. Since our structures are geometrically well-defined, each strand was modelled to generate the anticipated assembly with a minimal yield of byproducts. Previously, we have reported the design of DNA nanotubes consisting of 11 unmodified DNA strands using Gideon. 41 This software allowed us to develop the triangular rung unit with nominal strain between phosphate-backbone bonds and simplified the construction of the tubes with a defined architecture (Figure 3.2). Briefly, the size of every edge and whether it was more advantageous to add unpaired bases at the junction regions were also modelled via Gideon. These lengths resulted from the most relaxed and unstrained structure. After determining the dimension of each strand, the sequences were produced by CANADA 2.0 (available online), a software intended to reduce unwanted secondary interactions (Table 1). Finally, the Integrated DNA Technologies website was employed to verify that the produced sequences did not have any undesirable interactions (more than 5 bases) and that they are incapable of self-dimerizing. In this chapter, we study the effect of the addition of 6 DNA amphiphiles to our construct in two distinct regions and with different rotational freedom. At first, we examined the self-assembly behavior of the rung upon adding 3 DNA amphiphiles. Then we characterized the formation of the tubes in the presence of 6 DNA alkyl-conjugates.

Table 3.1. Sequences of all the strands used in this chapter

Name	Sequences 5' to 3'	ε ₂₆₀ (L.mole ⁻¹ .cm ⁻¹)
V	CTCAGCAGCGAAAAACCGCTTTACCACATTCGAGGCACGTTGTAC GTCCACACTTGGAACCTCATCGCACATCCGCCTGCCACGCTCTTA GCATAGGACGGCGGCGTTAAATA	1062100
C1	CGGTGCATTTCGACGGTACTTCGTACAACGTGCCTCGAATGTAGA GCGTGGCAGGCGGATGTGAAGCAGTTGCAGCGTACTCGT	803900
C2	TCGGCAGACTAATACACCTGTCGATGAGGTTCCAAGTGTGGATAG CTAGGTAACGGATTGAGC	623300
3'-HE(n)-8T-R1	TGCAACTGCTACCAGGTGTATTTTTTTTT-(HE)n	272200
3'-HE(n)-R1	TGCAACTGCTACCAGGTGTATT-(HE)n	207400
3'-HE(n)-8T-R2	TTACCTAGCTCCAGTACCGTCGTTTTTTTT-(HE)n	267200
3'-HE(n)-R2	TTACCTAGCTCCAGTACCGTCG-(HE)n	202000
3'-HE(n)-8T-R3-ov	GCCTGGCCTTGGTCCATTTGGTCCTATGCTTTGTAAAGCGGTTTTTT TTT-(HE)n	444300
3'-HE(n)-R3	GTCCTATGCTTTGTAAAGCGGT-(HE)n	207400
3'-Bio-ov*	CAAATGGACCAAGGCCAGGC-Biotin	198100
LS1	TTTTCGCTGCTGAGGTAAGCCTTCGGCGAGCATCTATCTA	563700
5'-HE(n)-8T-LS1*	(HE)n-TTTTTTTTCGGAGACA TAGATAGATGCTCGCCGAAGGCTTACCGACTTCGAG	497100
5'-HE(n)-LS1*	(HE)n-CGGAGACATAGATAGATGCTCGCCGAAGGCTTAC	337000
E1	CTCGAAGTCGGTAAGCCTTCGGCGAGCATCTATCTATGTCTCCGA AAAAAAA	506700
LS2	AGTCTGCCGACACAGAGATCAGTCGGAAGCATAATATCTTATGTT CGTGATAACGAGTACGC	618800
LS3	AAATGCACCGCACAGAGATCAGTCGGAAGCATAATATCTTATGTT CGTGATAGCTCAATCCG	615100
5'-HE(n)-8T-LS2/3*	(HE)n-TTTTTTTTTTATCACGAAC ATAAGATATTATGCTTCCGACTGATCTCTGTGCGACTTCGAG	565200
5'-HE(n)LS2/3*	(HE)n-TATCACGAACATAAGATATTATGCTTCCGACTGATC TCT GTG	406900
E2/3	CTCGAAGTCGCACAGAGATCAGTCGGAAGCATAATATCTTATGTT CGTGATAAAAAAAA	616200

To start with, three DNA amphiphiles (R1, R2 and R3) were hybridized to the rung as shown in Figure 3.2. We believe that the attachment of the hydrophobic units to the 3'-end of the DNA strands and the lack of rotational freedom played a key role in orienting these units to the outside of the triangular core (Figure 3.2). Such orientation prevents any intramolecular interaction between the alkyl chains within individual rung units. However, when spacers of 8 unhybridized thymine bases (8T) were added prior to the coupling of the hydrophobic chains, the latter benefit from an increased degree of freedom around the rung. To test whether the spacers provide enough flexibility to the alkyl chains to communicate intramolecularly, we hybridized three additional DNA amphiphiles to the linking strands LS1, LS2 and LS3 during the formation of the nanotubes. In this case, the hydrophobic units were attached to the 5'-end of the DNA strands allowing a separation of 32 and 36 bases pairs (bp) from the neighboring alkyl chains on the same side of the tubes. As such, in the presence of the spacers, the 6 DNA amphiphiles should be flexible enough to form a micellar microenvironment within the cavities of the tubes. Yet, in the absence of the spacers, intermolecular hydrophobic interactions between the nanotubes should be more favored.

3.4.3 DNA Synthesis and Purification

A. Unmodified DNA Strands

The strands were synthesized by automated solid-phase synthesis performed on a BioAutomation MerMade MM6 DNA synthesizer at 1 µmol scale. Strands labelled with fluorescent dyes or biotin were ordered from Integrated DNA Technologies (IDT). The synthesized strands were deprotected and cleaved from the support (controlled pore glass: CPG) after the addition of concentrated ammonium hydroxide solution (60°C, 16 hours). Polyacrylamide gel electrophoresis (PAGE: 20 x 20 cm vertical Hoefer 600 electrophoresis unit) was used to purify crude products (8-20%).

polyacrylamide/8M urea at constant current of 30 mA for two hours, with 1xTBE as a running buffer). Subsequent to the electrophoresis, the bands were excised, crushed then incubated in 11 mL of autoclaved water at 60°C for 12-16 hours. Size exclusion chromatography (Sephadex G-25) technique was employed to desalt the solution after drying the DNA samples to 1.5 mL. Finally, the strands were quantified (OD260) by UV/vis spectroscopy with a NanoDrop Lite Spectrophotometer and using IDT's extinction coefficient at 260.

B. DNA Amphiphiles (Trinh T. helped with the synthesis of some of these strands)

The synthesis of DNA was performed on a 1 µmole scale using the required nucleotides on a 1000 Å LCAA-CPG solid-support. Coupling efficiency was observed after elimination of the dimethoxytrityl (DMT) 5-OH protecting groups. DMT-dodecane-diol (cat.# CLP-1114) was purchased from ChemGenes (Figure 3.16). In a glove box under nitrogen atmosphere, DMTdodecane-diol was dissolved in acetonitrile and shaken for 10 mins to attain a final concentration of 0.1 M. Then, 0.25M of 5-(ethylthio)tetrazole in anhydrous acetonitrile was added to activate the DMT-dodecane-diol amidite and initiate the coupling reaction to DNA for 10 min. 3% dichloroacetic acid in dichloromethane was employed to remove DMT protecting group on the DNA synthesizer. When the synthesis was done, the solid support was treated with 28% aqueous ammonium hydroxide solution for 16-18 hours at 60°C in water bath. Then, the crude mixture was concentrated under reduced pressure at 60°C. Before carrying out high performance liquid chromatography (HPLC) on the 5'-end modified DNA amphiphiles (5'-HE(n)-8T-LS1*, 5'-HE(n)-LS1*, 5'-HE(n)-8T-LS2/3* and 5'-HE(n)-LS2/3* with n=4, 6, 8), the strands were filtered by 0.22 µm centrifugal filter. For R1, R2, R3 strands modified with HE units on the 3'-end, PAGE purification was performed followed by desalting using Sephadex.

OTMD
$$O-P-N(iPr)_2$$
 $O-CNEt$

Figure 3.16. DMT-dodecane-Diol phosphoramidite purchased from ChemGenes.

C. HPLC Purification

5'-HE(n)-8T-LS1*, 5'-HE(n)-LS1*, 5'-HE(n)-8T-LS2/3* and 5'-HE(n)-LS2/3* were purified by reverse-phase HPLC (RP-HPLC). Two mobile phases were TEAA and HPLC grade acetonitrile. Elution gradient used: 3-50% acetonitrile over 30 minutes at 60°C). Column used: Hamilton PRP 1 5 μm 2.1x150mm. Approximately 0.5 OD260 of crude amphiphiles was injected as a 20-50 μL solution in Millipore water and then detected using a diode array detector monitoring absorbance at 260nm. Figure 3.17 shows the separation between the unmodified DNA strands (peaks at 10 min) and the alkyl-DNA conjugates (peaks between 20-25 min). Note that the retention time increases as the length of the alkyl chains increases.

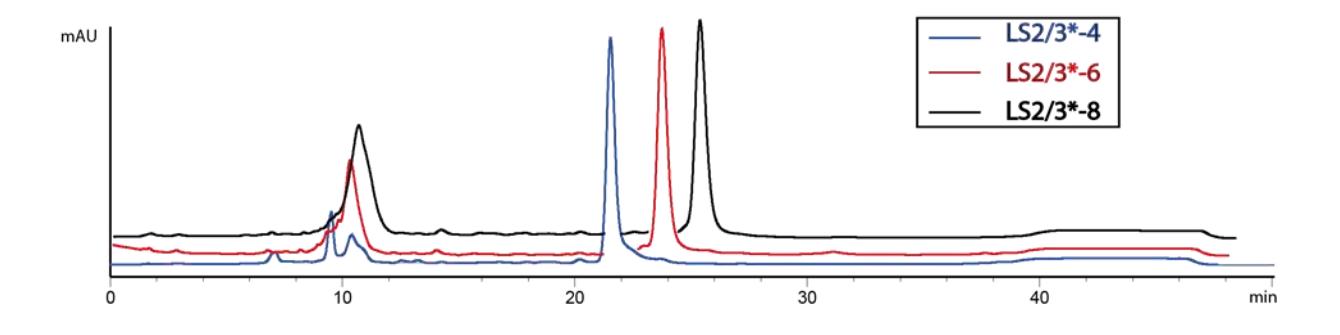


Figure 3.17. Reverse-phase HPLC traces of sequence-defined DNA amphiphiles.

3.4.4 Nile Red Encapsulation Protocol

DNA nanotubes at 75 nM in the presence of 6 DNA amphiphiles (with 8T spacers) were annealed following the aforementioned protocol. In separate glass vials, 0.75 μ L of 0.5 mM Nile Red solution in acetone was added, followed by drying the acetone at room temperature to achieve a dried film of Nile Red. To these vials, 50 μ L of tubes A4, A6, A8 were added separately at a final concentration of Nile Red = 7.5 μ M or 100x excess. The solution was mixed by a vortex mixer for 1 minute and gently shook in dark using the rotator for at least 12 hours. Excess Nile Red was removed by centrifugation at 13.4 krpm for 30 minutes in the cold room. To measure the fluorescent signal of the encapsulated Nile Red, 20 μ L of each sample were transferred to a 96 well-plate. BioTek Synergy well-plate fluorometer was employed to measure the fluorescence signal. The samples were excited at 535 nm with a slit width of 9 nm and the emission of Nile Red was monitored between 560 and 750 nm.

Next, we were interested to examine whether the degree of encapsulation correlates with the size of the hydrophobic chains. It would be challenging to use TIRFM for this study, because of the nanotube polydispersity (i.e. spots detected by TIRFM have nanotubes of different lengths). We thus carried out fluorescence ensemble measurements of the tubes A6-4 (6 DNA amphiphiles with 4 HE units each), A6-6 (6 DNA amphiphiles with 6 HE units each) and A6-8 (6 DNA amphiphiles with 4 HE units each), each incubated with the same amount of Nile Red, using a microplate reader. The results in Figure 3.18 suggest that tubes A6-8 have a higher encapsulation capacity than tubes A6-6, which in turn can encapsulate more guest molecules than A6-4. By varying the length of the DNA amphiphiles and changing the hydrophobicity of the microenvironment within the tubes, we are able to alter the encapsulation efficiency of Nile Red. Addition of the 3 erasing strands that remove the amphiphilic linking strands also results in loss of the intensity of Nile Red

in these ensemble measurements, consistent with conditional release of these guest molecules (tubes A3-6).

We were also interested in determining whether the size of the hydrophobic chains correlates with the encapsulation capacity of the bundles (Figure 3.18). Interestingly, both samples B6-6 and B6-8 encapsulated Nile red with a higher capacity than single tubes A6-4, A6-6 and A6-8 at the same concentration. However, bundles B6-8 did not show a dramatic increase in the fluorescence intensity of Nile Red compared to bundles B6-6.

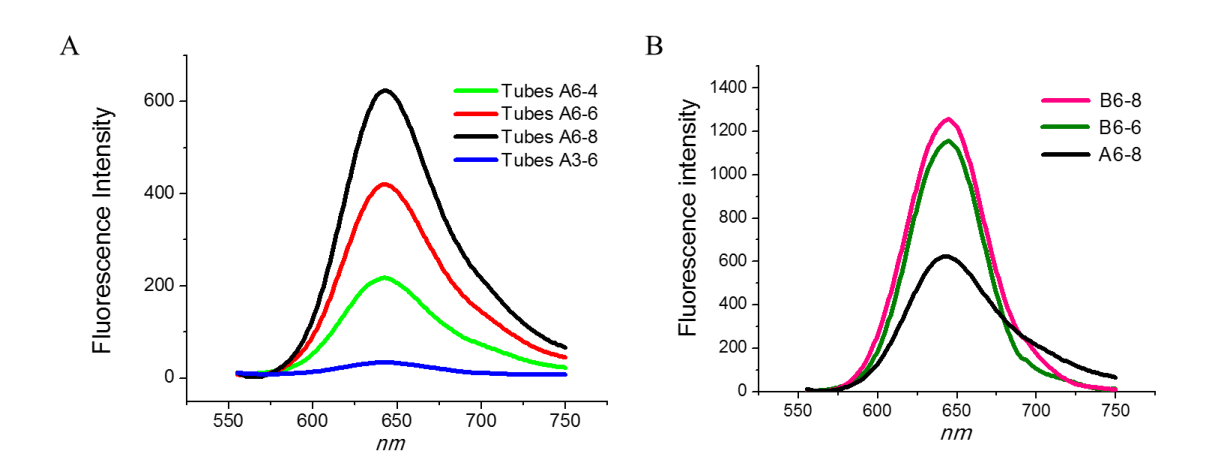


Figure 3.18. Emission spectra of Nile Red encapsulated within the hydrophobic pockets of (A) single nanotubes and (B) bundles.

3.4.5 Cellular Uptake Study (Performed by Dr. Vengut-Climent E.)

A. Confocal Lice-Cell Imaging

Images were collected and/or image processing and analysis for this manuscript was performed in the McGill University Life Sciences Complex Advanced BioImaging Facility (ABIF). Confocal life- cell imaging was performed with a Zeiss LSM 710 Confocal Microscope. Typically, HeLa cells were counted and seeded at a density of 250,000 cells/well in a 8-well plate with prewashed glass coverslips. Cells were allowed to recover for 24 h at 37 °C with 5% CO₂. Subsequently, cells were washed once with cold PBS, and then 200 µL of DMEM media supplemented with 10% (fetal bovine serum) FBS was added. Then, 30 ml DNA nanotubes samples were added (130 nM final concentartion). Cells were imaged during incubation at the following time points, 2h, 5h, 7h, 11h, 14h, 20h and 24h. All images were acquired using Zen Microscope Software and manipulated using ImageJ.

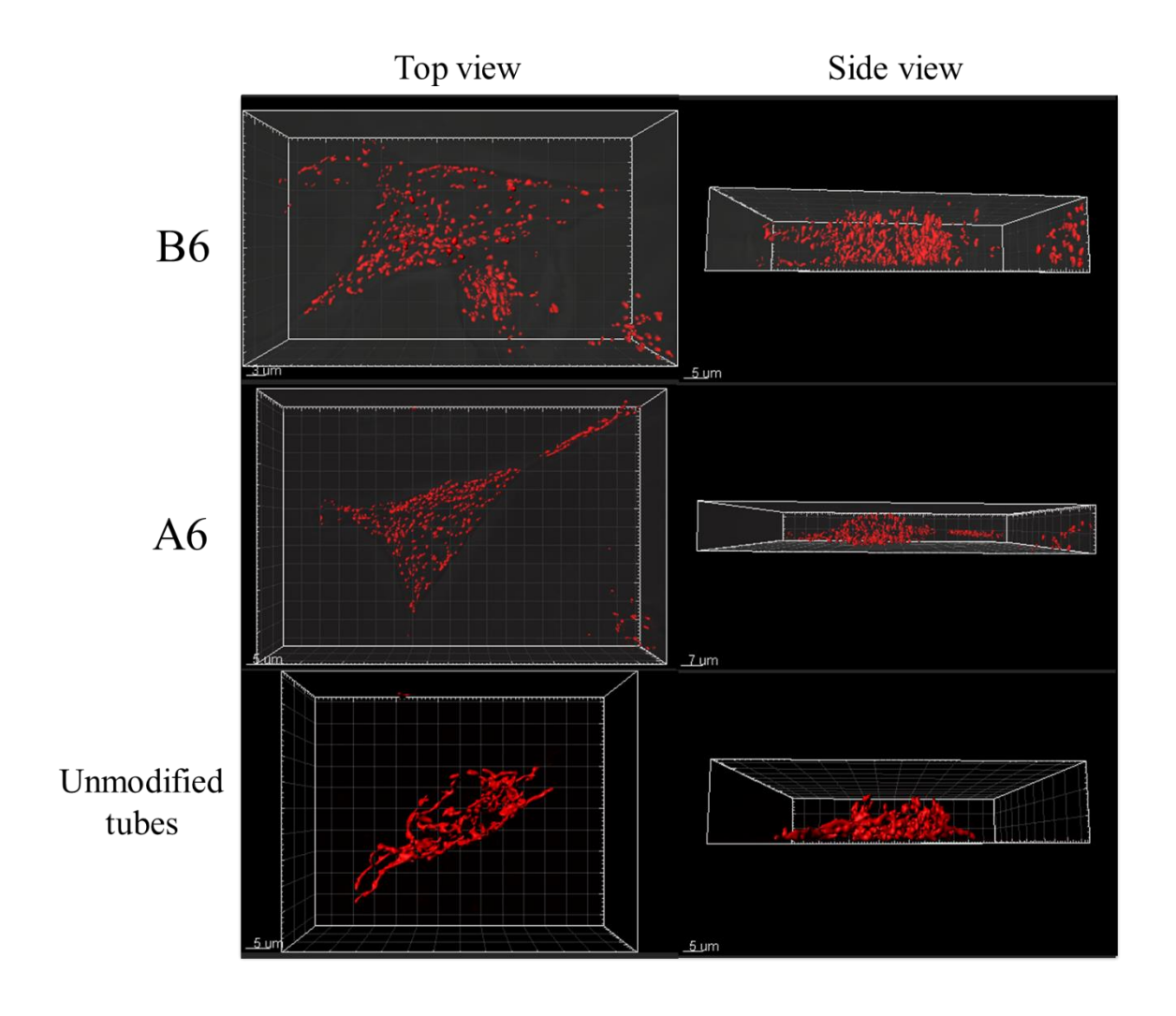
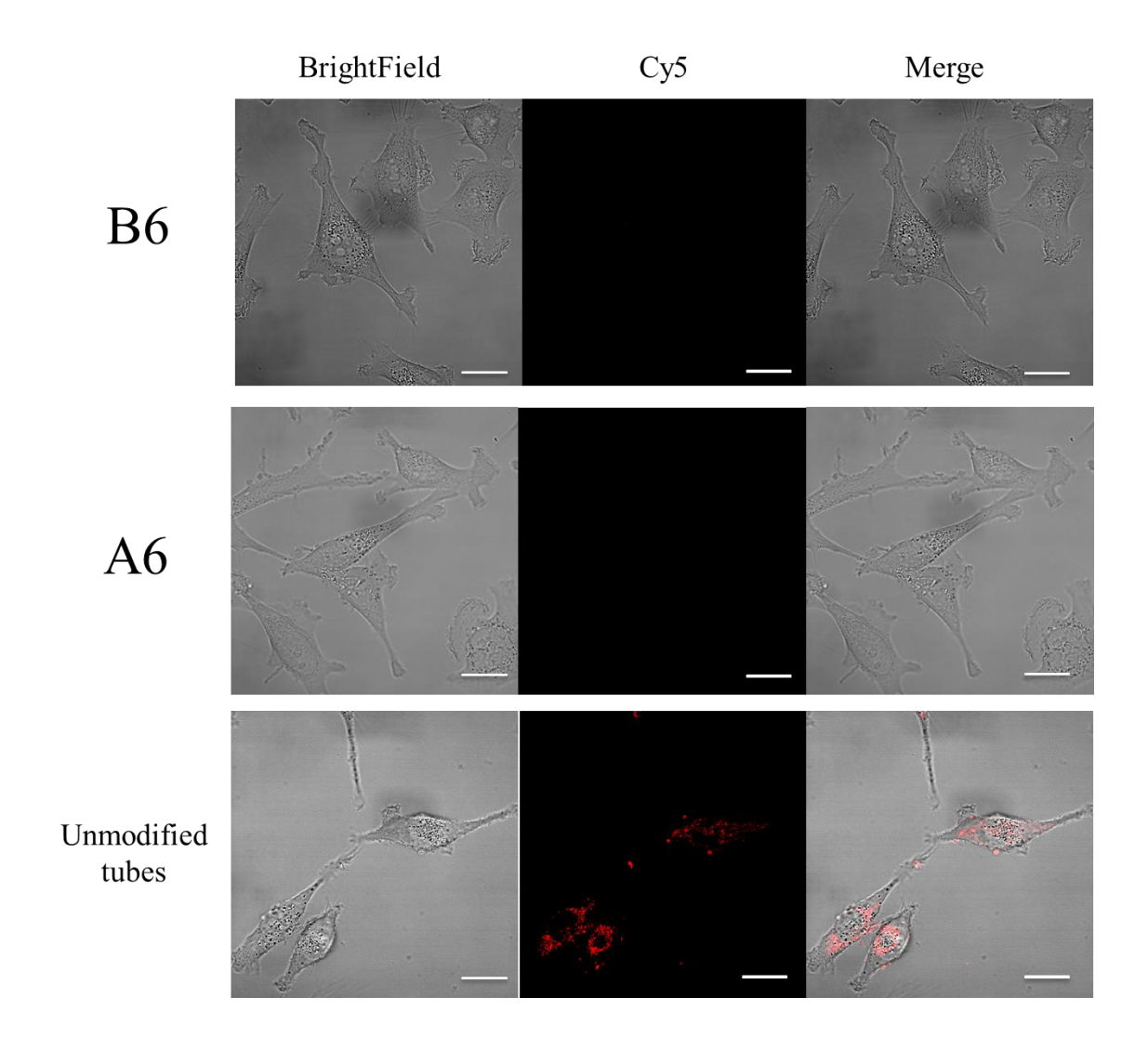


Figure 3.19. 3D reconstructed images of bundles/nanotubes incubated in HeLa cells for 24 h.

Using the same protocol, tubes A6, bundles B6 and the unmodified tubes were prepared. However, in order to visualize the Cy5 dyes (covalently linked to the rungs similar to the TIRFM section) via this technique, the concentration of each strand involved in the assembly was 1000 nM. As



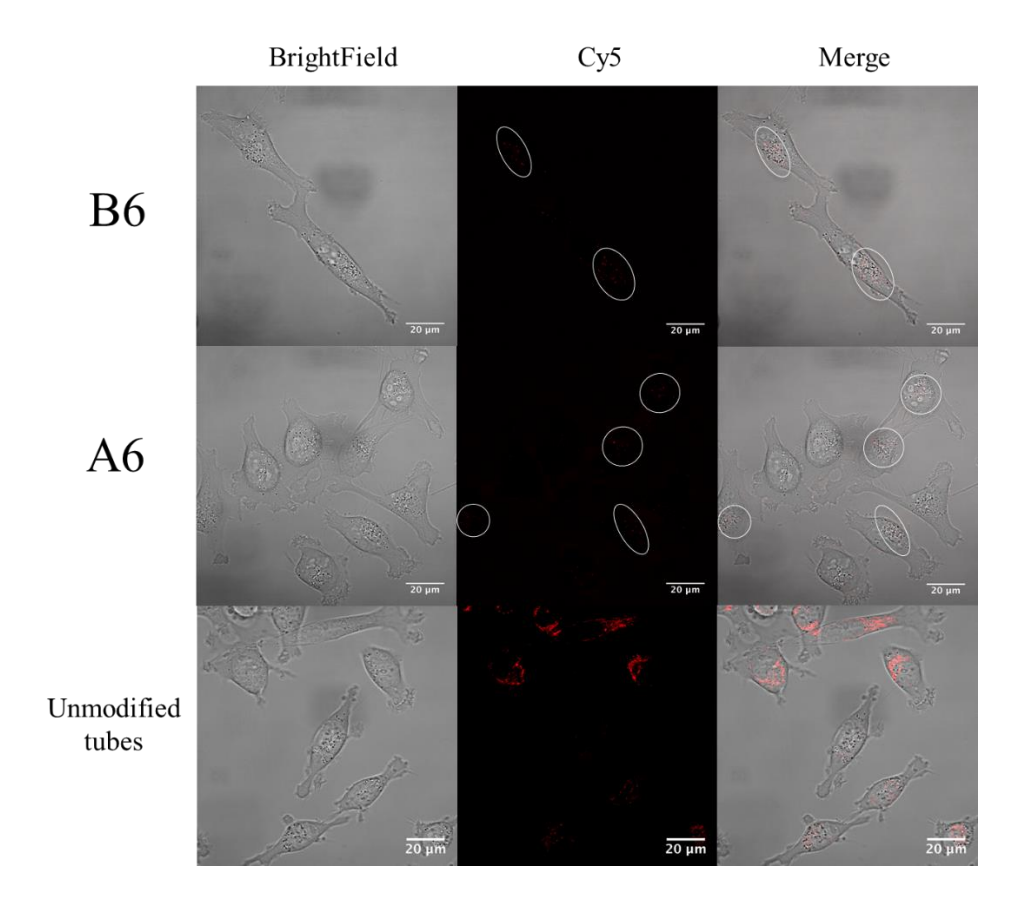


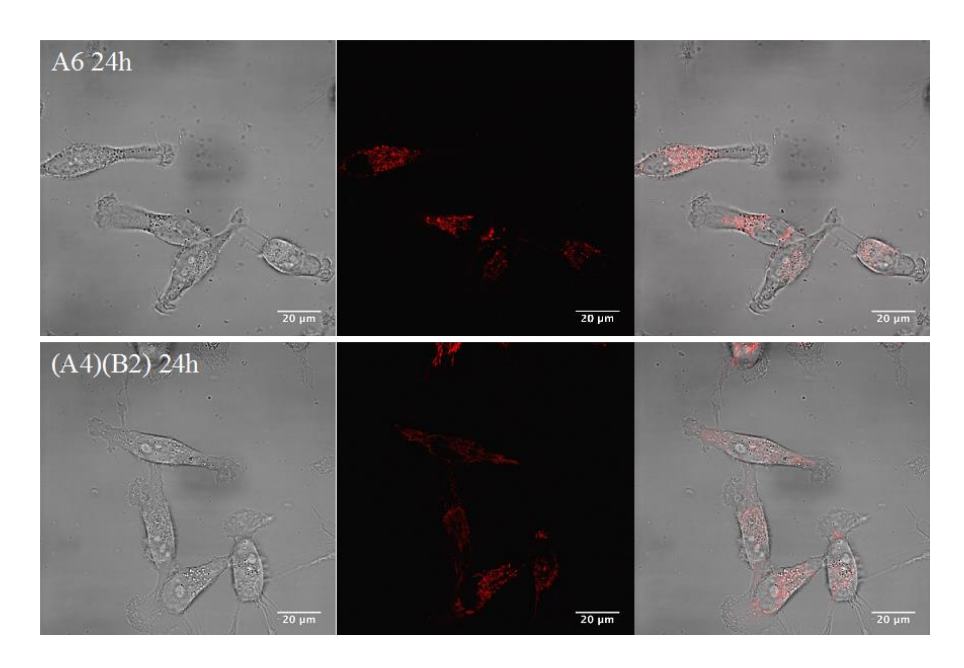
Figure 3.20. Spectral imaging of the bundles/nanotubes incubated in HeLa cells for 7 h(top) and 12 h (bottom).

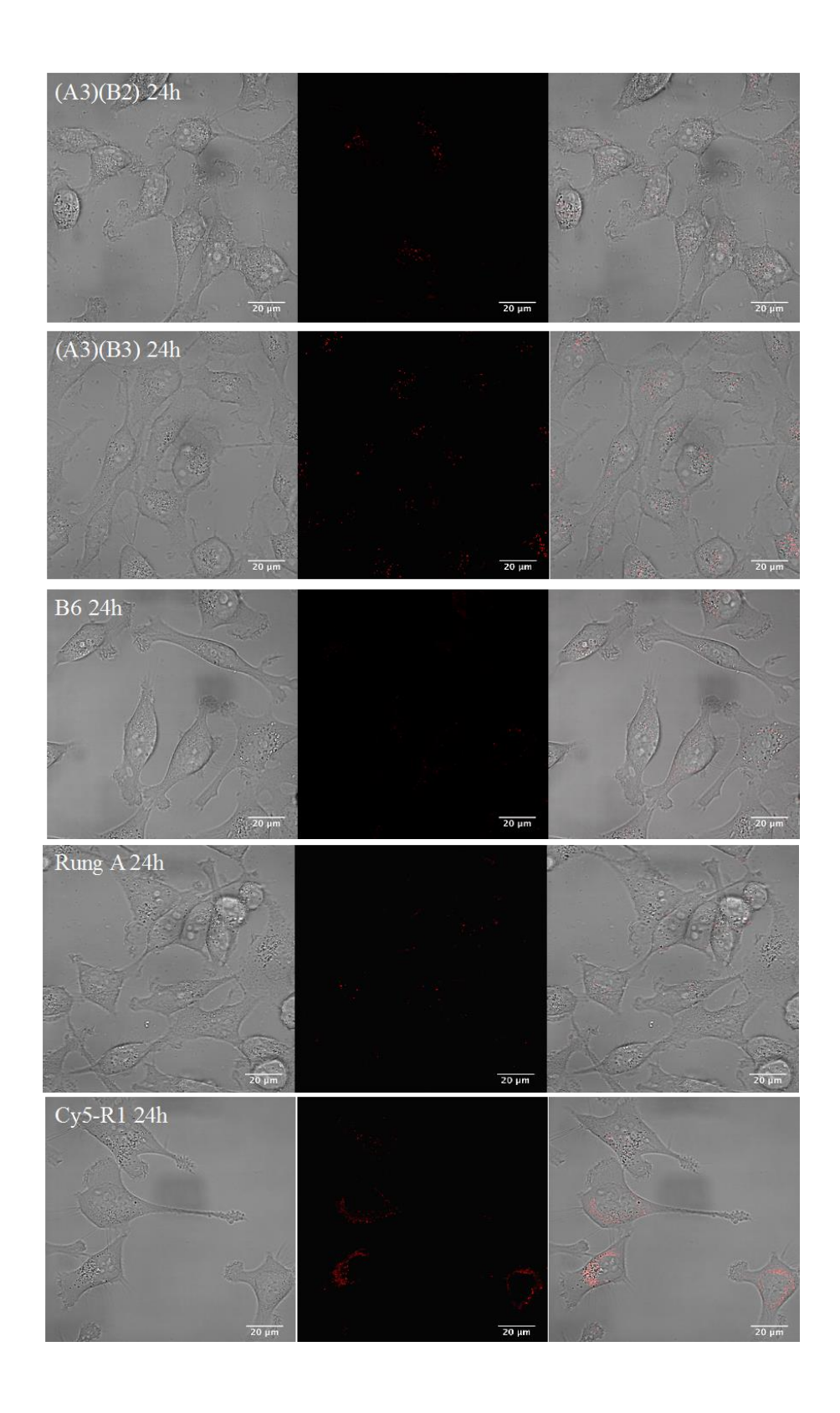
such, the formation of bundles was more favorable even for tubes A6 (see Figure 3.19). Figure 3.19 shows the 3-D reconstructed images of unmodified nanotubes and bundles under these conditions. All the samples were incubated in HeLa cells for 24h. The 3D reconstruction was made with Imaris software after collecting a z-stack using a 0.30 microm step.

To gain more insight on the kinetics of internalization of each system, we imaged them at different incubation times. Figure 3.20 shows the Cy5 and BrightField channels of bundles A6 and B6 as well as unmodified tubes at 7 and 12 hours. At 7 hours, the fluorescence signal of Cy5 attached to the bundles was not observed. On the other hand, we were able to visualize the internalization of the dye in the unmodified tubes samples at that time. The nanotubes formed aggregates in cell

medium and presented a fibrillar pattern intracellularly. At 12 hours, the fluorescence pattern of the unmodified tubes did not change, yet we started to observe a dim signal for the bundles. We noticed that these bundles follow a punctate pattern which is more characteristic of endosomal uptake.

The conversion of nanotubes A6 into bundles was examined using strand displacement strategy. In order to perform this experiment, we used again our initial conditions (75 nM) to prepare tubes A6. Then, we attempted to concentrate the samples by using a water pre-wetted 10k amicon. After centrifuging the amicon for 5 min at 13.8 rpm, water was discarded and the samples were centrifuged for 10-20 min at 7.5-10 rpm. Interestingly, the cellular uptake of A6, which is a fully formed nanotube composed of amphiphilic rungs and linking strands with an intramolecular association, showed the same internalization time and filament-like pattern displayed by the unmodified nanotube (Figure 3.21). Tube (A4)(B2) followed the same behavior inside the cells and did not behave like its component amphiphilic rungs. On the other hand, all the structures that exhibited a bundle-like morphology via AFM [(A3)(B2), (A3)(B3) and B6] showed a punctate fluorescence pattern intracellularly accompanied with a slower internalization time ~12 h.





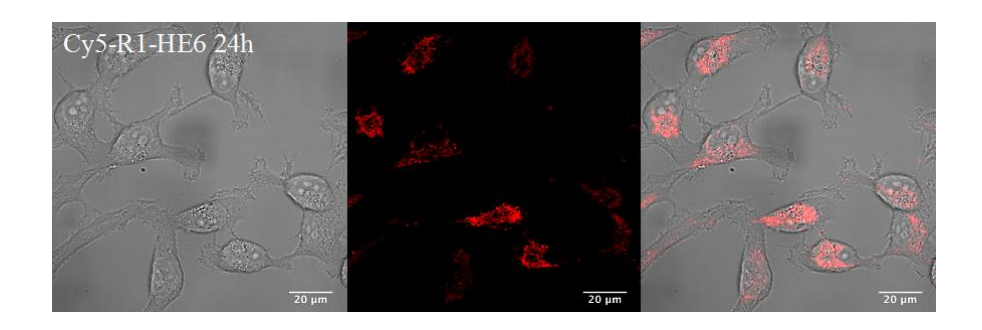


Figure 3.21. Spectral imaging of A6, (A4)(B2), (A3)(B2), (A3)(B3), B6, rung A, Cy5R1 and Cy5-R1-HE6 incubated in HeLa cells at 24 h.

B. Serum Stability Assays

We attempted to study the integrity of all previous structures via serum stability assays and followed the degradation of the bands over time by PAGE. We first prepared the samples under the conditions needed for confocal microscopy (1000 nM). Figures 3.22 shows the behavior of each structure at 0, 6, 9, 12 and 24 hours. We noticed that the disassembly of unmodified tubes started at 6 h until the end of the study. However, we were able to spot the non-penetrating bands even at 24 hours. As such, these bands can be attributed to the large aggregates we saw in cellular medium. We also examined bundles A6 and B6 which run similarly throughout the study. This observation was not surprising because we observed the same cellular uptake behavior via confocal microscopy. More importantly, amphiphilic rungs B showed the same degradation profile as the bundles. For instance, at 0 h, lower mobility bands appeared in both cases. These bands disappeared after 6 hours whereas the higher mobility bands remained until 24 h incubation time. The results support our hypothesis stating that unmodified tubes are more susceptible to nucleases degradation, yet the amphiphilic nanostructures are highly dependent on the concentration of Mg²⁺ and are most likely protected from serum enzymes.

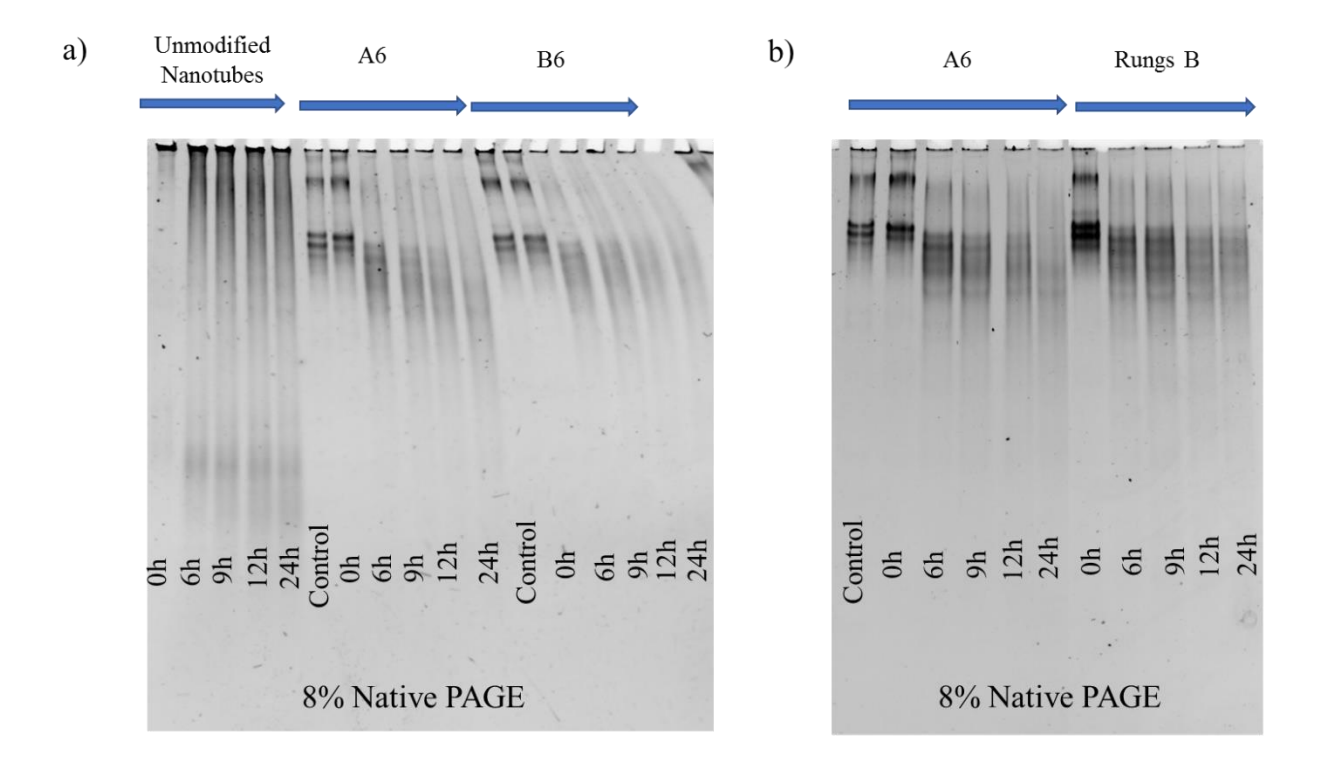


Figure 3.22. Serum stability assays, 8% PAGE displaying the integrity of: (a) unmodified nanotubes, bundles A6/B6 and (b) bundles A6 and rungs B over time. Control lanes represent the samples at low Mg²⁺ before the addition of the serum.

Finally, we examined the conversion of nanotubes A6 into bundles, using strand displacement strategy, via PAGE. In order to perform this experiment, we used again our initial conditions (75 nM) to prepare tubes A6. Then, we attempted to concentrate the samples by using a water prewetted 10k amicon. After centrifuging the amicon for 5 min at 13.8 rpm, water was discarded and the samples were centrifuged for 10-20 min at 7.5-10 rpm. Interestingly, tubes A6 did not fall apart and a non-penetrating band appeared throughout the study. This observation can be correlated to the uptake behavior of unmodified tubes instead of bundles since a fibrillar pattern was visualized under the confocal microscope after 7 hours incubation time. Furthermore, the punctate pattern monitored for structures (A3)(B2) and (A3)(B3) can be better explained with the gels in Figure 3.23 through the appearance of discrete bands over time. Again, the resulting bundles, from

replacing LS1s* and LS2/3s* by their analogues that lack the spacers, tend to disassemble under low Mg²⁺. Therefore, we only observe discrete bands that run similar to rungs B on PAGE.

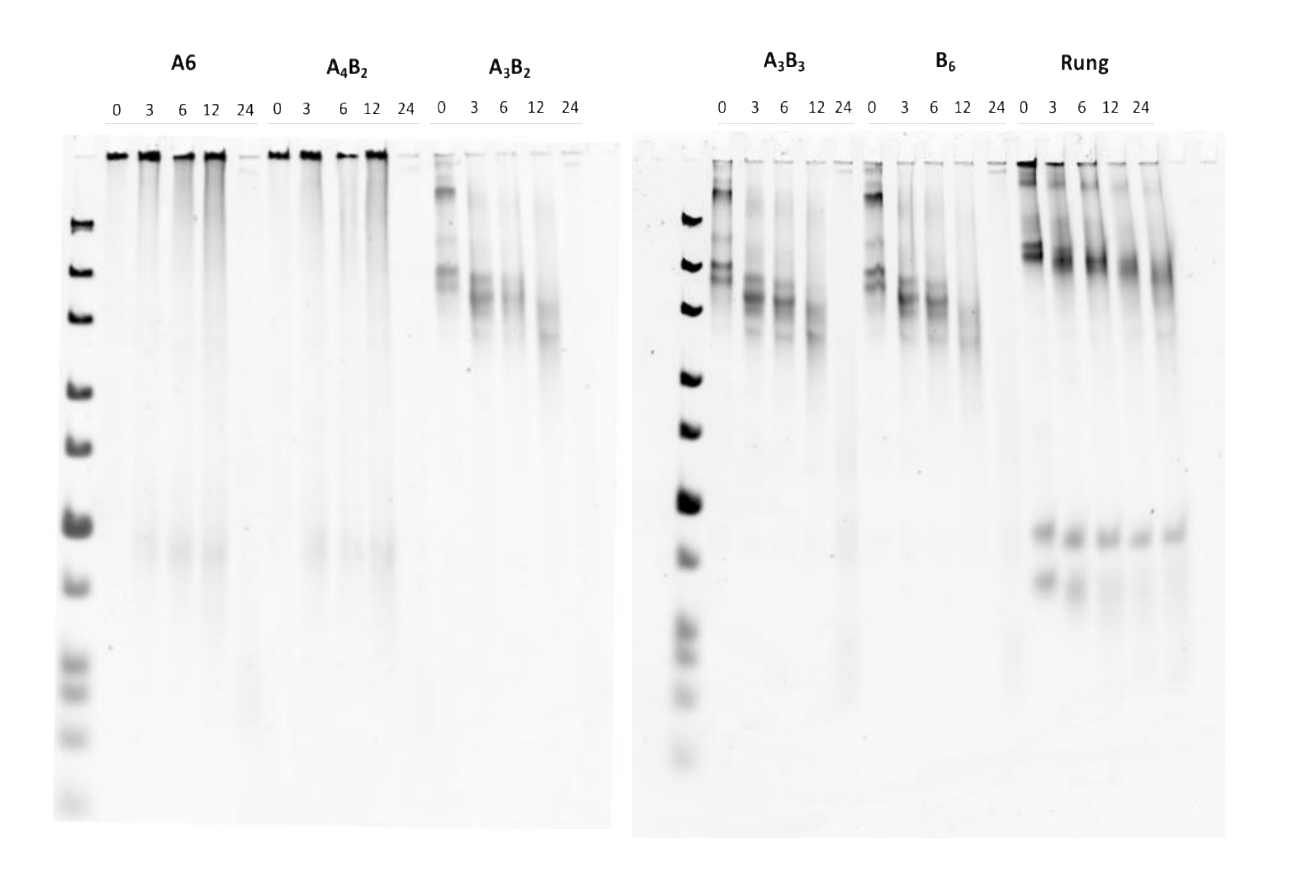


Figure 3.23. Serum stability assays, 8% PAGE displaying the integrity of tubes A6/(A4)(B2), bundles (A3)(B2)/(A3)(B3) and unmodified rungs at 3, 6, 12 and 24 hours. Control lanes represent the samples at low Mg^{2+} before the addition of the serum.

3.5 References

- (1) Cao, G. Nanostructures and nanomaterials: synthesis, properties and applications; World Sci., 2004.
- (2) Tapio, K.; Leppiniemi, J.; Shen, B.; Hytönen, V. P.; Fritzsche, W.; Toppari, J. J. *Nano Lett.* **2016**, *16*, 6780.

- (3) Srinivas, N.; Ouldridge, T. E.; Šulc, P.; Schaeffer, J. M.; Yurke, B.; Louis, A. A.; Doye, J. P.; Winfree, E. *Nucleic Acids Res.* **2013**, *41*, 10641.
- (4) Czogalla, A.; Franquelim, H. G.; Schwille, P. *Biophys. J.* **2016**, *110*, 1698.
- (5) Nalwa, H. S. J. Biomed. Nanotechnol. **2014**, 10, 1635.
- (6) Keyser, U. F. Nat. Nanotechnol. **2016**, 11, 106.
- (7) Rothemund, P. W. Nature 2006, 440, 297.
- (8) Ding, B.; Deng, Z.; Yan, H.; Cabrini, S.; Zuckermann, R. N.; Bokor, J. J. Am. Chem. Soc. 2010, 132, 3248.
- (9) Benson, E.; Mohammed, A.; Gardell, J.; Masich, S.; Czeizler, E.; Orponen, P.; Högberg, B. *Nature* **2015**, *523*, 441.
- (10) Schreiber, R.; Do, J.; Roller, E.-M.; Zhang, T.; Schüller, V. J.; Nickels, P. C.; Feldmann, J.; Liedl, T. *Nat. Nanotechnol.* **2014**, *9*, 74.
- (11) Yang, H.; McLaughlin, C. K.; Aldaye, F. A.; Hamblin, G. D.; Rys, A. Z.; Rouiller, I.; Sleiman, H. F. *Nat. Chem.* **2009**, *1*, 390.
- (12) Woo, S.; Rothemund, P. W. Nat. Chem. **2011**, *3*, 620.
- (13) Edwardson, T. G.; Carneiro, K. M.; McLaughlin, C. K.; Serpell, C. J.; Sleiman, H. F. *Nat. Chem.* **2013**, *5*, 868.
- (14) Chidchob, P.; Edwardson, T. G.; Serpell, C. J.; Sleiman, H. F. J. Am. Chem. Soc. 2016, 138, 4416.
- (15) List, J.; Weber, M.; Simmel, F. C. Angew. Chem. Intl. Ed. 2014, 53, 4236.
- (16) Serpell, C. J.; Edwardson, T. G.; Chidchob, P.; Carneiro, K. M.; Sleiman, H. F. *J. Am. Chem. Soc.* **2014**, *136*, 15767.

- (17) Edwardson, T. G.; Carneiro, K. M.; Serpell, C. J.; Sleiman, H. F. *Angew. Chem. Intl. Ed.* **2014**, *53*, 4567.
- (18) Chien, M. P.; Rush, A. M.; Thompson, M. P.; Gianneschi, N. C. *Angew. Chem. Intl. Ed.* **2010**, *49*, 5076.
- (19) Bousmail, D.; Amrein, L.; Fakhoury, J.; Fakih, H.; Hsu, J.; Panasci, L. C.; Sleiman, H. Chem. Sci. 2017.
- (20) Banga, R. J.; Meckes, B.; Narayan, S. P.; Sprangers, A. J.; Nguyen, S. T.; Mirkin, C. A. J. Am. Chem. Soc. **2017**, 139, 4278.
- (21) Chan, M. S.; Tam, D. Y.; Dai, Z.; Liu, L. S.; Ho, J. W. T.; Chan, M. L.; Xu, D.; Wong, M. S.; Tin, C.; Lo, P. K. *Small* **2016**, *12*, 770.
- (22) Chao, J.; Liu, H.; Su, S.; Wang, L.; Huang, W.; Fan, C. Small 2014, 10, 4626.
- (23) Wu, Y.; Sefah, K.; Liu, H.; Wang, R.; Tan, W. Proc. Natl. Acad. Sci. 2010, 107, 5.
- (24) Walsh, A. S.; Yin, H.; Erben, C. M.; Wood, M. J.; Turberfield, A. J. *ACS Nano* **2011**, *5*, 5427.
- (25) Chen, Y.-J.; Groves, B.; Muscat, R. A.; Seelig, G. *Nat. Nanotechnol.* **2015**, *10*, 748.
- (26) Chang, M.; Yang, C.-S.; Huang, D.-M. *ACS Nano* **2011**, *5*, 6156.
- (27) Bhatia, D.; Surana, S.; Chakraborty, S.; Koushika, S. P.; Krishnan, Y. *Nat. Commun.* **2011**, 2, 339.
- (28) Keum, J.-W.; Bermudez, H. Chem. Commun. 2009, 7036.
- (29) Rush, A. M.; Thompson, M. P.; Tatro, E. T.; Gianneschi, N. C. ACS Nano 2013, 7, 1379.
- (30) Agarwal, N. P.; Matthies, M.; Gür, F. N.; Osada, K.; Schmidt, T. L. Angew. Chem. 2017.
- (31) Sahoo, S. K.; Labhasetwar, V. *Drug Discov. Today* **2003**, *8*, 1112.
- (32) Lu, C.-H.; Willner, B.; Willner, I. ACS Nano **2013**, 7, 8320.

- (33) Farokhzad, O. C.; Langer, R. ACS Nano 2009, 3, 16.
- (34) Greenspan, P.; Mayer, E. P.; Fowler, S. D. J. Cell Biol. 1985, 100, 965.
- (35) Saadi, J.; Wennemers, H. *Nat. Chem.* **2016**.
- (36) Yurke, B.; Turberfield, A. J.; Mills, A. P.; Simmel, F. C.; Neumann, J. L. *Nature* **2000**, 406, 605.
- (37) Rahbani, J. F.; Hariri, A. A.; Cosa, G.; Sleiman, H. F. *ACS Nano* **2015**, *9*, 11898.
- (38) Li, J.; Pei, H.; Zhu, B.; Liang, L.; Wei, M.; He, Y.; Chen, N.; Li, D.; Huang, Q.; Fan, C. *ACS Nano* **2011**, *5*, 8783.
- (39) Jiang, Q.; Song, C.; Nangreave, J.; Liu, X.; Lin, L.; Qiu, D.; Wang, Z.-G.; Zou, G.; Liang, X.; Yan, H. *J. Am. Chem. Soc.* **2012**, *134*, 13396.
- (40) Rhee, W. J.; Bao, G. Nucleic Acids Res. **2010**, 38, e109.
- (41) Birac, J. J.; Sherman, W. B.; Kopatsch, J.; Constantinou, P. E.; Seeman, N. C. *J. Mol. Graph. Modell.* **2006**, *25*, 470.

Introduction to Chapter 4

In chapter 3, we explored the synthesis of higher-order DNA nanostructures through combining Watson-Crick base-pairing and hydrophobic interactions. Alternatively, chapter 4 illustrates a novel strategy to build super origami structures via DNA base-pairing exclusively. DNA origami is one of the most effective tools in producing a large addressable area for bottom-up construction of novel objects and devices at the nanometer-scale. However, many applications require bigger systems capable of scaling up the organization of materials with high precision and control. The main challenge lies in the size of the conventional single-stranded scaffold, typically 7249 nucleotides, used in most of the previous work. In chapter 4, we address this limitation by developing custom-made single-stranded scaffolds that bind pre-assembled origami tiles and induce their one-dimensional organization in high yields. Our synthetic method allowed us to convert multiple repetitive and unique sequences into correctly assembled large backbones, up to 1000 nucleotides, and finely tune the position and frequency of each unique building block. Granted with these regions, five origami tiles were successfully arranged in 1D by the aid of two scaffolds forming a nano-"railroad track". While the majority of the approaches aiming to assemble large origami fail in controlling the growth of superstructures, our technique enables the re-organization, removal and addition of tiles in a particular manner.

Chapter 4: Single-Stranded DNA Templates as 'Railroad Tracks' for Super-Origami Formation

Reproduced in part with permission from: "Sequential growth of long DNA strands with user-defined patterns for nanostructures and scaffolds", Hamblin G., Rahbani J. F., and Sleiman H. F. *Nature Commun.*, **2015**, *6*. Nature Publishing (2015).

Author Contributions: **Hsu J.** performed cloning of 500 mers and developed the design of 1000-nt scaffold. He also optimized ligation and transformation conditions of 1000 nt. **Chidchob P.** helped in the preparation of many origami tiles (~70% of 3-tiles system and ~20% of 5-tiles system) and performed gel electrophoresis experiments.

4.1 Introduction

The invention of DNA origami has enabled the assembly of two- and three-dimensional finite nanometer-sized objects with unique geometries and shapes. The use of DNA origami to organize biomaterials, and photonic components nanometers, and photonic them with myriad potential applications for drugs and biomolecular assays and novel materials. The technique is based on folding a long single-stranded circular DNA scaffold, typically 7.25 kilobase M13mp18 genome, into 2- or 3D shapes through its hybridization to hundreds of short staple strands. Because of the predesigned specific positioning of various functional entities during the assembly process of the nanostructures and its robustness as an assembly method, DNA origami is increasingly playing a crucial role in the evolving area of DNA nanotechnology. 21,22

However, a single origami offers around 200 templating sites and its surface area is mainly limited by the size of the single-stranded scaffold. To overcome this challenge and increase the size of origami structures, a variety of strategies have been examined. For instance, PCR-based methods were used to generate ssDNA of various lengths. Using PCR techniques, long DNA fragments from genomes, bigger than the length of M13mp18 strand used in most of origami designs, were amplified and extracted (Figure 4.1a). This technique allows scientists to modify the sequences of the original plasmid, hence producing a "recombinant plasmid". Nevertheless, the resulting long fragments require hundreds or thousands of staple short strands to create an origami tile. Ongoing efforts have also been optimizing inter-tile connections between individual origami structures to produce large 2D arrays (Figure 4.1b). ²⁶⁻²⁹ Other approaches include the functionalization of DNA strands with gold nanoparticles to induce the assembly of higher-order nanostructures (Figure 4.1c). At this level of complexity, thousands of strands are required and the size and geometry of the final products are not often well-controlled. Therefore, new methods for efficiently producing complex nanostructures without increasing the cost of synthesis are needed.

Long DNA strands consisting of repetitive sequences are valuable tools to build versatile three-dimensional (3D) nanostructures with symmetrical domains. Inspired by proteins, such as elastin, that comprise repeating peptide motifs, repetitive DNA backbones can also play a significant role in the self-assembly of robust nanomaterials without using hundreds of DNA strands. Our group has previously described a new route to create a DNA backbone, typically ~500 nucleotides (nt), in a temporally controlled way. A small set of short complementary DNA strands (42 nt) were added sequentially and ligated in-situ at each step, to produce a larger DNA backbone with sequence symmetry. The target product was then amplified via PCR, and converted to a single-

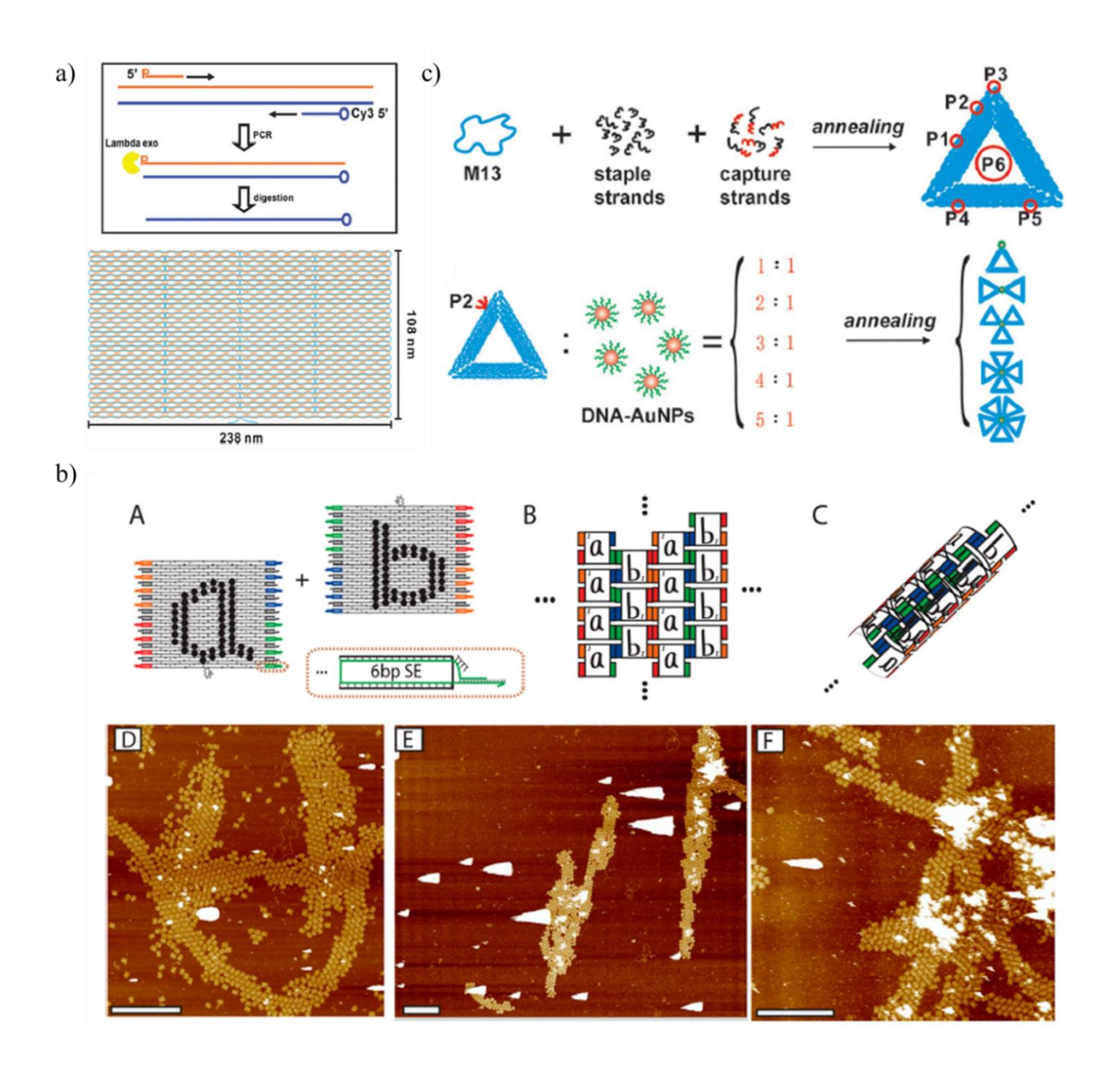


Figure 4.1. (a) Scheme showing the generation of a long DNA scaffold (~26 kb) via long-range PCR technique. In order to extract the single-stranded product, the 5'end of the desired strand was protected by Cy3 while the 5'end of its complementary strand was modified with a phosphate group to facilitate its degradation by λ exo-nuclease. The resulting scaffold required 792 staple strands to form a rectangular origami of 238 nm × 108 nm. Adapted with permission from reference 23 (Royal Society of Chemistry, 2012). (b) Schematic representation of two rectangular tiles having single-stranded extensions of 6 bases. Mixing the two tiles resulted in the formation of large 2D arrays (desired) and nanotubes (unintended). Scale bar for AFM images is 1 μm. Adapted with permission from reference 29 (ACS Publishing, 2016). (c) Schematic drawing of a flower-like super-origami mediated by AuNPs. Adapted with permission from reference 30 (Wiley-VCH, 2015).

stranded scaffold using magnetic beads or lambda exonucleases. Herein, we employ the Golden Gate strategy,³⁴ involving a restriction enzyme that cleaves the DNA fragment outside of its recognition site, and associated PCR procedures to generate ~1000 nt DNA backbones from the 500 nt pieces with predesigned site-specific asymmetry and repeating components. Since our scaffold can be extracted from a plasmid, we were able to easily modify its sequences through simple PCR reactions. Compared to other strategies, our technique is able to generate a wide range of products from the same starting materials, *e.g.* AAABBB patterns can be synthesized. Furthermore, the addressability of the single-stranded scaffolds allows the creation of higher-order DNA nanostructures without increasing synthetic costs.

In this work, we hybridized the vertical edges of pre-assembled DNA origami to our backbones ss[10], ~500 nt, and ss[20], ~1000 nt, to geometrically align three and five origami tiles respectively. A nano-"railroad track" was then developed by adding two sets of ss[20] backbones (one backbone hybridized to the top of the tiles and another to the bottom). This approach provides a unique platform for the modular re-organization of any tile, an option that has not been offered by previous methods. We believe that 2D/3D nanoarchitectures are also feasible by tuning the position of the unique sequences on the backbone. Future studies of design area and fine-tuning of binding interactions between the tiles are expected to scale up the production of complicated nanostructures for practical applications.

4.2 Results and Discussions

4.2.1 Synthesis of Single-stranded DNA Backbones ss-AB[10] (or ss[10])

The goal of our approach is to facilitate the assembly of higher-order DNA origami architectures. This requires the synthesis of a ssDNA scaffold that helps the association of a controlled number of origami tiles in high yields. With this in mind, we show the production of a set of ss DNA backbones of defined lengths. Our strategy allows us to modulate the sequences of the strands with full control over the location and number of repetitive and unique regions on the backbone. Therefore, we significantly diminish the number of components used, while preserving addressability.

The synthesis of the primary piece of DNA (462 nt) is based on the combination of a small set of short building blocks in the presence of ligase (4). The sequence of each duplex can be modified to generate a variety of patterns since each building block is included in the overall backbone. Previously, we demonstrated the formation of a backbone with an alternating A-B-A-B-A sequence pattern.³³ Each domain was composed of 42 nt corresponding to four helical turns. Figure 4.2 shows the four basic building blocks A^P, A, B and B^P that are hybridized to each other via 10bases overhangs. Note that the terminator blocks AP and BP contain unique sequences that are complementary to the primers used during PCR. They also consist of short unique sequences corresponding to the recognition sites of the restriction enzymes XbaI (in A^P) and EcoRI (in B^P). Starting with A^P, subsequent fragments were added sequentially as follows: B, A, B and A. In a separate eppendorf, the following building blocks were added to B^P: A, B, A and B. Figure 4.2b displays the growth of the 2 fragments ds[5]-A^P and ds[5]B^P and the formation of ds-AB[10] backbone upon their combination. The product was then purified via native AGE and the band containing ds-AB[10] was cut. However, since the efficiency of ligation is not 100%, the doublestranded fragment consisting of 10 building blocks might not be continuous (e.g. the 5' end of block A is not covalently linked to block B). Therefore, the isolated product ds-AB[10] was

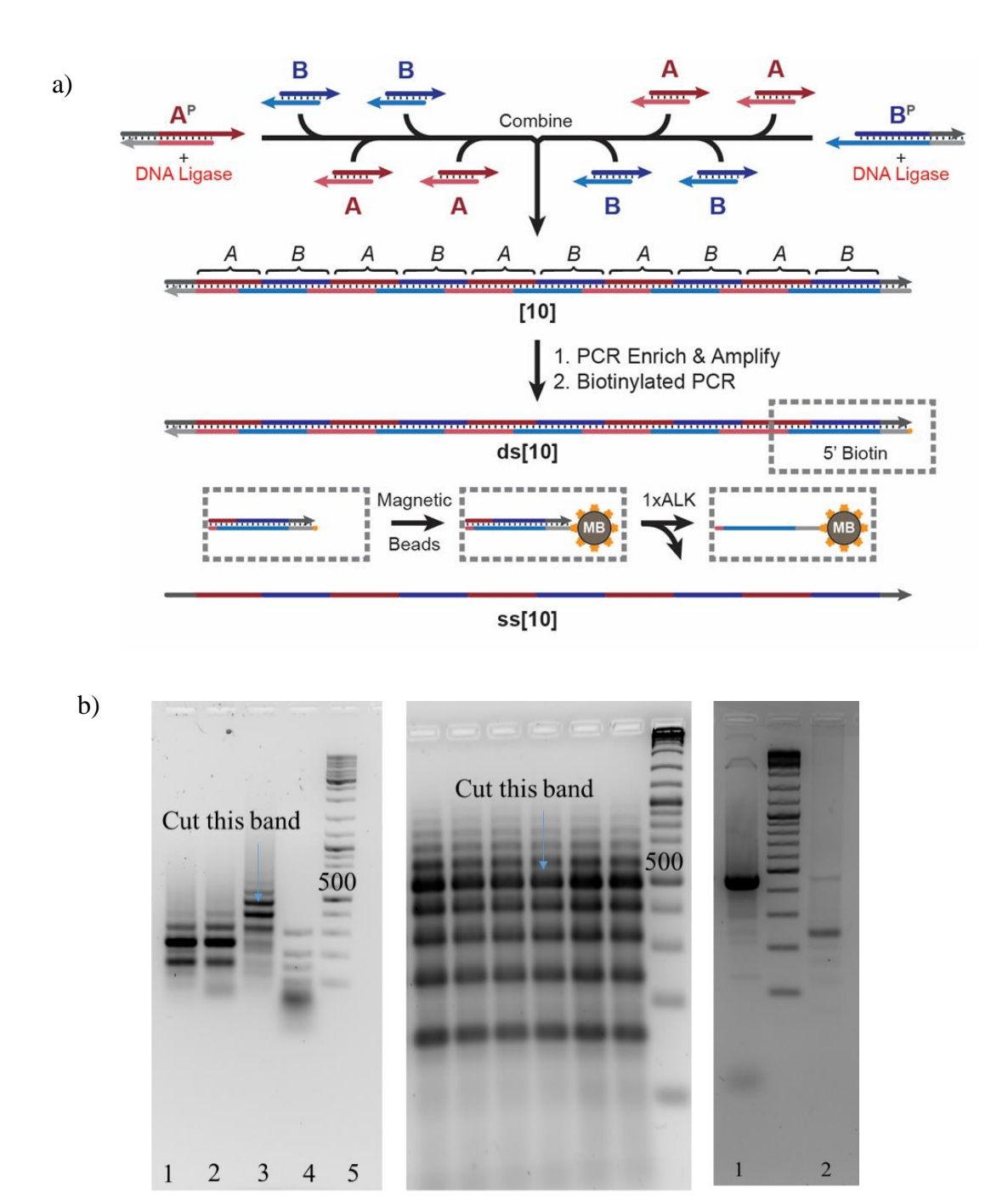


Figure 4.2. (a) Scheme showing the synthesis of a DNA backbone in a temporal controlled manner. Every fragment has overhangs at both ends allowing the four basic building blocks to hybridize. Adapted with permission from reference 33 (Nature Publishing Group, 2015). (b) Left: 2.5% native AGE in TAE buffer showing the growth of ds[10]. Lane 1: ds[5]-A^P, lane 2: ds[5]B^P, lane 3: nicked ds-AB[10], lane 4: ultra low ladder and lane 5: O'gene ladder. Middle: 2.5% AGE under denaturing conditions (with NaOH) displaying the unnicked backbone. Right: 2.5% AGE in TAE showing ds-AB[10] after PCR amplification (lane 1) and ss-AB[10] after magnetic beads separation.

purified again by AGE under denaturing conditions and the unnicked fragment was extracted then enriched by PCR (Figure 4.2b).

In order to use our scaffolds in building higher-order DNA nanoarchitectures, we employed PCR followed by magnetic beads separation to convert double-stranded backbones to their singlestranded form. To allow the binding of the double-stranded product to streptavidin-coated magnetic beads, we biotinylated the 5'end of the antisense strand (the sense that will not be used in future experiments) by using a biotinylated reverse primer (Figure 4.2a). However, prior to the incubation of the beads with ds-AB[10], we pre-treated them with 30 mM NaOH solution for 2 hours. This step is supposed to cleave the weakly bound streptavidin on the beads, hence minimizing byproducts. Later, ds-AB[10] was added to the beads in 0.5×SSC buffer at pH=7 for 2 hours (gently inverted to maximize binding). The single-stranded scaffold was obtained upon denaturing ds-AB[10] with a 20 mM solution of NaOH for 10 min. It is worthy to mention that both the concentration of the alkaline solution and the duration of incubation play a key role in determining the yield and the purity of ss-AB[10]. Incubation for a shorter time results in a low yield of ss[10], whereas keeping the mixture in contact with NaOH for a longer time can break the remaining weak biotin-streptavidin interaction. Similarly, using a concentration higher than 30 mM might have a greater impact on biotin/ streptavidin interaction. The supernatant containing the released ss-AB[10] product was finally recovered by ethanol precipitation. Figure 4.2b lane 2 shows a discrete band between 200 and 300 bp that corresponds to ss-AB[10]. Despite pre-treating the beads with NaOH, the non-penetrating band appearing in lane 2 is attributed to streptavidin proteins attached to 1-4 ss-AB[10] or ds-AB[10] and the lower mobility band around 500 bp corresponds to ds-AB[20] leftover.

4.2.2 Synthesis of Single-Stranded DNA Backbones ss[20] (developed by Hsu J.)

Over the past few decades, several approaches for building multigene circuits have been the crucial drivers of biological research and biotechnology. Nevertheless, the construction of genomes made up of repetitive DNA sequences remains unpredictable and time consuming. To overcome some of these challenges, ongoing efforts have been focusing on optimizing strategies such as Gibson assembly,³⁵ overlap-PCR on RCA (OERCA),³¹ iterative capped assembly (ICA)³⁶ and unique nucleotide sequence (UNS) guided assembly.³⁷ While each of these techniques presents many advantages, they suffer from poor fidelity (PCR-based methods and Gibson assembly), uncontrolled growth (OERCA) or they can still be time consuming (UNS guided assembly). Here, we used type II restriction enzyme (BsmBI) to combine two or more ds-AB[10] in the desired sequence (named M and N in Figure 4.3).

To start with, ds-AB[10] was digested by XbaI and EcoRI and ligated to digested pUC19 for cloning. We thought that this strategy will dramatically amplify our product, yet it is not a crucial step for the formation of ds[20]. Next, two sets of primers (each with a forward and a reverse primer) were designed such that the two amplified ds-AB[10]s from the plasmid contain type II restriction enzyme sites (BsmBI) and complementary sticky ends. In this work, we adapted Golden Gate assembly to create longer DNA fragments from the initial pieces for many reasons. Briefly, Type IIS restriction endonucleases are known to cleave DNA duplexes outside of their recognition sites, leaving behind unique sticky ends of 4 bases. Thus, the recognition site itself is eliminated and no scar sequence is inserted. After the digestion of two ds-AB[10]s (to produce M and N fragments) separately, we mixed the two backbones with digested pUC19 plasmid. During T7 ligation, the two pieces of DNA (M and N) came together in the right sequence and ligated to both ends of the open pUC19 through complementary sticky ends (Figure 4.3).

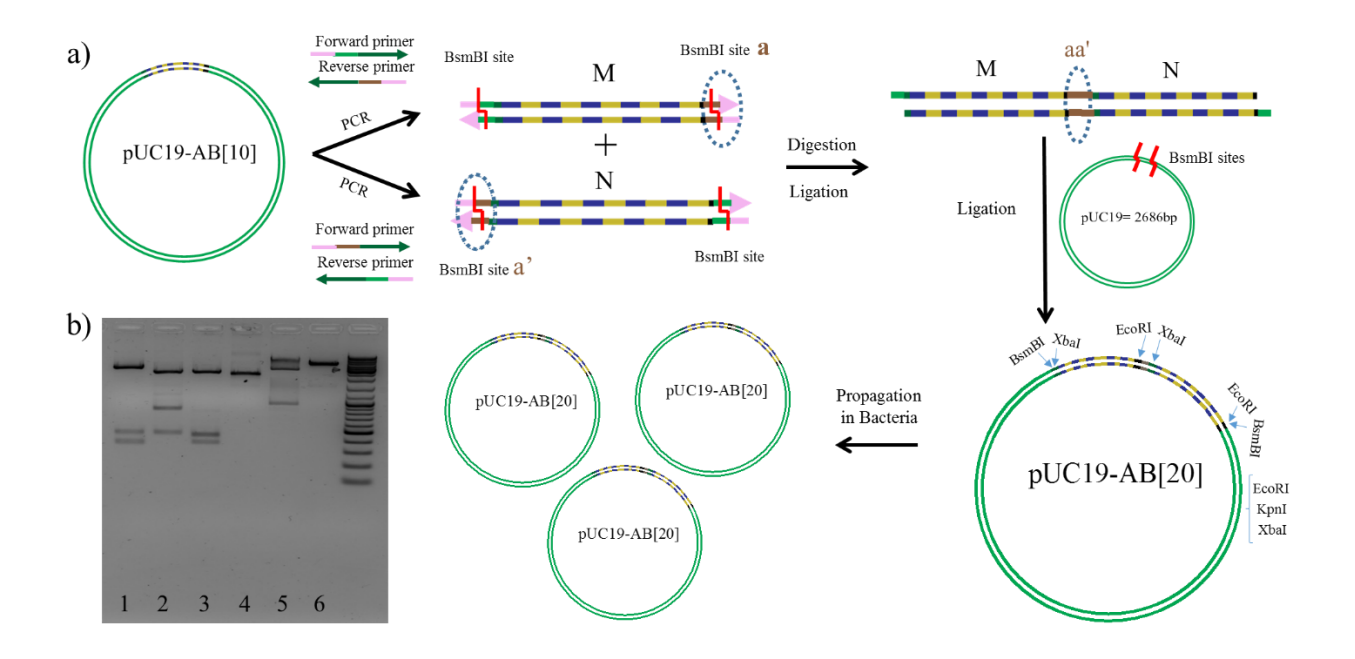


Figure 4.3. (a) Scheme illustrating the production of pUC19-AB[20] from pUC19-AB[10]. (b) AGE 2% in TAE buffer showing the insertion of the backbone into the plasmid. Lane 1: pUC19-AB[20] + EcoRI resulted in two fragments around 400 and 500 base pairs (bp) each , lane 2: pUC19-AB[20] + XbaI generated one DNA fragment ~500 bp and another ~1000 bp, lane 3: pUC19-AB[20] + EcoRI/XbaI, lane 4: pUC19-AB[20], lane 5: pUC19-AB[20] + BsmBI produced a fragment ~1000 bp corresponding to the size of our backbone and lane 6: pUC19-AB[20] + KpnI gave the linear pUC19-AB[20] product ~3600 bp.

To further examine the ligation of M+N to the digested pUC19, we run a native AGE prior to cloning. Figure 4.4 illustrates the successful insertion of the combined ds-AB[10] fragments into the plasmid (lane 1). Compared to lanes 3 and 4, the first lane displays three additional bands running around 500 (M or N), 1000 (M + N not ligated to plasmid) and 2000 bp (plasmid containing M+N) respectively. While the plasmid in lanes 3 and 4 was digested and ligated in the absence of the backbone, the plasmid in lane 8 was not. Note that the plasmid containing our 980 nt backbone was sequenced via Sanger methods (See section 4.4.6).

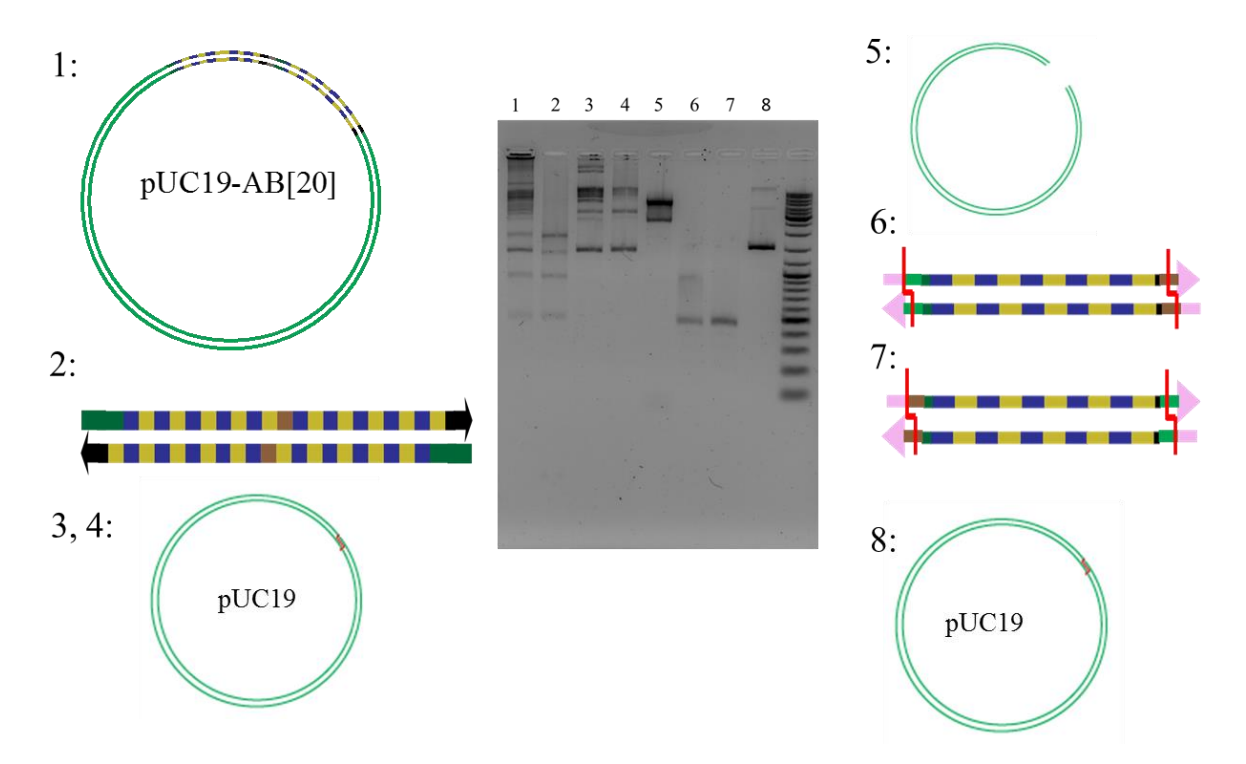
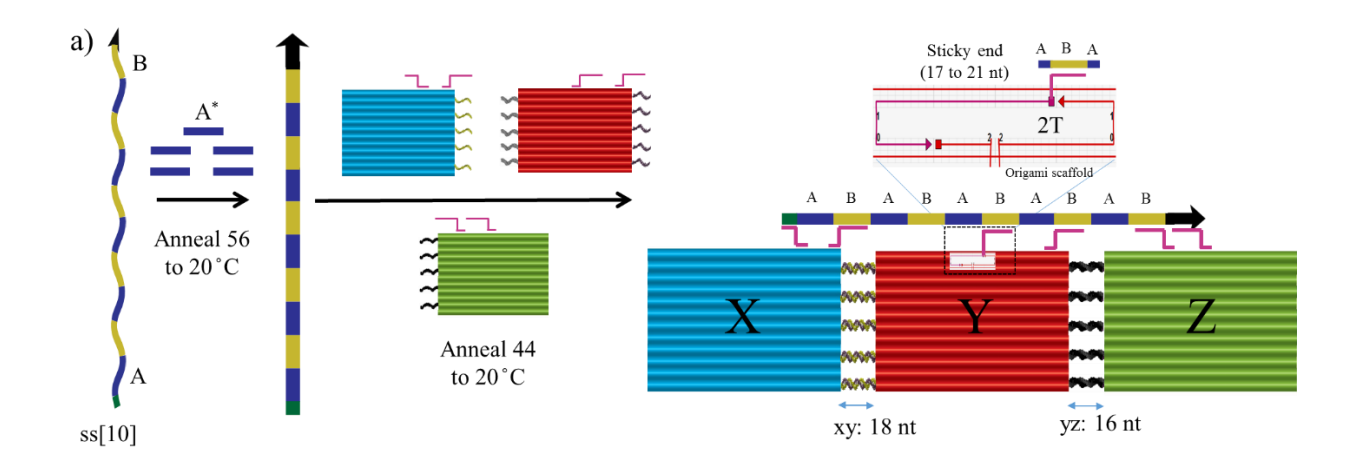


Figure 4.4. Native 2.5% AGE in TAE buffer displaying the comparison between the presence of ligase (Lanes 1 to 4) versus its absence (lanes 5 to 7). Lane 1: pUC19 + M + N, lane 2: M + N, lane 3: pUC19, lane 4: pUC19 (not purified), lane 5: pUC19 (not ligated), lane 6: M, lane 7: N and lane 8: pUC19 (not digested, nor ligated). Note that the all samples were digested except the ones in lane 8. Gel was performed by Hsu J.

4.2.3 Organization of Three Origami Tiles

In order to use our scaffolds (500 and 1000 nt) in building higher-order DNA nanoarchitectures, we employed PCR followed by magnetic beads separation to convert double-stranded backbones to their single-stranded form. We performed PCR on pUC19-AB[10] to extract ds-AB[10] and on pUC19-AB[20] to extract ds[20]. Alternatively, exonucleases (Lambda Exonuclease, T7 Exonuclease and Exonuclease III) can produce single-stranded fragments, when the 5'end of the ds scaffold is phosphorylated. One of the applications for these backbones is as addressable templates in extended DNA nanostructures. In several cases, the complexity of DNA

nanoarchitectures is associated with the number of unique sequences involved in the assembly. In principle, if these unique strands were replaced by repeating sequences, this would not only minimize the cost of the synthesis but also simplify the assembly. Here, we take advantage of the unique domains offered by our scaffolds to increase the addressability of the tiles and use the repeating patterns to expand the surface area of the structures. Sequentially grown DNA scaffolds offer an exceptional strategy to organize DNA origami tiles into various geometries and shapes. To validate this potential, we attempted initially to extend the assembly of higher-order DNA origami in 1-D. Individual tiles were first folded based on the method reported by Rothemund while heating the mixture at 95 °C then slowly cooling it down to 20 °C. 1 Separately, to increase the rigidity of the backbone, ss[10], the A pattern was hybridized to its complement A* (heated to 56°C then cooled to 22°C for ~1h). In this set of experiments, three tiles X5, Y5 and Z5 having the same core sequences but different attachment sites on the backbone were folded (Figure 4.5). For example, tile X can be connected to the backbone though 2 anchor points, one that is unique, complementary to the unique sequence on the 5'end of the backbone (22 bp), and another that is complementary to the block B (21 bp). Besides the two sticky ends extending from the vertical axis of each tile, we added 5 overhangs on the horizontal axis to improve the lateral cohesion strength between them. Figure 4.5 illustrates the inter-tile connection xy between tiles X5 and Y5 through 18 bp complementary ectensions and the connection yz between tiles Y5 and Z5 via 16 bp complementary extensions. To construct the 3-tile system, equimolar amounts of tiles X5, Y5 and Z5 (0.2 nM each) were mixed in 1xTAMg (12.5 mM of Mg²⁺), giving a final tile concentration of 0.6 nM. The ss[10]/A* solution was then added in 5 equimolar amount with respect to total tile concentration before annealing from 44 °C to 20 °C for ~45min. The final product was assessed by agarose gel electrophoresis and atomic force microscopy (AFM) in liquid conditions (Figure 4.5).



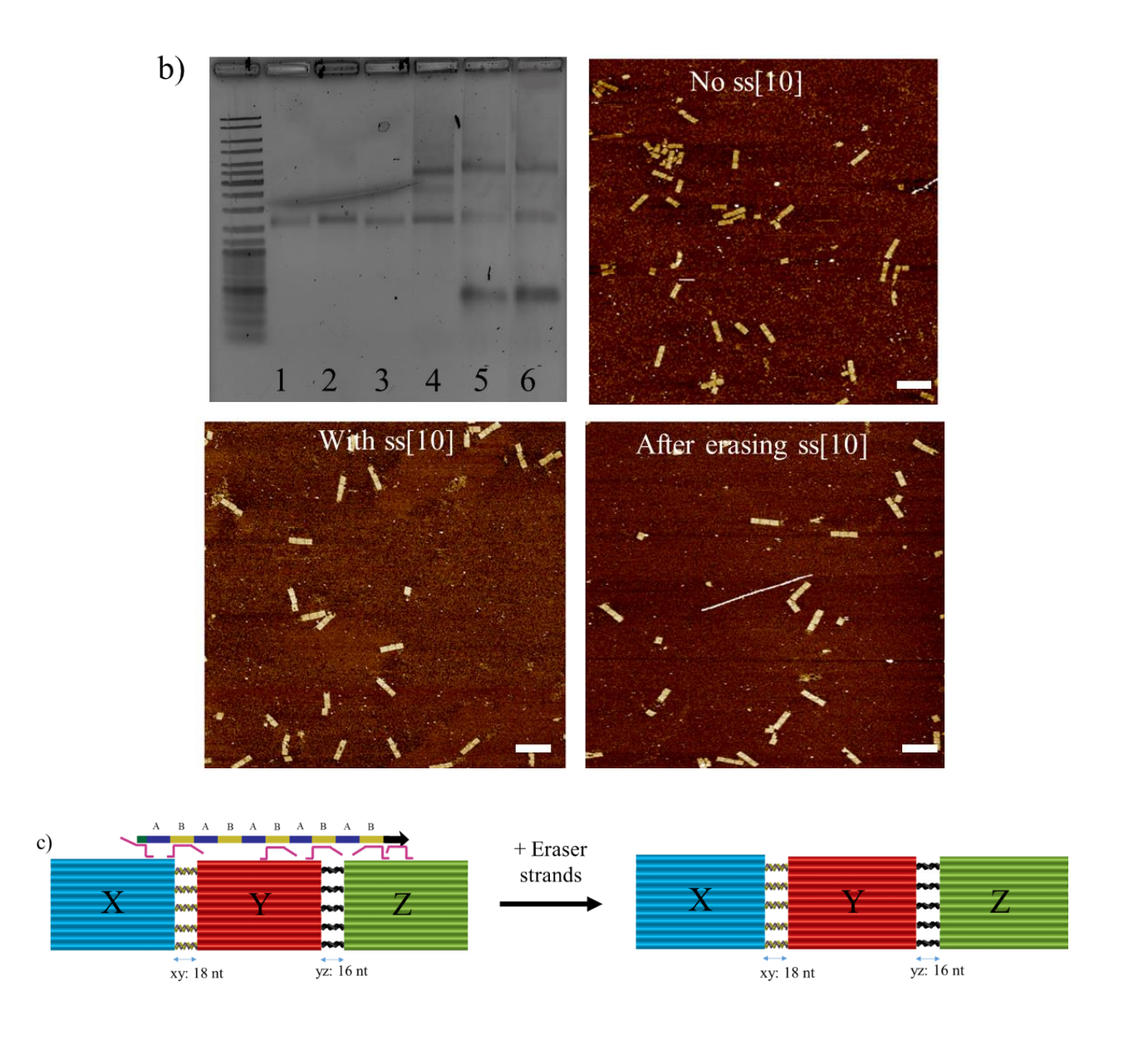


Figure 4.5. (a) Scheme depicting the one-pot assembly of 3-tile system in the presence of ss[10]. (b) Left: AGE 0.7% in TAMg. Lanes 1, 2 and 3 represent the individual tiles X5, Y5 and Z5. Lane 4: X5 + Y5 + Z5, lane 5: X5 + Y5 + Z5 before easing ss[10] and lane 6: X5 + Y5 + Z5 after easing ss[10]. Right: AFM micrographs demonstrating the effect of the external scaffold on organizing the tiles in 1-D. Even after removing the backbone, trimers were still the major product, scale bar 500 nm. Gel was performed by Chidchob P and the samples for AFM were prepared by him. (c) Schematic drawing of the removal of ss-AB[20] via strand displacement strategy.

In order to evaluate the effect of the backbone on the organization of the tiles in solution, we performed a statistical analysis on the AFM images taken with and without ss[10]. Interestingly in the presence of the backbone, linearly aligned trimers (3 tiles) constituted 71% of the overall mixture, whereas 22% only of the features were geometrically well aligned trimers in the absence of the backbone. Furthermore, the percentage of trimers (including the misaligned ones) when the backbone was hybridized to the tiles was 78% compared to 43% when it was not added. Therefore, ss[10] not only improved the formation yield of the trimers but also aligned them in a well-defined manner.

Next, we were interested in examining the stability of the trimers after the removal of the backbone. Thus, we added to each of the strands linking the tiles to the backbone a 10-base overhang (Figure 4.5c). Then, we organized the tiles X5, Y5 and Z5 in the presence of ss[10] through one-pot assembly. Addition of fully complementary erasing strands is expected to detach the backbone from each tile by strand displacement. Interestingly, the percentage of aligned trimers after removing the scaffold with respect to the other side-products was still significant. This observation is most likely due to the contribution of the backbone in the formation of trimers leading to 78% in yield. Yet, the removal of ss[10] seems to be possible afterwards without affecting much the stability of the whole system.

To maximize the cohesion strength between DNA tiles, an assembly of DNA origami containing 10 sticky ends of 16 (xy) and 18 (yz) complementary region each (X10, Y10, Z10) was performed (Figure 4.6). In the absence of the backbone, there were tile monomer, band smearing, and non-penetrating materials, which were likely to be aggregations of DNA tiles (lane 4, Figure 4.6). Addition of the backbone did not improve the trimer yield as expected, even at higher backbone concentration (lane 5-7). Atomic force microscopy (AFM) revealed that tile aggregates were the major product. This is likely due to strong cohesion between tiles and various possible connections between tiles (e.g., linear dimer, staircase dimer), which can easily result in aggregation.

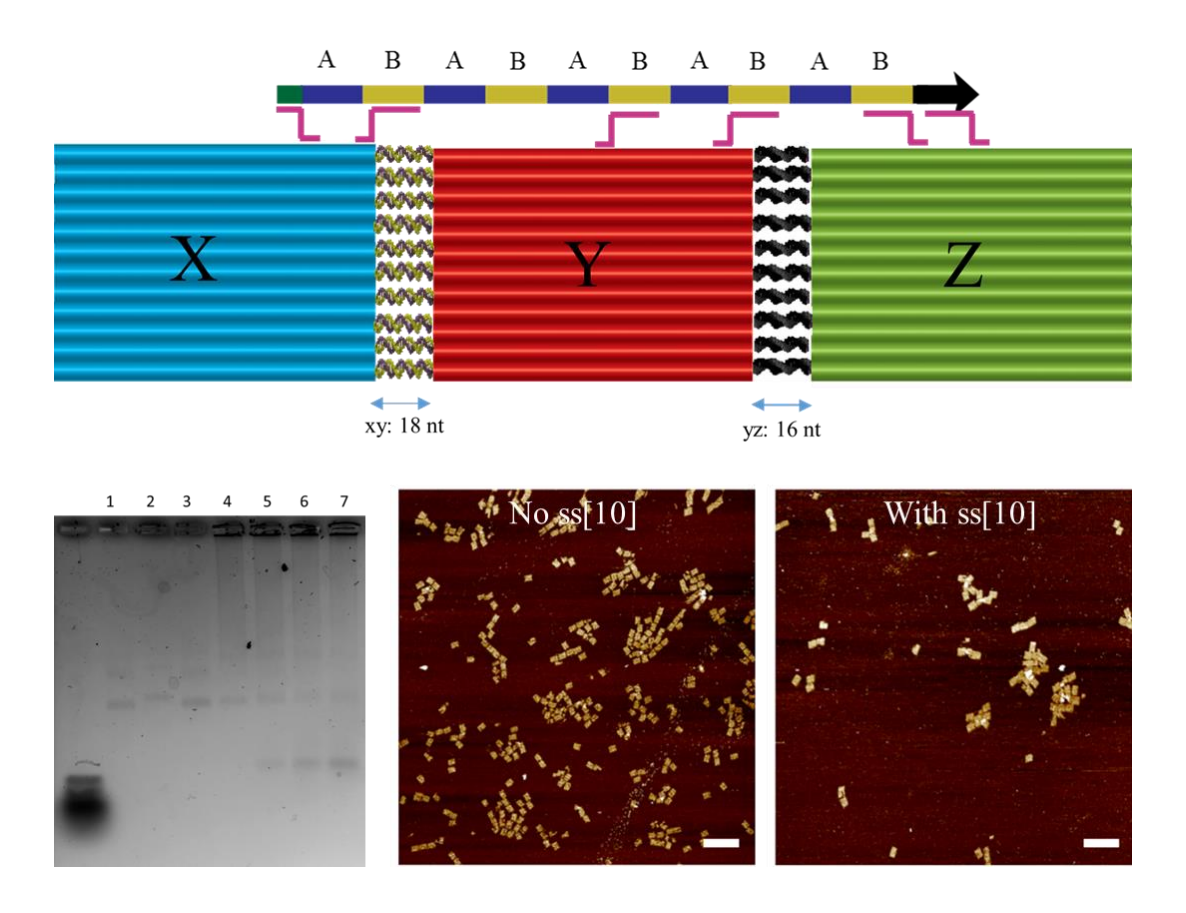


Figure 4.6. Top: Scheme showing 10 complementary extensions between X/Y tiles and Y/Z tiles. Bottom Left: 1% AGE in \times TAMg. Lane 1: X10, lane 2: Y10, lane 3: Z10, lane 4: X10+Y10+Z10, lane 5: (X10+Y10+Z10) + 5 equiv (ss[10]/A*), lane 6: (X10+Y10+Z10) + 10 equiv (ss[10]/A*) and lane 7: (X10+Y10+Z10) + 20 equiv (ss[10]/A*). Gel was performed by

Chidchob P. Right: AFM micrographs displaying the aggregation of three tiles in the absence and presence of ss[10]. Samples were prepared by Chidchob P.

Since the backbone is shown to improve the trimer yield as observed by AFM (Figure 4.5), we then followed the yield of trimers with respect to the concentration of ss[10] scaffolds. An efficient binding of the tiles to the backbone will, in theory, directly translate to more efficient alignment of the tiles on the backbone. Therefore, the titration of ss[10]/A* to the mixture X5+Y5+Z5 was carried out (Figure 4.7). Similar to Figure 4.5, the gel mobility decreased with increasing backbone concentration. However, the gel mobility became unchanged at 5 equivalents of the backbone with respect to total tile concentration. Thus, we decided to choose 5 equivalents of the backbone for all experiments. It is worthwhile mentioning that the sequential addition of the tiles to the backbone was also examined, please see section 4.4.7.

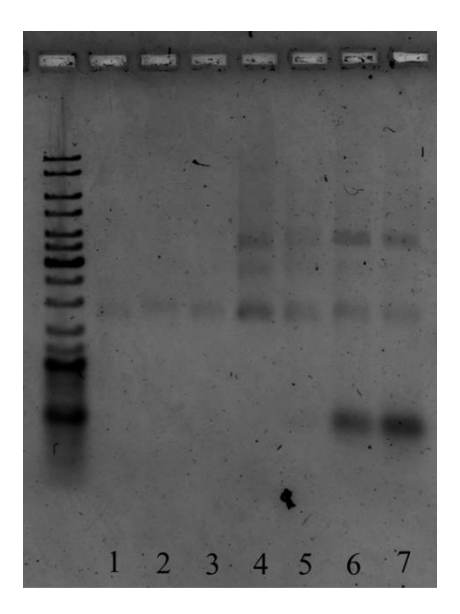


Figure 4.7. Titration of backbone to 3-tile system. Lane 1: X5, lane 2: Y5, lane 3: Z5, lane 4: X5 + Y5 + Z5 without $ss[10]/A^*$, lane 5: X5 + Y5 + Z5 with 1 equiv. $ss[10]/A^*$, lane 6: X5 + Y5 +

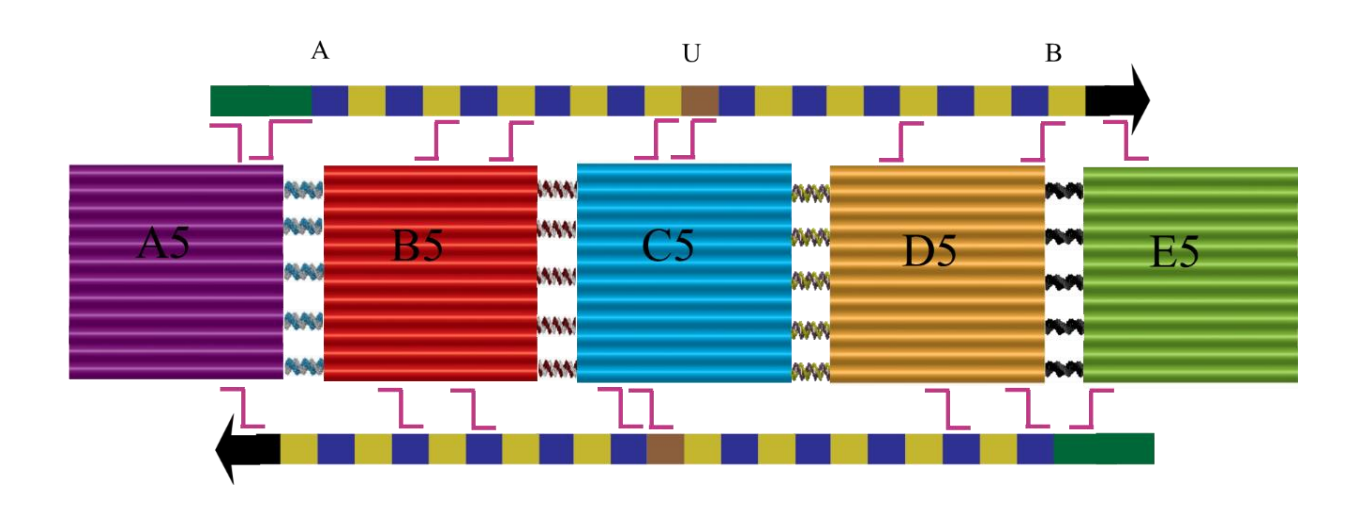
Z5 with 5 equiv. $ss[10]/A^*$ and lane 7: X5 + Y5 + Z5 with 10 equiv. $ss[10]/A^*$. Gel was performed by Chidchob P.

4.2.4 Self-Assembly of a Nano-Railroad Track

In the next set of experiments, we further examined the use of ss[20] scaffolds (980 mers) to organize five origami tiles in 1-D. Similar to ss[10], ss[20] was mixed with single-stranded A* at 1:10 ratio in TAMg, and the samples were annealed from 56°C to 20°C over 1 hour. To construct 5-tile system, equimolar amounts of tiles A5, B5, C5, D5 and E5 were mixed to give a final tile concentration of 1 nM. Then, ss[20]/A* solution was added in 5 equimolar amount with respect to total tile concentration before annealing from 44°C to 20°C over 4 hours. AGE and AFM were used to characterize the products.

In this section, we aimed initially at using 5 sticky ends (16 bp each) having the same sequences between two tiles e.g. tiles A5 and B5, yet a high amount of aggregates was observed on AFM (Figure 4.18). Therefore, we reduced the size of the overhangs to 10 bp and modified their sequences before proceeding with the one-pot assembly. Figure 4.8 displays the 1-D assembly of 5 origami tiles aided by ss[20]/A*. Unlike the 3-tile system, the addition of the backbone improved the yield of aligned pentamers from 19% to 38% only. This is most likely due to the increasing number of possible interactions between the tiles themselves or between the tiles and 1, 2 or more ss[20]. It also might be entropically more challenging to attach 5 tiles to a single backbone in an organized manner. In order to address this problem, we added on the vertical axis of each tile, opposite to the top sticky ends, new sticky ends that hybridize with the building block A of the backbone (Figure 4.8). To guide the assembly of the nano- "railroad track", 2 sets of ss[20] were mixed separately with single-stranded A* and B* respectively at 1:10 ratio from 56°C to 20°C.

Subsequently, 5 equivalents of ss[20]/A* and ss[20]/B* were added to the tiles (A5 to E5) before heating the mixture to 44°C then cooling it down to 20°C over 4 hour. The aim of this strategy is to improve the organization of pentamers by minimizing the non-desired interactions between the tiles and ss[20]. Interestingly, 5 tiles were successfully arranged by ss[10]/A* and ss[20]/B* scaffolds up to 66% (69% if we considered not well aligned pentamers) compared to 19% (30% including all types of pentamers) in the absence of any backbone. Accordingly, the percentage of tetramers decreased from 31% to 10%. The amount of trimers was reduced from 10% to 7% and the other misassembles features diminished from 29% to 14%. The results suggest that the "railroad" system is highly advantageous to assure the organization of the tiles in 1-D via maximizing the hybridization of the tiles to the backbone on both sides of the vertical axis. By using the railroad track system, we think that applications requiring larger areas than a single origami are achievable. The order and position of particular functional groups at the nanoscale precision can be adjusted by simply modifying the order of the building blocks on the backbone.



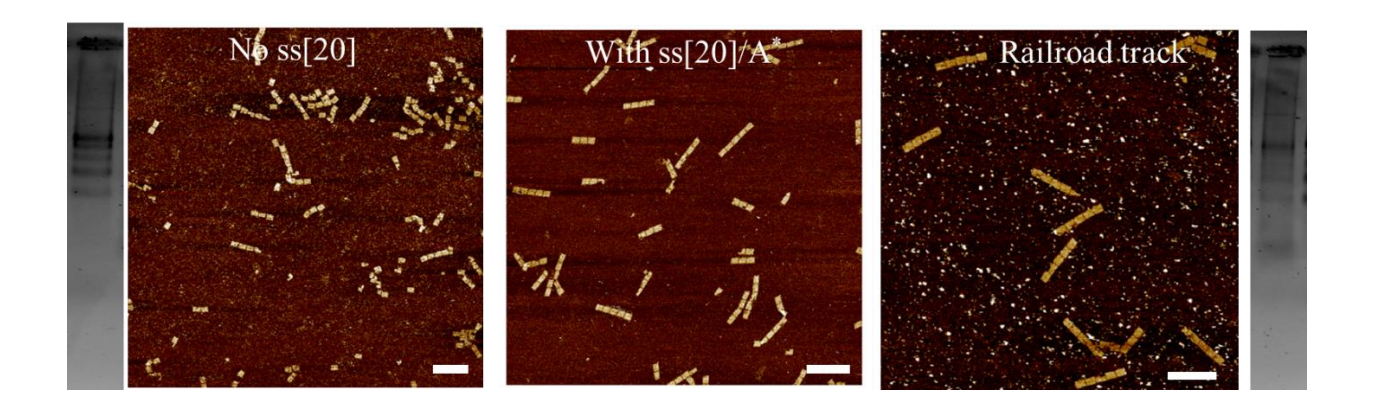


Figure 4.8. Figure 4. Top: Scheme displaying the railroad track in the presence of ss[20]/A* and ss[20]/B*. Bottom: AGE 1% in TAMg of the 5 tiles in the absence of the 2 backbones (left) and in the presence of the backbones (right). AFM micrographs showing the improvement of the yield of pentamers upon addition of ss[20]/A* and ss[20]/A* + ss[20]/B*, scale bar 500 nm.

4.3 Conclusions

In summary, we have developed a new strategy that borrows techniques from molecular biology to template the assembly of well-defined higher-order DNA nanostructures. Adapted from the Golden Gate method, we have synthesized DNA backbones of repetitive and unique sequences up to ~1000 nt in size. Since the sequences of the original building blocks were custom-made, we were able to control the frequency of the repetitive sequences and the order/position of the unique ones. Using BsmBI restriction enzyme, which cuts outside its recognition site, and in-situ ligation we combined 2 DNA strands (~500 nt each) and transformed the new construct into bacteria for cloning. Our approach is generally applicable to DNA fragments whether they are short or long, and allows the arbitrary positioning of unique and repetitive sequences. It is facile, relatively rapid compared to other techniques and requires the usage of one restriction enzyme to produce longer products. Here, we have demonstrated the impact of these scaffolds on the field of DNA nanotechnology. Our strategy will most likely also contribute to the growth of other fields that

require synthetic biological circuits such as the production of protein-polymers, biosensing and other biomedical applications.

For the DNA origami system to be integrated into a wide range of nanotechnology applications, procedures for assembling 1-D and 2-D structures must be simple, scalable and fast. Because our strategy involves the usage of cloned products and induces the organization of 3 to 5 tiles in high yields, it can be readily scaled up to match the requirements of some of these applications. Moreover, the addressability offered by the external scaffold plays an important role in determining the geometry and shape of the final construct. We anticipate that this technique can be extended to develop even larger structure, providing enough surface area to functionalize materials up to few micrometers. For instance, the successful assembly of super-origami structures on a large scale using routine routes employed industrially opens the doors to relate both top-down and bottom-up fabrication, hence, decreasing the reliance of future applications on the limited size of origami surface. In addition, applications such as directed multiplexed chemical reactions and molecular programming circuits (implemented in the development of biosensors and nanorobots) will highly benefit from the production of larger structures since the communication between the circuit components is amplified within the restricted area of the origami tiles.

4.4 Experimental

4.4.1 Materials

Acetic acid, boric acid, EDTA, urea, magnesium chloride, GelRed, tris(hydroxymethyl)aminomethane (Tris), D(+) glucose, 2-betamercaptoethanol, were purchased from Aldrich. Nucleoside (1000 Å)-derivatized LCAACPG solid support with loading densities of 25-40 µmol/g, Sephadex G-25 (super fine DNA grade), and reagents for automated DNA synthesis

were used as purchased from BioAutomation. Acrylamide (40%)/bis-acrylamide 19:1 solution and agarose were purchased from BioShop. All staple strands used for the assembly of origami were purchased from Bioneer. The scaffold M13mp18 single-stranded was purchased from New England Biolabs. AFM cantilevers were purchased from Asylum Research (model AC160TS) and RubyRed mica were ordered from Electron Microscopy Sciences. TBE buffer is composed of 90 mM Tris and boric acid and 1.1 mM EDTA, with a pH of ~8.3. TAMg buffer is composed of 45 mM Tris and 12.5 mM MgCl₂ with a pH of ~7.8 adjusted by glacial acetic acid. 1xTAE is composed of 45 mM Tris and 1 mM EDTA, with pH adjusted to 8.0 using glacial acetic acid. 1xOK buffer is composed of 50 mM Tris-HCl, 10 mM MgCl₂, 5 mM dithiothreitol (DTT), with a pH of 7.5. 1xQL buffer is composed of 66 mM Tris-HCl, 10 mM MgCl₂, 1 mM DTT, 1 mM ATP, 7.5% w/v PEG6000, with a pH of 7.6, and was made in-house as a 2x concentrate. 1xALK is composed of 30 mM NaOH and 1 mM EDTA. 1xSDA buffer is composed of 40 mM Tris, 10 mM MgCl2, 50 mM NaCl, 5 mM DTT, 100 μg/mL bovine serum albumin (BSA), and 500 μM of each dNTP. 0.5xSSC buffer is composed of 75 mM NaCl and 7.5 mM sodium citrate, with a pH of 7.0. Kits for Optikinase and Quick, T4 and T7 DNA ligase were purchased from New England Biolabs. A MyTaqTM HS Red PCR kit was purchased from CedarLane Laboratories. QIAquick Gel Extraction and PCR purification kits from Qiagen were used for extraction or cleanup of PCR products. FastDigest® XbaI and EcoRI were purchased from Life Technologies. rSAP (Shrimp Alkaline Phosphatase) was purchased from New England Biolabs. Streptavidin Magnesphere® Paramagnetic Particles were purchased from Promega. DH5α (Subcloning Efficiency Competent Cells) were purchased from Life Technologies. LB media is composed of 2.5 g BioTryptone, 2.5 g NaCl and 1.25 g Yeast Extract. PureLink Quick Plasmid DNA Mini/Maxi Prep Kits from Qiagen were used to isolate the plasmid.

4.4.2 Instrumentation

Standard automated oligonucleotide solid-phase synthesis was carried on a BioAutomation MerMade MM6 DNA synthesizer. UV-Vis quantifications were performed with a NanoDrop Lite Spectrophotometer. Polyacrylamide gel electrophoresis (PAGE) was carried out on a 20 x 20 cm vertical Hoefer 600 electrophoresis unit. Agarose gel electrophoresis (AGE) was performed on an Owl Mini gel electrophoresis unit. Thermal anneals, polymerase chain reaction (PCR), and enzymatic digestions were conducted using an Eppendorf Mastercycler Pro 96 well thermocycler. AFM was performed with a MultiModeTM MM8 SPM connected to a NanoscopeTM controller, from the Digital Instruments Veeco Metrology Group. The plasmids were sequenced using Sanger methods at McGill University Genome Center and Innovation Quebec.

4.4.3 Sequential Growth of ds[10]

A. DNA synthesis

The sequences of each building block were generated by CANADA version 2.0 (available online at http://ls11- www.cs.uni-dortmund.de/molcomp/downloads/), a program that intends to minimize undesired secondary interactions, and IDT DNA (Table 4.1). DNA synthesis was carried on a on a BioAutomation MerMade MM6 DNA synthesizer at 1 µmole scale. Deprotection and cleavage from the solid support was achieved through the addition of concentrated ammonium hydroxide (55°C, 14 hours). Crude products were then purified via polyacrylamide gel electrophoresis under denaturing conditions (4M urea). Following PAGE, the gel was visualized by UV light over a fluorescent TLC plate. The product was rapidly excised, then crushed and incubated in 11 mL of autoclaved water at 65°C overnight. Size exclusion chromatography

(Sephadex G-25) was used to desalt the samples. Finally, strands were quantified via a NanoDrop Lite Spectrophotometer (OD260) and using IDT's extinction coefficient at 260.

B. Temporal growth

Every strand having an internal 5'-terminus was phosphorylated by OptiKinase. The concentration of the strands was adjusted to 10 μM, with a 1xOptikinase buffer, 2.5 mM ATP, and 0.2 U/μL of OptiKinase. The mixture was incubated at 37°C for 40 min, then at 75°C for 10 min to inactivate the enzyme. It is worthy mentioning that the efficiency of Optikinase is around 60% according to the manufacturer. AB[10] was synthesized following the Sequential Growth procedure by Hamblin *et. al.*³³ It includes in-situ ligation, isolation of the ds[10] by native AGE, PCR enrichment and the separation of the non-nicked ds[10] via denaturing AGE. The duplex seeds used were A^Pxba, A, B, B^Peco; sequences can be found in table 4.1. In PCR enrichment, PrimerB2eco and PrimerA1xba were used for ds[10]; no additional restriction site was added through PCR.

Table 4.1. Duplex Seed Sequences for AB[10]

Name	Sequence (5' -> 3')	Length (bp)
Alpxba	AATTAAGATAGGCGCGGCTCTAGAGCGATATAATCTGG CTGCGCTTGAAACAACGGAAGGTCATGCTTTAGGA	73
A2pxba	TGACCTTCCGTTGTTTCAAGCGCAGCCAGATTATATCG CTCTAGAGCCGCGCCTATCTTAATT	63
A1	AATCTGGCTGCGCTTGAAACAACGGAAGGTCATGCTTT AGGA	43
A2	TGACCTTCCGTTGTTTCAAGCGCAGCCAGATTTCTTCT GATC	42
B1	ATCAAACCAAAGTTCAGCAACAGGCCGTTAAGGATCA	42

	GAAGA	
B2	CTTAACGGCCTGTTGCTGAACTTTGGTTTGATTCCTAA AGCA	42
B1peco	ATCAAACCAAAGTTCAGCAACAGGCCGTTAAGGATCA GAAGACGTAGTCCGAATTCACCTGCAA	64
B2peco	TTGCAGGTGAATTCGGACTACGTCTTCTGATCCTTAAC GGCCTGTTGCTGAACTTTGGTTTGATTCCTAAAGCA	74

4.4.4 Transformation of pUC19-AB[10] (Performed by Hsu J.)

Fist, ds[10] was amplified by PCR with annealing temperature 1-2 degree lower than that used in Sequential Growth. 1μg of ds[10] and 1μg of pUC19 were digested using FD EcoRI and FD XbaI (LifeTechnologies) for 1.5 hr at 37°C and purified using 2.5% and 1.2% (w/v) native agarose gel, respectively. The band from the gel was excised and the product was extracted by ethanol precipitation. Then 40ng of the digested backbone were ligated into 80ng of the digested plasmid using NEB T4 Ligase. We followed the manufacturer's manual for overnight or 10 min ligation. Finally, we transformed our insert into DH5α cells. Around 70 ng of ligated product was gently added to 50 μL aliquot of DH5α cells previously placed on ice. Then, the cells were heat shocked for 30 s at 42°C after 30 min incubation time. Lysogeny broth (LB) media was later added and the mixture was shaken at 225 rpm for 1 hour at 37°C. The transformation was plated on ampicillinagar and incubated overnight at 37°C. Few colonies were picked from the ligation plate and each one was used to inoculate 3 mL of LB media containing ampicillin (100 μg/mL) at 225 rpm and 37°C. PureLink Quick Plasmid DNA Mini Prep Kit was used to isolate the plasmid containing our insert.

In order to examine the sequence of our backbone within the plasmid, we submitted our samples for Sanger Sequencing to McGill University Genome Center and Innovation Quebec.

The observed sequence was the following:

NNNNNNcgatataatctggctgcgcttgaNNNacggaaggtcatgctttNNNNNNcaaaccaaagttcagcaacaggccg ttaaggatcagaagaaatctggctgcgcttgaaacaacggaaggtcatgctttaggaatcaaaccaaagttcagcaacaggccgttaaggat cagaagaaatctggctgcgcttgaaacaacggaaggtcatgctttaggaatcaaaccaaagttcagcaacaggccgttaaggatcagaag aaatctggctgcgcttgaaacaacggaaggtcatgctttaggaatcaaaccaaagttcagcaacaggccgttaaggatcagaagacaatctg gctgcgcttgaaacaacggaaggtcatgctttaggaatcaaaccaaagttcagcaacaggccgttaaggatcagaagacaatctg gctgcgcttgaaacaacggaaggtcatgctttaggaatcaaaccaaagttcagcaacaggccgttaaggatcagaagatcagaatccgaatt c

The red color represents the A block and the blue color represents the building block B.

The expected sequence is:

5'-

caggtcgactctagagcgatataatctggctgcgcttgaaacaacggaaggtcatgctttaggaatcaaaccaaagttcagcaacaggccgt taaggatcagaagaaatctggctgcgcttgaaacaacggaaggtcatgctttaggaatcaaaccaaagttcagcaacaggccgttaaggat cagaagaaatctggctgcgcttgaaacaacggaaggtcatgctttaggaatcaaaccaaagttcagcaacaggccgttaaggatcagaag aaatctggctgcgcttgaaacaacggaaggtcatgctttaggaatcaaaccaaagttcagcaacaggccgttaaggatcagaagagaaatctg gctgcgcttgaaacaacggaaggtcatgctttaggaatcaaaccaaagttcagcaacaggccgttaaggatcagaagaaatctg gctgcgcttgaaacaacggaaggtcatgctttaggaatcaaaccaaagttcagcaacaggccgttaaggatcagaagatcagaatcaaaccaaagttcagcaacaggccgttaaggatcagaatcagaacgaatcagaacaacggaaggtcatgctttaggaatcaaaccaaagttcagcaacaggccgttaaggatcagaatcagaactcgaatt cactggc-3'

After determining the plasmid with perfect backbone sequence we wanted to improve further the yield of our product. We used 50ng of this plasmid from Miniprep solution to transform 50μL of DH5α, via the same protocol. The next day, we picked a single colony using a sterile pipette tip and dropped it into 4.5 mL of LB with ampicillin to inoculate the media for 6 hrs at 225rpm, 37°C. Then we poured the media into 300mL of LB with ampicillin to inoculate further overnight. Finally, we used Maxiprep (Qiagen) to prepare a bulk quantity of the plasmid from the rest of the media. The yield was 850 ng/μL.

4.4.5 Magnetic Beads Separation of ss[10]

To isolate ds[10] from pUC19-AB[10], two primers that bind the flanking region of ds[10] were designed: Primer pUC19-AB10-For (caggicgactctagagcgatat) and primer pUC19-AB10-Rev (gccagtgaattcggactacg). Throughout this work, when designing a new primer, we avoided using any sequence included within the repeating pattern of ds[10] since it can introduce non-specific binding. Optimal PCR conditions intend to improve the yield of the desired product and minimize the amount of contaminants. This is achieved by: (i) using the gradient function on the thermal cycler to find out the best temperature, (ii) varying the amounts of pUC19-AB[10] and primers. Table 4.2 summarizes the final quantities we used to extract ds[10] from pUC19-AB[10]. Note that the extension of the primers occurred at 63°C. Before starting the conversion of ds[10] to its single-stranded analogue ss[10], the PCR products were purified via PCR purification kit. The remaining steps are described in section 4.2.1.

Table 4.2. Optimized PCR conditions to exctract ds[10] from pUC19-AB[10]

	μL
pUC19-AB[10] (20ng)	0.2
pUC19-AB10-For (0.5 μM)	0.5
pUC19-AB10-Rev (0.5 μM)	0.5
Autoclaved H ₂ O	18.8
MyTaq 2×mix	20

4.4.6 Synthesis of ds[20] and ss[20]

A. Synthesis of ds[20] (developed by Hsu J.)

Adapted from the Golden Gate assembly, type II restriction enzyme BsmBI was used to help linking 2 fragments of ds[10]. Because ds[10] was already inserted into pUC19, we had to design 4 primers (Primer A1p-pUC19-For, PrimerB2p-In-Rev, PrimerA1p-In-For and PrimerB2p-

pUC19-Rev) that introduce the corresponding complementary regions into ds[10] to synthesize ds[20]. As such, each primer was extended by 5 unique bases and a restriction site for the enzyme BsmBI (Figure 4.9). We made sure that all of the sticky ends are unique and do not overlap with each other besides than their own compatible ends. To generate the left fragment M, primer A1p-pUC19-For and primer B2p-In-Rev were used (In stands for the unique bases added to this primer allowing M to hybridize N). In a separate reaction mixture, primer A1p-In-For and primer B2p-pUC19-Rev were used to produce the right fragment N.

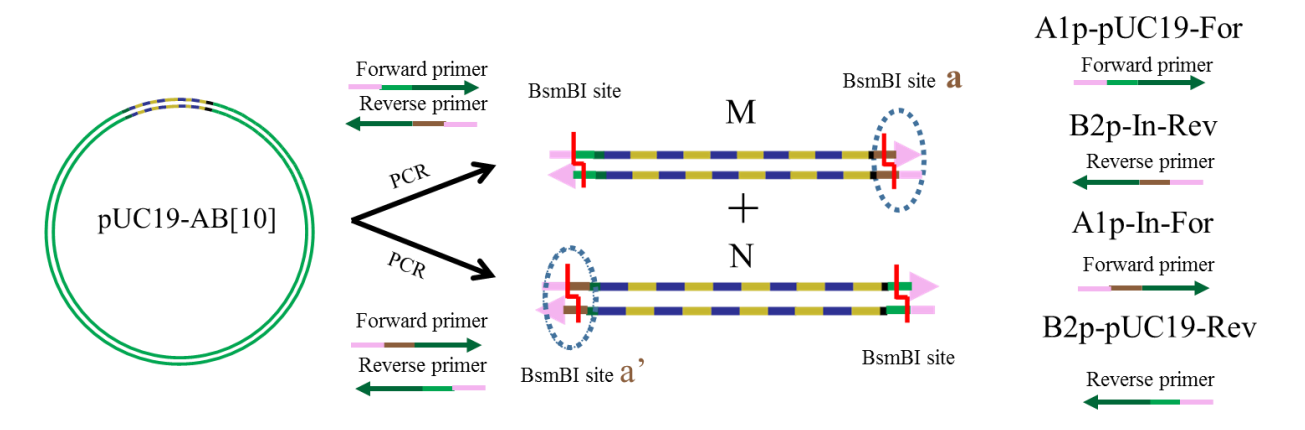


Figure 4.9. Scheme showing the generation of the two DNA fragments M and N via two PCR reactions.

ds[10] left fragment: M

TGCGTCCGTCTCGCGCGCAGGTCGACTCTAGAGCGATATaatctggctgcgcttgaaacaacggaag gtcatgctttaggaatcaaaccaaagttcagcaacaggccgttaaggatcagaagaaatctggctgcgcttgaaacaacggaaggtcatgct ttaggaatcaaaccaaagttcagcaacaggccgttaaggatcagaagaaatctggctgcgcttgaaacaacggaaggtcatgctttaggaatcaaaccaaagttcagcaacaggccgttaaggatcagaagaaatctggctgcgcttgaaacaacggaaggtcatgctttaggaatcaaaccaaagttcagcaacaggccgttaaggatcagaagaaatctggctgcgcttgaaacaacggaaggtcatgctttaggaatcaaaccaaagttcagcaacaggccgttaaggatcagaagaaatctggctgcgcttgaaacaacggaaggtcatgctttaggaatcaaaccaaagttcagcaacaggccgttaaggatcagaagaCGTAGTCCGAATTCACTGGCGGAGACGCA

PrimerA1p-pUC19-For

TGCGTCCGTCTCGCGCGCAGGTCGACTCTAGAGCGATAT

PrimerB2p-In-Rev

TGCGTCCGTCTCCGCCAGTGAATTCGGACTACG

ds[10] right fragment: N

TGCGTCCGTCTCGTGGCCAGGTCGACTCTAGAGCGATATaatctggctgcgcttgaaacaacggaagg tcatgctttaggaatcaaaccaaagttcagcaacaggccgttaaggatcagaagaaaatctggctgcgcttgaaacaacggaaggtcatgctt taggaatcaaaccaaagttcagcaacaggccgttaaggatcagaagaaatctggctgcgcttgaaacaacggaaggtcatgctttaggaat caaaccaaagttcagcaacaggccgttaaggatcagaagaaatctggctgcgcttgaaacaacggaaggtcatgctttaggaatcaaacca aagttcagcaacaggccgttaaggatcagaagaaatctggctgcgcttgaaacaacggaaggtcatgctttaggaatcaaacca aagttcagcaacaggccgttaaggatcagaagaaatctggctgcgcttgaaacaacggaaggtcatgctttaggaatcaaaccaaagttca gcaacaggccgttaaggatcagaagaCGTAGTCCGAATTCACTGGCTCCCGGAGACGCA

PrimerA1p-In-For

TGCGTCCGTCTCGTGGCCAGGTCGACTCTAGAGCGATAT

PrimerB2p-pUC19-Rev

TGCGTCCGTCTCCGGGAGCCAGTGAATTCGGACTACG

The PCR conditions are listed in Table 4.3. The reaction were carried on at 63°C annealing temperature.

Table 4.3. PCR conditions to generate M and N fragments

Left-500mer-Insert	(µL)	Right-500mer-Insert	(μL)
(or ds[10]-M)		(or ds[10]-N)	
pUC19-AB10 (20 ng)	0.461	pUC19-AB10 (20 ng)	0.461
Primer ApF	1.100	Primer AiF	1.362
$(0.625 \mu \text{M})$		$(0.625 \mu M)$	
Primer BiR	1.623	Primer BpR	0.767
$(0.625 \mu M)$		$(0.625 \mu M)$	
Autoclave H ₂ O	16.82	Autoclave H ₂ O	17.41
MyTaq 2×mix	20	MyTaq 2×mix	20

^{*} Primer ApF = PrimerA1p-pUC19-For; Primer BiR = PrimerB2p-In-Rev...so on

Following PCR purification of M and N, each backbone was digested with BsmBI for 16 hours at 37°C. The enzyme was then heated and inactivated for 20 min at 65°C. PCR purification kit was used to purify the two fragments and pUC19 prior to ligation. Table 4.4 summarizes the conditions employed for digestion. Later, digested pUC19 plasmid was mixed with M and N scaffolds in the presence of T7 ligase for 2 hours at room temperature (Figure 4.3). Table 4.5 summarizes the ligation conditions.

Table 4.4. Digestion conditions of pUC19 and M and N fragments with BsmBI

(µL)	pUC19 (1μg)	M (500ng)	N (500ng)
DNA (Insert OR	14.12	3.75	4.06
Plasmid)			
10X Tango Buffer	2	2	2
DTT (10mM)	2	2	2
dH2O	0.88	11.25	10.94
BsmBI	1	1	1

Table 4.5. Ligation conditions of pUC19 and M and N fragments with T7 ligase

pUC19 (100ng)	2.84 (35.2 ng/μL)
ds[10]-M Insert (18.5 ng)	0.877 (21.1 ng/μL)
ds[10]-N Insert (18.5 ng)	0.894 (20.7 ng/μL)
2X T7 Ligase Buffer	5
T7 Ligase	0.25
dH2O	0.139

B. Transformation of ds[20] into pUC19 (Followed Hsu J. conditions)

The ligation reaction (10 μ L) was used without further purification for transforming 90 μ L of MAX Efficiency DH5 α cells (LifeTechnologies), following the standard protocol provided. Positive and negative controls consisting of pUC19 digested and pUC19 intact were transformed

into the cells to compare with our product. Subsequent to picking the colonies from the ligation plates, each colony was inoculated overnight in a separate 3 mL of LB media containing ampicillin (100 µg/mL) at 225 rpm and 37°C. Finally, the plasmid was isolated using PureLink Quick Plasmid DNA Mini Prep Kit (eluted with 30 µL of EB) and the backbone ds[20] was screened via BsmBI. Table 4.6 displays one example in which colony 1 was screened for ds[20]. The mixture was incubated at 37°C for 1h.

Table 4.6. Digestion conditions of pUC19-[AB]20 with BsmBI

	Colony 1
DNA (50ng)	1.088
10x Tango Buffer	1
DTT (10mM)	1
dH2O	6.41
BsmBI (0.5U)	0.5

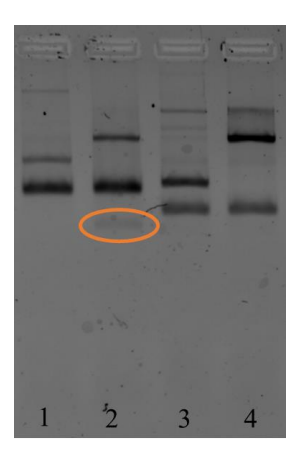


Figure 4.10. native AGE 2.5 % in TAE buffer showing one colony containing AB[20] (lanes 1 and 2) and another one that does not (lanes 3 and 4). Lanes 1 and 3: colonies were not treated with BsmBI, lanes 2 and 4: colonies were treated with BsmBI. Gel was performed by Hsu J.

C. Sequencing of pUC19-AB[20]

The same procedure for sequencing pUC19-AB[10] was followed to test the sequence of pUC19-AB[20]. Primers pUC19-AB20BB-FOR (ataagggcgacacggaaatg) and pUC19-AB20BB-REV (atcgcccttcccaacagtt) were used to perform the experiment. Note that every primer is able to sequence about 500bp from each end of the insert region. The samples were submitted for Sanger Sequencing to McGill University Genome Center and Innovation Quebec. From combining the two sequences given by the center, we found that our scaffold contains 1 substitution (highlighted in green) with respect to our theoretical expectations.

The observed sequence was:

D. Conversion of ds[20] to ss[20]

We followed the same protocol described in section 4.2.1 to generate ss[20] using Primer pUC19-AB20BB-PCR-FOR (cgtatcacgaggccctttc) and 5' biotinylated Primer pUC19-AB20BB-PCR-REV (gcttacagacaagctgtgac). We incubated the double-stranded backbone for 3 hours instead of 2 in 0.5×SSC buffer, while gently inverting the mixture, to maximize binding. Because ds[20] is longer than ds[10], increasing the incubation time is expected to improve the binding of

biotinylated ds[20] to the beads. Figure 4.11 lane 2 shows a discrete band around 500 bp that corresponds to ss[20]. It is noteworthy that improving the yield of ss[20] using this method is challenging. As described in the previous section, we attempted to increase the concentration of NaOH to enhance the separation of the double helix. However, an intense non-penetrating band was observed in the gel indicating the cleavage of biotin-streptavidin bond.

Alternatively, we optimized the conditions for using Lambda Exonuclease to generate ss[20] since it is faster and results in less byproducts (Figure 4.11). Table 4.7 summarizes the optimal conditions used to isolate ss[20] through Lambda Exonuclease method. Note that the same primers were used during PCR step before adding the exonuclease. In this case, the 5'end of the reverse primer was phosphorylated to facilitate the digestion of the antisense strand. The mixture was incubated at 37°C for 40 min then the enzyme was deactivated at 75°C for 15 min.

Table 4.7. Lambda Exonuclease digestion of ds[20]

ds[20] (180 ng/μL)	8.3 μL (60 ng/μL)
10x Lambda Exo Buffer	2.5 μL _(1×)
λ Exo (5000 Units/mL)	7.5 µl (1.5 U/µL)
dH2O	6.7 µL

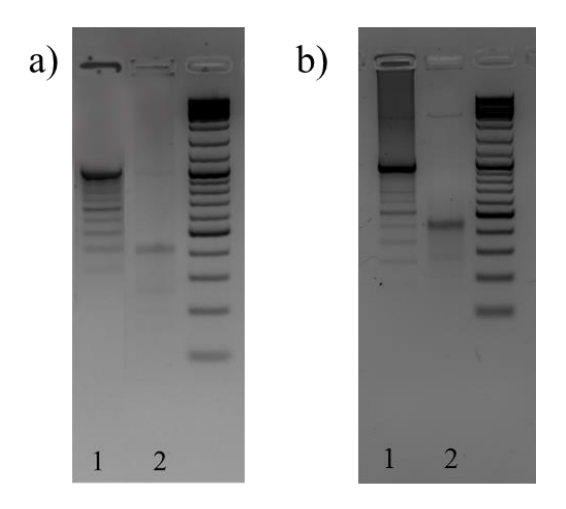


Figure 4.11. 2.5% AGE gel in 1×TAE buffer displaying the mobility shift between ds[20] and ss[20]. (a) via magnetic beads separation and (b) via Lambda Exonuclease technique. Lane 1: ds[20] and lane 2: ss[20].

4.4.7 Preparation of the 3-Tile System

A. Tile Assembly

The assembly of DNA tiles was based on the method reported by Rothemund¹ The long circular single-stranded viral scaffold M13mp18 was folded into rectangular tile with the aids of multiple short staple single-stranded DNA. The sequences of staple strands required for different tiles are listed in final section.

DNA tiles were assembled in one-pot annealing at 1 nM M13mp18 scaffold and 10 nM each staple strands in 1xTAMg buffer (45 mM Tris, 20 mM acetic acid, 12.5 mM MgCl₂·6H₂O at pH ~8.0). Then, 500 μL samples were heated to and held at 95°C for 5 min and slowly annealed to 20°C (-1°C/min). To remove excess staple strands, the samples were purified with 100kDa Amicon centrifugal filters (Millipore). First, 500 μL samples were centrifuged at 6000 rpm at 4°C for 5 mins. Then, 400 μL 1xTAMg was added and the samples were centrifuged at 5000 rpm at 4°C for 5 mins. This filtration step was repeated two more times. Approximately 50-100 μL samples were recovered, which can be stored at 4°C up to a week before use.

To determine the concentrations of DNA tiles, absorbance at 260 nm was measured by Biotek Synergy HT plate reader. The extinction coefficient of different DNA tiles can be approximated by equation (1)¹

$$\varepsilon = 6700 ds + 10000 ss$$
 (1)

where ds is the number of double stranded base pairs and ss is the number of single-stranded base. Using Beer-Lambert's law (A260 nm = ϵ bc, b = 1 cm), the concentrations of DNA tiles can be calculated.

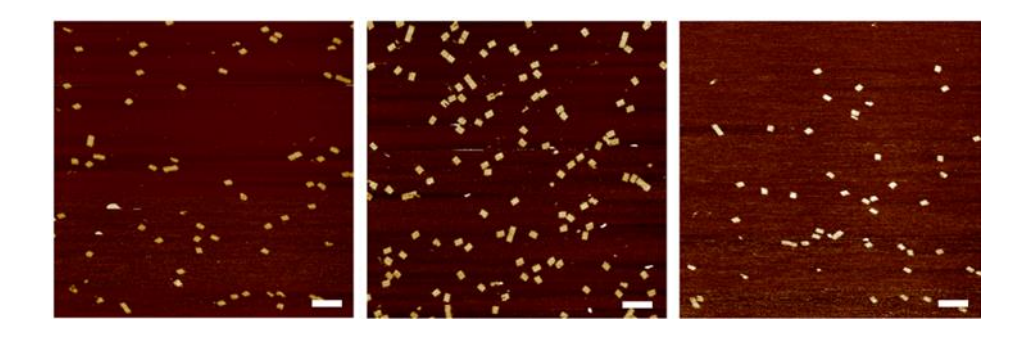


Figure 4.12. AFM micrographs showing the assembly of individual origami tiles, scale bar 500 nm.

B. Characterization of the 3-tile system (Gel and samples were prepared by Chidchob P)

We first attempted to increase a rigidity of single-stranded backbone, ss[10], by hybridizing A blocks of the backbones with its complements (A^*). Briefly, ss[10] was mixed with single-stranded A^* at 1:5 ratio in 1xTAMg, and the samples were annealed from 56°C to 20°C over 1 h. To construct 3-tile system, equimolar amounts of tile X, Y and Z (0.2 nM each) were mixed in 1xTAMg, which will give final tile concentration of 0.6 nM. Then, ss[10]/ A^* solution was added in 5 equimolar amount with respect to total tile concentration, i.e., 3 nM, before annealing from 44°C to 20°C over 4 hours. Agarose gel electrophoresis (AGE) was used to characterize the products by mixing 20 μ L samples with 4 μ L 6X loading dye then running on 1% AGE at 80 V for 2.5 h.

As one-pot assembly of 3-tile systems, which involved mixing together X5, Y5, Z5 and ss[10]/A*, was used in all previous experiment, we then investigated whether an order of addition of the tiles can improve the product formation. For example, X5 can bind first to the backbone and this preorganization may direct the binding of another two tiles to the backbone. As such, an assembly was performed in stepwise fashion: 1) annealing one of the tiles with the backbone from 44°C to 20°C, 2) adding the second tile and annealing from 44°C to 20°C, and 3) adding the third tile and annealing from 44°C to 20°C. In Figure 4.13, the stepwise assembly did not significantly improve the product formation (lane 6-9 VS lane 5). An exception was lane 8, which gave higher percentage of tile trimer, compared to other stepwise additions. The preorganization of the middle tile Y5 on the backbone seemed to be important for trimer formation. However, one-pot assembly showed significantly lower percentages of tile monomer and tile dimer.

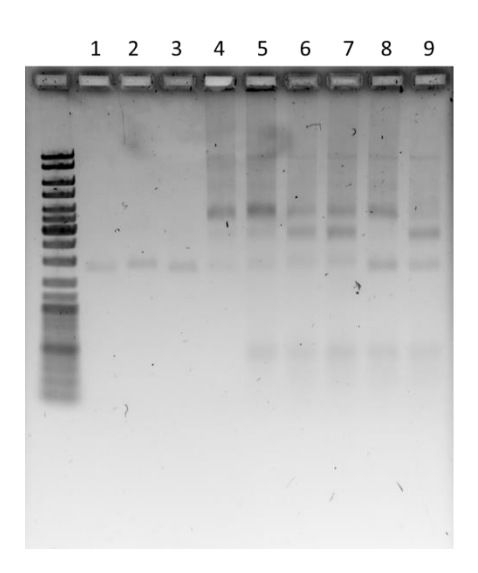


Figure 4.13. Step of tile additions. Lane 1: X5, lane 2: Y5, lane 3: Z5, lane 4: X5+Y5+Z5, lane 5: $(X5+Y5+Z5) + (ss[10]/A^*)$, lane 6: $(X5+(ss[10]/A^*) + Z5 + Y5$, lane 7: $(Z5+(ss[10]/A^*) + X5 + Y5$, lane 8: $(Y5+(ss[10]/A^*) + X5 + Z5$ and lane 9: $(X5+(ss[10]/A^*) + Y5 + Z5$. Gel was performed by Chidchob P.

Subsequent to the AGE experiments showing that the stepwise assembly starting by tiles Y5 and the backbone, followed by the addition of X5 and Z5 was effective, we carried on AFM measurements to study the amount of trimers with respect to monomers and dimers (Figure 4.14). Interestingly, the sequential addition of the tiles to ss[10] did not improve the yield of trimers compared to the one-pot strategy. We think that the one-pot assembly provides more binding sites to the backbone (3 tiles binding the scaffold simultaneously), hence it amplifies the effect of ss[10] on the construction of higher-order architectures.

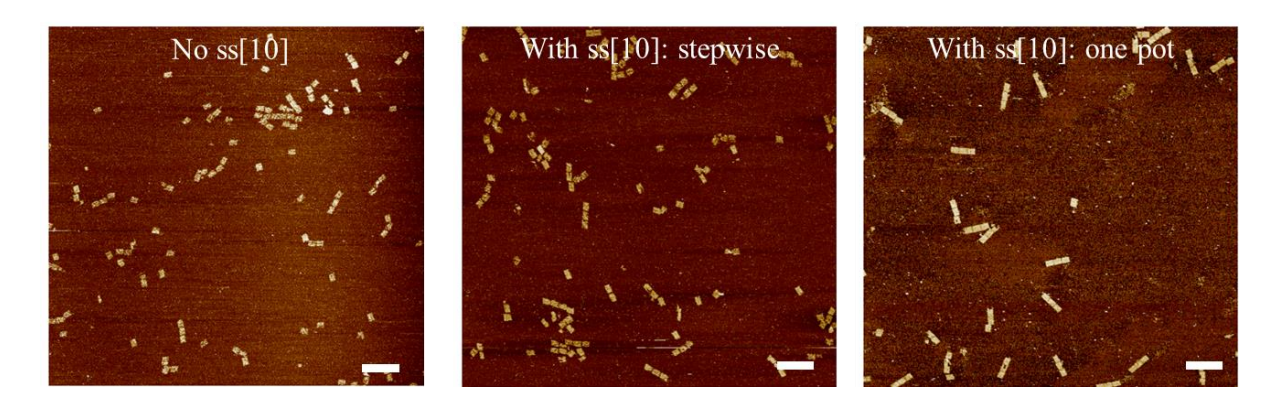


Figure 4.14. AFM micrographs displaying the stepwise assembly in the absence and presence of ss[10] versus one-pot assembly, scale bar 500 nm.

4.4.8 Preparation of the 5-tile System

The one-pot assembly of the 5-tile system follows the same protocol as the 3-tile system. ss[20] was first rigidified by hybridizing either A or B blocks of the backbones with their complements (A* or B*, respectively). We first attempted to hybridize one scaffold to tiles A5, B5, C5, D5 and E5, then examined the railroad system. Briefly, ss[20] was mixed with single-stranded A* or B* at 1:10 ratio in 1xTAMg, and the samples were annealed from 56°C to 20°C over 1 h. To construct

5-tile system, equimolar amounts of tiles A5, B5, C5, D5 and E5 (0.2 nM each) were mixed in 1xTAMg, which will give final tile concentration of 1 nM. Then, ss[20]/A* and/or ss[20]/B* solutions were added each in 5 equimolar amount with respect to total tile concentration before annealing from 44°C to 20°C over 4 hours. AGE (Figure 4.15) was used to characterize the products by mixing 20 μL samples with 4 μL 6X loading dye then running on 0.7% AGE at 80 V for 2.5 h. Lane 9 corresponds to the nanostructure with ss[20]/A* only and lane 8 to the railroad track in the presence of ss[20]/A* and ss[20]/B*. The results validate the AFM data shown in Figure 4.8 where 2 scaffolds were needed to enhance the formation yield of pentamers. Compared to lane 7, the railroad track system helped minimize other contaminants such as dimers, trimers and so on.

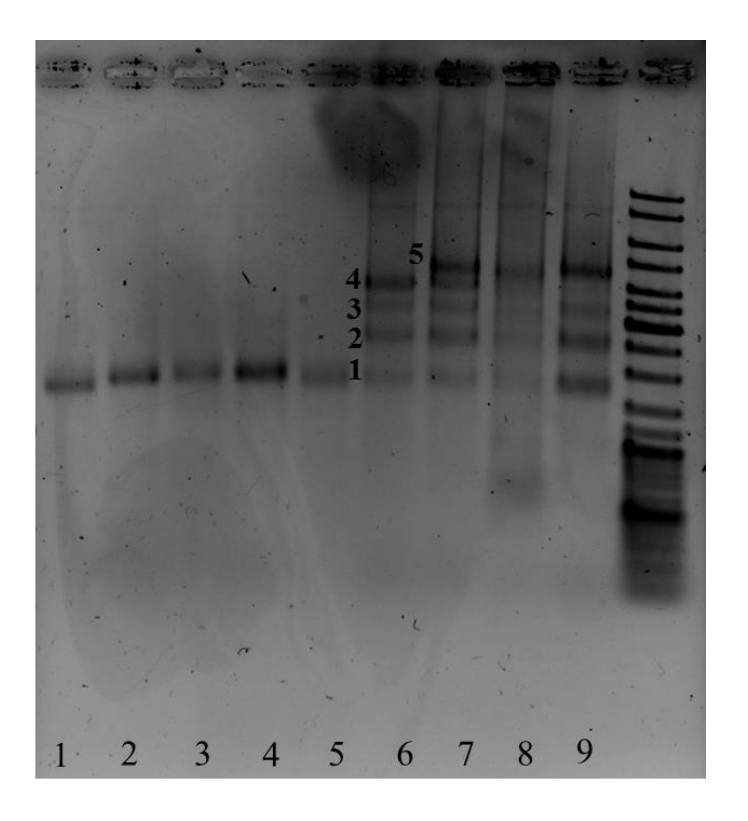


Figure 4.15. 1% AGE in 1×TAMg. Lane 1: A5, lane 2: B5, lane 3: C5, lane 4: D5, lane 5: E5, lane 6: A5 + B5 + C5 + D5, lane 7: A5 + B5 + C5 + D5 + E5, lane 8: A5 + B5 + C5 + D5 + E5 + ss[20]/A* + ss[20]/B* and lane 9: A5 + B5 + C5 + D5 + E5 + ss[20]/A*.

A quasi-quantitative analysis was performed on the gel to calculate the yield of pentamers. Simply, the intensity of the pentamers was divided by the intensity of the entire lane then multiplied by 100. We found that in the absence of backbones, ~27% of the products were pentamers, whereas the addition of scaffolds improved the yield to ~55%. We believe that the presence of two scaffolds increases the number of binding sites to the tiles and reduces the amount of undesired inter-tile connections.

In an attempt to further increase the yield of pentamers, we only added ss[20]/A* to the 5 tiles during 44 to 20°C cycle. Then, we incubated the mixture with ss[20]/B* at room temperature for 2 hours. The AGE gel in Figure 4.16 shows no significant enhancement in the yield of pentamers. Again, we believe that both backbones are needed to better organize the pentamers by minimizing the non-desired interactions and maximizing the hybridizing sites between tiles and backbones.

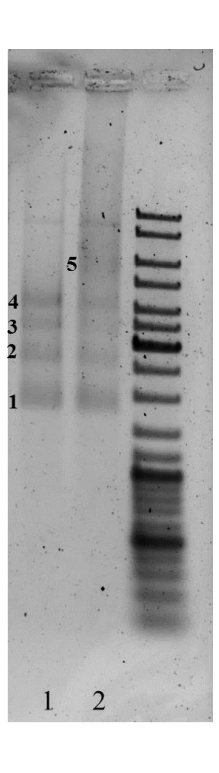


Figure 4.16. 1% AGE in 1×TAMg. lane 1: A5 + B5 + C5 + D5 + E5 and lane 2: $(A5 + B5 + C5 + D5 + E5 + ss[20]/A^*)$ at 44 to 20°C + ss[20]/B* at RT.

Next, we examined the ability of ss[20] to organize pentamers and improve their yields at room temperature. Thus, we annealed/cooled the mixture containing A5, B5, C5, D5 and E5 from 44°C to 20°C over 4 hours first, then added ss[20]/A* and ss[20]/B* at room temperature. Figure 4.17 displays a mixture of individual tiles, trimers, tetramers, pentamers and other misassembled nanostructures. Compared to the simultaneous addition of ss[20] to the tiles, the railroad track does not seem to improve the yield of pentamers significantly. Similar to the 3-tile system, we suppose that the interactions holding the pre-formed higher-order structures are difficult to re-arrange even after the addition of the backbones. As such, it is critical to add all the strands at the same time in order to promote the assembly of pentamers.

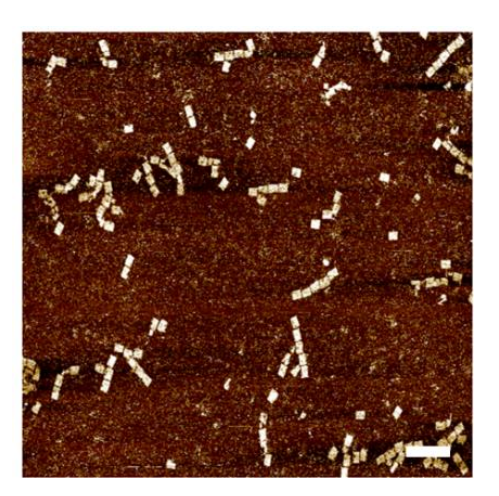


Figure 4.17. AFM micrograph displaying the assembly of 5 tiles with the 2 backbones at RT, scale bar 500 nm. Sample was prepared by Chidchob P.

Finally, we examined the organization of the 5 tiles using the same sticky ends between two tiles (with 16 bp complementary domains instead of 10). For example, the sequence of the 5 overhangs between tiles C and D is the same but different than the one between D and E. Similar to the 3-tiles system, we aimed at further decreasing the number of strands used and at increasing symmetry. However, the tiles did not arrange correctly and they aggregated instead (Figure 4.18). Furthermore, we increased the number of sticky ends, using the same sequences between the tiles, from 5 to 10. Figure 4.18b demonstrates the formation of aggregates on the mica surface. Thus, we decided to use 5 unique sticky ends to link the tiles.

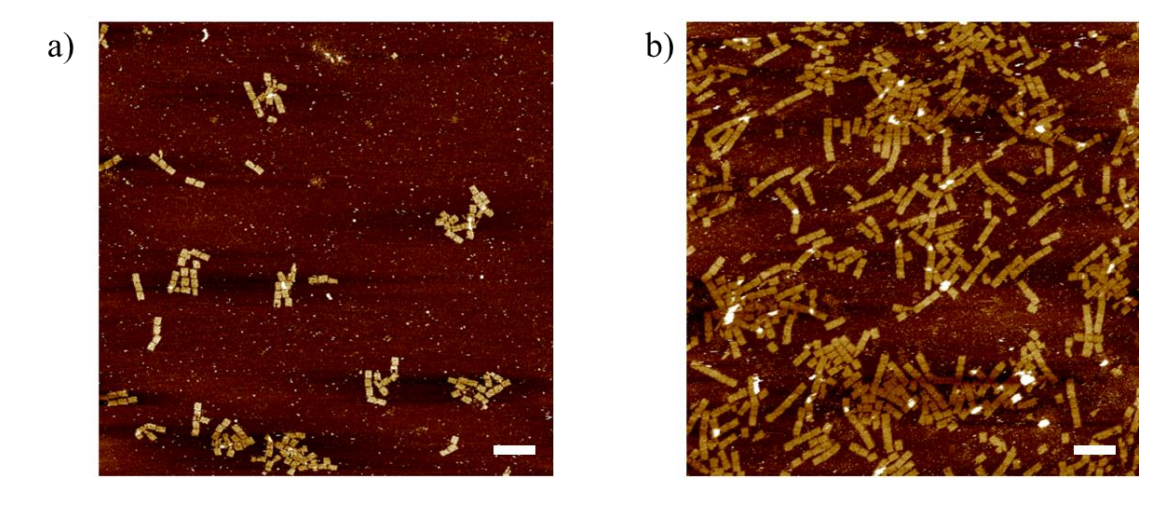


Figure 4.18. AFM micrographs depicting the formation of aggregates between the tiles when using (a) 5 sticky ends and (b) 10 sticky ends, scale bar 500 nm. Chidchob P. prepared the samples. Samples were prepared by Chidchob P.

4.4.9 Additional AFM images on 3- and 5-Tiles Systems

We present in this section additional AFM images that correspond to the railroad track system with ss[20]/A* and ss[20]/B* (Figure 4.20) and 3 tiles system with ss[10]/A*(Figure 4.19). These images were part of the data acquired to perform the statistical analysis on these nanostructures.

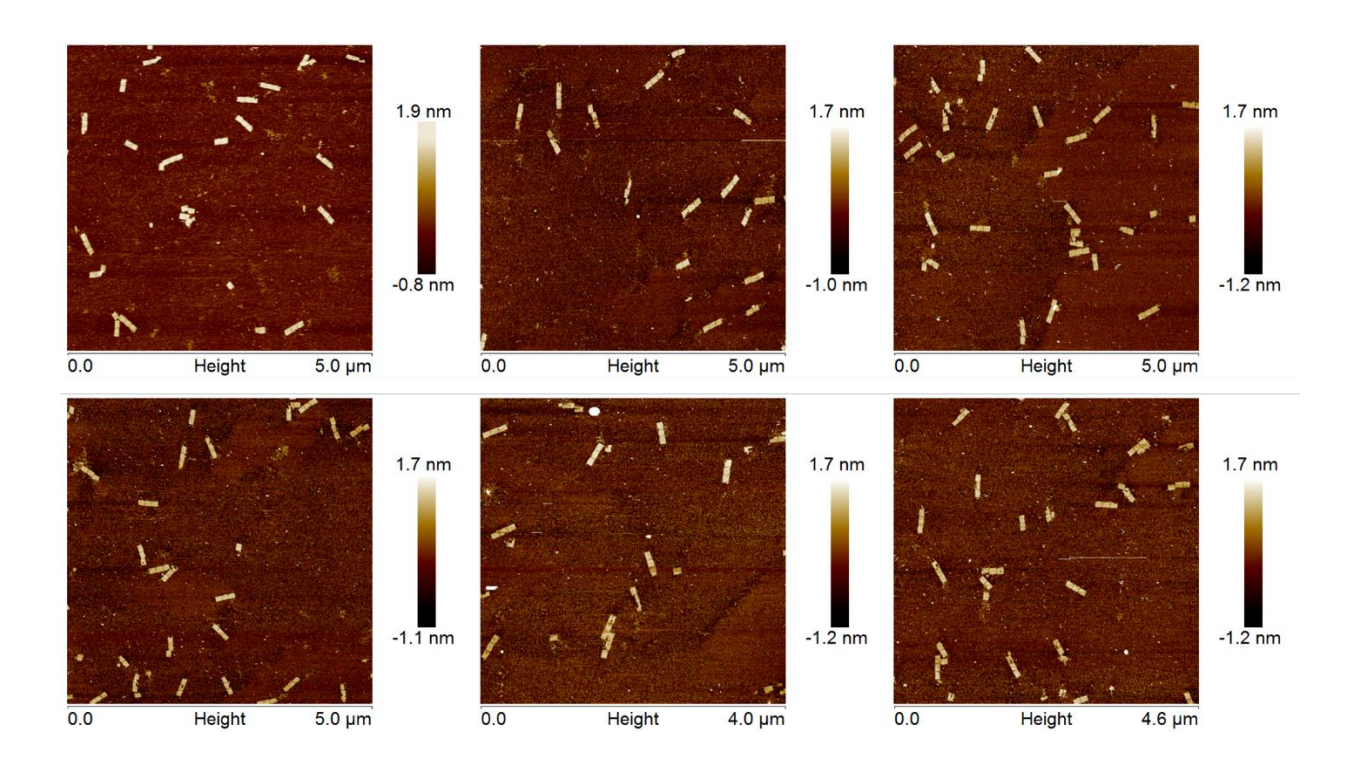
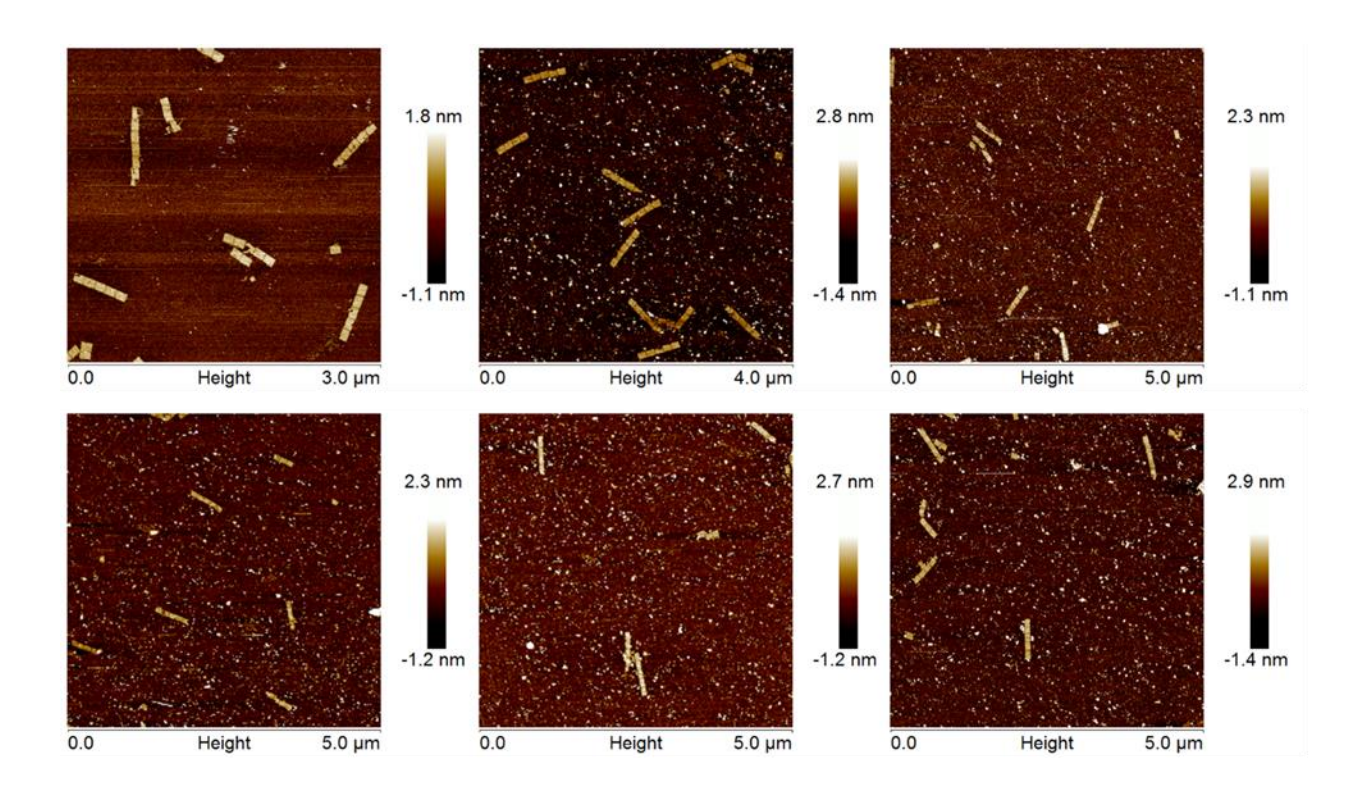


Figure 4.19. 3-tiles system



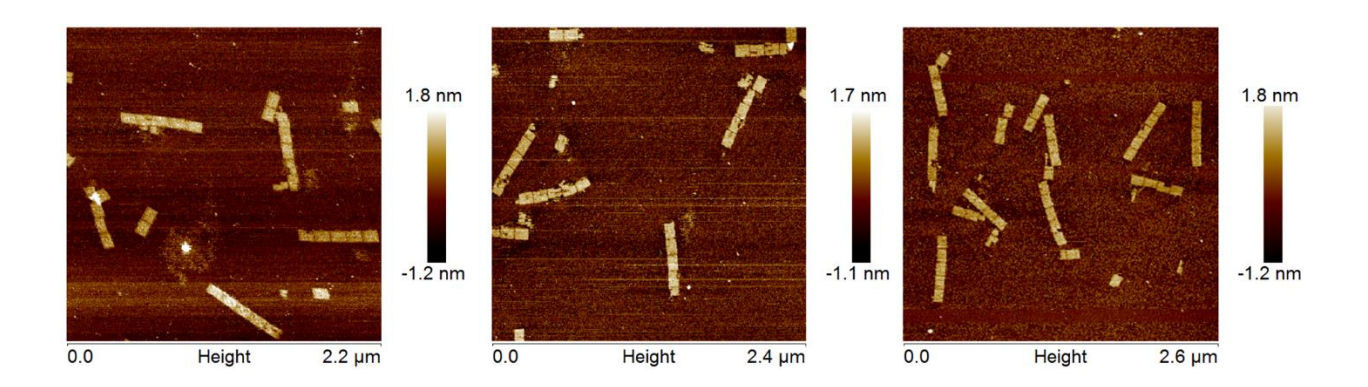


Figure 4.20. Railroad track system.

4.4.10 DNA Sequences

Table 4.8. Modification of staple strands in 3-tile system. 5 stands for 5 sticky ends between the tiles and 10 stands for 10 sticky ends linking the tiles.

Tile	Staple strand modifications
X5	X54, X100
	H134, H136, H137, H139, H158, H160
	102-A18, S103, 104-A18, S105, 106-A18, S107, 108-A18, S109, 110-A18, M111
Y5	Y52, Y132
	H134, H136, H137, H139, H158, H160
	102B, S103, 10B, S105, 106B, S107, 108B, S109, 110B, M111
	M205, 206-AC18, S207, 208-AC18, S209, 210-AC18, S211, 212-AC18, S213, 214-
	AC18, S215
Z 5	Z178, Z202
	H134, H136, H137, H139, H158, H160
	M205, 206BC, S207, 208BC, S209, 210BC, S211, 212BC, S213, 214BC, S215
X10	X54, X100
	H134, H136, H137, H139, H158, H160
	101-A18, 102-A18, 103-A18, 104-A18, 105-A18, 106-A18, 107-A18, 108-A18, 109-
	A18, 110-A18, M111
Y10	Y52, Y132
	H134, H136, H137, H139, H158, H160
	101B, 102B, 103B, 104B, 105B, 106B, 107B, 108B, 109B, 110B, M111
	M205, 206-AC18, 207-AC18, 208-AC18, 209-AC18, 210-AC18, 211-AC18, 212-
	AC18, 213-AC18, 214-AC18, 215AC-18, M216
Z10	Z178, Z202
	H134, H136, H137, H139, H158, H160

M205,	206BC,	207BC,	208BC,	209BC,	210BC,	211BC,	212BC,	213BC,	214BC,
215BC	, M216								

Note: The modifications of the staple strands required for 5-tile systems are listed in Table 4.11 and 4.12. The modified strands were used in place of unmodified strands of the same number for an assembly of different tiles.

Table 4.9. Modification of staple strands in 5-tile system. The same sequences were employed in each sticky end linking the same tiles.

Tile	Staple strand modifications
A5	A78, A100, A111
113	102A, S103, 104A, S105, 106A, S107, 108A, S109, 110A, M111
B5	B52, B132, B159, B73
	102B, S103, 104B, S105, 106B, S107, 108B, S109, 110B, M111
	M205, 206AC, S207, 208AC, S209, 210AC, S211, 212AC, S213, 214AC, S215
C5	C132, C156, C135, C113
	102C, S103, 104C, S105, 106C, S107, 108C, S109, 110C, M111
	M205, 206BC, S207, 208BC, S209, 210BC, S211, 212BC, S213, 214BC, S215
D5	D52, D180, D135, D197
	102D, S103, 104D, S105, 106D, S107, 108D, S109, 110D, M111
	M205, 206CC, S207, 208CC, S209, 210CC, S211, 212CC, S213, 214CC, S215
E5	E216, E205
153	206DC, S207, 208DC, S209, 210DC, S211, 212DC, S213, 214DC, S215
A10	A78, A100, A111
Alu	101A, 102A, 103A, 104A, 105A, 106A, 107A, 108A, 109A, 110A, M111
B10	B52, B132, B159, B73
Віо	M100, 101B, 102B, 103B, 104B, 105B, 106B, 107B, 108B, 109B, 110B, M111
	M205, 206AC, 207AC, 208AC, 209AC, 210AC, 211AC, 212AC, 213AC, 214AC,
	215AC, M216
C10	C132, C156, C135, C113
C10	M100, 101C, 102C, 103C, 104C, 105C, 106C, 107C, 108C, 109C, 110C, M111
	M205, 206BC, 207BC, 208BC, 209BC, 210BC, 211BC, 212BC, 213BC, 214BC,
	215BC, M216
D10	D52, D180, D135, D197
	M100, 101D, 102D, 103D, 104D, 105D, 106D, 107D, 108D, 109D, 110D, M111
	10100, 1010, 1020, 1030, 1040, 1000, 1070, 1000, 1070, 1100, 11111

	M205, 206CC, 207CC, 208CC, 209CC, 210CC, 211CC, 212CC, 213CC, 214CC,
	215CC, M216
E10	E216, E205
	206DC, 207DC, 208DC, 209DC, 210DC, 211DC, 212DC, 213DC, 214DC, 215DC,
	M216

Table 4.10. Modification of staple strands in 5-tile system. Each overhang (10 bases) is unique in this case.

A5(10)u	100, 101, 102A10(1), S103, 104A10(2), S105, 106A10(3), S107, 108A10(4), S109,
	110A10(5), S111
B5(10)u	B52, B132, B159, B73
	100, 101, 102B10(1), S103, 104B10(2), S105, 106B10(3), S107, 108B10(4), S109,
	110B10(5), S111
	205, 206AC10(5), S207, 208AC10(4), S209, 210AC10(3), S211, 212AC10(2), S213,
	214AC10(1), S215, 216
C5(10)u	C132 10b, C156 10b, C135 10b, C113 10b
	100, 101, 102C10(1), S103, 104C10(2), S105, 106C10(3), S107, 108C10(4), S109,
	110C10(5), S111
	205, 206BC10(5), S207, 208BC10(4), S209, 210BC10(3), S211, 212BC10(2), S213,
	214BC10(1), S215, 216
D5(10)u	D1 10b, D76 10b, D97 10b, D135 10b
	100, 101, 102D10(1), S103, 104D10(2), S105, 106D10(3), S107, 108D10(4), S109,
	110D10(5), S111
	205, 206CC10(5), S207, 208CC10(4), S209, 210CC10(3), S211, 212CC10(2), S213,
	214CC10(1), S215, 216
E5(10)u	E183 10b, E202 10b
	205, 206DC10(5), S207, 208DC10(4), S209, 210DC10(3), S211, 212DC10(2), S213,
	214DC10(1), S215, 216

Unmo	dified staple strands (1-216)	10	GCAATAGCGCAGATAGCCGAACAATTCAACCG
		11	CCTAATTTACGCTAACGAGCGTCTAATCAATA
2	AATGCCCCGTAACAGTGCCCGTATCTCCCTCA	12	TCTTACCAGCCAGTTACAAAATAAATGAAATA
3	TGCCTTGACTGCCTATTTCGGAACAGGGATAG	13	ATCGGCTGCGAGCATGTAGAAACCTATCATAT
4	GAGCCGCCCACCACCGGAACCGCGACGGAAA	14	CTAATTTATCTTTCCTTATCATTCATCCTGAA
5	AACCAGAGACCCTCAGAACCGCCAGGGGTCAG	15	GCGTTATAGAAAAAGCCTGTTTAGAAGGCCGG
6	TTATTCATAGGGAAGGTAAATATTCATTCAGT	16	GCTCATTTTCGCATTAAATTTTTGAGCTTAGA
7	CATAACCCGAGGCATAGTAAGAGCTTTTTAAG	17	AATTACTACAAATTCTTACCAGTAATCCCATC
8	ATTGAGGGTAAAGGTGAATTATCAATCACCGG		
9	A A A AGT A AT AT CTT ACCGA AGCCCTTCC AG AG	18	TTAAGACGTTGAAAACATAGCGATAACAGTAC

19	TAGAATCCCTGAGAAGAGTCAATAGGAATCAT	68	AAATCAATGGCTTAGGTTGGGTTACTAAATTT
20	CTTTTACACAGATGAATATACAGTAAACAATT	69	GCGCAGAGATATCAAAATTATTTGACATTATC
21	TTTAACGTTCGGGAGAAACAATAATTTTCCCT	70	AACCTACCGCGAATTATTCATTTCCAGTACAT
22	CGACAACTAAGTATTAGACTTTACAATACCGA	71	ATTTTGCGTCTTTAGGAGCACTAAGCAACAGT
23	GGATTTAGCGTATTAAATCCTTTGTTTTCAGG	72	CTAAAATAGAACAAAGAAACCACCAGGGTTAG
24	ACGAACCAAAACATCGCCATTAAATGGTGGTT	73	GCCACGCTATACGTGGCACAGACAACGCTCAT
26	TAGCCCTACCAGCAGAAGATAAAAACATTTGA	74	GCGTAAGAGAGCCAGCAGCAAAAAGGTTAT
29	CTGAAACAGGTAATAAGTTTTAACCCCTCAGA	77	TGCTCAGTCAGTCTCTGAATTTACCAGGAGGT
30	AGTGTACTTGAAAGTATTAAGAGGCCGCCACC	78	GGAAAGCGACCAGGCGGATAAGTGAATAGGTG
31	GCCACCACTCTTTTCATAATCAAACCGTCACC	79	TGAGGCAGGCGTCAGACTGTAGCGTAGCAAGG
32	GTTTGCCACCTCAGAGCCGCCACCGATACAGG	80	TGCCTTTAGTCAGACGATTGGCCTGCCAGAAT
33	GACTTGAGAGACAAAAGGGCGACAAGTTACCA	81	CCGGAAACACACCACGGAATAAGTAAGACTCC
34	AGCGCCAACCATTTGGGAATTAGATTATTAGC	82	ACGCAAAGGTCACCAATGAAACCAATCAAGTT
35	GAAGGAAAATAAGAGCAAGAAACAACAGCCAT	83	TTATTACGGTCAGAGGGTAATTGAATAGCAGC
36	GCCCAATACCGAGGAAACGCAATAGGTTTACC	84	TGAACAAACAGTATGTTAGCAAACTAAAAGAA
37	ATTATTTAACCCAGCTACAATTTTCAAGAACG	85	CTTTACAGTTAGCGAACCTCCCGACGTAGGAA
38	TATTTTGCTCCCAATCCAAATAAGTGAGTTAA	86	GAGGCGTTAGAGAATAACATAAAAGAACACCC
39	GGTATTAAGAACAAGAAAAATAATTAAAGCCA	87	TCATTACCCGACAATAAACAACATATTTAGGC
40	TAAGTCCTACCAAGTACCGCACTCTTAGTTGC	88	CCAGACGAGCGCCCAATAGCAAGCAAGAACGC
41	ACGCTCAAAATAAGAATAAACACCGTGAATTT	89	AGAGGCATAATTTCATCTTCTGACTATAACTA
42	AGGCGTTACAGTAGGGCTTAATTGACAATAGA	90	TTTTAGTTTTTCGAGCCAGTAATAAATTCTGT
43	ATCAAAATCGTCGCTATTAATTAACGGATTCG	91	TATGTAAACCTTTTTTAATGGAAAAATTACCT
44	CTGTAAATCATAGGTCTGAGAGACGATAAATA	92	TTGAATTATGCTGATGCAAATCCACAAATATA
45	CCTGATTGAAAGAAATTGCGTAGACCCGAACG	93	GAGCAAAAACTTCTGAATAATGGAAGAAGGAG
46	ACAGAAATCTTTGAATACCAAGTTCCTTGCTT	94	TGGATTATGAAGATGATGAAACAAAATTTCAT
47	TTATTAATGCCGTCAATAGATAATCAGAGGTG	95	CGGAATTATTGAAAGGAATTGAGGTGAAAAAT
48	AGATTAGATTTAAAAGTTTGAGTACACGTAAA	96	ATCAACAGTCATCATATTCCTGATTGATTGTT
49	AGGCGGTCATTAGTCTTTAATGCGCAATATTA	97	CTAAAGCAAGATAGAACCCTTCTGAATCGTCT
50	GAATGGCTAGTATTAACACCGCCTCAACTAAT	98	GCCAACAGTCACCTTGCTGAACCTGTTGGCAA
53	CCTCAAGAATACATGGCTTTTGATAGAACCAC	100	TTTTTATAAGTATAGCCCGGCCGTCGAG
54	TAAGCGTCGAAGGATTAGGATTAGTACCGCCA	101	AGGGTTGATTTTATAAATCCTCATTAAATGATATTC
55	CACCAGAGTTCGGTCATAGCCCCCGCCAGCAA	102	ACAAACAATTTTAATCAGTAGCGACAGATCGATAGC
56	TCGGCATTCCGCCGCCAGCATTGACGTTCCAG	103	AGCACCGTTTTTTAAAGGTGGCAACATAGTAGAAAA
57	AATCACCAAATAGAAAATTCATATATAACGGA	104	TACATACATTTTGACGGGAGAATTAACTACAGGGAA
58	TCACAATCGTAGCACCATTACCATCGTTTTCA	105	GCGCATTATTTTGCTTATCCGGTATTCTAAATCAGA
59	ATACCCAAGATAACCCACAAGAATAAACGATT	106	TATAGAAGTTTTCGACAAAAGGTAAAGTAGAGAATA
60	ATCAGAGAAAGAACTGGCATGATTTTATTTTG	107	TAAAGTACTTTTCGCGAGAAAACTTTTTATCGCAAG
61	TTTTGTTTAAGCCTTAAATCAAGAATCGAGAA	108	ACAAAGAATTTTAATTAATTACATTTAACACATCAAG
62	AGGTTTTGAACGTCAAAAATGAAAGCGCTAAT	109	AAAACAAATTTTTTCATCAATATAATCCTATCAGAT
63	CAAGCAAGACGCGCCTGTTTATCAAGAATCGC	110	GATGGCAATTTTAATCAATATCTGGTCACAAATATC
64	AATGCAGACCGTTTTTATTTTCATCTTGCGGG	111	AAACCCTCTTTTACCAGTAATAAAAGGGATTCACCAGTCACACGTTTT
65	CATATTTAGAAATACCGACCGTGTTACCTTTT	112	CCGAAATCCGAAAATCCTGTTTGAAGCCGGAA
66	AATGGTTTACAACGCCAACATGTAGTTCAGCT	113	CCAGCAGGGGCAAAATCCCTTATAAAGCCGGC
67	TAACCTCCATATGTGAGTGAATAAACAAAATC	114	GCATAAAGTTCCACACAACATACGAAGCGCCA

115	GCTCACAATGTAAAGCCTGGGGTGGGTTTGCC	163	${\tt GTTTGAGGGAAAGGGGGATGTGCTAGAGGATC}$
116	TTCGCCATTGCCGGAAACCAGGCATTAAATCA	164	CTTTCATCCCCAAAAACAGGAAGACCGGAGAG
117	GCTTCTGGTCAGGCTGCGCAACTGTGTTATCC	165	AGAAAAGCAACATTAAATGTGAGCATCTGCCA
118	GTTAAAATTTTAACCAATAGGAACCCGGCACC	166	GGTAGCTAGGATAAAAATTTTTAGTTAACATC
119	AGACAGTCATTCAAAAGGGTGAGAAGCTATAT	167	CAACGCAATTTTTGAGAGATCTACTGATAATC
120	AGGTAAAGAAATCACCATCAATATAATATTTT	168	CAATAAATACAGTTGATTCCCAATTTAGAGAG
121	TTTCATTTGGTCAATAACCTGTTTATATCGCG	169	TCCATATACATACAGGCAAGGCAACTTTATTT
122	TCGCAAATGGGGCGCGAGCTGAAATAATGTGT	170	TACCTTTAAGGTCTTTACCCTGACAAAGAAGT
123	TTTTAATTGCCCGAAAGACTTCAAAACACTAT	171	CAAAAATCATTGCTCCTTTTGATAAGTTTCAT
124	AAGAGGAACGAGCTTCAAAGCGAAGATACATT	172	TTTGCCAGATCAGTTGAGATTTAGTGGTTTAA
125	GGAATTACTCGTTTACCAGACGACAAAAGATT	173	AAAGATTCAGGGGGTAATAGTAAACCATAAAT
126	GAATAAGGACGTAACAAAGCTGCTCTAAAAACA	174	TTTCAACTATAGGCTGGCTGACCTTGTATCAT
127	CCAAATCACTTGCCCTGACGAGAACGCCAAAA	175	CCAGGCGCTTAATCATTGTGAATTACAGGTAG
128	CTCATCTTGAGGCAAAAGAATACAGTGAATTT	176	CGCCTGATGGAAGTTTCCATTAAACATAACCG
129	AAACGAAATGACCCCCAGCGATTATTCATTAC	177	TTTCATGAAAATTGTGTCGAAATCTGTACAGA
130	CTTAAACATCAGCTTGCTTTCGAGCGTAACAC	178	ATATATTCTTTTTCACGTTGAAAATAGTTAG
131	TCGGTTTAGCTTGATACCGATAGTCCAACCTA	179	AATAATAAGGTCGCTGAGGCTTGCAAAGACTT
134	GAATAGCCGCAAGCGGTCCACGCTCCTAATGA	182	TGGACTCCCTTTTCACCAGTGAGACCTGTCGT
135	GAGTTGCACGAGATAGGGTTGAGTAAGGGAGC	183	TGGTTTTTAACGTCAAAGGGCGAAGAACCATC
136	GTGAGCTAGTTTCCTGTGTGAAATTTGGGAAG	184	GCCAGCTGCCTGCAGGTCGACTCTGCAAGGCG
137	TCATAGCTACTCACATTAATTGCGCCCTGAGA	185	CTTGCATGCATTAATGAATCGGCCCGCCAGGG
138	GGCGATCGCACTCCAGCCAGCTTTGCCATCAA	186	ATTAAGTTCGCATCGTAACCGTGCGAGTAACA
139	GAAGATCGGTGCGGGCCTCTTCGCAATCATGG	187	TAGATGGGGGTAACGCCAGGGTTGTGCCAAG
140	AAATAATTTTAAATTGTAAACGTTGATATTCA	188	ACCCGTCGTCATATGTACCCCGGTAAAGGCTA
141	GCAAATATCGCGTCTGGCCTTCCTGGCCTCAG	189	CATGTCAAGATTCTCCGTGGGAACCGTTGGTG
142	ACCGTTCTAAATGCAATGCCTGAGAGGTGGCA	190	TCAGGTCACTTTTGCGGGAGAAGCAGAATTAG
143	TATATTTTAGCTGATAAATTAATGTTGTATAA	191	CTGTAATATTGCCTGAGAGTCTGGAAAACTAG
144	TCAATTCTTTTAGTTTGACCATTACCAGACCG	192	CAAAATTAAAGTACGGTGTCTGGAAGAGGTCA
145	CGAGTAGAACTAATAGTAGCAAACCCTCA	193	TGCAACTAAGCAATAAAGCCTCAGTTATGACC
146	GAAGCAAAAAAGCGGATTGCATCAGATAAAAA	194	TTTTTGCGCAGAAAACGAGAATGAATGTTTAG
147	TCAGAAGCCTCCAACAGGTCAGGATCTGCGAA	195	AAACAGTTGATGGCTTAGAGCTTATTTAAATA
148	CCAAAATATAATGCAGATACATAAACACCAGA	196	ACTGGATAACGGAACAACATTATTACCTTATG
149	CATTCAACGCGAGAGGCTTTTGCATATTATAG	197	ACGAACTAGCGTCCAATACTGCGGAATGCTTT
150	ACGAGTAGTGACAAGAACCGGATATACCAAGC	198	CGATTTTAGAGGACAGATGAACGGCGCGACCT
151	AGTAATCTTAAATTGGGCTTGAGAGAATACCA	199	CTTTGAAAAGAACTGGCTCATTATTTAATAAA
152	GCGAAACATGCCACTACGAAGGCATGCGCCGA	200	GCTCCATGAGAGGCTTTGAGGACTAGGGAGTT
153	ATACGTAAAAGTACAACGGAGATTTCATCAAG	201	ACGGCTACTTACTTAGCCGGAACGCTGACCAA
154	CAATGACACTCCAAAAGGAGCCTTACAACGCC	202	AAAGGCCGAAAGGAACAACTAAAGCTTTCCAG
155	AAAAAAGGACAACCATCGCCCACGCGGGTAAA	203	GAGAATAGCTTTTGCGGGATCGTCGGGTAGCA
158	AGTTTGGAGCCCTTCACCGCCTGGTTGCGCTC		
159	AGCTGATTACAAGAGTCCACTATTGAGGTGCC	1	CAAGCCCAATAGGAACCCATGTACAAACAGTT
160	ACTGCCCGCCGAGCTCGAATTCGTTATTACGC	28	CTCAGAGCCACCACCCTCATTTTCCTATTATT
161	CCCGGGTACTTTCCAGTCGGGAAACGGGCAAC	52	CCCTCAGAACCGCCACCCTCAGAACTGAGACT
162	CAGCTGGCGGACGACGACAGTATCGTAGCCAG	76	TATCACCGTACTCAGGAGGTTTAGCGGGGTTT

132	TGAGTTTCGTCACCAGTACAAACTTAATTGTA	Z178E		
156	TGTAGCATTCCACAGACAGCCCTCATCTCCAA	AAAAAAAAAATGGCAGGCGTCTTTGTTAGCTAAATTTCAACGTGAAA AAAGAATATAT		
180	CGTAACGATCTAAAGTTTTGTCGTGAATTGCG	Z202 AAAGGCCGAAAGGAACAACTAAAGCTTTCCAGTATCTGATCCTTAAC		
204	ACGTTAGTAAATGAATTTTCTGTAAGCGGAGT	GGCCTGTT		
205	TTTTCGATGGCCCACTACGTAAACCGTC			
206	TATCAGGGTTTTCGGTTTGCGTATTGGGAACGCGCG	A78 GGAAAGCGACCAGGCGGATAAGTGTTAAAGGGCCTCGTGATACG		
207	GGGAGAGGTTTTTGTAAAACGACGGCCATTCCCAGT	AI00 ATATCGCTCTAGAGTCGTTTTTATAAGTATAGCCCGGCCGTCGAG		
208	CACGACGTTTTTGTAATGGGATAGGTCAAAACGGCG	A111 ACCAGTAATAAAAGGGATTCACCAGTCACACGTTTTTTAGTGAATTCG		
209	GATTGACCTTTTGATGAACGGTAATCGTAGCAAACA	GACTACG		
210	AGAGAATCTTTTGGTTGTACCAAAAACAAGCATAAA	B52 CTTCTGATCCTTAACGGCCTTTCCCTCAGAACCGCCACCCTCAGAACT		
211	GCTAAATCTTTTCTGTAGCTCAACATGTATTGCTGA	GAGACT		
212	ATATAATGTTTTCATTGAATCCCCCTCAAATCGTCA	B73 GCCACGCTATACGTGGCACAGACAACGCTCATTTAAGCATGACCTTCC		
213	TAAATATTTTTTGGAAGAAAATCTACGACCAGTCA	GTTGTTT		
214	GGACGTTGTTTTCATAAGGGAACCGAAAGGCGCAG	B132 TTAACGGCCTGTTGCTGAACTTATTGAGTTTCGTCACCAGTACAAACT		
215	ACGGTCAATTTTGACAGCATCGGAACGAACCCTCAG	TAATTGTA		
216	CAGCGAAATTTTAACTTTCAACAGTTTCTGGGATTTTGCTAAACTTTT	B159 AGCTGATTACAAGAGTCCACTATTGAGGTGCCTTCCTTCC		
25	GAACGTGGCGAGAAAGGAAGGGAACAAACTAT	C113 CCAGCAGGGGCAAAATCCCTTATAAAGCCGGCTTTCGCTCTAGAGTC		
27	CGGCCTTGCTGGTAATATCCAGAACGAACTGA	GACCTGGC		
51	CCGCCAGCCATTGCAACAGGAAAATATTTTT	C132 ATCGCTCTAGAGTCGACCTGGTTTGAGTTTCGTCACCAGTACAAACTT		
75	GGAAATACCTACATTTTGACGCTCACCTGAAA	AATTGTA		
99	GAAATGGATTATTTACATTGGCAGACATTCTG	C135 GAGTTGCACGAGATAGGGTTGAGTAAGGGAGCTTCCTTCC		
133	CCCCGATTTAGAGCTTGACGGGGAAATCAAAA	AAGCGCA		
157	GTAAAGCACTAAATCGGAACCCTAGTTGTTCC	C156 GACTACGTCTTCTGATCCTTTTTGTAGCATTCCACAGACAG		
181	ACCCAAATCAAGTTTTTTGGGGTCAAAGAACG	TCCAA		
101		D52 GTTGCTGAACTTTGGTTTGATTTTCCCTCAGAACCGCCACCCTCAGAA CTGAGACT		
		D135		
		GAGTTGCACGAGATAGGGTTGAGTAAGGGAGCTTTTTCAAGCGCAGC CAGATT		
Modif	ied staple strands	D180		
X54	•	ACGGCCTGTTGCTGAACTTTGTTCGTAACGATCTAAAGTTTTGTCGTG AATTGCG		
	TAAGCGTCGAAGGATTAGGATTAGTACCGCCATTATATCGCTCTAGAG	D97		
X54E		CTAAAGCAAGATAGAACCCTTCTGAATCGTCTTTTTCCGTTGTTTCAA GCGCAGC		
CCTAATCC	AAAAAAAAACAGGTCGACTCTAGAGCGATATAATGGCGGTACTAAT TTCGACGCTTA	E205		
X100		CTAGAGTCGACCTGCGCGCGATTTTTTCGATGGCCCACTACGTAAACC GTC		
G	ATCCTTAACGGCCTGTTGCTGTTTTTATAAGTATAGCCCGGCCGTCGA	E216 AACTTTCAACAGTTTCTGGGATTTTGCTAAACTTTTTCTCCGGGAGCC		
Y52		AGTGAATTC		
TGAGACT	CCTTAACGGCCTGTTGCTGAATTCCCTCAGAACCGCCACCCTCAGAAC			
Y132		C113 10b CCA GCA GGG GCA AAA TCC CTT ATA AAG CCG GCT TAT TAT ATC GCT CTA GAG TCG A		
AGTACAA	TITITITITITGTTGCTGAACTTTGGTTTGATTTTTTGAGTTTCGTCACC ACTTAATTGTA	C132 10b CTA GAG TCG ACC TGG CCA GTG TTT GAG TTT CGT CAC CAG TAC		
Y132E	TACAATTAAGTTTGTACTGGTGACGAAACTCAAAAAATCAAACCAAA	AAA CTT AAT TGT A		
GTTCAGCA Z178	ACAAAAAAAAAAAAAAAAAAAAAAAAAAAAAAAAAAAA	C135 10b GAG TTG CAC GAG ATA GGG TTG AGT AAG GGA GCT TAG CAT GAC CTT CCG TTG TTT C		
TTTTTTTT	ATATATTCTTTTTTCACGTTGAAATTTAGCTAACAAAGACGCCTGCCA T	C156 10b CGT CTT CTG ATC CTT AAC GGC TTT GTA GCA TTC CAC AGA CAG CCC TCA TCT CCA A		

D76 10b TTC TGA TCC TTA ACG GCC TGT ATT ATC ACC GTA CTC AGG AGG TTT AGC GGG GTT T	110A-18 AATCAATATCTGGTCACAAATATCAAACCCTCCGCTCTCTCAAGTAGA
D97 10b CTA AAG CAA GAT AGA ACC CTT CTG AAT CGT CTT TTA AAG CAT GAC CTT CCG TTG T	AT
D135 10b $$ $$ GAG TTG CAC GAG ATA GGG TTG AGT AAG GGA GCT AGA CCT TCC GTT GTT TCA AGC G	206AC-18 CGGTTTGCGTATTGGGAACGCGCGGGGAGAGGATTCTACTTGAGAGA GCG
E183 10b TGG TTT TTA ACG TCA AAG GGC GAA GAA CCA TCT TTC GAC CTG CGC GCG AGA CGA A	207AC-18 TGTAAAACGACGGCCATTCCCAGTCACGACGTATTCTACTTGAGAGA
E202 10b AAA GGC CGA AAG GAA CAA CTA AAG CTT TCC AGT TGC TTA CAG ACA AGC TGT GAC C	GCG 208AC-18
H134	GTAATGGGATAGGTCAAAACGGCGGATTGACCATTCTACTTGAGAGA GCG
GAATAGCCGCAAGCGGTCCTCTTTTGAGGAACAAGTTTTCTTGTTCCA CGCTCCTAATGA	209AC-18 GATGAACGGTAATCGTAGCAAACAAGAGAATCATTCTACTTGAGAGA GCG
H136 GTGAGCTAGTTTCCTGTCCTCTTTTGAGGAACAAGTTTTCTTGTTGTA AATTTGGGAAG	210AC-18 GGTTGTACCAAAAACAAGCATAAAGCTAAATCATTCTACTTGAGAGA GCG
H137 TCATAGCTACTCACATTCCTCTTTTGAGGAACAAGTTTTCTTGTTAATT GCGCCCTGAGA	211AC-18 CTGTAGCTCAACATGTATTGCTGAATATAATGATTCTACTTGAGAGAG
H139 GAAGATCGGTGCGGGCTCCTCTTTTGAGGAACAAGTTTTCTTGTCTCT TCGCAATCATGG	212AC-18 CATTGAATCCCCCTCAAATCGTCATAAATATTATTCTACTTGAGAGAG
H158 AGTTTGGAGCCCTTCATCCTCTTTTGAGGAACAAGTTTTCTTGTCCGCC TGGTTGCGCTC	213AC-18 GGAAGAAAAATCTACGACCAGTCAGGACGTTGATTCTACTTGAGAGA
H160 ACTGCCCGCCGAGCTCTCCTCTTTTGAGGAACAAGTTTTCTTGTGAAT TCGTTATTACGC	GCG 214AC-18 TCATAAGGGAACCGAAAGGCGCAGACGGTCAAATTCTACTTGAGAGA
	GCG 215AC-18 GACAGCATCGGAACGAACCCTCAGCAGCGAAAATTCTACTTGAGAGA
M100 TATAAGTATAGCCCGGCCGTCGAG	GCG
M111 ACCAGTAATAAAAGGGATTCACCAGTCACACGTTTT	
M111 ACCAGTAATAAAAGGGATTCACCAGTCACACGTTTT M205 CGATGGCCCACTACGTAAACCGTC	101A
	${\bf AGGGTTGAATAAATCCTCATTAAATGATATTCACAAACAA$
M205 CGATGGCCCACTACGTAAACCGTC M216 AACTTTCAACAGTTTCTGGGATTTTGCTAAACTTTT	AGGGTTGAATAAATCCTCATTAAATGATATTCACAAACAA
M205 CGATGGCCCACTACGTAAACCGTC	AGGGTTGAATAAATCCTCATTAAATGATATTCACAAACAA
M205 CGATGGCCCACTACGTAAACCGTC M216 AACTTCAACAGTTTCTGGGATTTTGCTAAACTTTT 101A-18 AGGGTTGAATAAATCCTCATTAAATGATATTCACAAACAA	AGGGTTGAATAAATCCTCATTAAATGATATTCACAAACAA
M205 CGATGGCCCACTACGTAAACCGTC M216 AACTTCAACAGTTTCTGGGATTTTGCTAAACTTTT 101A-18	AGGGTTGAATAAATCCTCATTAAATGATATTCACAAACAA
M205 CGATGGCCCACTACGTAAACCGTC M216 AACTTCAACAGTTTCTGGGATTTTGCTAAACTTTT 101A-18	AGGGTTGAATAAATCCTCATTAAATGATATTCACAAACAA
M205 CGATGGCCCACTACGTAAACCGTC M216 AACTTCAACAGTTTCTGGGATTTTGCTAAACTTTT 101A-18	AGGGTTGAATAAATCCTCATTAAATGATATTCACAAACAA
M205 CGATGGCCCACTACGTAAACCGTC M216 AACTTCAACAGTTTCTGGGATTTTGCTAAACTTTT 101A-18 AGGGTTGAATAAATCCTCATTAAATGATATTCACAAAACAACGCTCTCT CAAGTAGAAT 102A-18 AATCAGTAGCGACAGATCGATAGCAGCACCGTCGCTCTCTCAAGTAG AAT 103A-18 TAAAGGTGGCAACATAGTAGAAAATACATACACGCTCTCTCAAGTAG	AGGGTTGAATAAATCCTCATTAAATGATATTCACAAACAA
M205 CGATGGCCCACTACGTAAACCGTC M216 AACTTCAACAGTTTCTGGGATTTTGCTAAACTTTT 101A-18	AGGGTTGAATAAATCCTCATTAAATGATATTCACAAACAA
M205 CGATGGCCCACTACGTAAACCGTC M216 AACTITCAACAGTTTCTGGGATTTTGCTAAACTTTT 101A-18	AGGGTTGAATAAATCCTCATTAAATGATATTCACAAACAA
M205 CGATGGCCCACTACGTAAACCGTC M216 AACTTCAACAGTTTCTGGGATTTTGCTAAACTTTT 101A-18	AGGGTTGAATAAATCCTCATTAAATGATATTCACAAACAA
M205 CGATGGCCCACTACGTAAACCGTC M216 AACTTICAACAGTTTCTGGGATTTTGCTAAACTTTT 101A-18	AGAGAGCG AGAGAGCG AGAGAGCG AATCAGTAGCGACAGATCGATAGCAGCACCGTATTACTTGAGAGAGC G AATCAGTAGCGACAGATCGATAGCAGCACCGTATTACTTGAGAGAGC G AAACAGTAGCGACAGATCGATAGCAGCACCGTATTACTTGAGAGAGC G AAACAGTAGCGACAGATCGATAGCAGCACCGTATTACTTGAGAGAGCC G AAACAGTAGCGACAACATAGTAGAAAATACATACAATTACTTGAGAGAGCC G ACACGGGAGAATTAACTACAGGGAAGCGCATTAATTACTTGAGAGAGA
M205 CGATGGCCCACTACGTAAACCGTC M216 AACTITCAACAGTTTCTGGGATTTTGCTAAACTTTT 101A-18	AGGGTTGAATAAATCCTCATTAAATGATATTCACAAACAA
M205 CGATGGCCCACTACGTAAACCGTC M216 AACTTCAACAGTTTCTGGGATTTTGCTAAACTTTT 101A-18 AGGGTTGAATAAATCCTCATTAAATGATATTCACAAAACAACGCTCTCT CAAGTAGAAT 102A-18 AATCAGTAGCGACAGATCGATAGCAGCACCGTCGCTCTCTCAAGTAG AAT 103A-18 TAAAGGTGGCAACATAGTAGAAAATACATACACGCTCTCTCAAGTAG AAT 104A-18 GACGGGAGAATTAACTACAGGGAAGCGCATTACGCTCTCTCAAGTAG AAT 105A-18 GCTTATCCGGTATTCTAAATCAGATATAGAAGCGCTCTCTCAAGTAG AAT 106A-18 CGACAAAAGGTAAAGTAGAGAAATATAAAGTACCGCTCTCTCAAGTAG AAT 107A-18 CGCGAGAAAACTTTTTATCGCAAGACAAAGAACGCTCTCTCAAGTAG	AGAGAGCG AGAGAGCG AATCAGTAGCGACAGATCGATAGCAGCACCGTATTACTTGAGAGAGC G 103A TAAAGGTGGCAACATAGTAGAAAATACATTACTTGAGAGAGC G 104A GACGGGAGAATTAACTACAAGGGAAGCGCATTAATTACTTGAGAGAGC G 105A GCTTATCCGGTATTCTAAATCAGATATACATTACTTGAGAGAGCG 106A CGACAAAAAGGTAAAGTAGAAAATACATACATTACTTGAGAGAGCC G 107A CGCGAGAAAACTTTTTATCGCAAGACAAAAGAAATTACTTGAGAGAGCC G 108A ATTAATTACATTTAACACATCAAGAAAACAAAAATTACTTGAGAGAGCC
M205 CGATGGCCCACTACGTAAACCGTC M216 AACTITCAACAGTTTCTGGGATTTTGCTAAACTTTT 101A-18	AGAGAGCG AGAGAGCG AATCAGTAGCGACAGATCGATAGCAGCACCGTATTACTTGAGAGAGC G 103A TAAAGGTGGCAACATAGTAGAAAATACATTACTTGAGAGAGC G 104A GACGGGAGAATTAACTACAGGGAAGCGCATTAATTACTTGAGAGAGC G 105A GCTTATCCGGTATTCTAAATCAGATATAAGAAGATTACTTGAGAGAGCC 106A CGACAAAAGGTAAAGTAGAGAATATAAAGTACATTACTTGAGAGAGCC G 107A CGCGAGAAAACTTTTTATCGCAAGACAAAAATTACTTGAGAGAGCC G 108A ATTAATTACATTTAACACATCAAGAAAAAAAAATTACTTGAGAGAGCC G
M205 CGATGGCCCACTACGTAAACCGTC M216 AACTITCAACAGTTTCTGGGATTTTGCTAAACTTTT 101A-18	AGAGAGCG AGAGAGCG AATCAGTAGCGACAGATCGATAGCAGCACCGTATTACTTGAGAGAGC G 103A
M205 CGATGGCCCACTACGTAAACCGTC M216 AACTTICAACAGTTTCTGGGATTTTGCTAAACTTTT 101A-18 AGGGTTGAATAAATCCTCATTAAATGATATTCACAAAACAACGCTCTCT CAAGTAGAAT 102A-18 AATCAGTAGCGACAGATCGATAGCAGCACCGTCGCTCTCCAAGTAG AAT 103A-18 TAAAGGTGGCAACATAGTAGAAAATACATACACGCTCTCTCAAGTAG AAT 104A-18 GACGGGAGAATTAACTACAGGGAAGCGCATTACGCTCTCTCAAGTAG AAT 105A-18 GCTTATCCGGTATTCTAAATCAGATAGAAGCGCTCTCTCAAGTAGA AT 106A-18 CGACAAAAGGTAAAGTAGAGAATATAAAGTACCGCTCTCTCAAGTAG AAT 107A-18 CGCGAGAAAACTTTTTATCGCAAGAACAAAGAACGCTCTCTCAAGTAG AAT 108A-18 ATTAATTACATTTAACACATCAAGAAAACAAACGCTCTCTCAAGTAG AAT	AGAGAGCG AGAGAGCG AATCAGTAGCGACAGATCGATAGCAGCACCGTATTACTTGAGAGAGC G 103A
M205 CGATGGCCCACTACGTAAACCGTC M216 AACTITCAACAGTTTCTGGGATTTTGCTAAACTTTT 101A-18	AGAGAGCG 102A AATCAGTAGCGACAGATCGATAGCAGCACCGTATTACTTGAGAGAGC G 103A TAAAGGTGGCAACATAGTAGAAAATACATTACTTGAGAGAGC G 104A GACGGGAGAATTAACTACAGGGAAGCGCATTAATTACTTGAGAGAGC G 105A GCTTATCCGGTATTCTAAATCAGATATAGAAGATTACTTGAGAGAGCG G 106A CGACAAAAGGTAAAGTAGAAAATATAAAGTACATTACTTGAGAGAGCG G 107A CGCGAGAAAACTTTTTATCGCAAGACAAAAATTACTTGAGAGAGC G 108A ATTAATTACATTTAACACATCAAGAAAAAATTACTTGAGAGAGCC G 109A TTCATCAATATAATCCTATCAGATGATGACAAAATTACTTGAGAGAGCCG 110A AATCAATATCTGGTCACAAATATCAAACCCTCATTACTTGAGAGAGCCG

208AC T	GTAATGGGATAGGTCAAAACGGCGGATTGACCCGCTCTCTCAAGTAA	213BC T	GGAAGAAAAATCTACGACCAGTCAGGACGTTGTAACTCAATGGACGC
209AC	GATGAACGGTAATCGTAGCAAACAAGAGAATCCGCTCTCTCAAGTAA	214BC	TCATAAGGGAACCGAAAGGCGCAGACGGTCAATAACTCAATGGACGC
T 210AC	GGTTGTACCAAAAACAAGCATAAAGCTAAATCCGCTCTCTCAAGTAA	T 215BC	GACAGCATCGGAACGAACCCTCAGCAGCGAAATAACTCAATGGACGC
T 211AC	CTGTAGCTCAACATGTATTGCTGAATATAATGCGCTCTCTCAAGTAAT	T	
212AC	CATTGAATCCCCCTCAAATCGTCATAAATATTCGCTCTCTCAAGTAAT	101C	
213AC	CATIONNICCCCCTCHINICATION	AGACCACT	AGGGTTGAATAAATCCTCATTAAATGATATTCACAAACAA
T	GGAAGAAAATCTACGACCAGTCAGGACGTTGCGCTCTCTCAAGTAA	102C	
214AC		C	AATCAGTAGCGACAGATCGATAGCAGCACCGTCACCACAAGACCACT
T T	TCATAAGGGAACCGAAAGGCGCAGACGGTCAACGCTCTCTCAAGTAA	103C	
		C	TAAAGGTGGCAACATAGTAGAAAATACATACACACCACAAGACCACT
215AC T	GACAGCATCGGAACGACCTCAGCAGCGAAACGCTCTCTCAAGTAA	104C	
1		C C	${\tt GACGGGAGAATTAACTACAGGGAAGCGCATTACACCACAAGACCACT}$
			GCTTATCCGGTATTCTAAATCAGATATAGAAGCACCACAAGACCACTC
101B	AGGGTTGAATAAATCCTCATTAAATGATATTCACAAACAA	105C	GCITATCCGGTATTCTAAATCAGATATAGAAGCACCACAGAGCACCACTC
ATTGAGTT	A	106C	CGACAAAAGGTAAAGTAGAGAATATAAAGTACCACCACAAGACCACT
102B	AATCAGTAGCGACAGATCGATAGCAGCACCGTAGCGTCCATTGAGTT	С	
A		107C	CGCGAGAAAACTTTTTATCGCAAGACAAGAACACCACAAGACCACT
103B	TAAAGGTGGCAACATAGTAGAAAATACATACAAGCGTCCATTGAGTT	С	
A		108C	ATTAATTACATTTAACACATCAAGAAAACAAACACCACAAGACCACT
104B	GACGGGAGAATTAACTACAGGGAAGCGCATTAAGCGTCCATTGAGTT	С	
A		109C	TTCATCAATATAATCCTATCAGATGATGGCAACACCACAAGACCACTC
105B	GCTTATCCGGTATTCTAAATCAGATATAGAAGAGCGTCCATTGAGTTA	110C	AATCAATATCTGGTCACAAATATCAAACCCTCCACCACAAGACCACTC
106B	CGACAAAAGGTAAAGTAGAGAATATAAAGTACAGCGTCCATTGAGTT		
A	conclusion and management of the concentration of t	206CC	CGGTTTGCGTATTGGGAACGCGCGGGGAGAGGGAGTGGTCTTGTGGT
107B	CGCGAGAAAACTTTTTATCGCAAGACAAAGAAAGCGTCCATTGAGTT	G	COOTTOCOTATTOGOAACGCCCCCCCCCAACAGGAAGGGAGTGGTCTTGTGGT
A	COCONOANACITITATCOCANOACAAAOAAAOCOTCCATTOAOTT	207CC	TGTAAAACGACGGCCATTCCCAGTCACGACGTGAGTGGTCTTGTGGTG
108B	ATTAATTACATTTAACACATCAAGAAAACAAAAGCGTCCATTGAGTT	208CC	
A	ATTACTTACACATCAAGAAAACAAAAGCOTCCATTGAGTT	G	GTAATGGGATAGGTCAAAACGGCGGATTGACCGAGTGGTCTTGTGGT
109B	TTCATCAATATAATCCTATCAGATGATGGCAAAGCGTCCATTGAGTTA	209CC	
110B	AATCAATATCTGGTCACAAATATCAAACCCTCAGCGTCCATTGAGTTA	G	GATGAACGGTAATCGTAGCAAACAAGAGAATCGAGTGGTCTTGTGGT
		210CC	
206BC		G	GGTTGTACCAAAAACAAGCATAAAGCTAAATCGAGTGGTCTTGTGGT
T	CGGTTTGCGTATTGGGAACGCGCGGGGAGAGGTAACTCAATGGACGC	211CC	CTGTAGCTCAACATGTATTGCTGAATATAATGGAGTGGTCTTGTGGTG
207BC		212CC	CATTGAATCCCCCTCAAATCGTCATAAATATTGAGTGGTCTTGTGGTG
T	TGTAAAACGACGGCCATTCCCAGTCACGACGTTAACTCAATGGACGC	213CC	
208BC		G	GGAAGAAAATCTACGACCAGTCAGGACGTTGGAGTGGTCTTGTGGT
T	GTAATGGGATAGGTCAAAACGGCGGATTGACCTAACTCAATGGACGC	214CC	
209BC		G	TCATAAGGGAACCGAAAGGCGCAGACGGTCAAGAGTGGTCTTGTGGT
Т	GATGAACGGTAATCGTAGCAAACAAGAGAATCTAACTCAATGGACGC	215CC	
210BC			${\tt GACAGCATCGGAACGAACCCTCAGCAGCGAAAGAGTGGTCTTGTGGT}$
Т	GGTTGTACCAAAAACAAGCATAAAGCTAAATCTAACTCAATGGACGC	G	
211BC	CTGTAGCTCAACATGTATTGCTGAATATAATGTAACTCAATGGACGCT	1010	
		101D	AGGGTTGAATAAATCCTCATTAAATGATATTCACAAACAA
212BC	CATTGAATCCCCCTCAAATCGTCATAAATATTTAACTCAATGGACGCT	GAGACATT	

102D	AATCACTACCOACACACTCCATACCACCACCTTTACTACTACTCACACAT		
T	AATCAGTAGCGACAGATCGATAGCAGCACCGTTTACTACTGAGACAT	102B10(1)	AATCAGTAGCGACAGATCGATAGCAGCACCGTAGCGTCCATT
103D	TAAAGGTGGCAACATAGTAGAAAATACATACATTACTACTGAGACAT	104B10(2)	${\sf GACGGGAGAATTAACTACAGGGAAGCGCATTACTTCGGCGAG}$
T		106B10(3)	CGACAAAAGGTAAAGTAGAGAATATAAAGTACAGTATCTTAT
104D	GACGGGAGAATTAACTACAGGGAAGCGCATTATTACTACTGAGACAT	108B10(4)	ATTAATTACATTTAACACATCAAGAAAACAAAGAACCTCATC
T		110B10(5)	AATCAATATCTGGTCACAAATATCAAACCCTCGTTCGTACGC
105D	GCTTATCCGGTATTCTAAATCAGATATAGAAGTTACTACTGAGACATT		
106D	CGACAAAAGGTAAAGTAGAGAATATAAAGTACTTACTACTGAGACAT	214BC10(1)	${\tt TCATAAGGGAACCGAAAGGCGCAGACGGTCAAAATGGACGCT}$
T		212BC10(2)	CATTGAATCCCCCTCAAATCGTCATAAATATTCTCGCCGAAG
107D	CGCGAGAAAACTTTTTATCGCAAGACAAAGAATTACTACTGAGACAT	210BC10(3)	${\tt GGTTGTACCAAAAACAAGCATAAAGCTAAATCATAAGATACT}$
T		208BC10(4)	${\tt GTAATGGGATAGGTCAAAACGGCGGATTGACCGATGAGGTTC}$
108D	ATTAATTACATTTAACACATCAAGAAAACAAATTACTACTGAGACATT	206BC10(5)	CGGTTTGCGTATTGGGAACGCGCGGGGGGGGGGGGGGGG
109D	TTCATCAATATAATCCTATCAGATGATGGCAATTACTACTGAGACATT		
110D	AATCAATATCTGGTCACAAATATCAAACCCTCTTACTACTGAGACATT	102C10(1)	AATCAGTAGCGACAGATCGATAGCAGCACCGTCACCACAAGA
		104C10(2)	GACGGGAGAATTAACTACAGGGAAGCGCATTACTATGTCTCC
206DC	CGGTTTGCGTATTGGGAACGCGCGGGGAGAGGAATGTCTCAGTAGTA	106C10(3)	CGACAAAAGGTAAAGTAGAGAATATAAAGTACGACAACGAGT
A		108C10(4)	ATTAATTACATTTAACACATCAAGAAAACAAAGTAAGCCATC
207DC	TGTAAAACGACGCCATTCCCAGTCACGACGTAATGTCTCAGTAGTA	110C10(5)	AATCAATATCTGGTCACAAATATCAAACCCTCTGGCACGTCA
A			
208DC A	${\tt GTAATGGGATAGGTCAAAACGGCGGATTGACCAATGTCTCAGTAGTA}$	214CC10(1)	TCATAAGGGAACCGAAAGGCGCAGACGGTCAATCTTGTGGTG
209DC		212CC10(2)	CATTGAATCCCCCTCAAATCGTCATAAATATTGGAGACATAG
A	GATGAACGGTAATCGTAGCAAACAAGAGAATCAATGTCTCAGTAGTA	210CC10(3)	GGTTGTACCAAAAACAAGCATAAAGCTAAATCACTCGTTGTC
210DC		208CC10(4)	GTAATGGGATAGGTCAAAACGGCGGATTGACCGATGGCTTAC
A	GGTTGTACCAAAAACAAGCATAAAGCTAAATCAATGTCTCAGTAGTA	206CC10(5)	CGGTTTGCGTATTGGGAACGCGCGGGGAGAGGTGACGTGCCA
211DC	CTGTAGCTCAACATGTATTGCTGAATATAATGAATGTCTCAGTAGTAA		
212DC	CATTGAATCCCCCTCAAATCGTCATAAATATTAATGTCTCAGTAGTAA	102D10(1)	AATCAGTAGCGACAGATCGATAGCAGCACCGTTTACTACTGA
213DC		104D10(2)	GACGGGAGAATTAACTACAGGGAAGCGCATTAAGTCTGCCGA
A	GGAAGAAAATCTACGACCAGTCAGGACGTTGAATGTCTCAGTAGTA	106D10(3)	CGACAAAAGGTAAAGTAGAGAATATAAAGTACCACATTCGAG
214DC		108D10(4)	ATTAATTACATTTAACACATCAAGAAAAACAAATAGTATTCCA
A	TCATAAGGGAACCGAAAGGCGCAGACGGTCAAAATGTCTCAGTAGTA	110D10(5)	AATCAATATCTGGTCACAAATATCAAACCCTCCTTGGCACAT
215DC			
A	GACAGCATCGGAACGAACCCTCAGCAGCGAAAAATGTCTCAGTAGTA	214DC10(1)	TCATAAGGGAACCGAAAGGCGCAGACGGTCAATCAGTAGTAA
		212DC10(2)	CATTGAATCCCCCTCAAATCGTCATAAATATTTCGGCAGACT
102A10(1)	AATCAGTAGCGACAGATCGATAGCAGCACCGTATTACTTGAG	210DC10(3)	GGTTGTACCAAAAACAAGCATAAAGCTAAATCCTCGAATGTG
104A10(2)	GACGGGAGAATTAACTACAGGGAAGCGCATTACGCTGCTGAG	208DC10(4)	${\tt GTAATGGGATAGGTCAAAACGGCGGATTGACCTGGAATACTA}$
106A10(3)	CGACAAAAGGTAAAGTAGAGAATATAAAGTACGATCAGTCGG	206DC10(5)	CGGTTTGCGTATTGGGAACGCGCGGGGAGAGGATGTGCCAAG
108A10(4)	ATTAATTACATTTAACACATCAAGAAAACAAACGTACGTCCA		
110A10(5)	AATCAATATCTGGTCACAAATATCAAACCCTCCAGAAAGCAT	S102	AATCAGTAGCGACAGATCGATAGC
		S103	TAAAGGTGGCAACATAGTAGAAAA
214AC10(1)	TCATAAGGGAACCGAAAGGCGCAGACGGTCAACTCAAGTAAT	S104	GACGGGAGAATTAACTACAGGGAA
212AC10(2)	CATTGAATCCCCCTCAAATCGTCATAAATATTCTCAGCAGCG	S105	GCTTATCCGGTATTCTAAATCAGA
210AC10(3)	GGTTGTACCAAAAACAAGCATAAAGCTAAATCCCGACTGATC	S106	CGACAAAAGGTAAAGTAGAGAATA
208AC10(4)	GTAATGGGATAGGTCAAAACGGCGGATTGACCTGGACGTACG	S107	CGCGAGAAAACTTTTTATCGCAAG
206AC10(5)	CGGTTTGCGTATTGGGAACGCGCGGGGAGAGGATGCTTTCTG	S108	ATTAATTACATTTAACACATCAAG

S109	TTCATCAATATAATCCTATCAGAT	S213	GGAAGAAAATCTACGACCAGTCA	
S110	AATCAATATCTGGTCACAAATATC	S214	TCATAAGGGAACCGAAAGGCGCAG	
S111	ACCAGTAATAAAAGGGATTCACCAGTCACACG	S215	GACAGCATCGGAACGAACCCTCAG	
		S216	AACTTTCAACAGTTTCTGGGATTTTGCTAAACTTTT	
S207	TGTAAAACGACGGCCATTCCCAGT			
S208	GTAATGGGATAGGTCAAAACGGCG			
S209	GATGAACGGTAATCGTAGCAAACA			
S210	GGTTGTACCAAAAACAAGCATAAA			
S211	CTGTAGCTCAACATGTATTGCTGA			
S212	CATTGAATCCCCCTCAAATCGTCA			

4.5 References

- (1) Rothemund, P. W. Nature **2006**, 440, 297.
- (2) Nangreave, J.; Han, D.; Liu, Y.; Yan, H. Curr. Opin. Chem. Biol. 2010, 14, 608.
- (3) Saccà, B.; Niemeyer, C. M. Angew. Chem. Intl. Ed. 2012, 51, 58.
- (4) Erben, C. M.; Goodman, R. P.; Turberfield, A. J. Angew. Chem. 2006, 118, 7574.
- (5) Ding, B.; Deng, Z.; Yan, H.; Cabrini, S.; Zuckermann, R. N.; Bokor, J. J. Am. Chem. Soc.2010, 132, 3248.
- (6) Hung, A. M.; Micheel, C. M.; Bozano, L. D.; Osterbur, L. W.; Wallraff, G. M.; Cha, J. N. Nat. Nanotechnol. **2010**, *5*, 121.
- (7) Tian, Y.; Wang, T.; Liu, W.; Xin, H. L.; Li, H.; Ke, Y.; Shih, W. M.; Gang, O. *Nat. Nanotechnol.* **2015**, *10*, 637.
- (8) Schreiber, R.; Santiago, I.; Ardavan, A.; Turberfield, A. J. ACS Nano 2016.
- (9) Yao, G.; Li, J.; Chao, J.; Pei, H.; Liu, H.; Zhao, Y.; Shi, J.; Huang, Q.; Wang, L.; Huang,W. Angew. Chem. 2015, 127, 3009.
- (10) Shen, X.; Asenjo-Garcia, A.; Liu, Q.; Jiang, Q.; García de Abajo, F. J.; Liu, N.; Ding, B. *Nano Lett.* **2013**, *13*, 2128.

- (11) Jiang, Q.; Song, C.; Nangreave, J.; Liu, X.; Lin, L.; Qiu, D.; Wang, Z.-G.; Zou, G.; Liang, X.; Yan, H. *J. Am. Chem. Soc.* **2012**, *134*, 13396.
- (12) Zhang, Q.; Jiang, Q.; Li, N.; Dai, L.; Liu, Q.; Song, L.; Wang, J.; Li, Y.; Tian, J.; Ding, B. *ACS Nano* **2014**, *8*, 6633.
- (13) Mikkilä, J.; Eskelinen, A.-P.; Niemelä, E. H.; Linko, V.; Frilander, M. J.; Törmä, P. i.; Kostiainen, M. A. *Nano Lett.* **2014**, *14*, 2196.
- (14) Acuna, G.; Möller, F.; Holzmeister, P.; Beater, S.; Lalkens, B.; Tinnefeld, P. *Science* **2012**, *338*, 506.
- (15) Pei, H.; Lu, N.; Wen, Y.; Song, S.; Liu, Y.; Yan, H.; Fan, C. Adv. Mater. 2010, 22, 4754.
- (16) Meng, H.-M.; Liu, H.; Kuai, H.; Peng, R.; Mo, L.; Zhang, X.-B. *Chem. Soc. Rev.* **2016**, 45, 2583.
- (17) Fu, Y.; Zeng, D.; Chao, J.; Jin, Y.; Zhang, Z.; Liu, H.; Li, D.; Ma, H.; Huang, Q.; Gothelf, K. V. J. Am. Chem. Soc. **2012**, 135, 696.
- (18) Schreiber, R.; Do, J.; Roller, E.-M.; Zhang, T.; Schüller, V. J.; Nickels, P. C.; Feldmann, J.; Liedl, T. *Nat. Nanotechnol.* **2014**, *9*, 74.
- (19) Jones, M. R.; Seeman, N. C.; Mirkin, C. A. Science **2015**, 347, 1260901.
- (20) Shaw, A.; Benson, E.; Högberg, B. r. ACS Nano 2015, 9, 4968.
- (21) Dietz, H. Nat. Nanotechnol. **2015**, 10, 829.
- (22) Suzuki, Y.; Endo, M.; Sugiyama, H. ACS Nano **2015**, 9, 3418.
- (23) Zhang, H.; Chao, J.; Pan, D.; Liu, H.; Huang, Q.; Fan, C. *Chem. Commun.* **2012**, 48, 6405.
- (24) Pound, E.; Ashton, J. R.; Becerril, H. A.; Woolley, A. T. *Nano Lett.* **2009**, *9*, 4302.
- (25) Zheng, L.; Baumann, U.; Reymond, J.-L. Nucleic Acids Res. 2004, 32, e115.

- (26) Wu, N.; Willner, I. Nano Lett. 2016, 16, 2867.
- (27) Chen, H.; Zhang, H.; Pan, J.; Cha, T.-G.; Li, S.; Andréasson, J.; Choi, J. H. *ACS Nano* **2016**, *10*, 4989.
- (28) Liu, W.; Zhong, H.; Wang, R.; Seeman, N. C. Angew. Chem. 2011, 123, 278.
- (29) Zenk, J.; Tuntivate, C.; Schulman, R. J. Am. Chem. Soc. **2016**, 138, 3346.
- (30) Yao, G.; Li, J.; Chao, J.; Pei, H.; Liu, H.; Zhao, Y.; Shi, J.; Huang, Q.; Wang, L.; Huang, W. *Angew. Chem. Intl. Ed.* **2015**, *54*, 2966.
- (31) Amiram, M.; Quiroz, F. G.; Callahan, D. J.; Chilkoti, A. Nat. Mater. 2011, 10, 141.
- (32) Simnick, A. J.; Lim, D. W.; Chow, D.; Chilkoti, A. J. Macromol. Sci., Part C: Polymer Reviews 2007, 47, 121.
- (33) Hamblin, G. D.; Rahbani, J. F.; Sleiman, H. F. *Nat. Commun.* **2015**, *6*.
- (34) Engler, C.; Kandzia, R.; Marillonnet, S. *PloS one* **2008**, *3*, e3647.
- (35) Gibson, D. G.; Young, L.; Chuang, R.-Y.; Venter, J. C.; Hutchison, C. A.; Smith, H. O. *Nat. Methods* **2009**, *6*, 343.
- (36) Briggs, A. W.; Rios, X.; Chari, R.; Yang, L.; Zhang, F.; Mali, P.; Church, G. M. *Nucleic Acids Res.* **2012**, *40*, e117.
- (37) Torella, J. P.; Lienert, F.; Boehm, C. R.; Chen, J.-H.; Way, J. C.; Silver, P. A. *Nat. Protoc.* **2014**, *9*, 2075.

Chapter 5:

Conclusions and Future Work

5.1 Conclusions

The principal premise of the work described in this thesis was to design and investigate strategies for generating higher-order DNA nanostructures with intrinsic dynamic behavior, while reducing synthetic effort. We first developed dynamic DNA nanotubes based on 11 unmodified short strands. Then, we introduced hydrophobic interactions to build 1D networks of DNA nanostructures and DNA nanotubes with hydrophobic environment. One of the main motivations behind exploring these systems was examining their cellular uptake behavior and building novel drug delivery vehicles. Finally, we attempted to produce super-origami structures without significantly increasing their synthetic costs. Our strategy improves the control over the final product and exhibits enhanced properties for practical applications.

In chapter 2, we have developed a new method to grow stable nanotubes with intrinsic dynamic behavior. Our tubes are constructed by hybridizing only 11 unmodified strands via sticky-end cohesion in less than 6 hours and are designed to have a unique architecture that is capable of cooperatively amplifying a stimulus into motion. We used the strand displacement strategy both on free nanotubes in solution and immobilized tubes on a solid support as a proof of concept to examine: (i) the stability of the single-stranded version of the design, (ii) the morphological shift between the single and double-stranded forms and (iii) how fast can our system respond to a stimulus. Second, we progressively shorten two sides of the nanotube while fixing the length of the third one. This, resulted in length mismatch in every repeat unit and caused an important

morphological shift from the original tubes. As observed by AFM and studied by single molecule photobleaching experiments, the tubes started to bend until the distortion is large enough to break them into shorter units. Thus, our strategy involves the rearrangement of DNA nanotubes in response to external stimuli and offers a new tool for drug delivery or materials organization.

In chapter 3, we introduced an orthogonal interaction to our nanotubes without changing the sequences of the original design. We reported the construction of a DNA nanotube with a switchable hydrophobic environment, and the characterization of its guest encapsulation and release behavior by single-molecule fluorescence microscopy. Under specific conditions, the hydrophobic association switched from intramolecular to intermolecular allowing the assembly of a long-range network held together through hydrophobic domains. A simple molecular spacer can thus switch the morphology from DNA nanotubes with an internal 'handshake' of the alkyl chains, to an external interaction that brings nanostructures and amphiphilic strands together into networks. Finally, we examined the cellular uptake of both systems in HeLa cells over time. When the alkyl chains are engaged in an intramolecular handshake, the tubes shed their dye-labelled strands within the cellular environment, which then co-localize with mitochondria. This behavior is similar to that of bare nanotubes without lipidic chains. On the other hand, the 1D-bundles with intermolecular hydrophobic association disassemble into alkyl coated smaller nanostructures. These structures protect their component strands from non-specific uptake and dye-directed mitochondrial localization, and instead enter cells slowly via endocytosis. Thus, both the presence of alkyl chains and their ability to result in an intramolecular interaction profoundly influence cellular uptake of their strands.

Chapter 4 described the creation of DNA "super-origami" without dramatically increasing the number of strands or the error rate during the assembly. This required the synthesis of a single-

stranded DNA (ssDNA) scaffold that helped the association of three and five origami tiles in 1D. With this in mind, we demonstrated the production of a set of long ss DNA backbones at defined lengths. Our strategy allowed us to modify the sequences of the strands with full control over the repetitive and unique regions on the backbone. Therefore, we significantly diminished the number of components used, while preserving addressability. Since DNA origami is currently one of the most successful approaches adopted in the field, our method offers a new way to build DNA nanostructures with even larger surface area. We hope that our platform will be further explored by scientists and engineers to construct more complex nanomaterials.

5.2 Suggestions for Future Work

Future work using our DNA nanotubes from Chapter 2 is already happening in our laboratory and in collaboration with Professor Cosa's Lab at McGill. As mentioned in Appendix A, we extended the linking strands on our tubes with 15-base polyadenine (polyA) sequence, then we added 3/20 nm AuNPs polyfunctionalized with 10/15-base polythymine (polyT) strands. Interestingly, long and organized fibers were observed via AFM under specific conditions. Ongoing efforts will focus on understanding the mechanism of assembly of these fibers. Parameters such as the size of AuNP's, the length of polyA/polyT sequences, the ionic strength of the solution and deposition conditions on mica surface should be further examined. Another study was carried out in our lab using this design based on conjugating proteins to the linking strands. The aim of this study is to: (i) provide a new synthetic route for the production DNA-Protein conjugates in a cost-effective manner and high yields and (ii) generate functionalized DNA nanotubes for theranostic applications.

The ability to reversibly switch between double- and single-stranded DNA nanotubes is a key characteristic of our design. Therefore, we are currently extensively investigating the kinetics of each step. Using single-molecule fluorescence microscopy, the effect of tube lengths on the strand displacement reaction can be revealed. This study is expected to help us design new generations of DNA nanotubes that better fit specific applications. For example, releasing cargo in response to biologically relevant triggers remains one of the exciting topics in the field. In this regard, the sequences on the linking strands will be modified to bind proteins such as thrombin and the stability of the tubes in the presence of the protein will be investigated.

The DNA nanotubes described in chapter 3 provide a great platform to encapsulate and conditionally release small molecules. Since it is challenging to predict the intracellular fate of these constructs, future work should aim at understanding their internalization mechanism and studying the role of alkyl chains in protecting DNA from degradation by nucleases. Another important consideration is incorporating targeting agents such as aptamers and folic acids in order to help our systems escape the lysosomes and release their cargo into specific organelles. Furthermore, synthesizing size-defined DNA nanotubes using the scaffold demonstrated in chapter 4 allows us to determine the optimal size of nanostructures entering the cells. Other factors including the rigidity of the constructs should be studied as well.

The strength of our approach described in chapter 4 lies not only in its ability to organize origami tiles but also in the addressability offered by the scaffold itself. For instance, when removing any of the 5 tiles, the backbones should still be able to successfully arrange the remaining tiles in a very well defined manner. To our knowledge, controlling the geometry of higher-order DNA nanoarchitectures is still a challenging task in the field. We believe that the introduction of custom-made external scaffolds to form extended DNA origami structures might solve some of

these problems by tuning the sequences of each building block on the DNA backbone. To further illustrate the versatility of this strategy, one could examine its capability to generate two-dimensional structures. We anticipate that this technique can be extended to develop even larger structures, providing enough surface area to functionalize materials up to few micrometers. In addition, because we are extracting our scaffolds from plasmids, polymerase chain reactions (PCR) can be employed to add unique sequences to the same scaffold, hence controlling the geometry of the final assembly.

5.2 List of Publications

- (1) Hamblin, G. D.; Rahbani, J. F.; Sleiman, H. F. *Nat. Commun.* **2015**, *6*, 1.
- (2) Rahbani, J.; Metera, K.; Sleiman, H. *Functional Metallosupramolecular Materials;* RSC Publishing, **2015**, 32.
- (3) Rahbani, J. F.; Hariri, A. A.; Cosa, G.; Sleiman, H. F. *ACS Nano* **2015**, *9*, 11898.
- (4) Rahbani, J. F.; Vengut-Climent E.; Chidchob P.; Gidi Y.; Trinh T.; Cosa G.; Sleiman H. F.; *Adv. Mater.* **2017,** Under Revision.
- (5) Luo X.; Chidchob P.; Rahbani J.; Sleiman H. F.; Small 2017, Under Revision.

Appendix 1:

Rearrangement of DNA Nanotubes into Long Fibers Mediated by Gold Nanoparticles

Author contributions: Saliba D. helped in preparing some samples (~40%) and synthesizing gold nanoparticles. He also performed gel electrophoresis experiments.

A1.1 Introduction

DNA nanotechnology provides an important route to arrange materials in a programmable fashion. In particular, DNA origami and other nanostructures have been widely employed to organize gold nanoparticles (AuNPs) in two-dimensional (2D) patterns, 1-3 and three dimensional (3D) photonic structures. 4.5 Our lab has recently reported a novel approach to transmit complex 2D patterns from DNA nanocages to AuNPs where the number and position of the oligonucleotides were determined by the scaffold. In this section, we explore the usage of AuNPs to induce the self-assembly of higher-order DNA nanostructures. Our strategy requires a limited number of DNA strands (11) and is not synthetically demanding. First, we studied by dry AFM the assembly of our nanotubes in the presence of AuNPs in magnesium buffer. Next, we examined the same mixture under various conditions including lower/higher DNA or AuNPs concentrations and in different buffers. Interestingly, long and organized fibers were only observed in magnesium buffer and under specific conditions. These results encouraged us to further explore the effect of salts deposition on the growth of these bundles. We believe that the simple addition of AuNPs to

our nanotubes offers a unique and inexpensive route to produce higher-order structures templated by these nanotubes, that are most likely salt-DNA composites.

A1.2 Results and Discussion

A1.2.1 System Design

The DNA triangular rung unit was assembled as described in chapter 2. Briefly, 6 strands (V, C1, C2, R1, R2 and R3) were mixed in equimolar amounts, with a final concentration of 240 nM in 1x TAMg (Tris base, acetic acid and magnesium chloride). The mixture was then annealed from 95 to 20°C over 3 h 40 min. In order to form the nanotubes, the first set of linking strands LS1/LS1* was added while heating the solution to 56°C then cooling it down to 22°C for 1 h. Finally, the remaining two linking strands LS2/LS2-3* and LS3/LS2-3* were added to close the tubes before annealing the mixture to 44°C then cooling it down to 22°C for 45 min.⁷

In this section, a few modifications were made to the design in order to allow its binding to AuNPs. First, we extended the 3' end of the three linking strands (LS1-3) and/or their complementary components (LS*1-3) by 15 polyadenine (polyA) bases. Then, we added the AuNPs decorated with 10 or 15 polythymine (polyT) bases. The sequences of the linking strands and their complementary strands were the same as the unmodified tubes, except an hexaethylene glycol (HEG) group was incorporated before adding the polyA sequence to enhance the flexibility of the overhang. All the strands were made via a DNA synthesizer and purified by gel electrophoresis.

During this study, we investigated the assembly of two types of modified nanotubes. The first one consisted of three extended polyA strands on LS*1-3 (NT3: Figure A1.1b) and the second one consisted of six poly A extensions, both on LS1-3 and LS*1-3 (NT6: Figure A1.1a). The

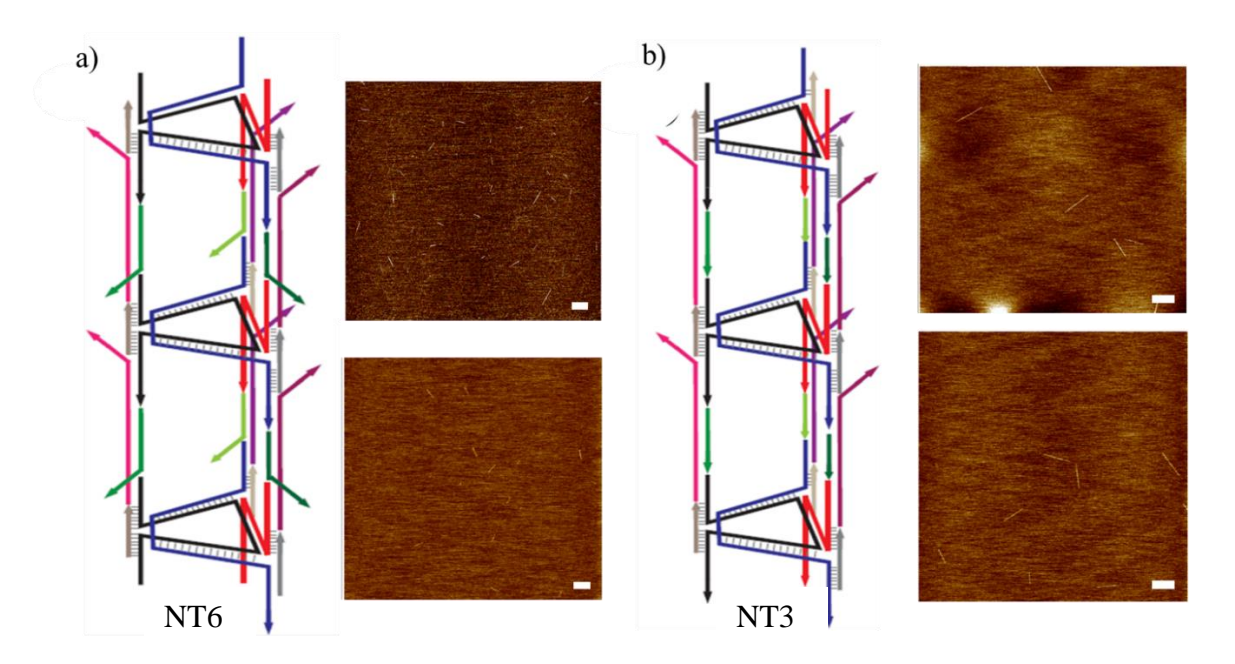


Figure A1.1. (a) AFM micrographs displaying the assembly of short (up to 300 nm) and straight nanotubes with 6 modified strands . (b) AFM micrographs displaying the assembly of big (up to 1 μ m) and straight nanotubes with 3 modified strands, scale bar 500 nm. Samples in part (a) were prepared by Saliba D.

assembly of both tubes was examined by AFM and AGE. Interestingly, AFM micrographs showed the growth of shorter features for NT6 compared to NT3 (Figure A1.1). This observation could be due to the additional steric effect of the overhangs on the three linking strands. However, both systems were bigger than the pores of agarose gel and appeared as non-penetrating bands as displayed in Figure A1.2.

A1.2.2 Self-Assembly of Long Fibers and Needle-Like Structures

The modified nanotubes were incubated with 10/15T-polyconjugated AuNPs (3 or 20 nm) at room temperature (RT) for 24 h. Remarkably, a precipitate was observed at that time and was characterized by 1% native AGE and AFM. This experiment was performed at two different

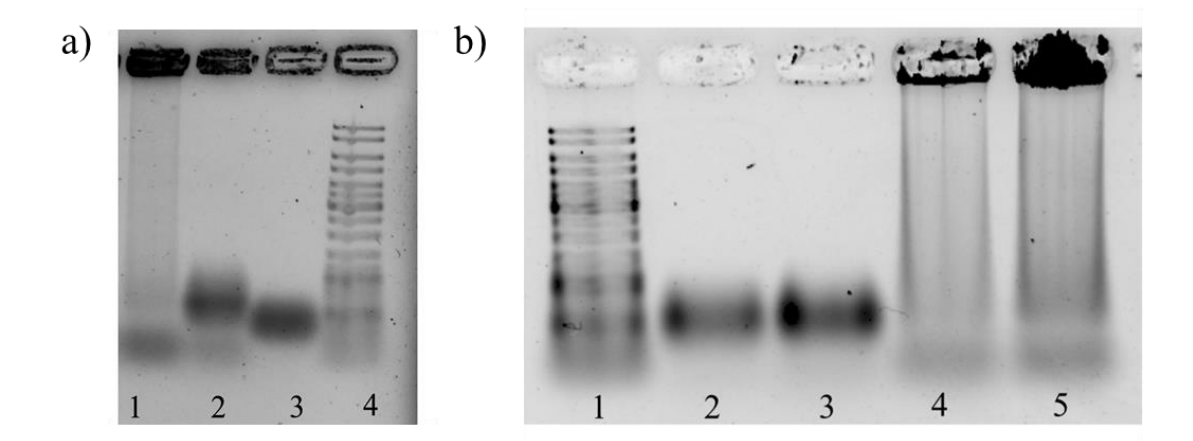


Figure A1.2. (a) 1% native AGE in 1×TAMg showing the assembly of unmodified nanotubes. Lane 1: fully formed nanotubes, lane 2: rung + LS1/LS1*, lane 3: rung unit and lane 4: OGen ruler. The DNA nanotubes are characterized by a non-penetrating band. (b) 1% native AGE in 1×TAMg showing the assembly of NT3 and NT6. Lane 1: OGen ruler, lane 2: rung + LS1/LS1*polyA, lane 3: rung + LS1polyA/LS1*polyA, lane 4: rung + LS1/LS1*polyA + LS2/LS2-3*polyA + LS3/LS2-3*polyA and lane 5: rung + LS1polyA/LS1*polyA + LS2polyA/LS2-3*polyA + LS3polyA/LS2-3*polyA. NT3 and NT6 are characterized by non-penetrating bands. Gels were performed by Saliba D.

concentrations of the nanotube building strands (50 nM and 400 nM) and at three different AuNPs/DNA equivalents (0.2, 1 and 2 equivalents). Interestingly, the AFM images for the 0.2 equivalents of 3 nm AuNPs-10T/NT3, at 50 nM showed a random aggregation of the nanotubes with the AuNPs, often arranged in a longitudinal fashion on the nanotubes. At 1 equiv. of AuNPs-10T/NT3, a flower-like structure with an underlying network of nanotubes was observed. At 2 equiv. of AuNPs-10T/NT3, structures consisting of parallel bundles of needle-like features, often arranged in a 'bow-tie' formed, and the AuNPs were no longer visible (Figure A3). Hence, we always added 2 equimolar mixture of AuNPs compared to DNA in future experiments.

Table A1.1 summarizes the effect of the AuNPs size on the assembly of fibers. The nanoparticles were functionalized with 10 or 15 polyT and were incubated with NT3 (nanotube with 3 A15 overhangs) and NT6 (nanotube with 6 A15 overhangs) at room temperature overnight.

Figure A1.4 displays the assembly of long fibers when tubes NT3 were incubated with 3 or 20 nm AuNPs-10/15T. The size of particles did not seem to play a major role in the assembly process in

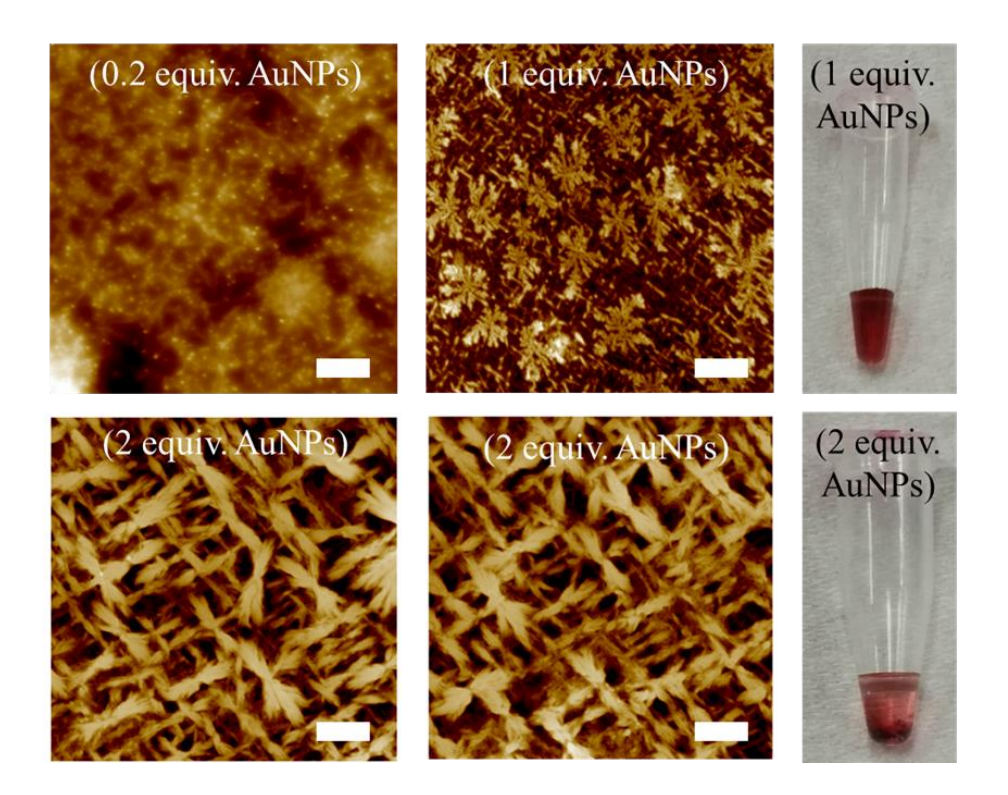


Figure A1.3. Left: AFM micrographs displaying the assembly of NT3 50 nM incubated with 0.2, 1 and 2 3 nm AuNP-10T/NT3 equivalents at RT. Right: Images showing the formation of precipitates at 2 AuNPs/NT3 equivalents. AFM at 0.2 equiv. was carried out by Saliba D.

Table A1.1. Effect of AuNPs size and polyT length on the formation of fibers.

	NT3*	NT6*
With 3 nm AuNPs-10T	Long fibers	Short needle-like
With 20 nm AuNPs-10T	Long fibers	Short needle-like
With 3 nm AuNPs-15T	Long and more organized fibers	Short needle-like
With 20 nm AuNPs-15T	Very long and organized fibers	Short needle-like

^{*}NT3 and NT6 50 nM were incubated with 2 equivalents of AuNPs at RT for 24 h.

the presence of AuNPs-10T. However, incubating the mixture with 20 nm AuNPs-15T caused the growth of very well organized and long fibers. While it is logical for larger AuNPs to bind more nanotubes, we are still examining the mechanism of formation of such long features and whether it is related to the size of AuNPs. Note that the height of all AFM images reached ~100 nm. Therefore, we assumed that working under dry AFM conditions might affect the local concentrations of AuNPs/DNA and induce the growth of these bundles. We also believed that the heights obtained by AFM can be directly related to the unwashed salts on mica surface. In order to study the effect of salts on the assembly of bundles, we first repeated the AFM measurements under dry conditions after washing the mica surface with autoclaved water. Later, we attempted to observe the same samples under AFM liquid conditions. Interestingly, the integrity of the fibers (e.g. NT3 + 3 nm AuNPs-15T) was not completely lost after washing the samples three times with water and the height of AFM images decreased by 20 nm (Figure A1.4). Next, we deposited the samples on the surface of mica, waited 1 hour for them to dry, then carried on AFM measurements under liquid conditions. We thought that acquiring the images under these conditions may minimize the effect of the salt layers on the surface of mica. The integrity of the fibers was partially preserved and the heights of the AFM micrographs decreased to ~50 nm. Finally, we performed AFM measurements under normal liquid conditions where the samples were deposited for 3 min on mica before adding the buffer solution. Figure A1.4 shows the disassembly of some of these bundles while the integrity of many features was preserved. It is likely that the features observed are salts that are templated by an underlying nanotube-gold nanoparticle structure. To have a better understanding about the behavior of the bundles under liquid conditions, future experiments should focus on designing highly stable bundles where the interaction between the tubes and the AuNPs is stronger than 15 polyA/T, as well as salts with reduced water solubility.

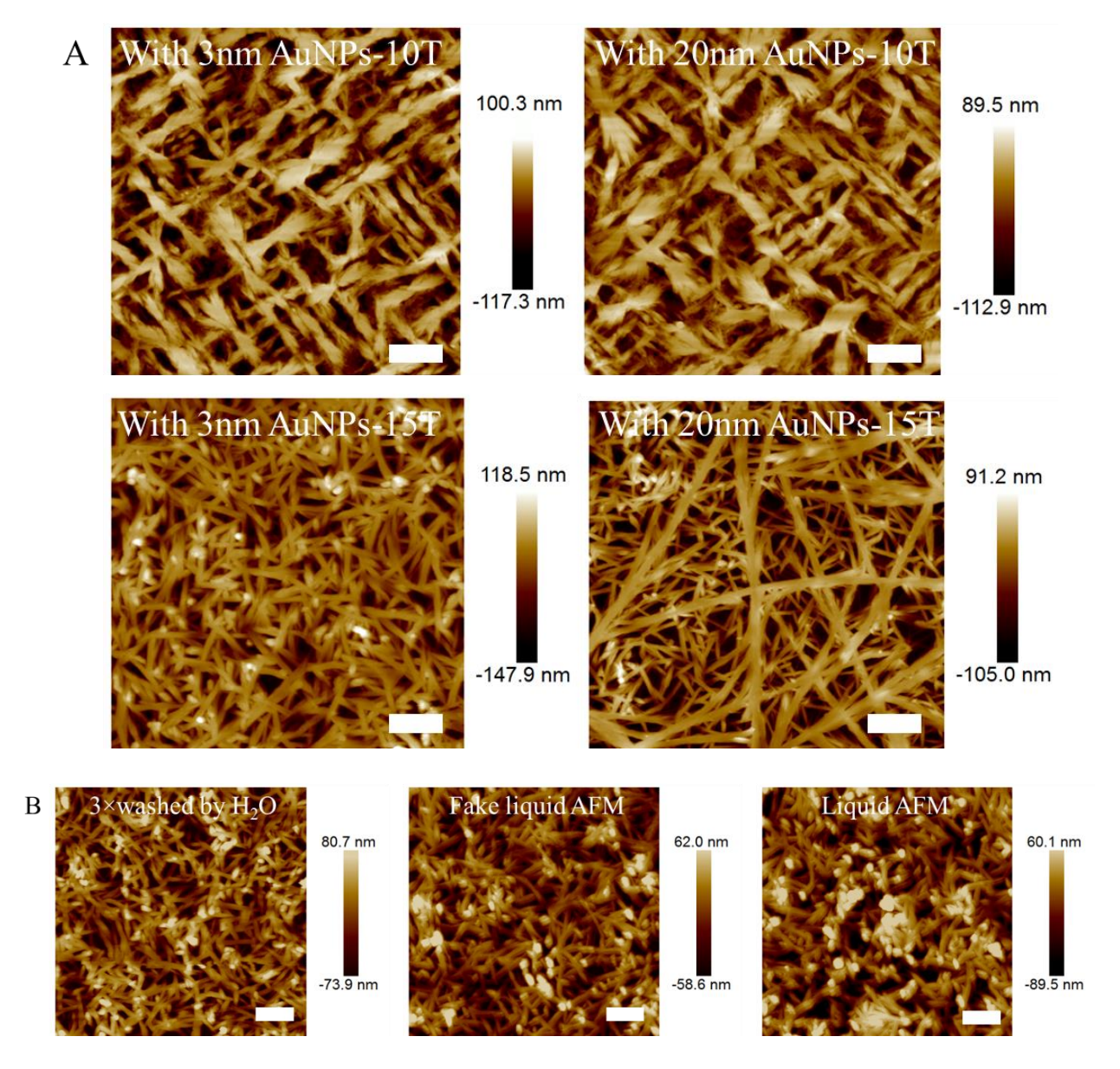


Figure A1.4. (A) AFM micrographs showing the effect of AuNPs size and polyT length on the formation of fibers made up of NT3 50 nM/AuNPs. (B) AFM images displaying the morphology of the bundles (NT3 at 50 nM + 2equiv. 3 nm AuNPs-15T) at different experimental conditions. Scale bar, 500 nm. Samples with 20 nm AuNPs were prepared by Saliba D.

The same experiments were repeated to examine the morphological changes of tubes NT6 in the presence of 2equiv. of 3/20 nm AuNPs-10/15 T. Remarkably, small needle-like structures that are comparable in size to tubes NT6, in the absence of AuNPs, were observed by dry AFM (Figure

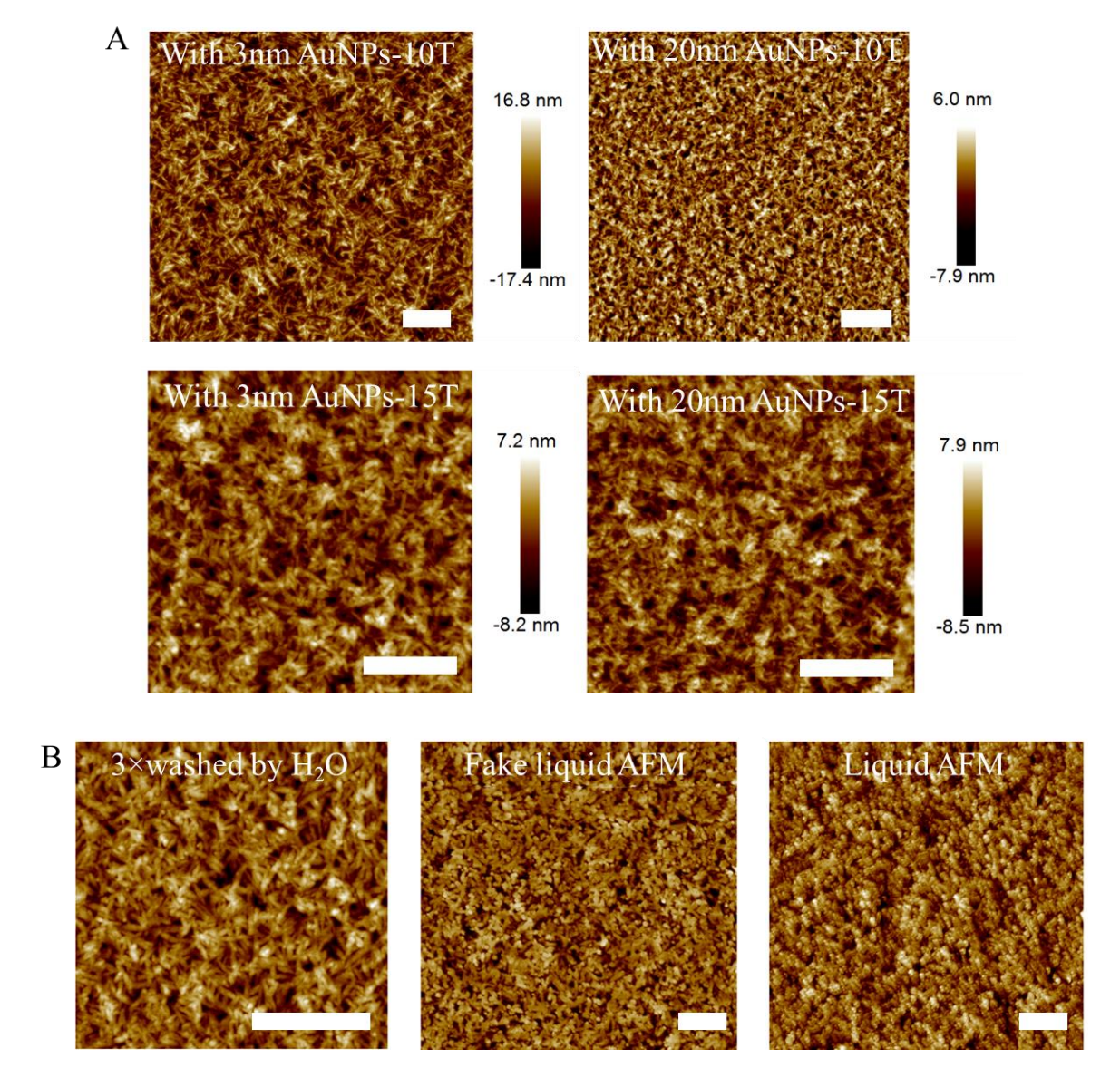


Figure A1.5. (A) AFM micrographs showing the effect of AuNPs size and polyT length on the formation of fibers made up of NT6 50 nM/AuNPs. (B) AFM images displaying the morphology of the needle-like structures (NT6 at 50 nM + 2equiv. 3 nm AuNPs-10T) at different experimental conditions. Scale bar, 500 nm.

A1.5). Since smaller tubes were originally formed (up to 300 nm), increasing the size of AuNPs or the length of polyT sequence did not significantly affect the shape and geometry of bundles. More importantly, although we used the same deposition conditions on the mica surface (same salt concentrations), the height of the AFM micrographs was ~5 nm. This observation suggests that the

long fibers described previously are most probably not the sole result of random salt deposition on the mica surface, as they are affected by the DNA/gold template. In addition, when we visualized the small needle-like structures under liquid conditions, the integrity of most of the structures was lost indicating that 10 or 15 A/T interaction is not strong enough to perform AFM measurements under liquid conditions, or that the crystallized salt layer is dissolving under the conditions of the experiment.

In the next set of experiments, we monitored the morphological changes of tubes NT3 incubated overnight with 2 equiv. of 3 nm AuNPs-10T at room temperature. The only difference is the concentration of the strands constituting the tubes. Here, the tubes were prepared at 400 nM, deposited on the mica surface and examined by dry AFM. Figure A1.6 depicts the assembly of large and thick bundles that almost covered the entire field of view. Assuming that salts play a more important role at higher concentrations, we continued to prepare our samples at 50 nM.

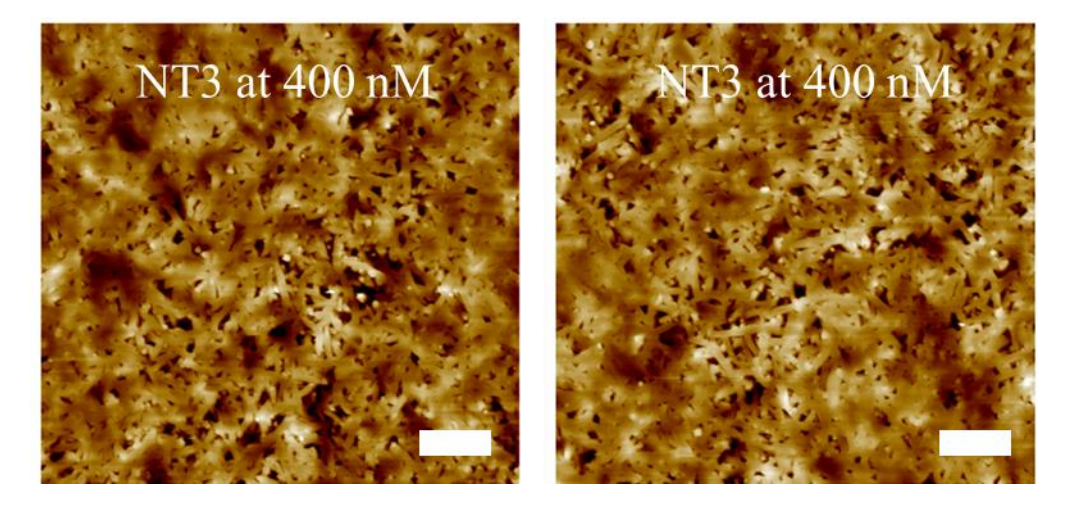


Figure A1.6. AFM micrographs of fibers made up of NT3 at 400 nM + 2equiv. 3 nm AuNPs-10T. Scale bar, 500 nm.

Finally, we investigated the assembly of long fibers in other tris (hydroxymethyl) aminomethane) buffers and in phosphate buffer PBS. We prepared tubes NT3 50 nM in 1×TANi before incubating the mixture with 3 nm AuNPs-15T at RT. Interestingly, no fibers were observed under AFM dry conditions. Similarly, small AuNPs aggregates were spotted when the samples were prepared in 1×TACa. Figure A1.7 shows the formation of salts patterns on the mica surface after depositing a mixture of NT3/AuNPs in PBS. While we are still studying the effect of buffers on the growth of these bundles, the presence of Mg²⁺ seems essential to facilitate the interaction between nanotubes and AuNPs. Future studies should focus on determining the amount of magnesium needed for these long fibers to form, and the composition of these fibers.

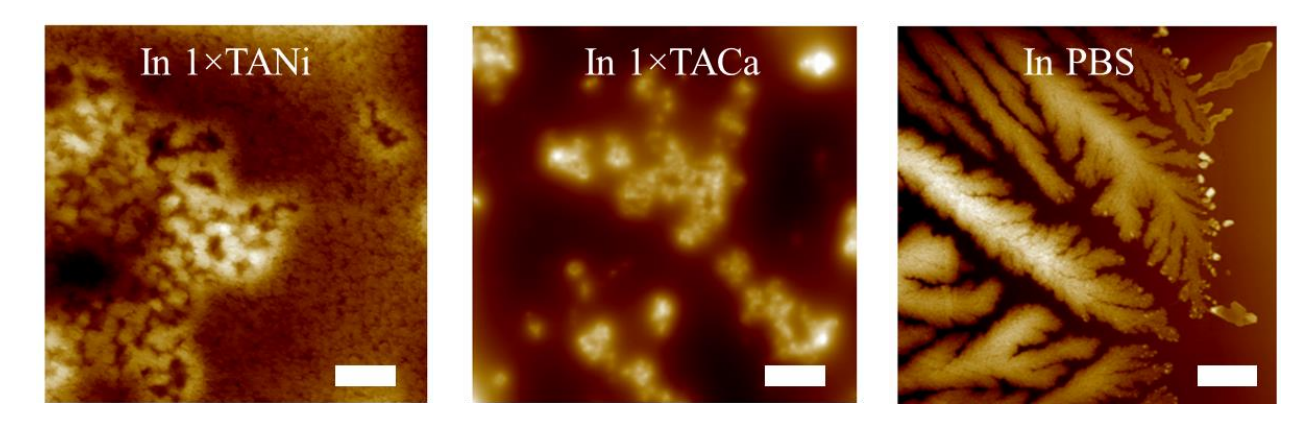


Figure A1.7. AFM micrographs showing no fibers formation when incubating NT3 with 3 nm AuNPs-15T at RT. Scale bar, 500 nm. Samples were prepared by Saliba D.

A1.3 Conclusions

In conclusion, we attempted in this section to develop a novel strategy to generate higher order DNA nanostructures without involving synthetically challenging procedures or hundreds of DNA strands. Preliminary data show the growth of short and long fibers when A15-labelled DNA

nanotubes were mixed with T15-labelled gold nanoparticles in tris magnesium buffer, and deposited on a solid surface. Factors such as the quantity of DNA, concentration and size of AuNPs, concentration and nature of cations in solution and salt deposition on the mica surface play a crucial role in determining the final shape and geometry of these fibers. Tubes bearing three polyA sequences grew up to 1 μ m, hence long and organized bundles were assembled when AuNPs were added. On the other hand, tubes having six polyA sequences did not grow more than 300 nm, thus needle-like structures were observed by AFM after the addition of AuNPs. Further examination of the assembly conditions and the composition of these fibers will allow us to use them as platforms for the templation of a wide range of functional materials and biomaterials.

A1.4 Experimental

A1.4.1 Materials

Solid support (1000Å 1 µmole universal CPG, cat.# MM1-3500-1) columns and standard reagents used for automated DNA synthesis and Sephadex G-25 were used as purchased from BioAutomation. Thiol-Modifier C6 S-S phosphoramidite (cat.# 10-1936-90) was purchased from Glen Research. DMT-Hexaethylene-Glycol phosphoramidite (HEG, cat.# CLP-9765) was purchased from ChemGenes Corporation. 40% acrylamide/bis-acrylamide 19:1 solution, N,N,N',N'-tetramethylethane-1,2-diamine (TEMED), ammonium persulfate, tris(hydroxymethyl)-aminomethane (Tris), urea, ethylenediaminetetraacetate (EDTA) and agarose were purchased from Bioshop Canada Inc. and used as supplied. GelRed nucleic acid stain in water (cat.# 41003) was obtained from Biotium Inc. Acetic acid, ammonium hydroxide and boric acid were used as received from Fisher Scientific. Gold(III) chloride trihydrate, magnesium chloride, sodium chloride, Bis(p-sulfonatophenyl)phenylphosphine dihydrate dipotassium salt (BSPP) and other

chemicals were purchased from Sigma-Aldrich and used as received. 1xTBE buffer is composed of 90 mM Tris, 90 mM boric acid, 1.1 mM EDTA with a pH of \sim 8.3. 1×TBEN buffer contains additional 100 mM NaCl. 1xTAMg buffer is composed of 40 mM Tris, 12.5 mM MgCl2, with pH adjusted to 7.8 \pm 0.1 using glacial acetic acid.

A1.4.2 Instrumentation

Standard DNA oligonucleotides synthesis was carried out on a BioAutomation MerMade MM6 DNA synthesizer. DNA quantification measurements were performed by UV absorbance on a NanoDrop Lite spectrophotometer from Thermo Scientific. Agarose gel electrophoresis (AGE) experiments were performed on a Thermo ScientificTM OwlTM EasyCastTM B1 Mini Gel Electrophoresis System and polyacrylamide gel electrophoresis (PAGE) experiments on a 20 × 20 cm vertical Hoefer 600 electrophoresis unit. BioTek Synergy HT Multi-Detection Microplate Reader was used for gold nanoparticle (AuNP) quantification. Centrifugation for AuNP workup was performed on an Eppendorf 5702R Centrifuge while centrifugation for sample washing in the Amicon Ultra 0.5 mL centrifugal filters (100 kDa) was performed on a SorvallTM LegendTM Micro 21 Centrifuge. Multimode 8 scanning probe microscope (Bruker) was employed to acquire AFM images.

A1.4.3 Synthesis of Gold Nanoparticles (Performed by Saliba D.)

AuNPs with a diameter of 3 and 20 nm were synthesized by the reduction of tetrachloroauric acid (HAuCl4; Sigma-Aldrich). Before the synthesis, all glassware was cleaned with and aqua regia solution (3:1 hydrochloric acid: nitric acid) then rinsed thoroughly with distilled water. Next, 100 mL of a solution of 1% w/v of HAuCl₄ was brought to 60°C for the 3 nm AuNPs and to boiling

for the 20 nm AuNPs. Under vigorous stirring, 20 mL of a mixture of 4.0 mL of 1.0 % w/v of sodium citrate tribasic, 5.0 mL of 1.0 % w/v of tannic acid, 5.0 mL of 3.46 mg/ml of potassium carbonate and 6.0 mL of MilliQ water for the 3 nm AuNPs and 2.6 mL of 1.0 % w/v of sodium citrate tribasic for the 20 nm AuNPs were added very quickly. After the color had changed from pale gray to wine red, the solution was heated for another 30 min at the same temperature as before. Next, the citrate shell surrounding the AuNPs was exchanged for a more stable phosphine ligand shell. For this, 40 mg of bis-p-sulfonatophenyl- phenylphosphine dihydrate dipotassium salt (BSPP; Sigma-Aldrich) was added to the colloidal AuNPs solution (100 mL) and was stirred overnight for total passivation of the AuNPs surface. An aqueous saturated NaCl solution was added dropwise until a color change from red to dark blue was observed, indicating the aggregation of the AuNPs. The solution was then centrifuged for 30 min at 4.4 G; the clear supernatant was discarded, and the precipitated particles were resuspended using the smallest amount of an aqueous 3.5 mM BSPP solution.

Next, the resuspended solution was run on a purification 1x TBE (Tris base, boric acid, EDTA) agarose gel (3% for the 3 nm and 1.5% for the 20 nm AuNPs) for 2 h 30 min at 100 (V). The purple band was divided into sub bands of 0.5 cm each and excised with a scalpel where the AuNPs were separated from the gel by microelution at 300 (V) for 2 h in 0.5x TBE. The collected AuNPs suspension was concentrated by ultrafiltration with a prewetted (1xTBE) 10 kDa molecular weight cutoff filter (Amicon Ultra, AMD Millipore) at 14.8 G for 5 min. The concentration was determined photometrically at 450 nm assuming a molar extinction coefficient of 7.2×10⁶ L.mol⁻¹.cm⁻¹ and 5.4×10⁸ L.mol⁻¹.cm⁻¹ for the 3 nm and 20 nm AuNPs, respectively.

Finally, the AuNPs were conjugated to thiol-modified oligonucleotides (3'-ThiolC6-T10). First, the thiol-modified oligonucleotides were incubated with AuNPs in 1x TBENa buffer for 1h

at 50°C at a ratio of 1:100 (AuNP/DNA) for the 3 nm AuNPs and 1:400 for the 20 nm AuNPs. The sodium chloride was added to maximize the oligonucleotide density on the AuNP's surface. The excess of oligonucleotides was removed by three ultrafiltration and washing steps (400 μ L of 1x TBENa buffer per step) with a prewetted 50 kDa molecular weight cutoff filter (Amicon Ultra, AMD Millipore) at 14.8 G for 5 min. The concentration was determined photometrically at 450 nm, as mentioned before.

A1.4.4 DNA Sequences

All the sequences used in this appendix are summarized in table A1.2.

Table A1.2. Sequences of the strands used to build the nanotubes.

Name	Sequence $(5' \rightarrow 3')$			
V	CTCAGCAGCGAAAAACCGCTTTACCACATTCGAGGCACGTTGTAC			
	GTCCACACTTGGAACCTCATCGCACATCCGCCTGCCACGCTCTTAG			
	CATAGGACGGCGCGTTAAATA			
C1	CGGTGCATTTCGACGGTACTTCGTACAACGTGCCTCGAATGTAGA			
	GCGTGGCAGGCGATGTGAAGCAGTTGCAGCGTACTCGT			
C2	TCGGCAGACTAATACACCTGTCGATGAGGTTCCAAGTGTGGATAG			
	CTAGGTAACGGATTGAGC			
R1	TGCAACTGCTACCAGGTGTATT			
R2	TTACCTAGCTCCAGTACCGTCG			
R3	GTCCTATGCTTTGTAAAGCGGT			
LS1	TTTTCGCTGCTGAGGTAAGCCTTCGGCGAGCATCTATCTA			
	CGTATTTAACGCCGCC			
LS1*	CGGAGACATAGATAGATGCTCGCCGAAGGCTTAC			
LS1*polyA	CGGAGACATAGATAGATGCTCGCCGAAGGCTTACAAAAAAAA			
	AAAAA			
LS2	AGTCTGCCGACACAGAGATCAGTCGGAAGCATAATATCTTATGTT			
	CGTGATAACGAGTACGC			
LS3	AAATGCACCGCACAGAGATCAGTCGGAAGCATAATATCTTATGTT			
	CGTGATAGCTCAATCCG			
LS2/3*	TATCACGAACATAAGATATTATGCTTCCGACTGATCTCTGTG			
LS2/3*polyA	TATCACGAACATAAGATATTATGCTTCCGACTGATCTCTGTGAAAA			
	AAAAAAAAA			

A1.5 References

- (1) Le, J. D.; Pinto, Y.; Seeman, N. C.; Musier-Forsyth, K.; Taton, T. A.; Kiehl, R. A. *Nano Lett.* **2004**, *4*, 2343.
- (2) Zheng, J.; Constantinou, P. E.; Micheel, C.; Alivisatos, A. P.; Kiehl, R. A.; Seeman, N. C. *Nano Lett.* **2006**, *6*, 1502.
- (3) Teshome, B.; Facsko, S.; Keller, A. *Nanoscale* **2014**, *6*, 1790.
- (4) Nykypanchuk, D.; Maye, M. M.; Van Der Lelie, D.; Gang, O. *Nature* **2008**, *451*, 549.
- (5) Auyeung, E.; Cutler, J. I.; Macfarlane, R. J.; Jones, M. R.; Wu, J.; Liu, G.; Zhang, K.; Osberg, K. D.; Mirkin, C. A. *Nat. Nanotechnol.* **2012**, *7*, 24.
- (6) Edwardson, T. G.; Lau, K. L.; Bousmail, D.; Serpell, C. J.; Sleiman, H. F. *Nat. Chem.* **2016**, *8*, 162.
- (7) Rahbani, J. F.; Hariri, A. A.; Cosa, G.; Sleiman, H. F. *ACS Nano* **2015**, *9*, 11898.